THE UNIVERSITY OF MICHIGAN

INDUSTRY PROGRAM OF THE COLLEGE OF ENGINEERING

COMPREHENSIVE CAVITATION DAMAGE DATA FOR WATER AND VARIOUS LIQUID METALS INCLUDING CORRELATIONS WITH MATERIAL AND FLUID PROPERTIES

Ramon Garcia

A dissertation submitted in partial fulfillment
of the requirements for the degree of
Doctor of Philosophy in the
University of Michigan
Department of Nuclear Engineering
1966

September, 1966

IP-745

Engn
UMR
1579

COMPREHENSIVE CAVITATION DAMAGE DATA FOR WATER AND

VARIOUS LIQUID METALS INCLUDING CORRELATIONS

WITH MATERIAL AND FLUID PROPERTIES

by
Ramon Garcia

A dissertation submitted in partial fulfillment
of the requirements for the degree of
Doctor of Philosophy in the
University of Michigan
1966

Doctoral Committee:

Professor Frederick G. Hammitt, Chairman
Professor Richard K. Brown
Associate Professor Julian R. Frederick
Professor William Kerr
Associate Professor Edward A. Martin
Professor Clarence A. Siebert

Doctoral Committee:

       Professor Frederick G. Hammitt, Chairman
       Professor Richard K. Brown
       Associate Professor Julian R. Frederick
       Professor William Kerr
       Associate Professor Edward A. Martin
       Professor Clarence A. Siebert

TABLE OF CONTENTS

LIST OF TABLES

x

LIST OF FIGURES

xix

CHAPTER I

INTRODUCTION AND LITERATURE SURVEY

A. Introduction

Cavitation can be described as a hydrodynamic phenomenon which relates to the formation and collapse of vapor bubbles in a liquid. In general terms, these bubbles form in regions where the local pressure is reduced below the vapor pressure at that temperature and start to collapse as soon as the local pressure exceeds the vapor pressure. While this definition implies a distinction between phase transitions associated with reduction of pressure at constant ambient temperature, on the one hand, and addition of heat at constant pressure (i.e., boiling), on the other, heat transfer effects may play an important role in many cases of cavitating liquids. Such effects are especially important in liquids near their boiling points in the undisturbed condition. From a purely physical-chemical point of view, of course, no distinction need be made between boiling and cavitation, at least insofar as the question of inception is concerned, and many of the basic physical ideas regarding inception, vapor mass transfer, and condensation apply equally in either case.

The bubble collapse associated with cavitation can be considered as giving rise either to a shock wave which is propagated through the

fluid, or to a small high-velocity liquid jet, in either case terminating at the wall of the fluid container. The effects produced as a consequence of cavitation are twofold. First, for flow processes, it generally decreases the transferable energy and causes a loss in efficiency. Secondly, destruction (damage) of the material may take place when the shock wave or liquid jet terminates on structural material surfaces. Thus, it becomes necessary to investigate carefully those conditions resulting in cavitation and the damage suffered by various materials.

Since the cavitation damage process is apparently very closely related to damage from droplet or particle impingement or conventional erosion,* the damage data so obtained for various structural materials is also to some extent applicable to the resistance of these materials to these other forms of attack, so that the fields of droplet erosion in wet vapor streams (as in turbines or other two-phase flow passages), rain erosion of high-speed aircraft, micrometeorite bombardment of space vehicles, etc., are involved.

For the past two hundred years the phenomenon of cavitation has been known, and the accompanying losses of component performance and material damage have been of considerable concern to the designers of fluid machinery since the turn of the century. In the earliest considerations of the cavitation phenomenon the primary fluid of importance

---

*Reference 1 includes many papers on the relations between these various forms of attack. Also ASTM Committee G-2 has recently been formed to attempt to relate these various phenomena and form applicable test standards.

was water, as this was the basic fluid used in fluid machinery until recent times. At the present, however, liquid metals, cryogenics, organics, and other fluids have come into prime consideration as heat transfer agents and as working fluids in thermodynamic cycles.

The successful pumping and handling of high-temperature liquid metals, wherein cavitation itself is a problem, is of considerable importance in the present and future space program, particularly from the viewpoint of power generation using nuclear heat sources and liquid metal Rankine cycle power conversion equipment. As has been recently demonstrated, damaging cavitation attack can occur in bearings,[2] close-clearance passages,[3] etc., as well as pumps.[4,5] Recent theoretical studies[6] emphasize, in addition, a form of microcavitation that may also occur in many high-performance bearing applications and even in components such as gear teeth, so that the pitting which is often found in such units may well be a result of a form of cavitation. The same problems are, of course, also important in the conventional nuclear power plant program,[3] which includes several existing and projected reactor systems using liquid metals as the coolant. Hence, the prediction of cavitation performance and damage in a variety of fluid-material environments at various temperatures becomes of great importance. The high developmental costs for the component machinery and the difficult handling problems encountered with liquid metals make the full scale component testing and the materials-screening programs, which have been necessary in many cases, highly undesirable and very costly.

In the SNAP[*] application the minimization of size and weight and the maximization of temperature are of over-riding importance, so that the fluid-handling equipment, which must utilize high velocity flow rates and minimum suppression heads, must be designed to operate under conditions approaching cavitation or actually in a cavitating regime. In addition, long unattended life is desired for many such units. Hence, it becomes necessary to know realistically under what conditions cavitation can be anticipated, and the quantity and quality of damage to be expected for a given degree of cavitation, since it may not be possible or desirable to avoid the cavitating regime entirely by over-conservative design, as has been the practice for conventional applications.

The objectives of the present study include the determination of the cavitation resistance of potentially useful alloys in water at room temperature and in liquid metals at elevated temperatures, and the determination of material-fluid parameters to correlate damage and allow its à priori prediction.

B. Historical Background

The possibility of the occurrence of cavitation due to pressure changes in a flowing liquid was recognized by Euler[7] as early as 1754 in his treatise on hydraulic turbines. Reynolds,[8] in the last decade of the nineteenth century, produced and observed cavitation in a glass

---

[*]Acronym for System for Nuclear Auxiliary Power.

venturi tube at room temperature. These dates indicate the early spo-
radic interest in the problem. However, the major early analyses of
importance were those by Besant[9] in 1859 and Rayleigh[10] in 1917. The
accompanying loss of component performance and the destructive action of
cavitation were first noted in connection with a British destroyer's
propellers in 1895.[11] Other early users of fluid handling machinery who
investigated cavitation were Barnaby,[12] Parsons and Cook,[13] Sir Charles
Parsons,[14] Wagenbach,[15] and Fottinger.[16] Following the work of these
early pioneers, numerous investigators have devoted major efforts to
studying the details of this phenomenon over the past fifty years.

In the 1930's the laboratory testing of various materials in
order to determine their resistance to cavitation damage came into wide-
spread use, and several different methods of testing were developed.
These experimental facilities may be grouped into two categories: those
that depend on inducing low pressures as a result of high velocities in
flowing liquids or motion through a stationary liquid; and those that
produce cavitation by means of local, periodic, accelerations in an
otherwise stationary liquid. The first group includes devices such as
venturi tubes, objects immersed in constant area sections of cavitation
tunnels, and disks rotating in otherwise stationary liquid with through-
holes to generate cavitation upon test specimens inserted in the disk,
while the second depends on alternating pressure fields such as are pro-
duced by acoustic or other acceleration-producing devices. In addition
to such equipment, other types of "impact" producing devices, such as
liquid jets impinging on specimens, have also been used, since the

damage from such tests appears to be very similar to cavitation damage.

Venturi sections, which are simply convergent-divergent nozzles, or modifications thereof, were among the first flow devices used in the study of cavitation damage under laboratory conditions. Fottinger[16] in 1926 and Schroter[17] in 1932 utilized such a device to produce cavitation, the extent and intensity of which could be controlled, and made to occur in a region where a test specimen could be inserted. Mousson (1937)[18] and Lichtman et al (1958)[19] also performed studies in such nozzles. Most recently is the very extensive work of Hammitt[20,21] and Robinson,[22] who conducted studies both in water and mercury in a cavitating venturi. Since many machines operate under conditions of high velocity flow similar to that achieved in the venturi test sections, the venturi test is considered to be quite representative of field conditions.

Cavitation damage tests have also been performed in large cavitation tunnels which operate on principles similar to a wind tunnel. The cavitation is generally produced on a body of revolution or a hydrofoil placed in the fluid stream. Such devices have been described by Robertson[23] and Wright,[24] while Knapp (1955)[25] carried out cavitation damage experiments in such a tunnel. These tunnels are seldom used for damage tests because of the expense of operation, the relatively complicated procedures required in installing experiments, and the length of time they must operate to obtain measurable weight loss.

A device that has been used in recent years for studies of cavitation damage is a rotating disk on which cavitation is induced in a

separated flow region. Basically, such devices consist of a disk with holes near the periphery with axis parallel to the disk axis, rotated at high speeds in a chamber filled with the test fluid in which the ambient pressure can be controlled. Several specimens can be mounted on the disk and subjected to the cavitation cloud which is produced downstream of the holes. Such devices have been used and described by Rasmussen[26] and by Lichtman et al.[19] Very recently, a rotating disk assembly was utilized by Wood et al[27] to obtain cavitation damage data in water and by Kelly, Wood, et al[28] to obtain data in liquid metals.

Many investigators have used a variety of acoustic devices which produce cavitation by means of local, periodic, accelerations. The most common device of this type is the magnetostriction oscillator. The magnetostrictive effect is exhibited by the ferromagnetic materials, which, under the influence of an alternating magnetic field, show a periodic change in length. The first magnetostriction oscillator used for cavitation tests was developed by Gaines[29] in 1932. Kerr[30] and Schumb et al[31] in 1937 published extensive results obtained with such a device. Nowotny,[32] Leith and Thompson,[33] Rheingans,[34] Plesset,[35] and Thiruvengadam et al[36] also contributed valuable data and information accumulated over the years with this laboratory test device. Very recently, the vibratory apparatus has been used to test materials in high-temperature liquid metals as sodium,[3,37,38,39] and as part of this thesis investigation in lead-bismuth alloy,[40,41] mercury,[39,42] and lithium.[43]

Acoustic field generators comprise another type of laboratory device used to study effects of cavitation damage on materials. In this

case cavitation is produced by imposing a focused acoustic field in a liquid. The cavitation occurs in regions of maximum pressure amplitude. A very economical cavitation generator using barium titanate transducers to produce an acoustic field in a resonant container has been developed by Ellis.[44] The operating frequencies used with this device are 18 Kc./sec. and 24 Kc./sec. Another type of acoustic field generator, operating at frequencies from 400 to 1000 Kc./sec. has been used in experiments by Lichtman et al.[19]

One other type of apparatus, namely impact testing devices, should also be mentioned along with the venturi test section, cavitation tunnel, rotating disk, magnetostriction oscillator, and acoustic field generator used in laboratory cavitation tests. Although the impact of water drops is not per se a cavitation process, the use of such impact tests was important in early examinations of the mechanism of cavitation damage since it was assumed that the processes were analogous.[*] In order to examine the question of whether the mechanism of cavitation damage was associated with mechanical erosion, de Haller (1933)[45] ran experiments in which small rods fastened to the periphery of a wheel rotating at a high rate of speed, were passed through a high speed water jet. More recently, Hobbs[46] used a similar device in which a high velocity liquid jet impinged on multiple test specimens mounted on a rotating disk. A similar device is now in use also at the Chatou laboratory of Electricité de France.

---

[*]According to present theory, this assumption appears justified.

Each of the above-mentioned laboratory test devices has been used by many other investigators in the determination of the cavitation resistance of various materials as part of materials-screening programs currently being undertaken throughout the world. Of these devices the venturi test sections and cavitation tunnels are considered to be quite representative of field conditions encountered in rotating machinery. However, damage appears only after very lengthy operation, and the resulting costs are sometimes prohibitive. The rotating disk device and magnetostriction oscillator produce considerable damage in comparatively short periods of time and, hence, lend themselves nicely to materials-screening programs involving a variety of materials and several fluid conditions. Such apparatus is sometimes referred to as an "accelerated" cavitation test device due to the intense degree of cavitation produced and resulting extensive damage to test specimens.

Corrosion is often present when cavitation occurs, and many investigators have studied the combined interaction of these two damaging mechanisms.[47,48,49] Plesset[48] proposed a pulsing technique using a magnetostriction oscillator, whereby a short period of cavitation is followed by a longer non-cavitating interval, and concluded that such a test produces more meaningful results in cases where corrosion is important. The accumulated non-cavitating time allows a more realistic opportunity for any corrosion mechanism to manifest itself on the test specimen. In a purely cavitating experiment of the accelerated type, the test time involved might be so short that the corrosion contribution to the total damage mechanism would be negligible as compared to field

conditions, and, hence, the results misleading. Such pulsing apparatus can be used for both steady and pulsed cavitation studies. Hence, the effect of corrosion damage can be quantitatively determined.

C. Problem Statement

In a prototype system, the damage due to cavitation appears usually only after fairly lengthy operation under design conditions. Hence, it is clear that if a systematic study is to be made, involving a variety of materials and numerous plant conditions, it will be necessary to expend large amounts of time and money. An alternate approach, sacrificing direct applicability to some extent in the interests of economy, is to accelerate the cavitation losses by employing any one of the several laboratory techniques, previously discussed, which have been developed for this purpose. The most commonly-used method which is also employed in our own laboratory is a flowing tunnel system utilizing a venturi test section and a centrifugal pump to circulate the test fluid around a closed loop. This system has been described elsewhere.[50] As mentioned previously, the venturi is reasonably similar to actual flow systems, but at the same time damage occurs only rather slowly. As an alternative to a flowing system, an acoustic vibratory device was chosen for this investigation. This accelerated acoustic system makes use of a piezoelectric transducer[51] and will be described in detail later. Damage is accumulated at a very rapid rate compared to the venturi system, and, hence, large numbers of potentially useful materials can be tested in a variety of fluid-temperature environments at an economical cost.

In addition, this device makes it possible to conduct tests at elevated

temperatures in liquid metals with relatively little trouble. Compar-

able tests conducted in a flowing venturi system would involve a myriad

of additional problems and prohibitive cost.

In the past, the utility of accelerated acoustic cavitation dam-

age results has been limited because no direct correlation with cavita-

tion in a flowing system has been available. However, if such a corre-

lation could be formulated, it might be possible to substitute

relatively economical acoustic testing for tests in a tunnel facility.

Our own laboratory has conducted cavitation tests in both water and mer-

cury in venturi facilities[20,21,22] for the past several years and has

accumulated much useful data over this period of time. It is expected

that the accelerated cavitation data obtained with the vibratory facil-

ity in this investigation can be compared with the tunnel results, so

that a correlation can be obtained, allowing a more direct application

of the accelerated test results.

In addition to the cavitation testing program, it is essential

to determine the applicable mechanical properties of the materials

tested at the test temperatures so that a correlation between resistance

to this form of two-phase attack and some combination of the mechanical

properties can be obtained. Applicable mechanical properties certainly

might include the ultimate tensile strength, yield strength, hardness,

strain energy to failure, elongation, reduction in area, elastic modu-

lus, etc. Since many fluid-temperature combinations are involved in

this investigation, it is expected that any correlation of cavitation

data certainly will have to account for changes in fluid properties.

Applicable fluid properties for such a comprehensive correlation might

include density, surface tension, net positive suction head,[*] bulk mod-

ulus, kinematic viscosity, specific heat, thermal conductivity, heat of

vaporization, thermal diffusivity, Prandtl Number, and vapor pressure.

Thus, one would expect a complete correlation of cavitation damage data

to involve both mechanical properties of the test materials and fluid

properties at the applicable temperatures.

Hence, the objectives of the present investigation are as

follows:

1) Develop a practical laboratory device for obtaining cavitation

    damage data in a wide variety of fluids (including liquid

    metals) at temperatures as high as 1500°F under conditions of

    controlled purity utilizing an inert cover gas.

2) Utilizing the accelerated vibratory device developed for this

    program, determine the cavitation resistance of a wide variety

    of useful materials (involving a considerable range of mechani-

    cal properties) including stainless steels, carbon steel, tool

    steels, refractory alloys, aluminum, copper, nickel, brass,

    plastics, etc., in water at 70°F, in mercury at 70°F and 500°F,

    and in lead-bismuth alloy and lithium at 500°F and 1500°F.

3) Obtain a comprehensive correlation of the cavitation damage

    data with applicable material and fluid properties utilizing a

---

[*]Fluid "head" above vapor, i.e., NPSH $= \dfrac{p - p_v}{\rho}$, where p, p_v,
and ρ are the local pressure, vapor pressure, and fluid density,
respectively.

suitable computer program, so that one might be able to predict

à priori the behavior of a new material under a given set of

fluid-temperature conditions.

4) Develop a relationship or correlation between the damage

incurred in the flowing venturi device operated by this labora-

tory and the damage obtained in the accelerated vibratory facil-

ity studies.

CHAPTER II

EXPERIMENTAL EQUIPMENT

A. Facility Selection

1. Introduction

As discussed previously, there are many types of accelerated

cavitation research facilities available. These include the tunnel

facility and its variations, the rotating disk device, and the several

acoustic facilities. Early in the investigation by this laboratory, it

was decided to develop an acoustic cavitation unit since the tunnel

facility was already available and it was felt that the rotating disk

device would involve excessive costs. It was further felt that it would

be much more feasible to obtain data in liquid metals at elevated tem-

peratures with an acoustic facility, as opposed to any alternative sys-

tems. Hence, an investigation of the various types of acoustic

approaches was made.

The types of transducers that would lend themselves nicely to

acoustic cavitation facilities are:[52,53]

a) Crystal oscillators - These utilize the piezoelectric effect,

which is reversible. The range of frequencies used is very

wide, the upper limit being about 10,000 Mc./sec.

b) Magnetostrictive oscillators - These devices make use of the

phenomenon of magnetostriction, which is also reversible. The

upper frequency limit is of the order of 100 Kc./sec.

It should be noted that there are several other types of transducers

available, such as electromagnetic transducers, electrostatic trans-

ducers, etc., but it was felt that only the two approaches mentioned

above were suitable, considering the experimental program which was

proposed.

2. Piezoelectric Effect

Crystal oscillators make use of one of two types of crystal

for generating ultrasonic waves. One type of crystal displays the

piezoelectric effect and the other the electrostrictive effect. The

piezoelectric effect, which was first discovered by the Curie brothers

in 1880, occurs in crystals having axes of non-symmetry. Suppose a slab

or disk of such a crystal is cut with its parallel surfaces lying normal

to an axis of non-symmetry. On subjecting this slab to a mechanical

stress, equal and opposite electric charges appear on the parallel sur-

faces. Provided that the crystal is not strained beyond the elastic

limit, the magnitude of the charge density (or dielectric polarization)

is directly proportional to the applied stress. The converse effect was

predicted by Lippman in 1881, and discovered experimentally by the Curie

brothers in the same year. When an electric field is applied in the

direction of an axis of non-symmetry, the slab is mechanically strained,

the amount of strain being proportional to the intensity of the applied

field. From a consideration of the principle of conservation of energy, the direct and converse piezoelectric effects may be shown to be equal and opposite, i.e., the effect is reversible. It is the converse piezo-electric effect that is used in designing an ultrasonic transducer of this type for cavitation investigations. An alternating electric field is applied to the parallel surfaces of a piezoelectric crystal, and the resulting rapid variation of length of the crystal is transmitted along an exponential or stepped horn which is fitted with a suitable test specimen. The specimen then oscillates with a frequency equal to that of the applied electric field, and with an amplitude proportional to the magnitude of the applied field. These horns will be described later. Crystals exhibiting the piezoelectric effect include quartz, Rochelle salt, tourmaline, and lithium sulphate. Each crystal has a natural fre-quency of vibration dependent on the dimension of the crystal. If the natural frequency corresponds to the applied frequency of the electric field, the amplitude of vibration of the crystal is a maximum. Unfor-tunately, many piezoelectric materials are deliquescent and can only be used in controlled surroundings.

3. Electrostrictive Effect

The electrostrictive effect occurs in all dielectrics and is a phenomenon analogous to magnetostriction, which will be described later. For most materials, the electrostrictive effect is negligible, but in certain dielectrics, called ferroelectrics, the effect is strongly pronounced. The application of an electric field in a given

direction produces a mechanical strain, the magnitude of which is proportional to the square of the applied field strength (as opposed to the piezoelectric effect where the strain is proportional to the applied field), and is thus independent of the sense of the field. Consequently a positive strain may occur for both positive and negative values of the exciting field. Electrostrictive materials can be made to exhibit the piezoelectric effect if they are properly polarized. This can be done permanently by heating the materials to a temperature above the Curie point (i.e., the temperature at which electrostriction disappears) and then allowing them to cool slowly in a strong electric field oriented in the direction in which one intends to apply the exciting field. Provided that the exciting field is small compared with the initial polarizing field, the strain will vary sinusoidally at the frequency of the sinusoidally varying exciting field. A polarized ferroelectric transducer appears to display the same effect as a piezoelectric transducer, and for this reason it is commonly referred to as being piezoelectric. At present, barium titanate and lead zirconate are the substances most widely used for electrostrictive applications. For the construction of this type of transducer, many small crystallites of ferroelectric material, together with suitable additives, are bonded together to form a ceramic of the required shape. Because these materials are polycrystalline, they have the advantage over naturally occurring piezoelectric crystals in that they are isotropic and do not have to be cut along specified axes. Such electrostrictive materials lend themselves nicely to the type of acoustic cavitation facility envisioned for this study.

4. Magnetostrictive Effect

Magnetostriction occurs with ferromagnetic materials and certain non-metals called ferrites. The magnetostrictive effect was discovered by Joule in 1847, and the converse effect by Villari in 1868. When a rod or bar of ferromagnetic or ferrimagnetic material is subjected to a magnetic field, it experiences a change in length. Conversely, a mechanical stress applied to a rod or bar causes a change in intensity of magnetization. The magnetostrictive effect, which is analogous to the electrostrictive effect described above, is prominent for materials such as nickel, iron, and cobalt. Whether there is an increase or decrease in length depends entirely on the nature of the material and on the strength of the applied magnetic field, and this is independent of the direction of the field. For purposes of cavitation investigation, an alternating magnetic field might be applied to a ferromagnetic material, the resulting rapid variation in length of the material constituting a standing wave generator. The ferromagnetic material may be coupled to an exponential or stepped horn which in turn would accommodate the test specimen. The standing wave would exist throughout the assembly. If the assembly is of a suitable length, e.g., equal to the wavelength of the sound wave propagated within it, then the amplitude of vibration at the tip of the assembly would be a maximum and give rise to a rapid variation of local pressure at the tip of the assembly, which, for purposes of cavitation investigations, is immersed in a liquid. If the pressure variation is such that the local pressure is reduced below the vapor pressure of the liquid at the existing

temperature, then the phenomenon of cavitation occurs. The details of the design of such a transducer assembly will be discussed later. However, at this point, a decision must still be made as to which of the approaches described above is to be pursued.

5. Choice of Accelerated Cavitation Device

The choice is one between the piezoelectric, electrostrictive, or magnetostrictive devices described above. Much work has been reported utilizing the magnetostrictive transducers, and hence it might be reasonable to adopt such a device on this basis. However, the power requirements and cooling problems can be somewhat severe, and perhaps the cost higher than the alternatives. Further, since a local vendor was available to help in the design of either the piezoelectric or electrostrictive-type transducers, it was felt that this approach should be adopted. The amplitude obtained with such generators is of the same order as that obtained with the magnetostrictive devices, and it is believed that the efficiency of energy conversion with the piezoelectric devices is greater than that obtained with the magnetostrictive generators. In summary, it was felt that a piezoelectric cavitation generator would be entirely suitable for the studies envisioned in that flexibility in the design permitted many changes, heat losses were kept at a minimum, crystal temperature did not exceed the Curie point with a feasible cooling arrangement, amplitude of vibration was sufficient, and cost was nominal. Pure lead zirconate ($PbZrO_3$) is a non-ferroelectric, but if mixed with more than 10 mole % lead titanate ($PbTiO_3$), it acquires ferroelectric properties. Hence, in view of the previous

discussion, a polarized lead zirconate-titanate ceramic, which exhibits
the piezoelectric effect, was chosen as the crystal for the transducer
assembly. This crystal has the following desirable properties:

a) Satisfactory piezoelectric characteristics for the required
   modes of vibration.

b) Homogeneous throughout.

c) Capable of being worked to the desired shape and size.

d) Variations of its properties with temperature are minimal.

e) Internal friction is low.

f) Chemically and physically stable.

g) Retains its piezoelectric properties over the complete range of
   temperatures for which it is to be used.

h) Results in satisfactory matching with both the electrical cir-
   cuit and the medium of propagation for efficient energy
   transfer.

The ultrasonic transducer utilizing the piezoelectric crystal
selected must satisfy the following general requirements:

a) It must be operable (i.e., able to produce appreciable cavita-
   tion activity) in fluids ranging in density from 1-15 grams/cc.

b) It must be capable of operating in fluids whose temperatures
   range from 70°F to 1500°F.

c) It must be so constructed that the amplitude of vibration can be
   accurately and conveniently measured.

d) The stepped and/or exponential horns employed are to be remov-
   able and interchangeable (i.e., easily replaced).

e) The exponential horn will be designed so as to accommodate the test specimens.

f) Provision is to be made for fastening the transducer to the fluid container without appreciably reducing the amplitude of vibration at the horn tip.

B. Description of Overall System

A general description and discussion of the major features of the University of Michigan high-temperature ultrasonic cavitation vibratory facility will be given here. Succeeding sections will describe the various components in detail. Figure 1 is a schematic block diagram of the high-temperature ultrasonic vibratory facility showing the audio oscillator, power amplifier, transducer-horn assembly, test specimen, oscilloscope, frequency counter, high-temperature furnace and cavitation vessel, and accelerometer. The signal supplied by the variable frequency audio oscillator is amplified and applied to the piezoelectric crystals. The resultant periodic motion of the crystals effectively constitutes a standing wave generator with the amplitude of the standing wave being increased as it traverses the exponential horn assembly. The use of exponential horns as velocity transformers in this fashion was first suggested by Mason.[54] The movement of the horn tip, to which a test specimen has been attached, results in a rapid variation in local pressure, causing the periodic formation and collapse of an intense cavitation cloud. The final result is an accelerated erosion of the test specimens subjected to the collapsing bubble cloud. The materials of interest can be tested in a variety of fluids over a wide temperature
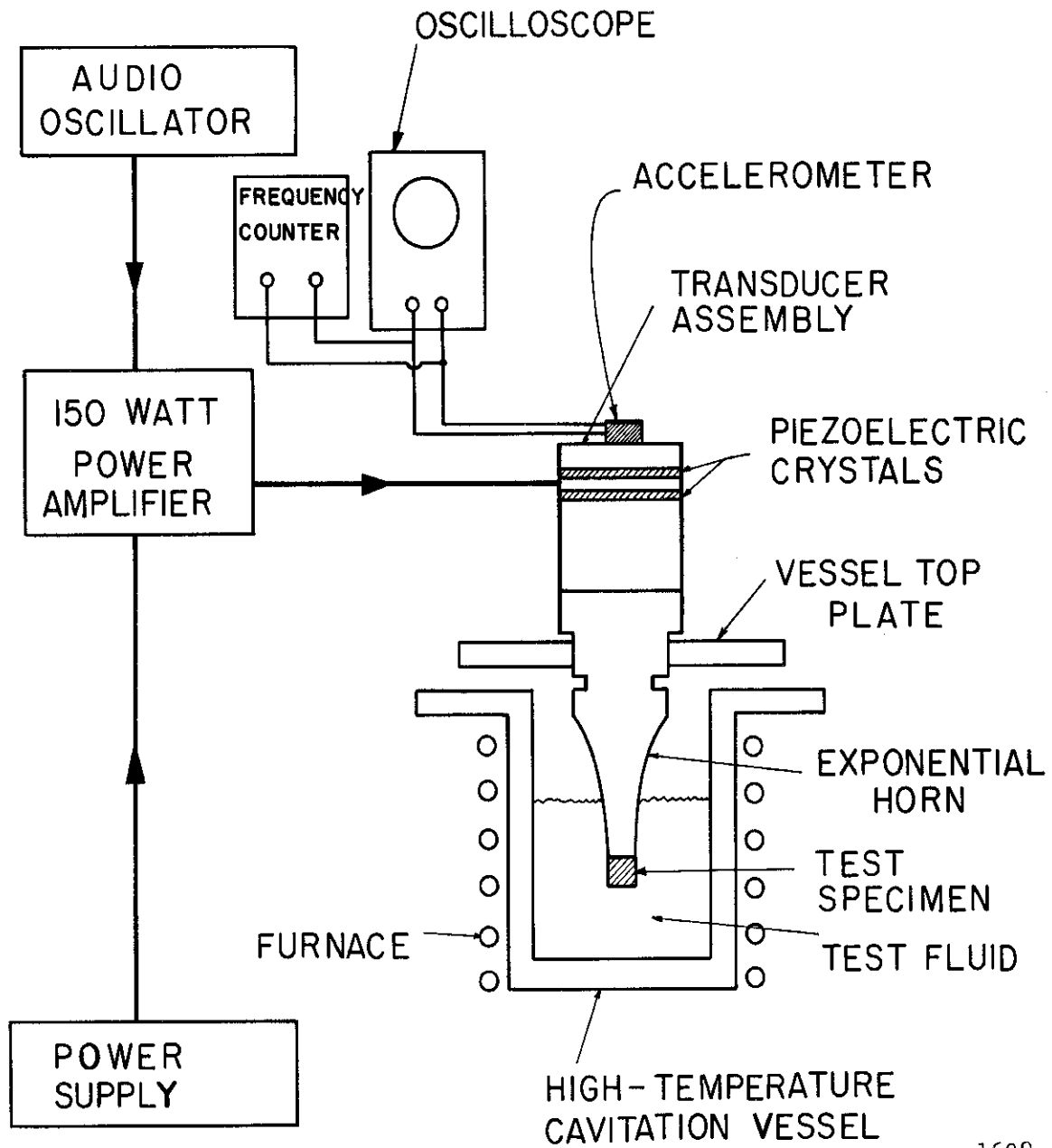
Fig. 1.--Block diagram of the high-temperature ultrasonic vibratory facility.

range. For studies at elevated temperatures the transducer-horn

assembly is attached to the special cavitation vessel which is filled

with the appropriate fluid. Figure 2 is a photograph of the facility

showing the audio oscillator, power amplifier, voltmeter, oscilloscope,

timer, temperature controller, furnace, and the transducer-horn assembly

installed in the high-temperature cavitation vessel. The vessel is

inserted in the furnace. The line running to the vessel supplies argon

as a cover gas for the fluid.

The cavitation facility has been completely calibrated and oper-

ated at fluid temperatures in excess of 1500°F at a frequency of approx-

imately 20 Kc./sec. and double amplitude of $\sim$ 2 mils. It is capable of

operation with a variety of fluids.

C. Ultrasonic Transducer Assembly

As mentioned previously, the ultrasonic cavitation facility con-

sists of a variable frequency audio oscillator and power amplifier which

supply a voltage of suitable magnitude and frequency directly to elec-

trodes attached to the piezoelectric crystal (in this case lead

zirconate-titanate). The applied voltage causes the crystal to alter-

nately expand and contract its length by $\sim$ 0.1 to 0.2 mils. In order

to produce cavitation in various liquids, it is desirable to amplify

this minute movement of the lead zirconate-titanate crystal. This can

be done by attaching either a stepped or exponential horn assembly to

the crystal transducer section. The horn acts as a velocity trans-

former, increasing the velocity of the standing waves propagated by the
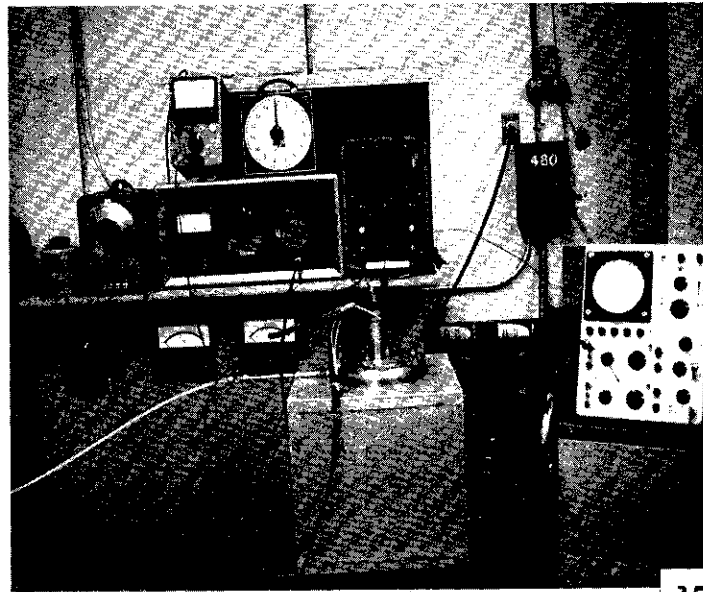
Fig. 2.--Photograph of the high-temperature cavitation facility.

crystal. As a result, the maximum amplitude of the horn tip may be as great as 2 to 3 mils. The amplification obtained with a stepped horn is a function of the ratio of the end diameters while the amplification obtained with an exponential horn is a function of the ratio of the end areas.[53] An exponential horn was chosen to minimize the stress problems within the horn assembly. With the stepped horn, stresses at the interface can cause the horn to fracture at this point. The general features of the ultrasonic transducer assembly are indicated in Figure 3.

There are two lead zirconate-titanate crystal wafers in the driver so that both ends of the transducer can be grounded. If only one crystal had been used, one end of the transducer would have been at a voltage above ground. This represents an undesirable situation. The aluminum disk shown between the two crystal wafers is suitably bonded to each of the crystals and represents one of the electrodes (high volt- age). An internal bolt, suitably insulated, contacts the steel counterweight, passes through both crystals and the separating aluminum disk, and terminates in the lower aluminum section. As a result, the steel counterweight, the upper surface of the top crystal wafer, and the lower surface of the lower crystal wafer are electrically the same point (ground). Hence, the second electrode is attached to the upper steel counterweight. The aluminum sleeve serves the purpose of making a firm attachment to the lower crystal. It is then possible to easily and quickly attach various exponential and stepped horns to this upper assembly without having to bond the crystal to a new horn surface each time. The horn made for the transducer was exponential in form, as noted, and fabricated of type 303 stainless steel.

5/8 - 20

STEEL COUNTERWEIGHT

HEX. HEAD CAP SCREW

ALUMINUM SPACER

LEAD ZIRCONATE - TITANATE
CRYSTALS

ALUMINUM SLEEVE

3/8 - 28

STAINLESS STEEL
HORN

1/4 - 28

TEST SPECIMEN

1/2

1/4

1/16

1/4

1/4

1/2

1/2

1/2

4 1/16

1 3/4

1 3/4

9 5/16

11/16

1/16

3/16

5 1/4

2 9/16

5/8

A

1/16

9/16

1/16

1 1/4

1453

SECTION A - A'
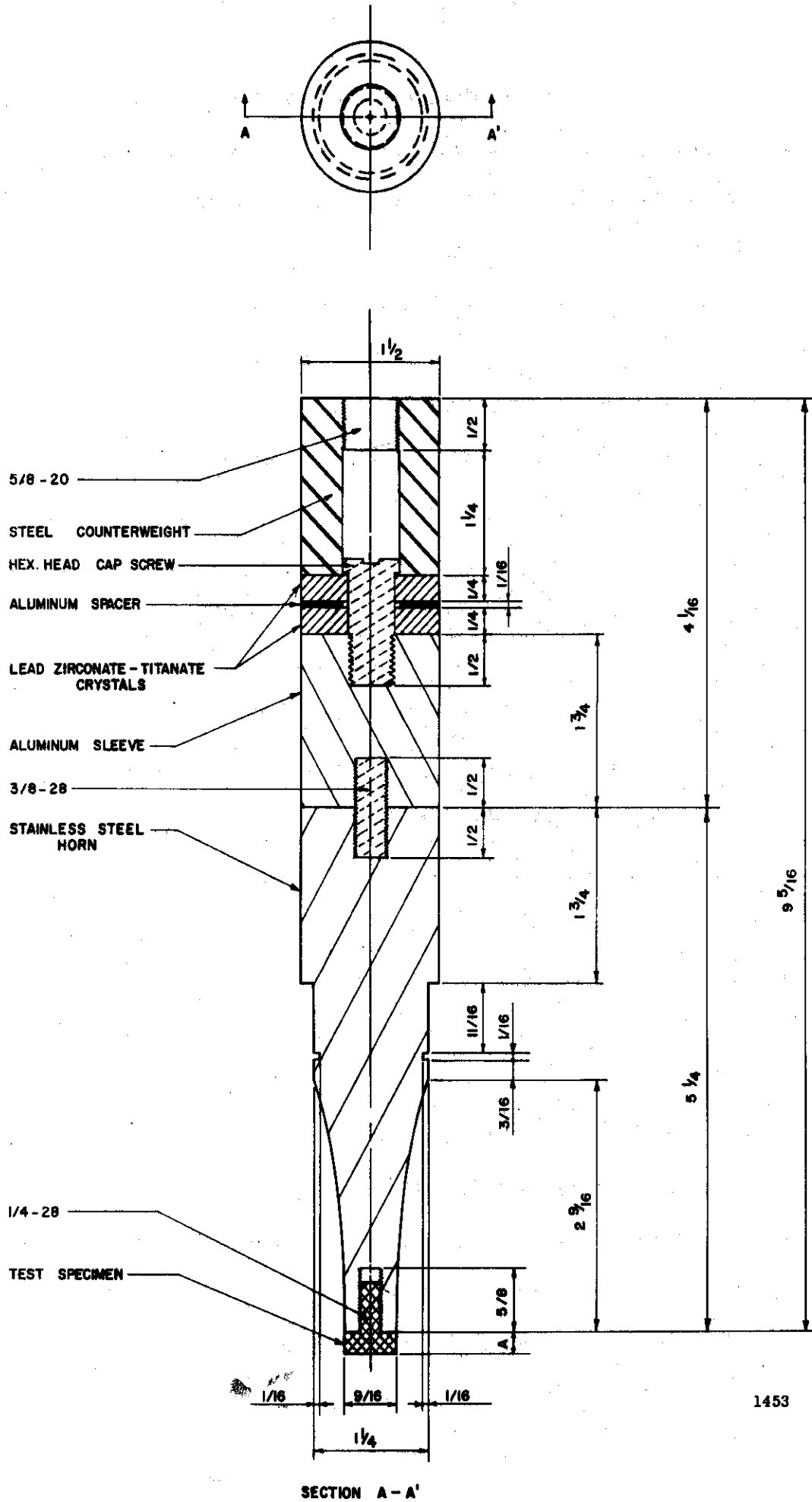
Fig. 3.--Exponential horn and ultrasonic transducer assembly.

The standing waves generated by the continual vibration of the crystal wafers are propagated throughout the length of the transducer assembly. It is necessary to achieve a proper acoustic match between the various materials making up the assembly if efficient transfer of energy is to be realized. If one considers the reflection and transmission of plane waves at the interface of two materials, it can be shown that the reflection coefficient approaches zero and the transmission coefficient approaches unity as the acoustic impedances of the two media approach one another. The acoustic impedance is given by the product of the density of the medium and the velocity of sound propagated within it. In the case of aluminum and stainless steel, the velocity of sound in each is approximately the same, namely, $\sim$ 16,000 feet/second. However, the densities of the materials differ by about a factor of three. Thus, the acoustic impedance of the aluminum is 1.7 x 10^7 kg./m.^{2}sec., while that of the stainless steel is 4.7 x 10^7 kg./m.^{2} sec. Hence, at the interface of these two materials one would expect a transmission coefficient of approximately 0.75, or 75%, which indicates that the media are quite well matched and efficient transfer of energy is taking place across the interface. This is a very important consideration in the design of such a transducer in that poor selection of materials can result in large degree of reflection at the interface, and hence a very inefficient transducer.

A final important consideration in the design of such a transducer is concerned with the dimensions of the upper driver section and the exponential horn assembly. Typically, the length of the upper

driver section and the exponential horn would each be equal to half the

wavelength of the acoustic oscillation propagated in it. Figure 4 is a

schematic of a typical waveform showing the position of the nodes and

anti-nodes along the length of the transducer assembly. It is clear

that maximum amplitude is necessary at the tip of the horn assembly to

which the test specimen is attached. Hence, the horn tip must corres-

pond to an anti-nodal point of the standing wave propagated throughout

the assembly. Further, it is clear also that if an attachment of the

horn assembly is to be made to a stationary container of some type, this

point of attachment must correspond as closely as possible to a nodal

point of the standing wave, i.e., a point of zero amplitude. Due to

symmetry, it is clear that the aluminum spacer electrode located between

the two crystal wafers must be a point of zero amplitude, a nodal point.

Many variations are possible here, but it is seen from Figure 4 that an

anti-node will exist at the tip of the horn and a node will exist at

the mid-point of the horn assembly if both the horn assembly and the

upper driver section are made equal to one-half wavelength of the stand-

ing wave propagated within the assembly. As mentioned previously, the

velocity of sound in both aluminum and stainless steel is approximately

equal, namely, $\sim$ 16,000 feet/second. Hence, it is possible to compute

either the length of the transducer, given the applied frequency, or to

compute the frequency, given the length. Of course, a convenient

length, neither very small nor large, is desired. If a total length of

10 inches is chosen for the assembly, the required applied frequency is

easily determined from the familiar relation:
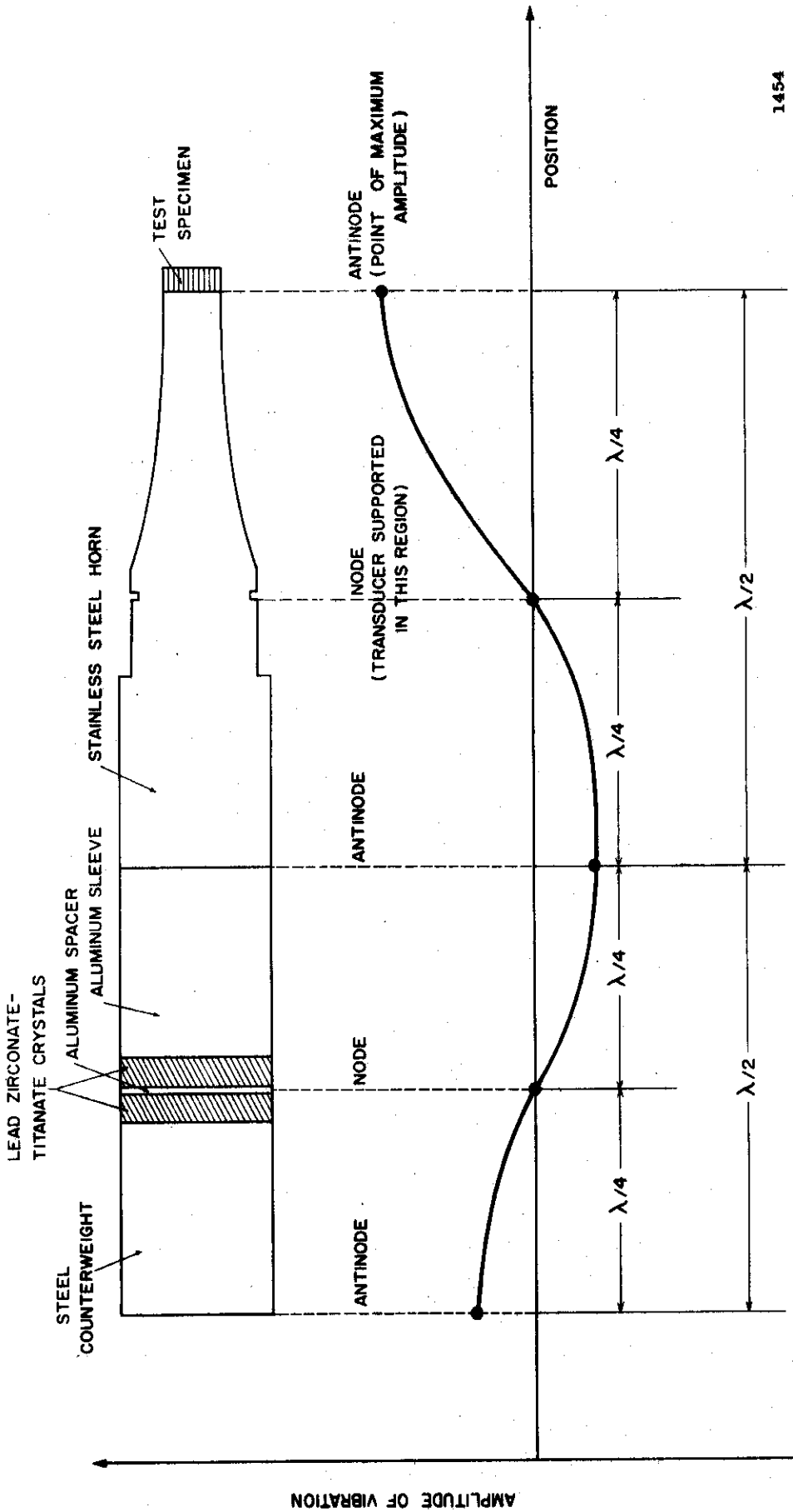
Fig. 4.--Typical waveform showing position of nodes and anti-nodes on transducer assembly.

$$c = f\lambda$$

where:

  c = velocity of sound

  f = applied frequency

  λ = wavelength of sound

For the case above, the frequency determined in this fashion is found to be $\sim$ 20 Kc./sec. Such a frequency can be easily supplied by a standard variable-frequency audio oscillator. The stainless steel horn is approximately 5 inches in length, while the upper driver assembly is about the same length. Hence, the transducer is referred to as a full wavelength transducer and the horn as a half wavelength horn.

Figure 4 also shows schematically the velocity transformer action of the exponential horn, as the amplitude of the standing wave propagated within the assembly is increased due to the exponential variation in cross-sectional area.

D. Test Specimens

1. Effect of Density on Specimen Size

Since this study includes the testing of many different specimen materials, varying widely in density, and since it is necessary to maintain uniform weight of the specimens to obtain an approximately equal resonant frequency for all cases, the length of the various specimens will vary with the density of the material. Figure 5 is a curve of specimen length, A, versus density of specimen material. The required specimen weight is 9.4 $\pm$ 0.1 g. The volume of the mounting hardware for
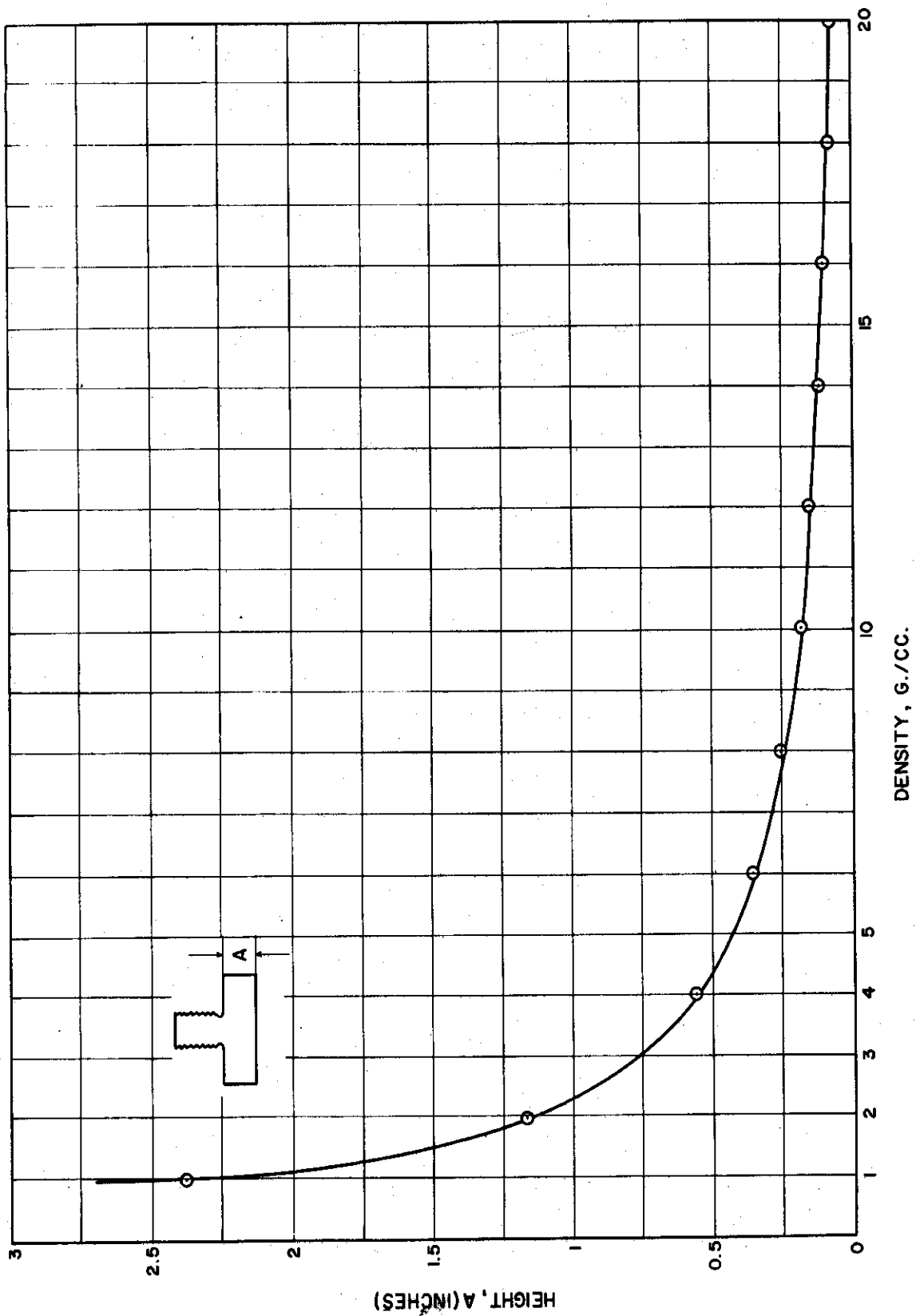
Fig. 5.--Effect of density on cavitation test specimen size.

1459

each specimen is constant, and this was determined by a weight measurement of the complete specimen. Hence, the required weight must be realized by suitable adjustment of the specimen face thickness, A, which can be easily computed.

2. Standard Cavitation Test Specimen

Figure 3 clearly indicates the point of attachment of the test specimen at the tip of the ultrasonic transducer assembly. The details of the standard cavitation test specimen are shown in Figure 6. These specimens are screwed into the end of the horn and tightened with a special wrench which does not in any way damage the specimen or remove material from it, as shown by repeated tests. The required dimensions "A" and "B" vary with the density of the material. The dimension "A" may be determined from Figure 5, while the length of the threaded hardware section (B - A) is generally held constant at 3/8 in.

3. Special Cavitation Test Specimens

A number of the materials tested in this program could not be machined in the form of the standard cavitation test specimen shown in Figure 6 due to very low density, brittle nature of some of the materials, unavailability of bar stock of the required material, and difficulty in machining and providing the material with a threaded length. In each case a special specimen was designed to overcome the problems encountered so as to achieve satisfactory operation.

Plexiglas was one such material that required a special design for the test specimen. Due to the low density of the Plexiglas

$\frac{1}{4} - 28 - \text{UNF}$

UNDERCUT

SHARP
CORNERS

B ± .005

A ± .005

—.547 ± .001—
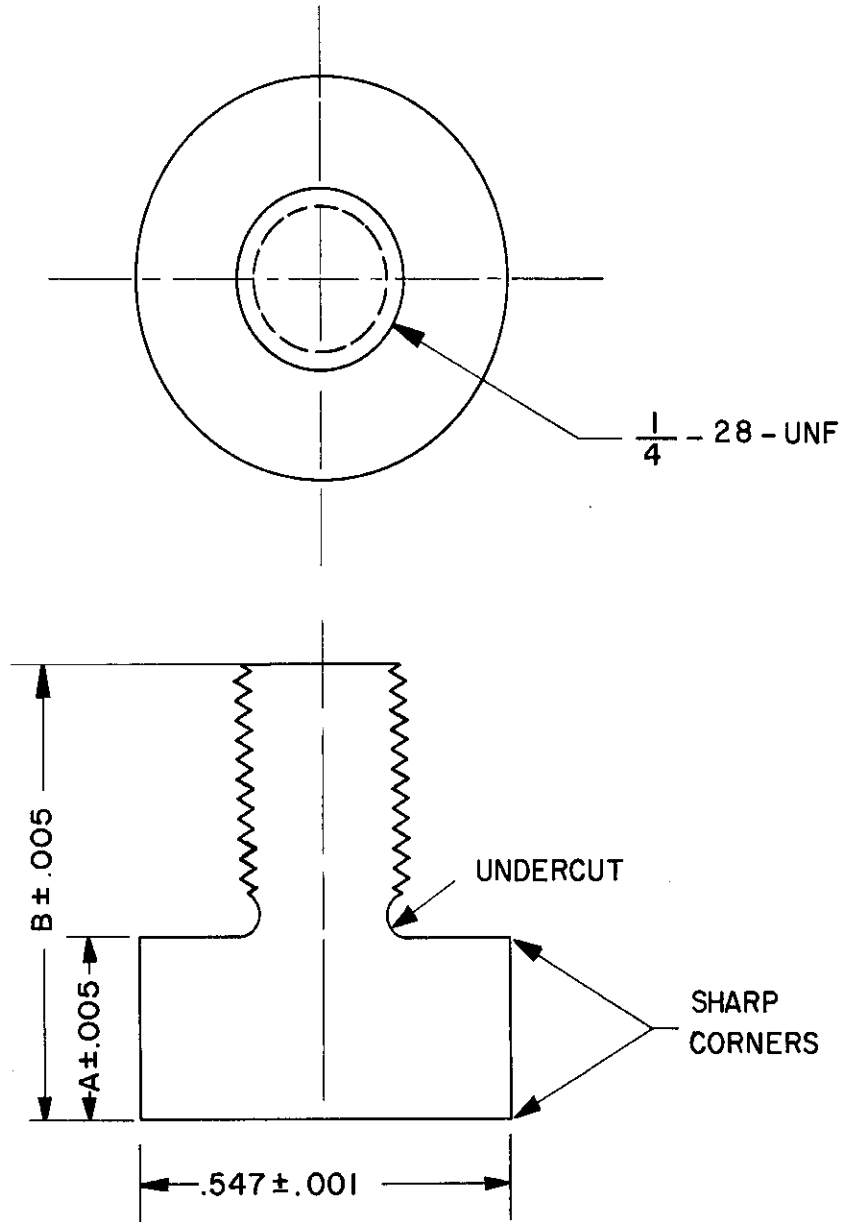
NOTE :
DIMENSIONS "A" & "B"
VARY WITH SPECIMEN MATERIAL

1455

Fig. 6.--Standard cavitation test specimen.

(compared to the other materials tested) and its brittle nature, it was completely impractical to fabricate standard cavitation test specimens as shown in Figure 6. The low density would result in an unusually large "A" dimension (and hence appreciably change the resonant frequency of operation), while the brittle nature of the material made it impossible to firmly affix a specimen to the ultrasonic horn without damage to the threaded portion. It is necessary that the specimen be firmly and tightly attached to the horn tip so that the ultrasonic energy is properly transmitted across the interface for efficient operation. Hence the design shown in Figure 7 consisting of a Plexiglas test specimen with internal thread and a separate stainless steel mounting stud was adopted and proved to be satisfactory. The mounting stud results in a firm attachment of the Plexiglas cylinder to the horn tip without damage to the Plexiglas internal threads since this connection need only be made once. The high density of the steel also allows the required specimen weight to be obtained without an unduly long specimen. Thus, this design overcomes all of the problems encountered with the standard cavitation test specimen.

Another material tested that posed similar problems to the Plexiglas was the material, graphitar. Graphitar is formed from carbon and graphite powders which are compacted under high unit pressures and then furnaced at temperatures up to 4500°F, and is of wide technological importance in connection with seals and bearings. It has a relatively low density and is brittle and porous. For these reasons the identical test specimen design adopted for the Plexiglas was also used for the

1/4−28

1/4−28

1/2

3/4

7/8

.547±.001

PLEXIGLAS CAVITATION
SPECIMEN

STAINLESS STEEL
MOUNTING STUD
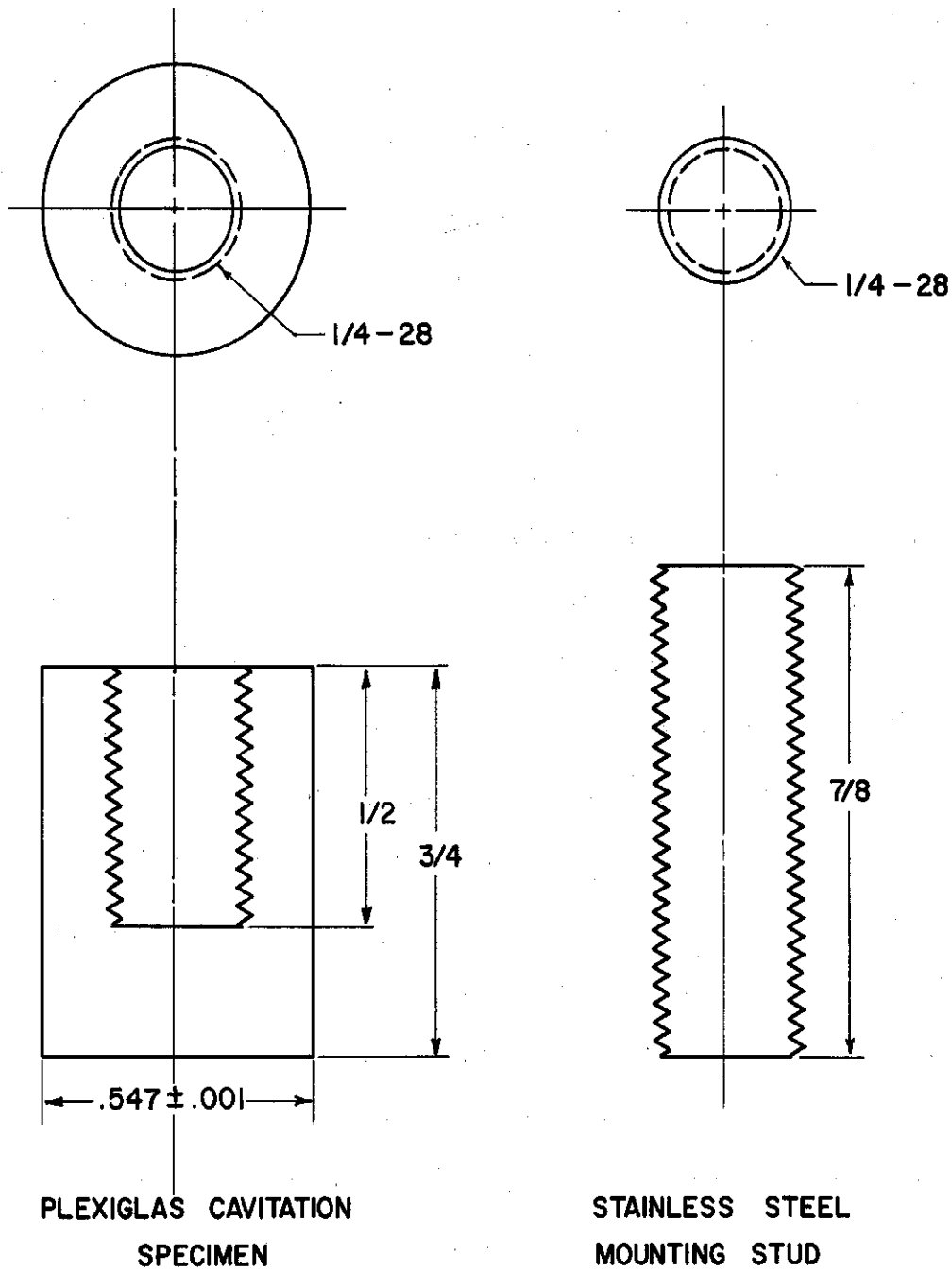
1771

Fig. 7.--Special Plexiglas cavitation test specimen and mounting stud.

graphitar material and found to be completely satisfactory (Figure 7).

It was desired to test in the vibratory facility the identical heat-treats of Cu, Cu-Zn, Cu-Ni and Ni that had been previously tested in the venturi loop facility. Since these materials were available only in sheet stock 1/16 in. thick, it was necessary to design a special specimen consisting of an adaptor of a suitable material and a disk of the desired test material. Means of attaching the disk to the adaptor had to be provided so that a firm bond would result. This is necessary so that the ultrasonic energy is efficiently transferred across the interface. Hence the design shown in Figure 8, consisting of a brass adaptor and a disk of the desired material, was adopted and proved to be satisfactory. The disk is fastened to the adaptor with soft solder. Various epoxies and cements were attempted as a bonding material initially, but the bond was immediately destroyed upon initiation of the test. The acoustic impedance of the soft solder is on the order of that of both the brass adaptor and disk materials, while the epoxies and cements possessed a very low acoustic impedance due to negligible elastic properties. The arrangement shown in Figure 8 results in a standard specimen weight of 9.4 ± 0.1 g., as desired.

Finally, it was not convenient to fabricate a standard cavitation test specimen from single-crystal tungsten, which was also included in the cavitation testing program. Single-crystal tungsten is very difficult to machine using standard techniques, and due to the lack of a suitable grinder for forming the threaded portion of the specimen, alternate designs were considered. It was found feasible to produce a

1/4 –28

BRASS ADAPTOR

UNDERCUT

.58"

.14"

DISC OF
TEST MATERIAL

.06

0.547 ± .001

SOFT SOLDER BOND
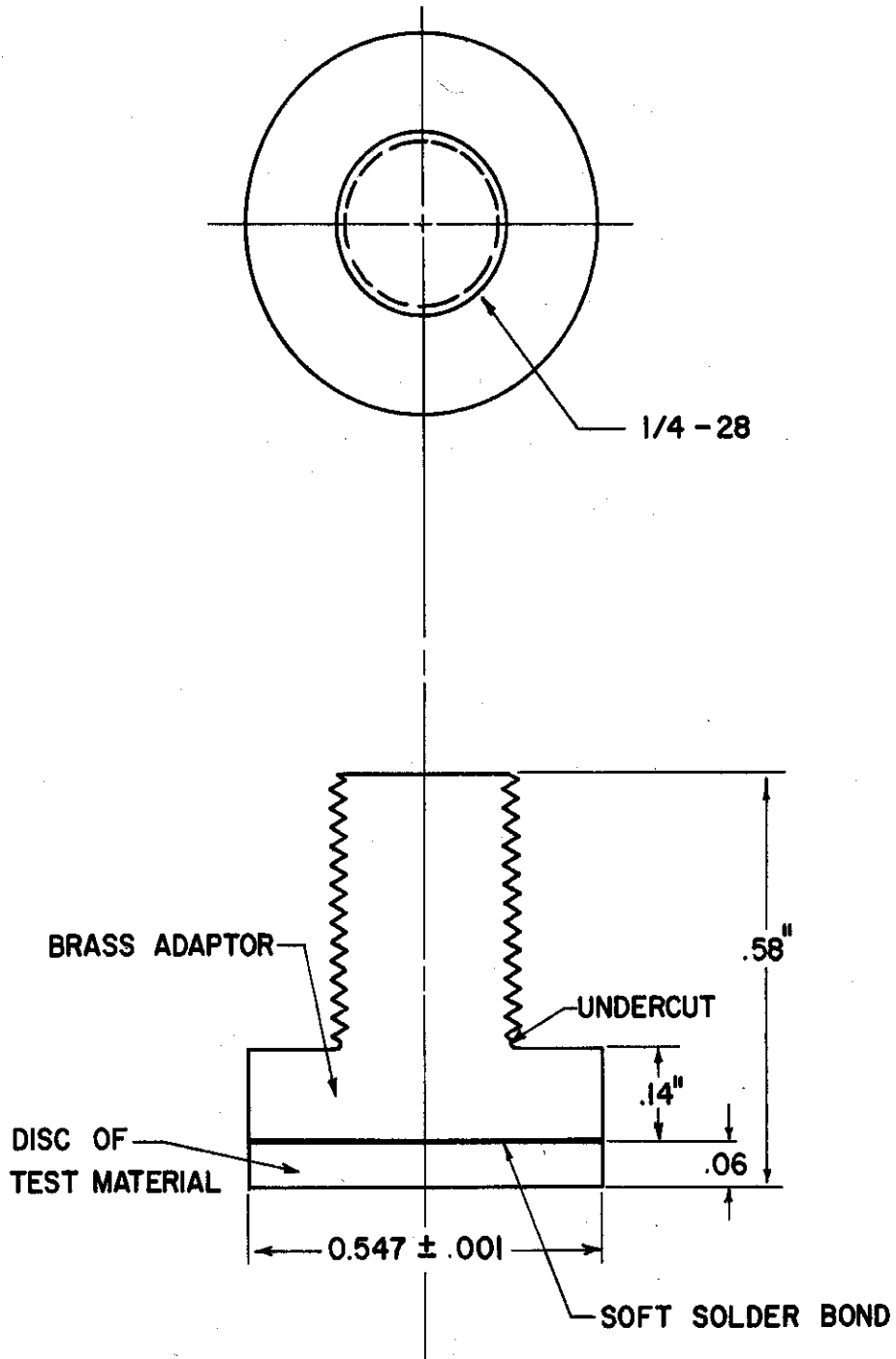
1776

Fig. 8.--Special cavitation test specimen for Cu, Cu-Zn, Cu-Ni,
and Ni.

simple disk of single-crystal tungsten by grinding, but it was still

necessary to affix the disk firmly to the ultrasonic horn. Initially,

an attempt was made to use epoxy resin to attach the tungsten disk to a

stainless steel adaptor. However, as mentioned previously, little suc-

cess was achieved with various epoxies and cements which were tried for

this purpose due to negligible elastic properties and very low impact

strength. As a result the epoxy bond immediately fractured at the start

of the test.* Finally, the design shown in Figure 9 was found to be

satisfactory. Here, a simple disk of single-crystal tungsten has been

attached to a stainless steel adaptor with silver solder. The silver

solder was found to form a very suitable bond between the tungsten and

stainless steel, and resulted in satisfactory transmission of the

acoustic energy across the interface. The diameter of the tungsten disk

(1/2 in.) was slightly smaller than the diameter of the stainless steel

adaptor (.547 in.) due to unavailability of single-crystal tungsten in a

larger size at the time of the tests.

Thus, all materials tested in this program were fabricated as

per Figure 6, with the exception of the special circumstances and diffi-

culties encountered with a few materials, as discussed above.

E. High-Temperature Cavitation Vessel

1. Design Philosophy and Criteria

Since one of the major objectives of the present experimen-

tal cavitation program is to obtain damage data at elevated temperatures

---

*At a later date a suitable epoxy (Loctite Bonding Kit #2508 -
Loctite Corp.) for attaching specimen disks to adaptors was found and
used for certain plastic materials where other methods of attachment
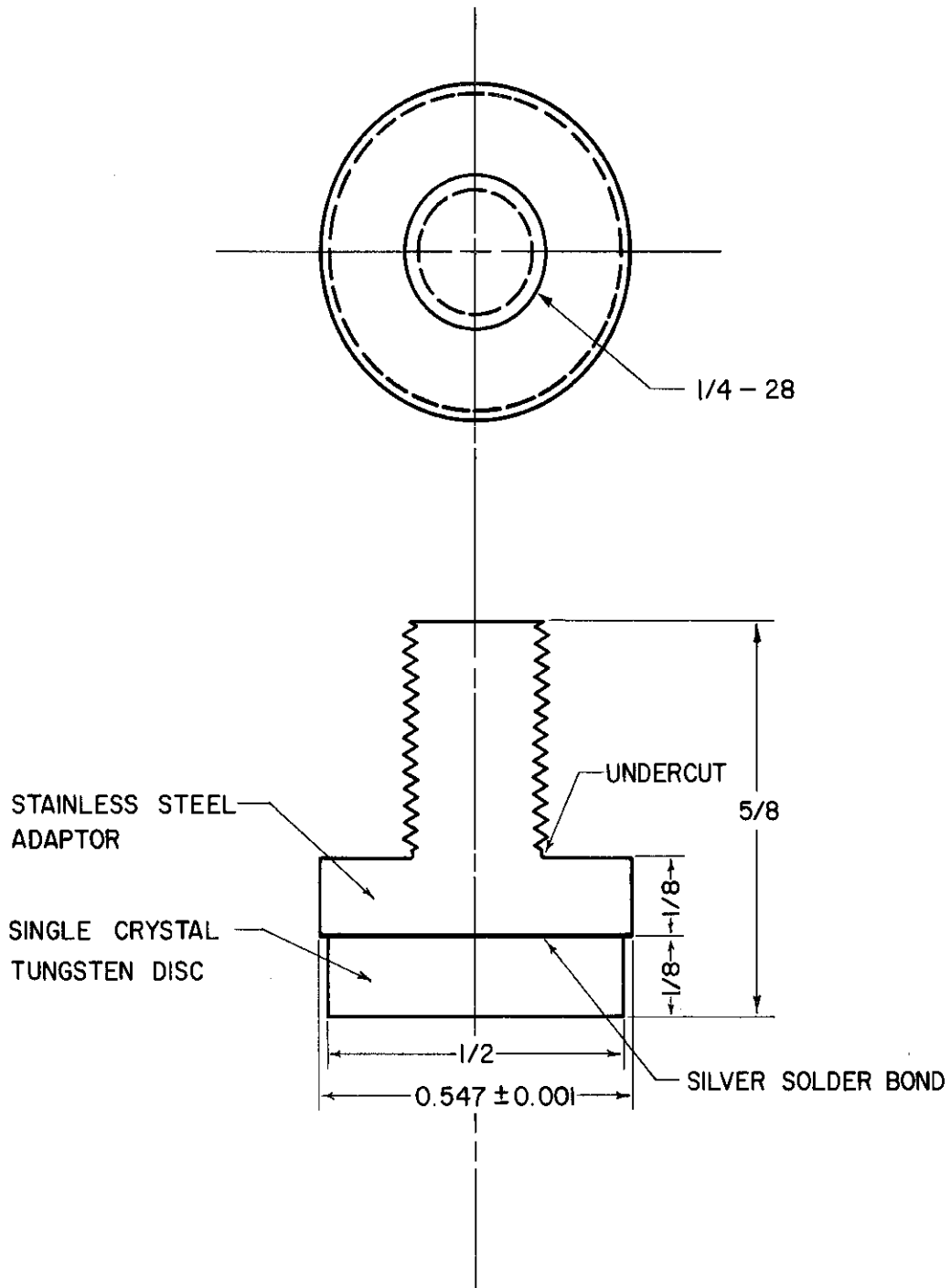
Fig. 9.--Special single-crystal tungsten cavitation test
specimen.

in liquid metals, it was necessary to give consideration to the design

of a suitable high-temperature facility. Basically, such a facility

would include a suitable closed vessel for containment of the test

fluid, and for support of the transducer assembly, means for introduc-

tion and removal of the test fluid into and out of the cavitation ves-

sel, means for controlling the oxide concentration in the test fluid

where applicable, the necessary furnace for obtaining the desired tem-

perature in the test vessel, and a suitable controller for maintaining

the fluid temperature at the desired level within satisfactory limits.

Clearly, various other auxiliary items such as "O" rings, snap rings,

thermocouples, cover gas supply, valves, etc., would be necessary to

complete the system. Detailed consideration will now be given to the

design of the cavitation vessel, a furnace for obtaining the desired

temperature level, and a suitable temperature controller for maintaining

the test temperature at the desired level.

The design of the high-temperature cavitation vessel will be

considered first. The range of temperatures considered is from approx-

imately room temperature to 1500°F. The room temperature tests are nec-

essary for comparison with similar cavitation tests conducted in the

venturi facilities operated by this laboratory. The 1500°F temperature

level corresponds closely to typical operating temperatures encountered

in SNAP reactor power plants utilizing Rankine cycles. The range of

pressures considered in this design will extend from normal atmospheric

---

were not feasible. For high-temperature applications the "Chemgrip-HT"
(Chemplast, Inc.) is recommended.

pressure to a maximum pressure of 50 psig. The high-pressure operation would be necessary in tests with fluids such as sodium at 1500°F due to the excessively large vapor pressure at this temperature. Thus the 50 psig maximum pressure figure was selected as certainly sufficient for such tests and also practical. Argon was chosen as a suitable inert cover gas. Operation with lithium, which is a very reactive liquid metal, will be assumed as a reference for the discussion that follows. Investigations with sodium or potassium could be conducted with almost no modifications to the procedure utilized for lithium. In tests with lead-bismuth, mercury, and water a much simpler procedure was used since maintenance of fluid purity is not nearly as difficult as with the alkali liquid metals.

The problem of maintaining fluid purity for repetitive runs where numerous intermediate inspections and weighings are required is a difficult problem when the test fluid is an alkali liquid metal. The usual solutions that have been applied to this problem in the past include the utilization of a large dry-box which encloses the complete experimental apparatus, or an elaborate plumbing system which allows the liquid metal to be transferred to and from the experimental vessel by pressurization. The dry-box approach is very expensive and is complicated by the fact that a range of dry-box pressures would be required for suitable operation. The plumbing system would involve a need for several valves, system pressurization for fluid transferral, trace heaters for lines, hot traps, cold traps, etc., for purification. Both of these approaches were unsuitable for the present investigation

because of these many problems and the fact that the financial resources were limited to a modest sum. Hence, we adopted the following procedure for the tests conducted in lithium.

In order to minimize the formation of oxides when very reactive liquid metals are being used as the test fluid, the liquid metal was charged into the cavitation vessel in the form of a solid cylindrical ingot, properly sized to fit into the vessel and fill it, upon melting, to the desired level. The solid ingot, supplied by the manufacturer in an individual hermetically sealed container, was first placed in a clean stainless steel beaker which fit snugly into the cavitation vessel and provided for easy removal and disposal at the conclusion of a test. The loading operation was carried out at room temperature (where oxidation would be at a minimum rate) in a glove box under an argon atmosphere. The sealed vessel was then removed from the glove box and placed in the furnace where the liquid metal was brought to the required test tempera- ture. Each test was conducted with a new, fresh lithium ingot. This procedure eliminated the need for transferring the molten liquid metal to and from the experimental vessel while the test fluid was in the liquid state and eliminated the need for trace heaters, line heaters, hot traps, cold traps, valves, etc., from the system design. The need for an expensive pressurized dry-box arrangement was also eliminated. Such a procedure resulted in a very economical design and kept oxide contamination relatively uniform and at a minimum, since a fresh ingot was used for each test. Various procedures were developed to remove the ultrasonic transducer and specimen from the cavitation vessel at the

conclusion of the test in a very safe manner. These will be discussed later.

Figure 10 is a schematic representation of the test vessel, showing the ultrasonic transducer assembly supported by the vessel top plate. The two "O" ring seals required, the position of the thermocouple, the argon gas inlet, and the cooling coil are also noted.

The level of the liquid metal or other test fluid in the vessel can be measured with a suitable fast response thermocouple. The thermocouple will be attached to the top plate with an adjustable immersion packing gland. The adjustable packing gland makes it possible to measure the liquid metal level at any required submergence of the test specimen. For this design, a test specimen face submergence of one inch was chosen so that small differences in submergence between runs will not have a large effect. When the liquid level reaches the thermocouple tip, there will be a step increase in the thermocouple reading because of the large difference between the film coefficient for the argon-thermocouple sheath interface and the liquid metal-thermocouple sheath interface. The film coefficient of heat transfer between the argon gas and the metal sheath of the thermocouple is much less than that between the liquid metal and the metal sheath of the thermocouple. Heat is always being conducted up the metal sheath of the thermocouple to the stainless steel top plate, and this heat must be supplied from the medium surrounding the thermocouple (argon gas or liquid metal). When the surrounding medium is argon gas, the temperature difference between the argon gas and the metal sheath of the thermocouple is greater than

20 KC HIGH
VOLTAGE LINE

LEAD ZIRCONATE-
TITANATE CRYSTALS

ULTRASONIC TRANSDUCER & HORN

$\frac{3}{8}$-14-1$\frac{1}{2}$ HEX HEAD BOLT

THERMOCOUPLE

COPPER COOLING COIL

"O" RING

SOLDER

"O" RING

LIQUID
LEVEL

TOP PLATE

ARGON
INLET

TEST SPECIMEN

TEST FLUID

CAVITATION VESSEL

1464
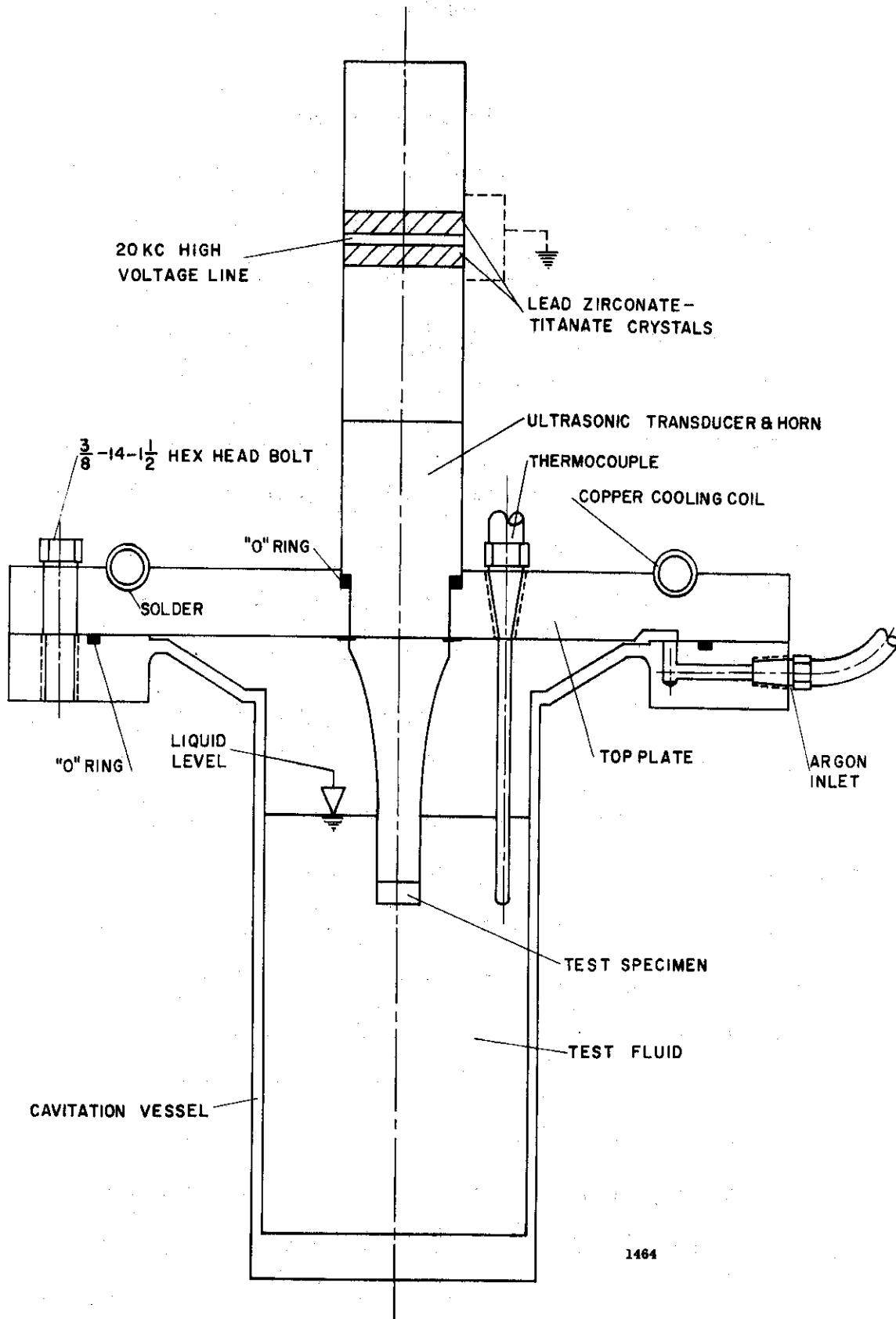
Fig. 10.--High-temperature cavitation vessel and ultrasonic
transducer.

the temperature difference between the liquid metal and the metal sheath of the thermocouple when the surrounding medium is liquid metal. This is due to the lower film coefficient at the argon-thermocouple sheath interface. This thermocouple is also used for measurement of the temperature of the test fluid in the vicinity of the test specimen.

Once the liquid metal has been introduced into the vessel and liquefied, the pressure and temperature can be adjusted to the desired operational conditions. Argon is supplied to the system from the side of the bottom flange (Figure 10).

As indicated in Figure 10, the liquid metal is to be maintained at a maximum temperature of 1500°F only a few inches from the flange-plate assembly, and about 8 inches from the crystals, which must be maintained at a temperature not to exceed about 150-200°F. Thus, special heat transfer, thermal stress, and sealing considerations arise. In general, the vessel wall and cone supporting the flange-plate assembly is made to minimum wall thickness, consistent with stress requirements, to minimize heat conduction to the flange-plate assembly. Heat is also unavoidably transferred to the flange-plate assembly by conduction through the horn and by convection and radiation in the argon cover gas. The heat is removed from the flange-plate assembly by a cooling coil, and the flange-plate assembly cross-section is thick enough so that temperature gradients in it are small. Hence, its temperature must be close to that of the cooling medium. This allows the use of conventional organic sealing materials such as rubber "O" rings, and assures that the allowable crystal temperature will not be exceeded.

The details of the construction are discussed more fully below.

The cylindrical section of the vessel is made from type 316 stainless steel pipe. The top plate is fabricated of type 304 stainless steel, 3/4 in. thick. Since it will not come into direct contact with any of the test fluids and will not operate at excessively high temperature, this material is adequate. The substantial thickness was chosen to facilitate heat conduction to the cooling medium. The top plate is provided with an access hole for the thermocouple and a centrally-located opening to accommodate the transducer horn. Figure 10 indicates the details of the top plate design.

The section connecting the lower flange and the cylindrical vessel has been designed in the shape of a cone to minimize thermal stresses due to the large temperature gradients in this region.

2. Method of Fastening Transducer to Vessel

The problem of attaching the horn at or near a nodal point to the top plate is quite unique in that a good seal is required between the plate and the horn, but at the same time the horn cannot be grasped in such a manner that the amplitude of vibration is reduced. To establish the seal, a rubber or teflon "O" ring with dimensions 1 1/4 in. x 1 1/2 in. x 1/8 in. is provided to slip around the transducer horn and to seat in the groove provided in the top plate. The horn is held in a proper axial position by fastening a snap ring around the horn directly below the top plate. This arrangement provides the required squeeze on the "O" ring. It has been shown experimentally that this arrangement

does provide a positive seal and does not result in a decrease in horn amplitude because the "0" ring is soft enough not to restrain the low amplitude, high frequency vibration at this point. A patent application has been filed for this arrangement under the title, "Seal Holder Device for Ultrasonic Vibratory Unit." Alternative approaches have involved a steel bellows attachment which is subject to fatigue failure, and the complete enclosing of the entire unit in a dry-box (which solution was beyond our financial capability). The snap ring employed is of type 304 stainless steel. The arrangement has functioned over a total of 1000 hours and numerous assemblies and disassemblies without difficulty.

The seal between the top plate and the upper flange section of the cavitation vessel is maintained by means of a rubber or teflon "0" ring of dimensions 7 1/2 in. x 7 3/4 in. which seats in a groove provided in the upper flange section. The cooling arrangement previously described allows the use of a soft seal at this point, thus obtaining more positive sealing than experience indicates might be obtained from gaskets suited to high-temperature service.

A 1/2 in. O.D. Schedule 20 copper tubing cooling system is provided to remove the heat conducted to the top plate by means of the transducer horn assembly and the vessel proper. The copper tubing is seated in a groove provided in the top of the top plate and brazed into position to provide good thermal contact. Flexible tygon tubing from the inlet and outlet provide cooling water to and from the copper tubing. Calculations[55] have shown that the available tap water flow is sufficient to remove the heat transferred to the top plate.

The top plate is firmly attached to the cavitation vessel by means of six cap screws which are inserted into the top plate and terminate in the upper flange of the vessel proper.

F. Furnace Requirements

The furnace which was chosen for providing the heat to attain the test temperatures desired is fitted with an opening of suitable dimensions so that the vessel is easily accommodated. Since the heating chamber is of a length somewhat greater than the length of the vessel, it was decided to attach to the bottom of the cavitation vessel a heat conducting extension, to provide more area to receive radiant heat from the furnace windings and also more cooling area on shut-down. This conductive skirt, 7" long with 3 1/8" I.D. and 4" O.D., was made of aluminum-bronze material, chosen because of its high thermal conductivity and excellent high-temperature properties and ability to withstand corrosion. Without such a skirt, an appreciable portion of the heaters making up the furnace would have been radiating heat across the vessel at each other. Such operation could cause burnout of the heaters. More important, though, in order to achieve reasonable heat-up times for the tests envisioned, it was necessary to provide as much thermal power as possible in the furnace. Hence, the conductive aluminum-bronze skirt was designed. It is shown in Figure 11, attached to the high-temperature cavitation vessel by means of set screws.

Due to the operating temperatures of the system, the stress limitations of the materials used at these temperatures must be

20 KC HIGH VOLTAGE LINE

LEAD ZIRCONATE-TITANATE CRYSTALS

"O" RINGS

ULTRASONIC TRANSDUCER & HORN

SNAP RING

THERMOCOUPLE
COOLING COIL

VESSEL TOP PLATE

ARGON INLET

CAVITATION VESSEL

TEST SPECIMEN

FURNACE

INSULATION

TEST FLUID

CERAMIC FURNACE VESSEL

HEATING ELEMENT

ALUMINUM-BRONZE
CONDUCTIVE SKIRT

FURNACE SUPPORT
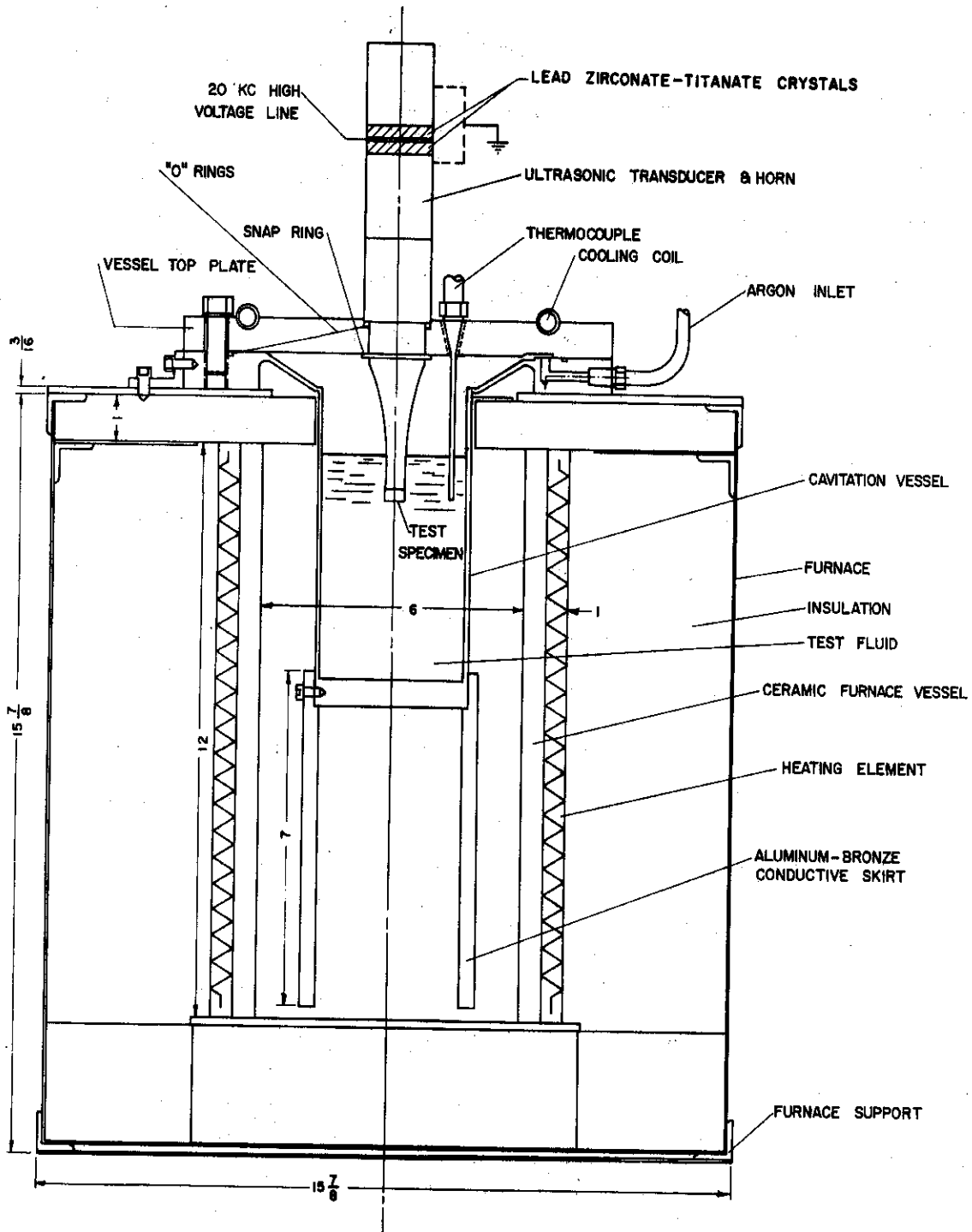
1463

Fig. 11.--High-temperature cavitation vessel and ultrasonic transducer assembly mounted in furnace.

considered. The short-term tensile strength of type 316 stainless steel

drops from approximately 90,000 psi to approximately 20,000 psi when

heated from 70°F to 1500°F, and becomes almost negligible at approxi-

mately 2000°F. Since the forging point of stainless steel is 2100-

2300°F, the system could conceivably operate up to approximately 2000°F

for short periods of time at low pressures. However, for operation

above about 1500°F, it might be wise to use more exotic materials, e.g.,

various refractory alloys, which have improved high-temperature

properties.

The discontinuity stress values, i.e., stress at sharp corners,

etc., should also be investigated, and are presented in reference 55,

along with the stress calculations, assumptions, simplifications, and

any necessary clarifying figures. Appendix A summarizes the major

assumptions and results of the necessary heat transfer calculations.

Calculations[55] indicated that the heating losses due to conduc-

tion in the cavitation vessel would be approximately 2800 Btu/hour, or

about 800 watts. In order to achieve a heat-up time of one hour, which

was deemed reasonable for a test at 1500°F, it was then necessary to

have at least a power input of 2000 watts. Many inquiries were made of

commercial vendors as to the feasibility of supplying a furnace of such

a power rating which could also accommodate the cavitation vessel. In

the meanwhile, it was found that a suitable furnace (Figure 11) existed

in the Department of Chemical and Metallurgical Engineering at this

University, and this was made available by Professor C. A. Siebert of

that department for the experiments of this laboratory. The furnace was

in the shape of a cube, 16" on an edge. The outer covering consisted of 1/16 in. sheet metal. The bulk of the sheet metal box was filled with suitable insulation, but centrally located in the enclosure was an alundum crucible about which were wound the heater coils. Alundum cement was then used to cover the coils. The dimensions of the furnace chamber formed by the crucible were 6 in. diameter x 12 in. length. The crucible was open at both ends. However, it rested in an upright position on a layer of firebrick positioned at the bottom of the sheet metal frame. A similar layer of firebrick was positioned at the top of the furnace and provided with an access hole 4 in. in diameter. The thickness of the top layer of firebrick was 1 1/4 in. This layer of firebrick was covered by a steel end plate 1/8 in. thick and fitted with a centrally-located access hole 5 1/2 in. in diameter. The 4 in. access hole in the firebrick closely approximates the diameter of the cavitation vessel. It was felt that heat losses would be greater if the 6 in. hole available in the crucible were not decreased in this manner. This end plate provides a suitable surface to support the cavitation vessel, i.e., the lower surface of the upper flange of the cavitation vessel is in direct contact with the carbon steel end plate and rests on it. The power rating of the furnace is 3000 watts at 220 volts, and hence is ample for the purposes of this investigation.

Figure 11 shows the high-temperature cavitation vessel and ultrasonic transducer assembly mounted in the furnace. The furnace is supported in a simple Unistrut frame structure.

G. Temperature Controller Requirements

A Foxboro automatic temperature controller was also provided by Professor Siebert from the Department of Chemical and Metallurgical Engineering for control of the furnace temperature. A thermocouple was embedded in the alundum cement surrounding the heating element, and is thus in close proximity to the heating element. This should reduce any cycling problems. The controller has an upper temperature limit of 2500°F, which is considerably above the maximum temperature planned for the experiments. It is an ON-OFF type controller equipped with a standard mercury switch. When the process temperature is below the set point, the full 220 volts is applied to the windings of the furnace. When the process temperature exceeds the set point, the mercury switch opens, reducing the voltage to zero. Once the desired temperature is reached, it is possible to achieve somewhat finer control by reducing the voltage applied to the windings by means of a variac. Thus, perhaps only 100 volts is necessary to compensate for the heat losses once equilibrium has been reached. Figure 12 is a schematic indicating the relationship and connections necessary to achieve this fine control. The primary voltage supply, variac, furnace, thermocouple, and controller are shown. The thermocouple used for temperature control in this application is of chromel-alumel. The automatic temperature controller is driven by a small motor requiring a 220 volt supply.

220 VOLTS

MERCURY SWITCH
ON CONTROLLER

PRIMARY

VARIAC

SECONDARY
0 - 220 V

FURNACE

THERMOCOUPLE

HEATING ELEMENT
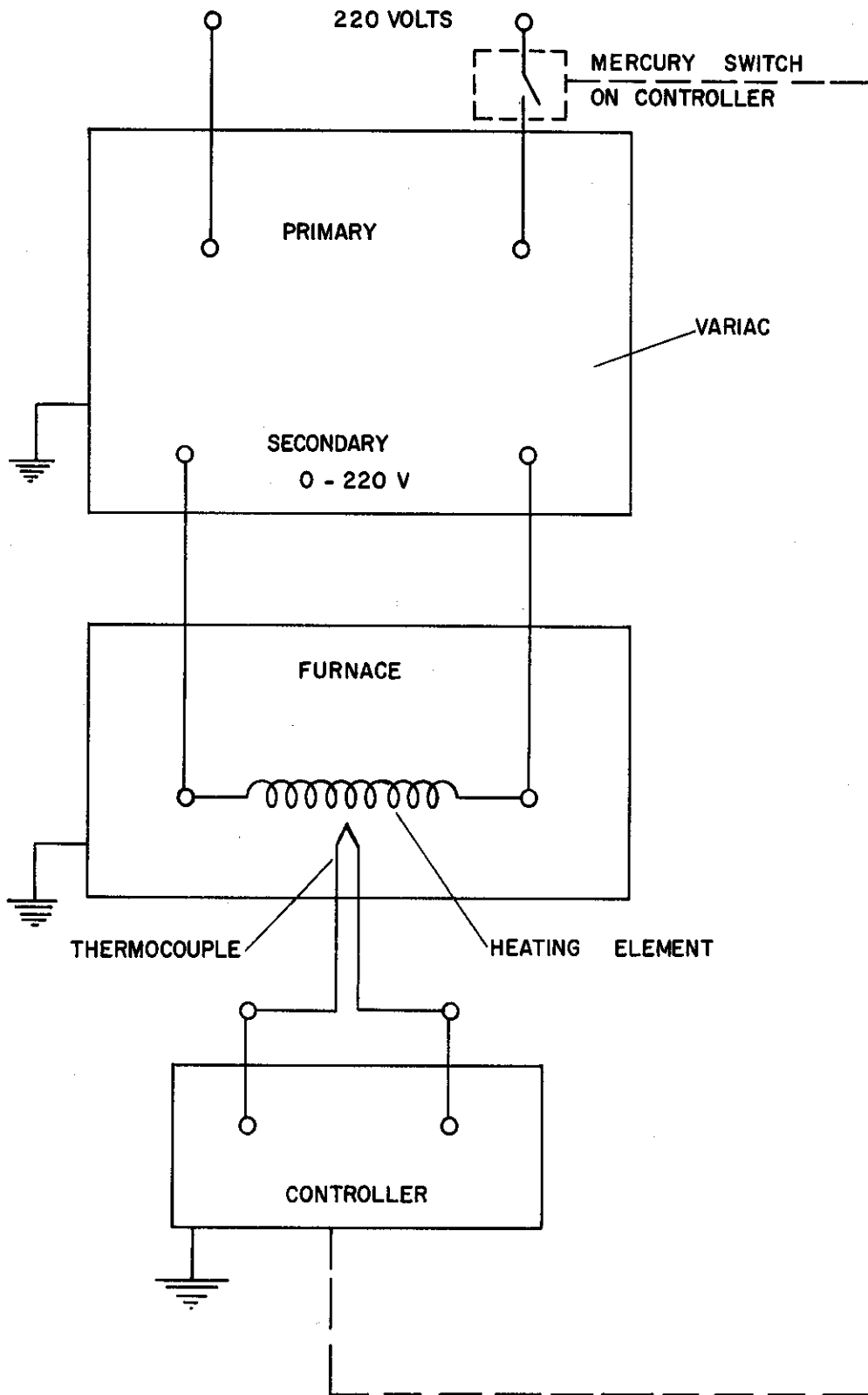
CONTROLLER

1465

Fig. 12.—Schematic of variac, furnace, and temperature controller.

H. Accelerometer Assembly[57]

1. Introduction

It has been shown by several investigators[36,48,56] that the amount of damage sustained by the test specimen is heavily dependent on the amplitude of the horn tip to which the specimen is attached, and this is, of course, also to be expected on theoretical grounds. In fact, there exists a minimum threshold amplitude for a given facility[48] below which no damage is suffered by the test specimen, either due to the complete lack of cavitation for this amplitude or the insufficient shock pressures generated by bubble collapse. Hence, it is clear that it will be necessary to determine the amplitude of the specimen with reasonable accuracy, and to maintain this amplitude within acceptable limits for the duration of a test. In addition, it is important that any given amplitude be reproducible for future investigations so that comparisons may be drawn between various specimen material-fluid-temperature combinations. The problem of amplitude measurement is made difficult since the amplitudes characteristic of the magnetostrictive and piezoelectric devices used for ultrasonic cavitation studies are in the range of 1 to 5 mils, while the frequency of operation is generally 15 to 20 Kc./sec. Other investigators[36,48] have utilized a "voice coil" arrangement, which surrounded the exponential section of the horn, to determine the amplitude of the device. During operation, a voltage is induced in the voice coil which, hopefully, is proportional to the amplitude at the horn tip by the cyclic change in inductance due to the variable area portion of the horn which is enclosed by the coil. One

difficulty which has been experienced with this and similar arrangements is that it is also sensitive to the electromagnetic radiation from the driving amplifier, etc., which then gives a very misleading output. The output from the voice coil may be displayed on an oscilloscope or fed to a vacuum tube voltmeter and/or frequency counter for analysis. This arrangement, as well as all others which seem feasible, requires that an absolute determination of the amplitude of the horn tip be made by direct observation in air (or conceivably in a transparent liquid) utilizing a suitable high-power microscope. Such a calibration would result in a plot of absolute amplitude of the horn tip versus the voltage output from the voice coil, and would enable one to determine the amplitude easily in any fluid as long as the characteristics of the exponential horn-voice coil system were not changed by the conditions of the surrounding environment, which includes the horn and fluid temperature, fluid density, viscosity, etc. This calibration is particularly necessary since it would be difficult to directly observe the motion of the horn tip during a test in water, and impossible during an investigation in an opaque fluid, e.g., liquid metals at elevated temperatures, where the vessel would also be opaque. Hence, it is necessary to be able to easily measure some secondary quantity that is directly related to the absolute amplitude in a reproducible and reliable manner.

In the case of our experiments, some of which have been conducted in liquid metals at temperatures up to 1500°F, it is not possible to utilize a voice coil arrangement, as described previously, because of the severe environment surrounding the exponential portion of the horn.

Thus, it was necessary to determine the amplitude in our investigations by some other method.

Since the horn tip approximately describes simple harmonic motion, the vertical displacement measured from some suitable datum plane taken as the origin is given by:

$$y = A \sin \omega t \qquad (1)$$

where:

        y = displacement at time, t

        A = maximum amplitude

        ω = 2π x frequency of vibration

        t = time

Hence, the acceleration, a, can be determined by differentiating expression (1) twice:

$$a = -A\omega^2 \sin \omega t = -y \omega^2 \qquad (2)$$

When $y = y_{max.} = A$, $a = a_{max.} = -A\omega^2$ (3)

Thus, it is seen that the acceleration at the horn tip is proportional to the amplitude at the horn tip.[*] This suggests the use of a suitable commercially available accelerometer whose voltage output would be proportional to measured acceleration and, hence, amplitude, at a given frequency. Such an accelerometer could be mounted at some point along the transducer horn assembly where the temperature variation is very

---

[*]The acceleration, being directly related to the acoustic pressure induced in the fluid, is seen to be a quantity more closely related to the cavitation phenomenon than the amplitude itself.

slight during the investigations. Hence, its operation would be unaffected by the severe environment existing at the horn tip. Nevertheless, for a fixed accelerometer position, it would be possible to determine a suitable calibration of absolute amplitude (as determined by direct visual microscopic observation in air) versus voltage output from the accelerometer. Such a calibration would be valid for operation of the transducer-horn assembly at elevated temperatures since the accelerometer responds to changes in acceleration only, assuming that the ratio between acceleration at the specimen face and at the accelerometer position remains constant even when the transducer is exposed to a severe temperature gradient. The approximate validity of this assumption seems intuitively reasonable.

2. Accelerometer Description

The requirements of a suitable accelerometer for this application include an ability to operate at a frequency of 20 Kc./sec., which is the normal frequency of operation of our ultrasonic cavitation facility. In addition, the sensitivity of the accelerometer must be sufficiently large so that the output can be easily measured with an oscilloscope and/or vacuum tube voltmeter. The weight of the accelerometer should be a minimum so as to only slightly disturb the ultrasonic unit. The accelerometer chosen for this application was the Glennite accelerometer Model #CA260502, supplied by Gulton Industries, Inc., of Metuchen, New Jersey. This accelerometer has a sensitivity of 1.32 mv. /g^* over a wide frequency range, a resonant frequency of 138 Kc./sec., a

---

$^*g$ = acceleration due to gravity, taken as 980 cm./sec.^{2} at sea level.

nominal frequency range extending from 3 cps to 20 Kc./sec., a nominal acceleration range from 0 to 2000 g,[*] a transverse response of only 1.7%, and a weight of 1.3 grams. It is easily mounted to the transducer-horn assembly at a suitable location by means of a threaded stud. A consideration of equation (3) above shows that for a frequency of 20 Kc./sec., and an amplitude of only 0.1 mils, the maximum acceleration would be approximately 2000 g.[*] Hence, the output from the accelerometer would be approximately 2.5 volts, which is easily measured. It should be noted that an acceleration of approximately 2000 g[*] constitutes the upper limit of applicability of any accelerometer, due to mechanical limitations of the design.

It was decided to mount the accelerometer at the top of the transducer assembly, as shown in Figure 1. Such a location resulted in easy access to the unit with respect to cable attachment, and the temperature at this location was shown to be less than 100°F, even when the test fluid was at 1500°F. Although the acceleration at this location is considerably less than at the horn tip, it was felt that the sensitivity of the accelerometer was large enough to provide a suitable output voltage for measurement. In fact, the acceleration at the horn tip is so large (approximately 50,000 g[*]) that an accelerometer mounted in this vicinity would be immediately destroyed upon operation of the unit, even if operated in air rather than a high-temperature fluid. Since the transducer assembly had been fitted with a tapped hole (5/8-20) at its top when it was initially constructed, an aluminum adaptor was

---

[*]Ibid., p. 57.

fabricated which attached to the top of the transducer assembly. The accelerometer was then firmly screwed into the aluminum adaptor with a torque wrench. Because of the high frequency of operation and the resultant low impedance of the accelerometer (approximately 20,000 ohms at 20 Kc./sec.), it is possible to feed the signal from the accelerometer directly to an oscilloscope or vacuum tube voltmeter, each of which has an input impedance of several megohms. As a result, in this application, a cathode follower or other similar impedance matching device is not necessary.

3. Accelerometer Calibration

As previously noted, it is necessary to calibrate the accelerometer once it is mounted in a fixed position, i.e., determine the relationship between the voltage output from the accelerometer and the amplitude at the horn tip. The necessary calibration was performed in air at 70°F with the transducer-horn assembly mounted in the top plate. The complete assembly was supported so that the axis of the transducer was vertical, corresponding to normal operation of the unit. A Unitron Metallurgical Microscope fitted with an eyepiece which contained a uniformly graduated scale was employed for the absolute amplitude measurements. Previously, the graduated scale had been calibrated by observing a specimen of known dimensions at a magnification of 400. It was found that 8 divisions on the eyepiece scale corresponded to a length of 1 mil, the complete scale having a length of 100 divisions. Since earlier visual amplitude measurements[51] had established that the

amplitude of vibration of the horn tip was in the range of 1 to 3 mils, it was felt that the sensitivity obtained at a magnification of 400 would be sufficient for the measurements. The test specimen at the end of the horn was backlighted with a General Radio Company Type 1531-A Strobotac which was adjusted to a suitable frequency so that it was possible to observe the motion of the horn tip as it vibrated between the extremities of travel. For a given test specimen, the voltage applied to the piezoelectric crystals was varied over a wide range (at a fixed frequency of 20 Kc./sec., which corresponds to the resonant frequency of the transducer-horn assembly), and the peak-to-peak amplitude of vibration of the horn tip was observed under the microscope at a magnification of 400. By means of the calibrated eyepiece and stroboscope, it was possible to note easily the number of divisions corresponding to the specimen motion, and hence determine the absolute amplitude, knowing the calibration of the graduated scale. For each value of absolute amplitude observed, the output from the accelerometer was fed to a Ballantine Laboratories, Inc., Model 300-G Vacuum Tube Voltmeter with a scale range from 1 mv. to 1000 volts RMS.[*] Thus, it was possible to determine corresponding values of the absolute amplitude and voltage output from the accelerometer. The procedure was repeated for three test specimens, one each of stainless steel, aluminum, and a tantalum-base alloy, covering a density range from 2.77 g./cc. to 17.6 g./cc. All specimens weighed 9.4 ± 0.1 grams. After many measurements were made, it was felt that

---

[*]Root-mean-square voltage.

the reproducibility of data was within a tolerance of 1 scale division on the calibrated eyepiece, or approximately 0.1 mils. Also, the visual measurement accuracy was estimated to be within a tolerance of 1 scale division, or approximately 0.1 mils.

For various horn tip amplitudes the output from the accelerometer was also fed directly to a Tektronix, Inc., Type 502A Dual-Beam Oscilloscope for visual display and analysis. Hence, it was also possible to determine the frequency of vibration of the transducer-horn assembly by determining the frequency of the accelerometer voltage waveform.

The results obtained in this investigation are presented in Table 1, which lists corresponding values of variac voltage (proportional to crystal voltage), accelerometer voltage output (RMS) as measured by the vacuum tube voltmeter, accelerometer voltage output (peak-to-peak) as measured by the oscilloscope, and absolute amplitude (peak-to-peak) of the horn tip. It was found that the results were identical for each of the three specimens employed within the margin of experimental error. Note that the maximum amplitude measured was 3 mils (peak-to-peak), which corresponds to an acceleration of approximately 100,000 g (peak-to-peak) at the horn tip. Equation (3) was used for this computation. At this amplitude the peak-to-peak accelerometer output voltage was 16 volts, which corresponds to an acceleration of approximately 12,000 g (peak-to-peak) at the opposite end of the transducer-horn assembly where the accelerometer is mounted. This value of acceleration was computed assuming an accelerometer sensitivity of

TABLE 1

AMPLITUDE MEASUREMENT DATA

Experimental Conditions:

1) Transducer-horn assembly mounted in vessel top plate and held in a vertical position by usual mounting device

2) Surrounding medium is air at 70°F

3) Microscope magnification = 400X

4) Eyepiece calibration: 8 divisions = .001" = 1 mil

5) Stroboscope frequency = 3300 flashes/minute

6) Frequency of vibration of transducer-horn assembly = 20.3 Kc./sec.

7) Test specimens were 304 stainless steel, 2024-T351 aluminum, and T-111 (Ta-base alloy); data applies to all materials.

8) Accelerometer mounted at top of transducer-horn assembly

	Accelerometer Voltage Output		
Variac Voltage	VTVM(RMS)*	CRO(P-P)**	Amplitude(P-P)
60 V	0 V	0 V	0 mils
70	0.9	3.0	0.5
80	1.8	6.0	1.0
90	2.9	8.0	1.5
100	4.1	10.0	2.0
110	5.2	13.0	2.5
120	6.0	16.0	3.0

*Voltage measured by vacuum tube voltmeter, root-mean-square.

**Voltage measured by cathode-ray oscilloscope, peak-to-peak.

1.32 mv./g, which represents a careful calibration supplied by the manu-

facturer. This calibration is stated to be valid even at the very high

values of acceleration involved in this investigation as long as the

accelerometer is not damaged, and the frequency of operation (20 Kc./

sec.) is a factor of 3 or 4 below the resonant frequency of the accel-

erometer (138 Kc./sec.) so as to avoid accelerometer resonance effects.

It is interesting to note that the acceleration (and hence amplitude) is

approximately 8 times greater at the horn tip where the specimen is

located than at the opposite end of the horn where the accelerometer is

located. This is very reasonable since in an exponential assembly of

this type, the amplitude of vibration varies inversely as the cross-

sectional areas of the ends of the exponential assembly.[53,54] In our

case, the cross-sectional area at the top of the transducer-horn

assembly is approximately 9 times greater than the tip cross-sectional

area. Both ends of the horn assembly correspond to antinodal points of

the standing waves propagated within the transducer.[51]

In Table 1, values of accelerometer voltage measured by the

oscilloscope (peak-to-peak voltage) should be about 2.8 times as great

as the values of accelerometer voltage measured by the vacuum tube volt-

meter (RMS voltage), if the horn tip describes simple harmonic motion.

The ratio of the corresponding voltage values varies from 2.5 to 3.3,

which is reasonable, since the measurement error in reading the oscil-

loscope waveforms is at least 10%, and the motion of the horn tip is not

exactly simple harmonic in nature.

A plot of absolute amplitude of vibration of the horn tip in

mils (peak-to-peak) versus accelerometer voltage output (as measured by

an RMS vacuum tube voltmeter) is presented in Figure 13. Note that the

relationship is nearly linear, which corresponds to equation (3). This

calibration makes it possible to determine the amplitude of the horn tip

during an investigation in any fluid environment by monitoring the out-

put from the accelerometer mounted at the opposite end of the trans-

ducer-horn assembly.

4. Summary and Conclusions

An accurate method for measuring the amplitude of vibration

at the tip of an ultrasonic transducer assembly has been developed. The

method consists of monitoring the voltage output from a Glennite accel-

erometer, Model #CA260502, mounted at the top of the transducer assembly

where it is readily accessible. The absolute amplitude of vibration at

the opposite end of the horn assembly to which test specimens are

attached is desired. A calibration of absolute amplitude at the horn

tip versus the voltage output from the accelerometer makes it possible

to determine the desired amplitude during any investigation. The major

features of this system are as follows:

a)   The accelerometer is able to operate at frequencies in the

vicinity of 20 Kc./sec.

b)   The accelerometer has a sensitivity of 1.32 mv./g, which makes

it ideal for amplitude measurements in the range 1-3 mils.

c)   The accelerometer is mounted at the top of the transducer-horn

assembly where it is easily accessible and at a point where the

temperature never exceeds 100°F, even when the test specimen is
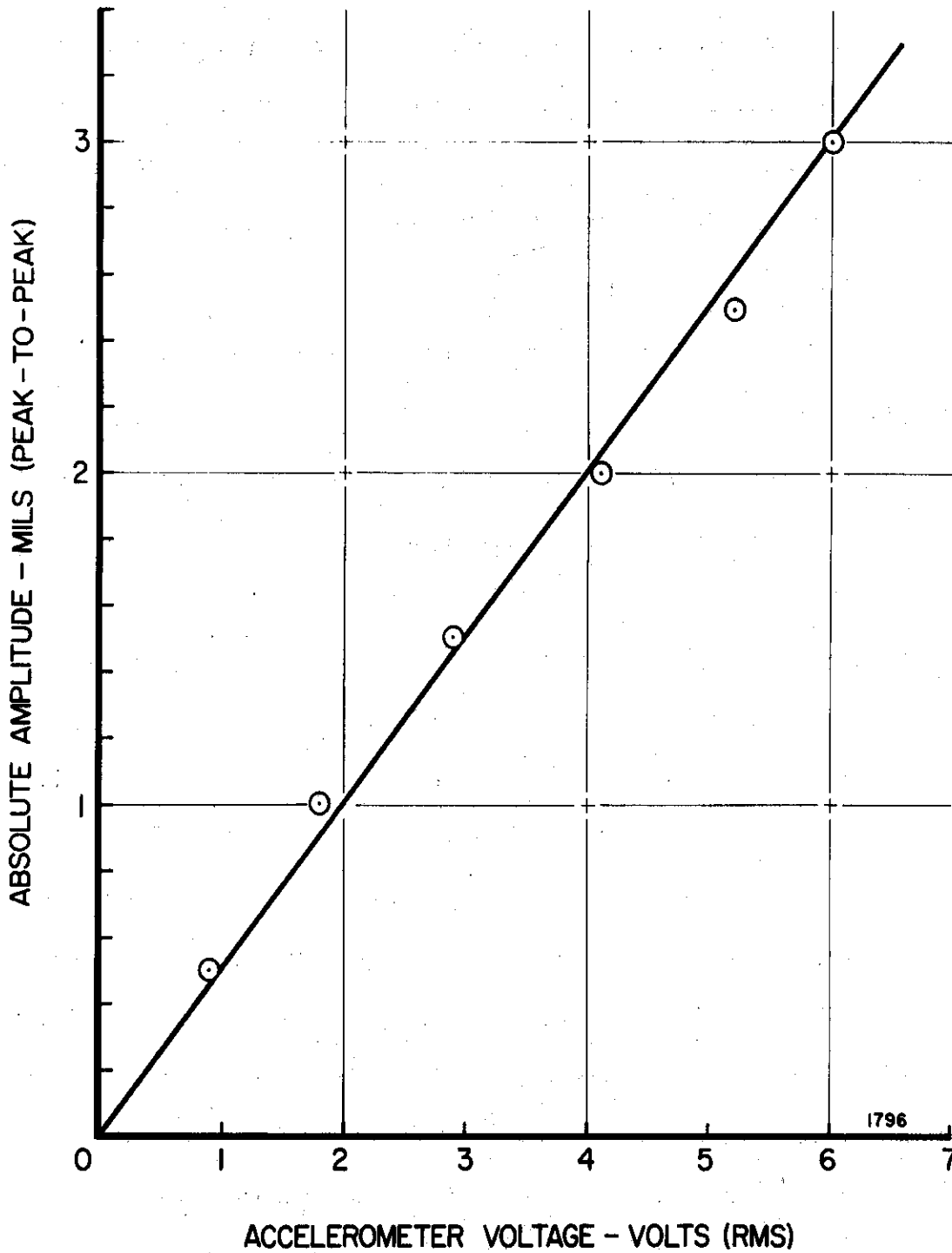
Fig. 13.--Calibration curve for accelerometer.

immersed in a fluid at 1500°F. Hence, the accelerometer is never exposed to a severe environment, thus insuring relatively trouble-free operation.

d) The voltage output from the accelerometer is proportional to the acceleration to which it is subjected, and hence the amplitude at the point of mounting. Thus, the output is also proportional to the amplitude at the tip of the transducer, since the system is acoustically coupled.

The major observations made during the investigation are as follows:

a) The maximum amplitude measured at the horn tip was 3 mils (peak-to-peak), which corresponded to an accelerometer voltage of 6 volts RMS.

b) The relationship between absolute amplitude and accelerometer voltage is nearly linear (Figure 13).

c) The ratio of peak-to-peak accelerometer voltage to RMS acceler-ometer voltage varies from 2.5 to 3.3 for this investigation.

d) The calibration obtained is independent of test specimen density, over the complete range tested ($\sim$ 2.7 to 17.7 g/cc.).

e) The oscilloscope waveforms of voltage output from the accelerom-eter confirm the frequency of vibration of the transducer-horn assembly, namely 20 Kc./sec.

f) The acceleration at the horn tip is approximately 100,000 g (peak-to-peak), i.e., $\pm$ 50,000 g, whereas it is only about 12,000 g (peak-to-peak) at the point where the accelerometer is

mounted, as expected, due to the difference in cross-sectional

area at the two locations.

g) The absolute amplitude of vibration can be determined visually

within a tolerance of $\pm$ 0.1 mils.

J. Special Hardware

It was noted previously that the ultrasonic horn utilized in

this investigation was of type 303 stainless steel. When tests are con-

ducted at elevated temperature with cavitation specimens whose coeffi-

cient of thermal expansion is considerably less than that of type 303

stainless steel, improper operation may result if necessary precautions

are not taken. The combination of the type 303 stainless steel ultra-

sonic horn and a stainless steel or carbon steel cavitation specimen

does not result in any problem since the coefficients of thermal expan-

sion are nearly identical. However, with the high coefficient of

thermal expansion ultrasonic horn (type 303 stainless steel) and various

low coefficient of thermal expansion cavitation specimens (T-111, T-222,

Mo-1/2Ti, and Cb-1Zr) an axial gap may develop at the interface between

the cavitation specimen and the ultrasonic horn at high temperature,

particularly at 1500°F. Hence, for this type of test, special hardware

is necessary to eliminate this effect as the gap would result in

improper transmission of the acoustic energy across the interface and a

reduced amplitude at the test specimen face. The cavitation results

would be greatly in error.

For the tests at 1500°F in lead-bismuth alloy and lithium spe-

cial hardware was designed and fabricated. The design consists of five

separate items of hardware. Item (1) is a modified ultrasonic horn
fabricated of type 303 stainless steel. It is shown in Figure 14. Its
design is similar to the standard ultrasonic horn shown in Figure 3,
except that it is about 1 1/4 inches shorter than the standard horn.
Item (2) shown in Figure 15 is an adaptor stud made of the refractory
alloy T-222(A). Any of the refractory materials used in this investiga-
tion, such as T-222, Mo-1/2Ti, or Cb-1Zr, would have been suitable for
this stud as long as the coefficient of thermal expansion matched that
of Item (3), shown in Figure 16. Item (3) consists of an ultrasonic
horn adaptor, also fabricated of the refractory alloy T-222(A). This
ultrasonic horn adaptor must be fabricated of material having a coeffi-
cient of thermal expansion nearly equal to that of the refractory mater-
ials to be tested. Fortunately, the T-111, T-222, Mo-1/2Ti, and Cb-1Zr
have nearly identical coefficients of thermal expansion. The stud in
Figure 15 (Item 2) is used to attach the ultrasonic horn adaptor shown
in Figure 16 (Item 3) to the modified ultrasonic horn shown in Figure
14 (Item 1). The refractory cavitation test specimens are then attached
to the tip of the assembly resulting from Items (1), (2), and (3). Such
an arrangement eliminates any problems concerned with differential
expansion, and results in intimate contact being maintained at the
interface of the ultrasonic horn adaptor and the refractory cavitation
specimen. Intimate contact is also achieved at the interface of the
modified ultrasonic horn and the ultrasonic horn adaptor, since the con-
necting adaptor stud has a coefficient of thermal expansion equal to
that of the ultrasonic horn adaptor and less than that of the modified

ITEM I: MODIFIED ULTRASONIC HORN
MATERIAL: TYPE 303 STAINLESS STEEL

3/8-24
2 HOLES

1.491

5/8

1.750

1.247

.044

.682

.043

4

.220

13°

15/16

.0625 x .500 D
COUNTERBORE

9/16

.655
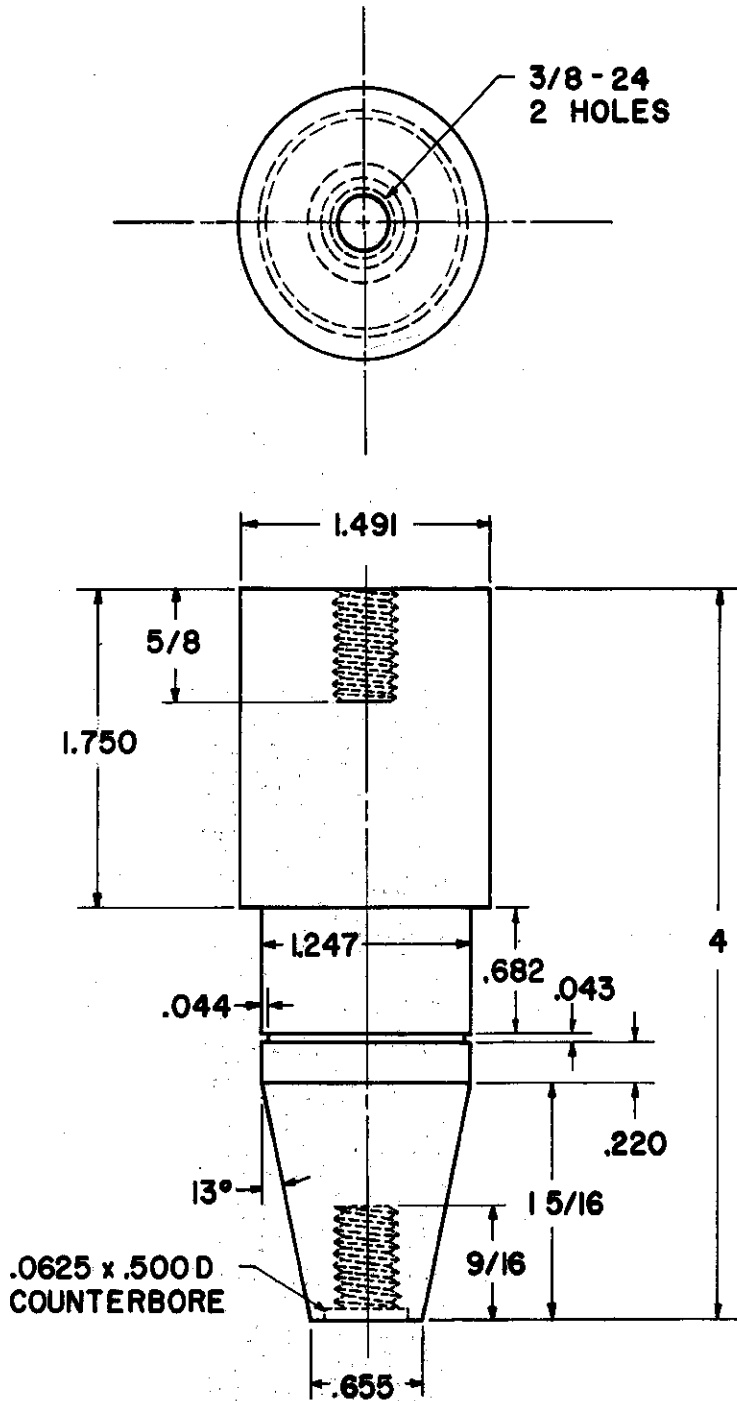
TOLERANCES
DECIMAL: ±.001"
FRACTIONAL: ±1/32

1979

Fig. 14.--Modified ultrasonic horn.

ITEM 2: ADAPTOR STUD
MATERIAL: T-222 (A)

3/8-24

1980

Fig. 15.--Adaptor stud.

ITEM 3: ULTRASONIC HORN ADAPTOR
MATERIAL: T-222 (A)

Fig. 16.--Ultrasonic horn adaptor.

horn. Thus, any differential expansion in this region would result in a tighter bond at this interface. The temperature existing at this interface during operation of the assembly is much lower than that existing at the interface of the cavitation test specimen and the ultrasonic horn adaptor. Hence, less expansion would be expected.

The arrangement described above was used successfully to test the refractory specimens at 1500°F. At 500°F it was found that the differential expansion was so slight as to not affect the operation of the standard ultrasonic horn (Figure 3) with the refractory specimens attached directly to it.

When testing types 304 and 316 stainless steel at 1500°F, the standard ultrasonic horn (Figure 3) was used, since the coefficients of thermal expansion of both the horn and the specimens were nearly identical. Since the special adaptor hardware described previously was used when testing the refractory specimens at 1500°F, it was felt that it would be instructive to experimentally compare the operation of the two systems. To do this, it was necessary to fabricate a modified cavitation specimen of type 304 stainless steel to be used in conjunction with the ultrasonic horn adaptor (Figure 16). The modified cavitation specimen is shown in Figure 18 as Item (5). It is attached to the ultrasonic horn adaptor by means of the modified cavitation specimen stud shown in Figure 17 as Item (4). This stud is made of Cb-1Zr(A), but any of the other refractory materials previously mentioned would have been suitable for this item of hardware. With this arrangement at high temperature, the high thermal expansion coefficient cavitation specimen would expand

ITEM 4: STUD FOR MODIFIED CAVITATION SPECIMEN
MATERIAL: Cb-1 Zr (A)

1/4-28

1/2
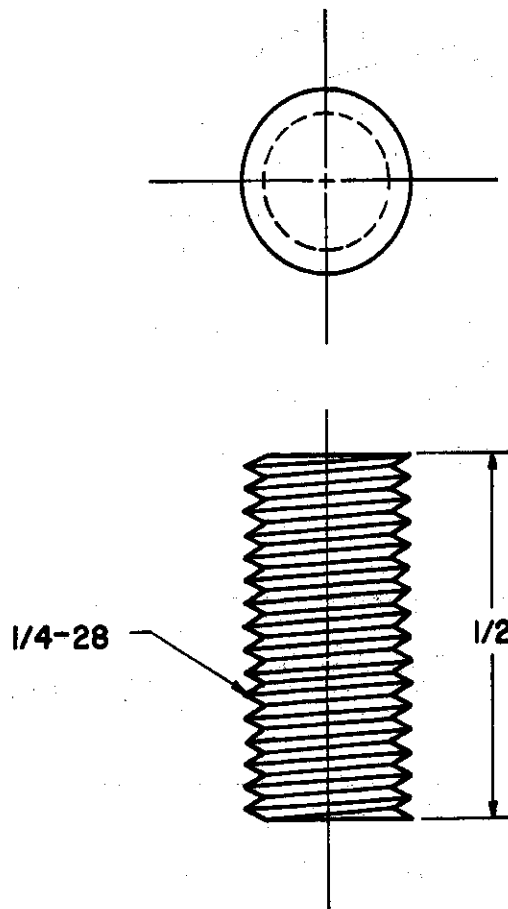
Fig. 17.--Stud for modified cavitation specimen.   1982

ITEM 5: MODIFIED CAVITATION SPECIMEN
MATERIAL: TYPE 304 STAINLESS STEEL
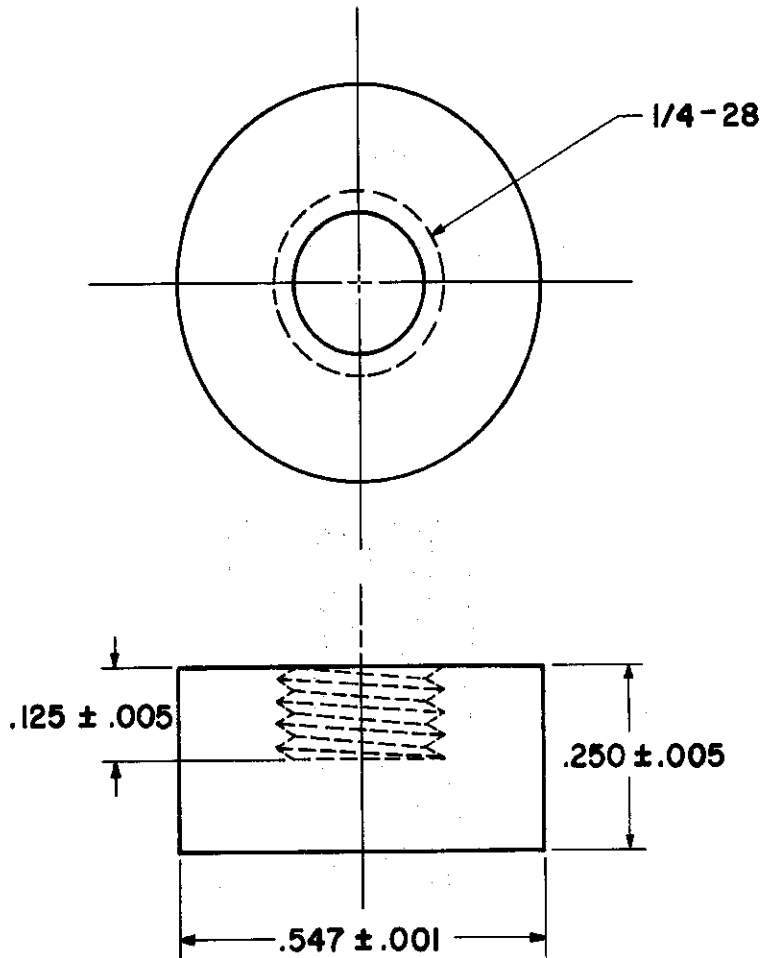
Fig. 18.--Modified cavitation specimen.   1983

more than the low coefficient stud or the low coefficient adaptor.

Hence, an axial gap would not develop at the interface between the high

coefficient cavitation specimens and the low coefficient adaptor. Of

course, this arrangement is not necessary when testing the type 304 and

type 316 stainless steel cavitation specimens as the standard ultrasonic

horn (made of type 303 stainless steel) can then be utilized. However,

both arrangements were employed to test stainless steel in lead-bismuth

at 1500°F in order to compare the systems. The test results differed by

3%, thus verifying the proper operation of both systems.

Items (1) through (5) are shown in an assembly drawing (Figure

19) which clearly indicates the order of assembly of the hardware. A

patent application has been made to cover the special hardware

assemblies described in this section.

MODIFIED ULTRASONIC
HORN (ITEM I)

ADAPTOR STUD
(ITEM 2)

ULTRASONIC HORN
ADAPTOR (ITEM 3)

SPECIMEN STUD
(ITEM 4)

MODIFIED CAVITATION
SPECIMEN (ITEM 5)
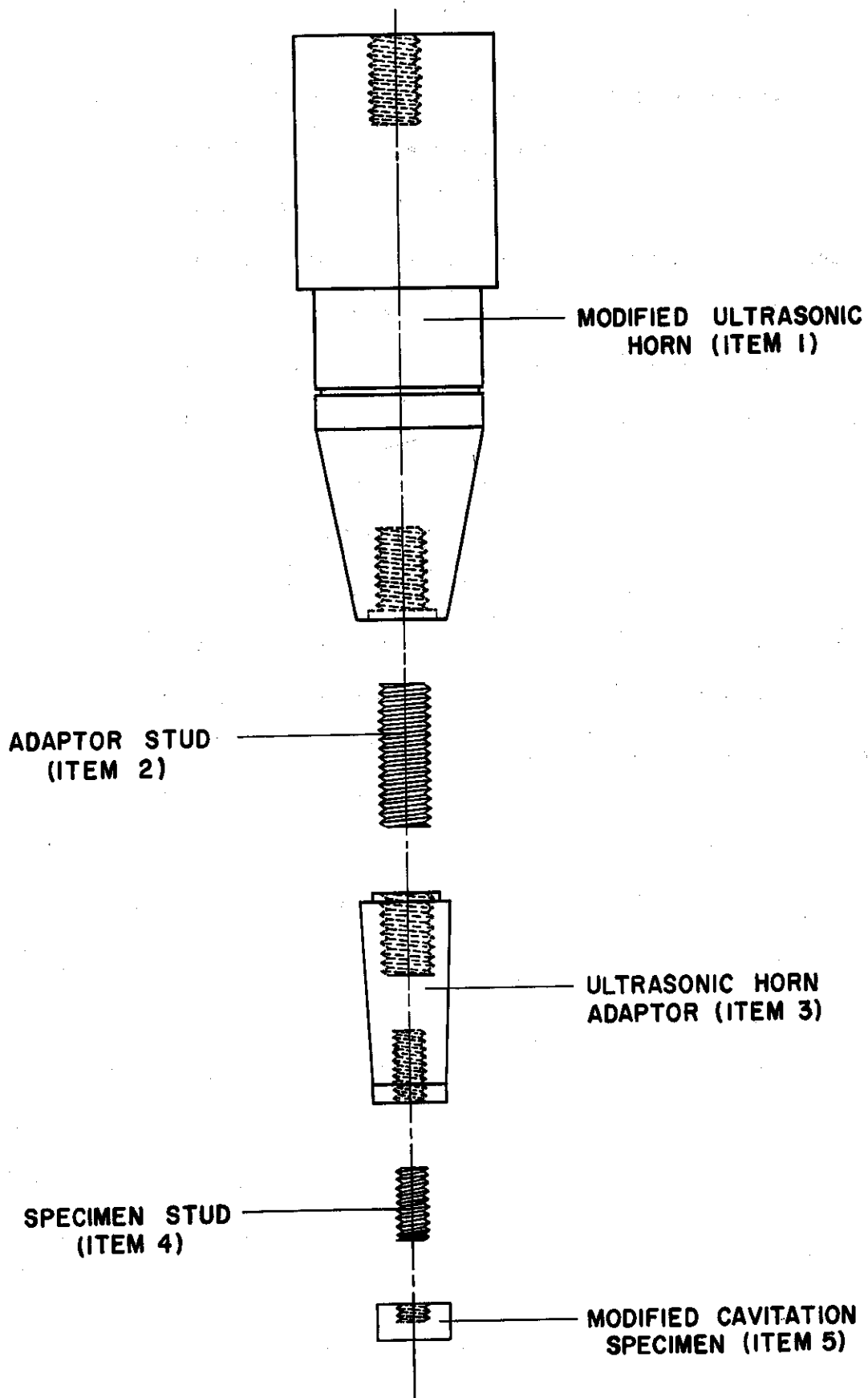
1984

Fig. 19.--Assembly drawing of modified ultrasonic horn, adaptor
stud, ultrasonic horn adaptor, specimen stud, and modified cavitation
specimen.

CHAPTER III

EXPERIMENTAL INVESTIGATIONS

A. Objectives of Experimental Program

Utilizing the high-temperature vibratory device developed for

this program, it was desired to determine the cavitation resistance of a

wide variety of potentially useful materials (involving a considerable

range of mechanical properties) in a wide variety of fluids over a full

temperature range in an attempt to learn more about the cavitation dam-

age process as it is affected by fluid and material properties. Mater-

ials included are stainless steels, carbon steel, refractory alloys,

aluminum, copper, nickel, brass, plastics, etc., and the fluids to be

used are water at 70°F, mercury at 70°F and 500°F, and lead-bismuth

alloy and lithium at 500°F and 1500°F. Table 2 summarizes the specimen

material-fluid-temperature combinations which were studied in this

investigation. The composition of the various refractory alloys is

given along with the annealing temperatures and duration of anneal for

the various Cu, Cu-Zn, Cu-Ni, and Ni materials tested.

In addition, several potential bearing materials were tested to

further widen the material property range. These were the tool steel

alloy BG-42 (a modified 440-C stainless steel), Blue Chip Tool Steel

-77-

TABLE 2

SPECIMEN MATERIAL-FLUID-TEMPERATURE
COMBINATIONS INVESTIGATED

	Fluid			
Material	Water 70°F	Mercury 70°F	Mercury 500°F	Pb-Bi & Li 500°F & 1500°F
1100-0 Al (U-M)	X	...	...	...
2024-T351 Al (U-M)	X	...	...	...
6061-T651 Al (U-M)	X	...	...	...
304 Stainless Steel (U-M)	X	X	X	X
316 Stainless Steel (U-M)	X	X	X	X
Hot-Rolled Carbon Steel (U-M)	X	X	X	...
T-111 (Ta-8W-2Hf) (P & W)	X	X	X	X
T-222 (Ta-9.5W-2.5Hf-.05C) (P & W)	X	X	...	...
T-222(A) (P & W)	...	...	X	X
Mo-1/2Ti (P & W)	X	X	X	X
Cb-1Zr (P & W)	X	X	X	X
Cb-1Zr(A) (P & W)	X	X	X	X
Plexiglas (U-M)	X	X	...	...
Cu(60% cold-worked) (U-M)	X	...	...	...
Cu(900°F anneal, 1 hour) (U-M)	X	...	...	...
Cu(1500°F anneal, 1 hour) (U-M)	X	...	...	...
Cu-Zn(60% cold-worked) (U-M)	X	...	...	...
Cu-Zn(850°F anneal, 1 hour) (U-M)	X	...	...	...
Cu-Zn(1400°F anneal, 1 hour)(U-M)	X	...	...	...
Cu-Ni(60% cold-worked) (U-M)	X	...	...	...
Cu-Ni(1300°F anneal, 1 hour)(U-M)	X	...	...	...
Cu-Ni(1800°F anneal, 1 hour)(U-M)	X	...	...	...
Ni(75% cold-worked) (U-M)	X	...	...	...
Ni(1100°F anneal, 1 hour)(U-M)	X	...	...	...
Ni(1600°F anneal, 1 hour)(U-M)	X	...	...	...

Notes:
1) "X" indicates test conducted for this specimen material-fluid-temperature combination.
2) The notations (U-M) and (P & W) following the specimen materials indicate the source of the material, namely, The University of Michigan and Pratt & Whitney Aircraft (CANEL), respectively; whereas the notation (A) denotes an annealed condition of the material.

(18-4-1[*] tool steel), Mo-1/2Ti, Cb-1Zr(A), two grades of graphitar,

single-crystal tungsten, and teflon-coated type 304 stainless steel.

These were tested in mercury at various temperatures, and in water at

70°F. The various materials tested in this program along with the

fluid-temperature combinations involved are summarized in Table 3.

B. Experimental Test Conditions

Initially, each of the specimens was weighed on a precision bal-

ance to an accuracy of 0.01 mg., and then attached to the tip of the

stainless steel exponential horn, whereupon the entire unit was

assembled.

The tests in lead-bismuth alloy and lithium at 500°F and 1500°F

and the tests in mercury at 70°F and 500°F were conducted in the 316

stainless steel cavitation vessel previously described. The investiga-

tions in water at 70°F were conducted in a Plexiglas cavitation vessel

whose inside dimensions were identical to those of the 316 stainless

steel container. The Plexiglas vessel permits visual observation of

the bubble cloud and continuous monitoring of the condition of the

specimen surface during a test.

At elevated temperatures the test fluid was maintained at the

required temperature by the temperature controller, which allowed tem-

perature variations of less than 5°F.

The specimens were oscillated at approximately 20 Kc./sec. with

the exception of the 1500°F tests where the resonant frequency

---

[*]The 18-4-1 designation denotes a tool steel containing 18%
tungsten, 4% chromium, and 1% vanadium.

TABLE 3

MATERIALS TESTED IN BEARING PROGRAM

70°F Mercury	350°F Mercury	500°F Mercury
Graphitar-Grade 50(U-M)	Teflon-Coated 304 SS(U-M)	BG-42 (R_c = 47)(TRW)
Graphitar-Grade 80(U-M)		BG-42 (R_c = 53)(TRW)
		BG-42 (R_c = 64)(TRW)
		Blue Chip Tool Steel (TRW)
70°F Water		
		Mo-1/2Ti (P & W)
Single-Crystal Tungsten(U-M)		Cb-1Zr(A) (P & W)

NOTE:

The notations (TRW), (P & W), and (U-M) following the specimen materials indicate the source of the material, namely, Thompson-Ramo-Wooldridge, Pratt & Whitney Aircraft (CANEL), and The University of Michigan, respectively; whereas the notation (A) denotes an annealed condition of the material. The grades of graphitar are designations of the United States Graphite Company.

was reduced to $\sim$ 18 Kc./sec. by the reduction in sonic velocity in the high-temperature portion of the horn. The frequency, however, can be measured with an accuracy of $\pm$ 0.002 Kc./sec. The submergence of the horn tip was held constant at 1 1/2 $\pm$ 1/8 inches in all fluids, while the double amplitude at the specimen was maintained at 2 $\pm$ 0.1 mils for all the tests, as determined by the precision accelerometer previously described.[57]

The argon cover gas was maintained over the test fluids at a pressure that was a function of the fluid-temperature combination being investigated. The value of argon cover gas pressure is chosen for a given fluid-temperature combination such that the suppression pressure, i.e., the difference between local pressure at the specimen face and vapor pressure of the fluid, is approximately constant for all investigations involving a variety of fluid-temperature combinations. The lead-bismuth tests at 500°F and 1500°F and the mercury tests at 70°F were conducted at a slight overpressure (0.5 psig) to prevent inward leakage of oxygen, and the corresponding suppression pressure was used for the remainder of the tests. The mercury tests at 500°F then required an argon pressure of 2.4 psig, the lithium tests at 500°F required 1.1 psig, the lithium tests at 1500°F required 1.2 psig, and the water tests at 70°F an argon pressure of 1.5 psig. The variation is due to the different densities and vapor pressures of these fluids at the various test temperatures. While a constant suppression head (pressure/density) rather than pressure may have been desirable for considerations of fluid-dynamic modeling, the pressure capabilities of the

equipment were not adequate to allow this course to be pursued.

Total test duration varied for the different materials and was always sufficient to obtain a good determination of damage rate, which, neglecting the very early portion of the test, was found to be essentially constant for most of the tests within the total accumulated damage obtained. Test duration was thus a function of the fluid and fluid temperature, and differed widely for the various materials. The appropriate test duration for each material-fluid-temperature combination will be discussed in more detail later. The tests were terminated when the complete face of the specimen was damaged, and an approximately uniform rate of damage established. Frequent inspections and weighings were made during the tests to monitor the condition of the specimen surface and establish the rate of weight loss.

Heating time from 500°F to 1500°F for the lead-bismuth and lithium tests proved to be approximately 1 1/2 hours. Cooling time from 1500°F to 500°F is approximately five hours.

Since the piezoelectric crystals must be maintained at a temperature below 150°F, the top plate of the cavitation vessel is cooled by circulating water as previously described. In addition, a fan in close proximity to the crystals provides additional cooling.

The tests in each fluid generally required special handling procedures that were a function of the fluid-temperature combination. These will be described in the appropriate sections.

C. Cavitation Studies in Lead-Bismuth
Alloy at 500°F and 1500°F

1. Experimental Procedure

The seven materials tested in lead-bismuth alloy (70% lead-30% bismuth) at 500°F and 1500°F were 304 stainless steel (U-M), 316 stainless steel (U-M), T-111 (P & W), T-222(A) (P & W), Mo-1/2Ti (P & W), Cb-1Zr (P & W), and Cb-1Zr(A) (P & W). Standard cavitation test specimens, as shown in Figure 6, were machined from available bar stock. The required dimensions "A" and "B" for the seven materials tested are listed in Table 4. These dimensions provide a standard specimen weight of 9.4 ± 0.1 g.

The vapor pressure of lead-bismuth at both 500°F and 1500°F is approximately zero. The argon cover gas pressure was maintained over the molten lead-bismuth throughout the tests at both 500°F and 1500°F at a slight overpressure of 0.5 psig to prevent in-leakage of oxygen. The corresponding suppression pressure, 15.3 psig, was then maintained constant for all the tests in all fluids.[*]

At 500°F the specimens were subjected to the cavitation environment for a total test period of 12 hours with the exception of the Cb-1Zr(A) which showed gross erosion after 8 hours of testing. Preliminary tests had indicated that when this gross erosion was achieved, the damage rate starts to vary substantially from the relatively constant value obtained once damage had become fairly uniform. Hence, it is not

---

[*]Changes in atmospheric pressure from day to day have been assumed negligible.

TABLE 4

SPECIMEN DIMENSIONS

Material	"A"	"B"
304 Stainless Steel	.250"	.625"
316 Stainless Steel	.250"	.625"
Hot-Rolled Carbon Steel	.250"	.625"
T-111	.085"	.460"
T-222	.085"	.460"
T-222(A)	.085"	.460"
Mo-1/2Ti	.175"	.550"
Cb-1Zr	.220"	.595"
Cb-1Zr(A)	.220"	.595"
1100-0 Aluminum	.820"	1.195"
2024-T351 Aluminum	.820"	1.195"
6061-T651 Aluminum	.820"	1.195"
BG-42 (all heat-treats)	.250"	.625"
Blue Chip Tool Steel	.220"	.595"

desired to carry the tests to very heavy damage conditions. At 2 hour

intervals the specimens were visually examined, photographed, and care-

fully weighed. Then the test was resumed. At each examination excess

lead-bismuth adhering to the test specimen was removed by quickly heat-

ing the specimen with a propane torch to a temperature just above the

melting point of the lead-bismuth (approximately 350°F). The excess

fluid was then separated from the test specimen by a quick blast of com-

pressed air. The process was rapid enough so that only negligible oxi-

dation occurred.

For the tests at 1500°F all transfers of the specimens to and

from the high-temperature cavitation vessel were made at a temperature

of 500°F. Since the lead-bismuth is not grossly and rapidly affected by

exposure to atmosphere, no special provisions as the use of pre-cast

sealed ingots previously described for the lithium were necessary. The

fact that there was no substantial intergranular corrosion during the

test is shown by the photomicrograph of Figure 20. The type 316 stain-

less steel specimen shown here was tested in lead-bismuth alloy at

1500°F for 6 hours. The magnification is 1000X. In Figures 21 and 22

photomicrographs of the surface of the same type 316 stainless steel

specimen are shown at a magnification of 500X. There is no evidence of

corrosion at the surface but this may be due to surface cleaning by the

cavitation process. The fact that the non-cavitated parts of the speci-

men were not corroded shows that corrosion in the absence of cavitation

was negligible. The effects of corrosion in the vibratory type test

have been previously examined by Plesset.[48] After securing the
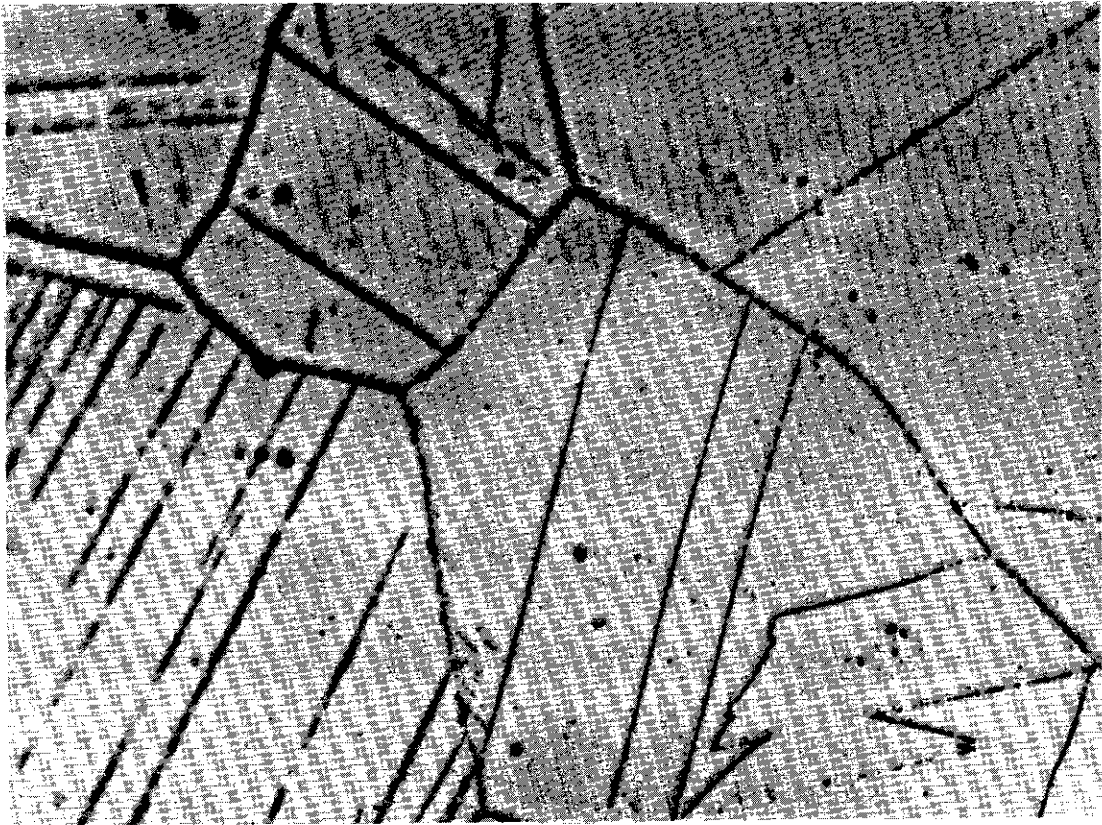
1947

Fig. 20.--Photomicrograph of type 316 stainless steel specimen tested in lead-bismuth alloy at 1500°F (interior of specimen, magnification 1000X).
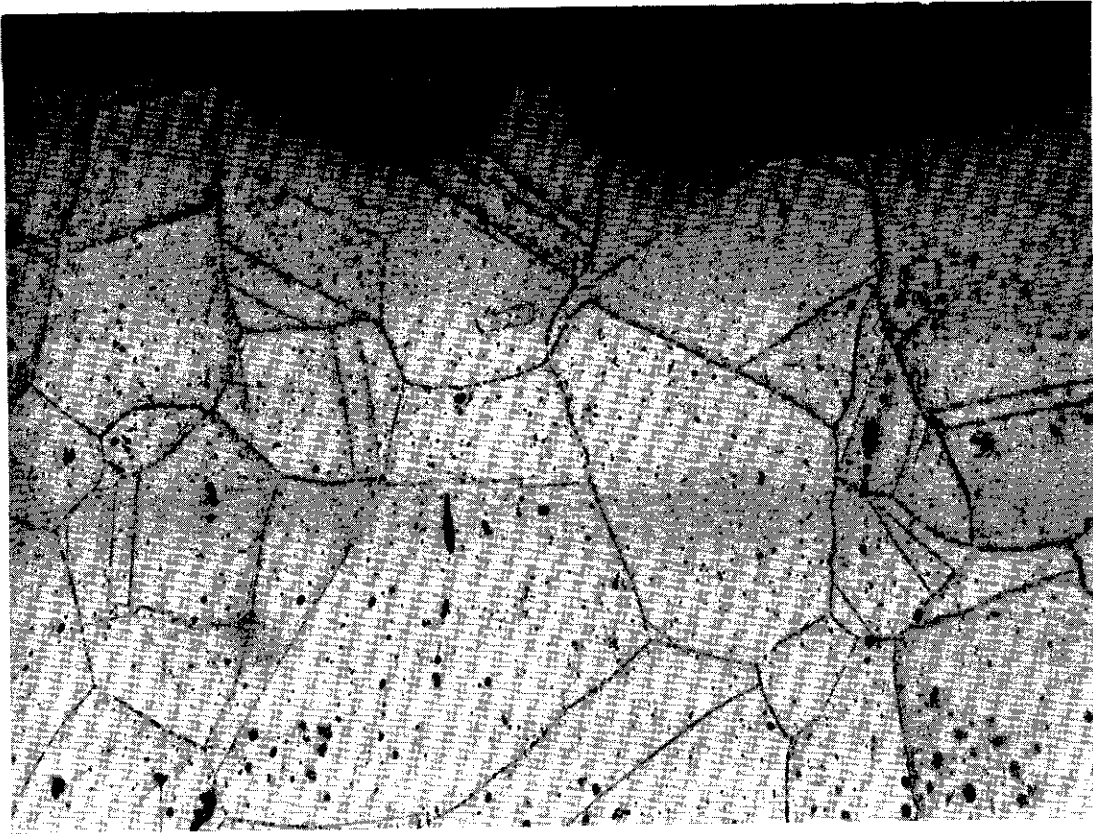
1945

Fig. 21.--Photomicrograph of type 316 stainless steel specimen tested in lead-bismuth alloy at 1500°F (specimen surface, magnification 500X).

1946

Fig. 22.--Photomicrograph of type 316 stainless steel specimen tested in lead-bismuth alloy at 1500°F (specimen surface, magnification 500X).

ultrasonic transducer assembly to the top plate of the cavitation vessel
and bolting the top plate in place, the temperature of the lead-bismuth
alloy was increased to 1500°F by means of the automatic temperature con-
troller. At the conclusion of the test the temperature was reduced to
500°F again so that the specimen could safely be removed from the end of
the exponential horn and visually examined and weighed. Also, it was
desired not to expose the test materials to the atmosphere at 1500°F
where reaction rates would no doubt be considerably greater than at
500°F.

The seven specimens tested for cavitation resistance at 1500°F
were subjected to the cavitation environment for varying lengths of
time, the stainless steel being exposed for 5-6 hours and the refractory
alloys for a total of 10 hours. At appropriate intervals the specimens
were visually examined, photographed, and carefully weighed. Then the
test resumed. Excess lead-bismuth alloy was removed from the specimens
using the procedure outlined earlier. It was not possible to examine
the refractory materials as frequently as the stainless steels because
of numerous mechanical problems that were encountered with these mater-
ials. On several occasions the refractory specimens fractured during
disassembly at the point where the threaded length joins the cylindrical
button portion of the specimen, thus voiding the test. Hence, extreme
care had to be exercised during assembly and disassembly, so that it was
not desired to repeat this operation any more often than necessary. As
a result, the refractory specimens were examined, photographed, and
weighed after 4 hours of testing, and again after a total of 10 hours in
the cavitation environment.

2. Experimental Results at 500°F

The cavitation results obtained at 500°F in lead-bismuth alloy will be displayed as accumulative weight loss versus test duration, and also as accumulative mean depth of penetration (MDP) versus test duration. The mean depth of penetration, computed assuming that the weight loss is smeared uniformly over the cavitated specimen surface, is felt to be more physically meaningful than weight loss, since it is generally the total penetration of a particular component by cavitation erosion that would render it unfit for service. Of course, neither weight loss nor MDP is sensitive to damage distribution and form, i.e., damage may vary from isolated deep pits to relatively uniform wear, depending on material-fluid combination. Obviously, a "figure of merit" such as MDP takes into account the large variation in density that may occur within a set of test materials.

The appropriate expression for computing the MDP of a given material is of the form:

$$MDP \text{ (mils)} = C \cdot W$$

where W is the weight loss expressed in mg. and C is a constant for the given material. Values of the constant, C, for computing the MDP of all the materials tested, along with their densities, are presented in Table 5.

Figure 23 is a plot of accumulative weight loss versus test duration for the seven materials tested, while Figure 24 is the corresponding plot of accumulative MDP versus test duration. The results presented in Table 6 are the slopes of these curves.

TABLE 5

RELATION BETWEEN WEIGHT LOSS AND MDP
(MDP = C·W)

Material	Density	Constant C*
1100-0 Aluminum	2.77 g./cc.	.0935
2024-T351 Aluminum	2.77	.0935
6061-T651 Aluminum	2.77	.0935
304 Stainless Steel	7.85	.033
316 Stainless Steel	7.85	.033
Hot-Rolled Carbon Steel	7.85	.033
T-111	17.66	.0147
T-222	17.66	.0147
T-222(A)	17.66	.0147
Mo-1/2Ti	10.22	.0253
Cb-1Zr	8.72	.0296
Cb-1Zr(A)	8.72	.0296
Plexiglas	1.23	.210
Cu (60% cold-worked)	8.97	.0288
Cu (900°F anneal, 1 hour)	9.04	.0287
Cu (1500°F anneal, 1 hour)	9.06	.0286
Cu-Zn (60% cold-worked)	8.61	.0300
Cu-Zn (850°F anneal, 1 hour)	8.62	.0300
Cu-Zn (1400°F anneal, 1 hour)	8.62	.0300

TABLE 5--Continued

Material	Density	Constant c*
Cu-Ni (60% cold-worked)	9.05 g./cc.	.0287
Cu-Ni (1300°F anneal, 1 hour)	9.05	.0286
Cu-Ni (1800°F anneal, 1 hour)	9.02	.0287
Ni (75% cold-worked)	8.97	.0288
Ni (1100°F anneal, 1 hour)	9.00	.0288
Ni (1600°F anneal, 1 hour)	9.00	.0288
BG-42 (all heat-treats)	7.85	.033
Blue Chip Tool Steel	8.70	.0296
Graphitar-Grade 50	1.70	.152
Graphitar-Grade 80	1.80	.144
Single-Crystal Tungsten	19.30	.0161

*Valid when MDP is expressed in mils and W is expressed in mg.
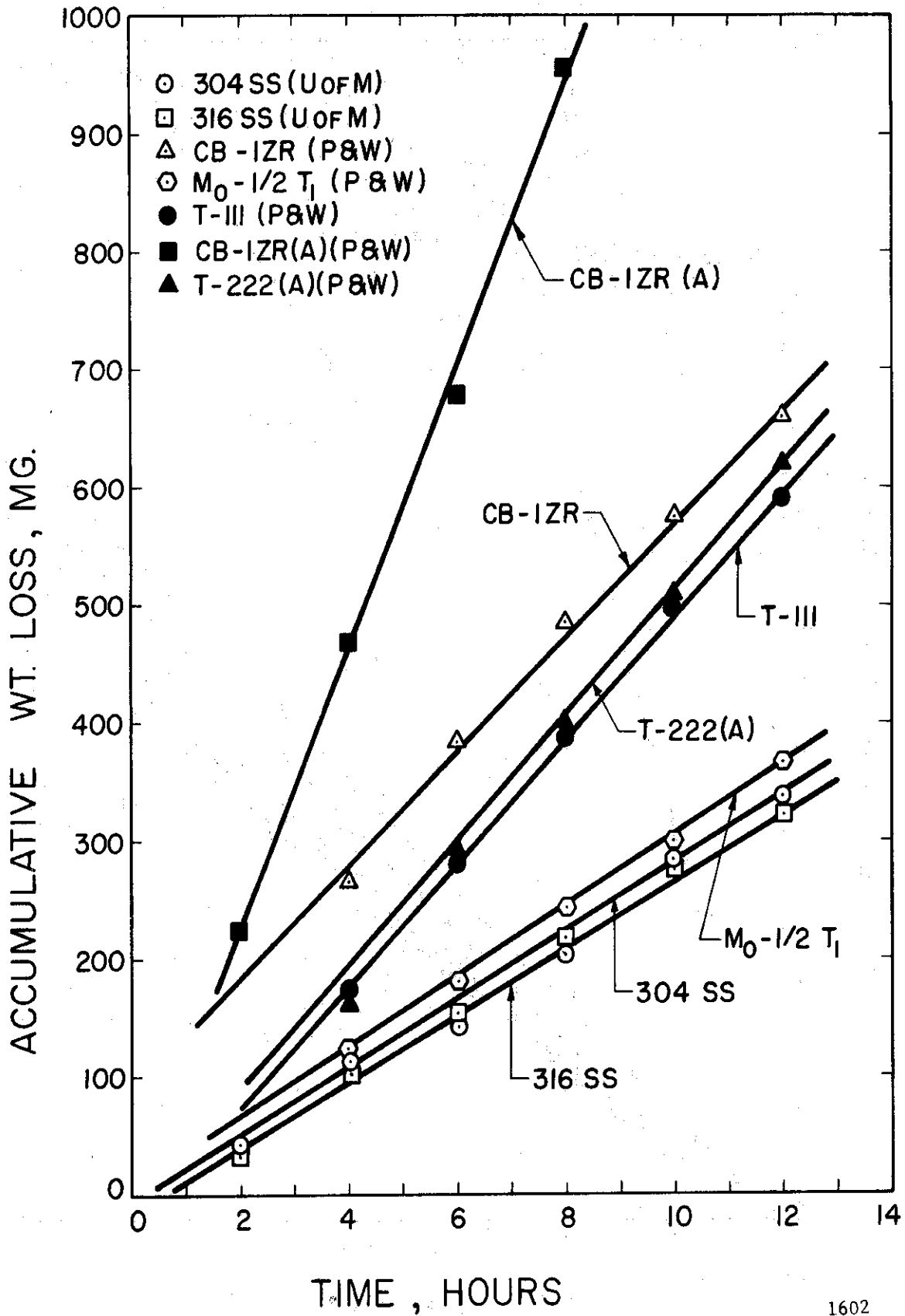
Fig. 23.--Effect of cavitation test duration on weight loss at 500°F in lead-bismuth alloy.
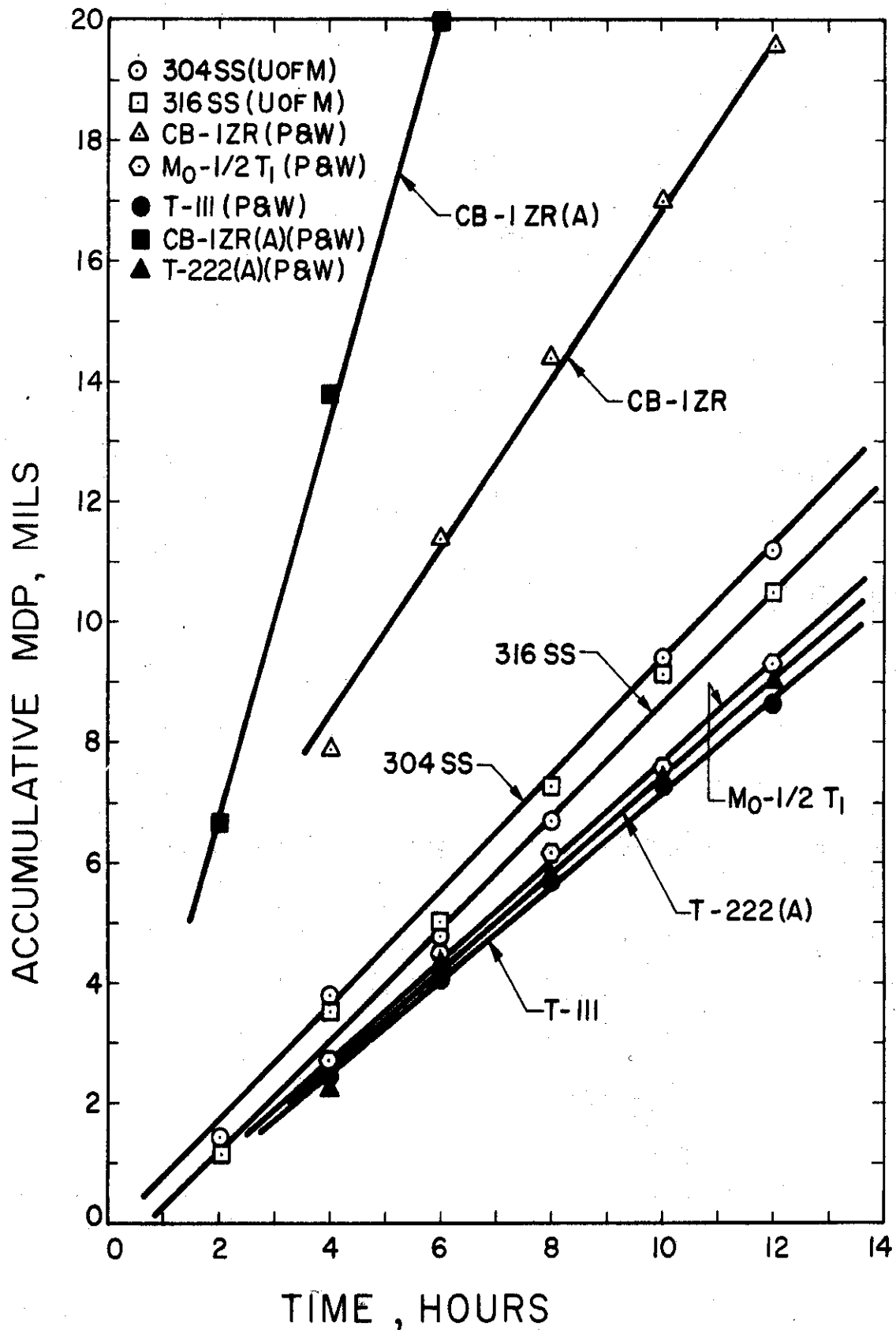
Fig. 24.--Effect of cavitation test duration on MDP at 500°F in lead-bismuth alloy.

TABLE 6

SUMMARY OF CAVITATION RESULTS IN LEAD-BISMUTH AT 500°F

Material	Avg. Wt. Loss Rate	Average MDP Rate
T-111 (P & W)	49.1 mg./hr.	.72 mils/hr.
T-222(A) (P & W)	51.6	.76
Mo-1/2Ti (P & W)	30.7	.78
316 SS (U-M)	26.6	.88
304 SS (U-M)	28.2	.93
Cb-1Zr (P & W)	55.1	1.63
Cb-1Zr(A) (P & W)	119.5	3.54

On the basis of MDP it is clear that the alloy T-111 has exhib-
ited the greatest resistance to cavitation damage in this experiment,
although T-222(A), Mo-1/2Ti, 304 stainless steel, and 316 stainless
steel are also quite cavitation resistant relative to the Cb-1Zr and the
Cb-1Zr(A). The Cb-1Zr(A) suffered gross damage after 8 hours of test-
ing. The other materials were tested for a total of 12 hours. It is
clear from Figures 23 and 24 that the rate of erosion for each individ-
ual material was approximately constant throughout the test, except for
the very initial part. It is also significant that at 500°F the stain-
less steels tested fared almost as well as the refractory alloys T-111,
T-222(A), and Mo-1/2Ti.

Photographs of the test specimens before exposure and at the
conclusion of the cavitation experiment are presented in Figure 25. The
effect of the cavitation erosion action of the collapsing bubble field
is quite apparent. Note the generally uniform dispersion of pitting
over the entire surface except for a relatively undamaged thin rim
around the outside. This eventually leads to a cupped specimen surface
which affects the bubble cloud and damage rate.

3. Experimental Results at 1500°F

The cavitation results obtained at 1500°F in lead-bismuth
alloy are also presented as accumulative weight loss versus test dura-
tion and also as accumulative mean depth of penetration (MDP) versus
test duration. The expressions given previously for MDP as a function
of weight loss (Table 5) are, of course, applicable at 1500°F* also.

---

*The damage measurements are, of course, made at room

BEFORE EXPOSURE   500°F.   1500°F.
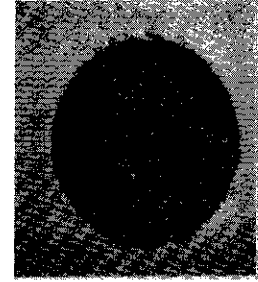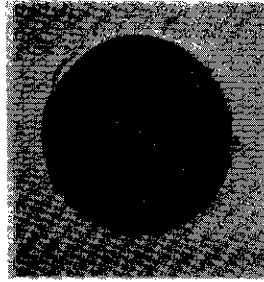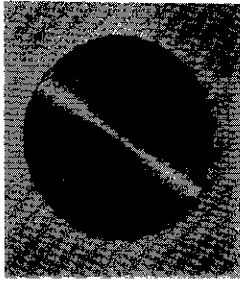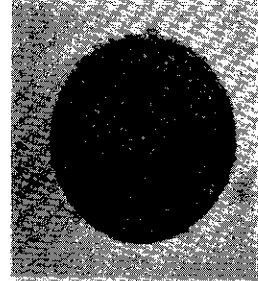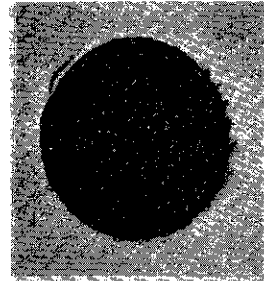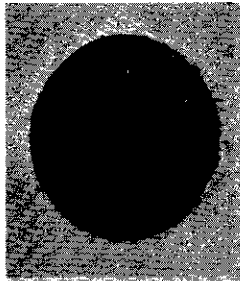
304 Stainless Steel   304 Stainless Steel   304 Stainless Steel
      (U-M)   12 Hour Exposure   5 Hour Exposure

316 Stainless Steel   316 Stainless Steel   316 Stainless Steel
      (U-M)   12 Hour Exposure   6 Hour Exposure
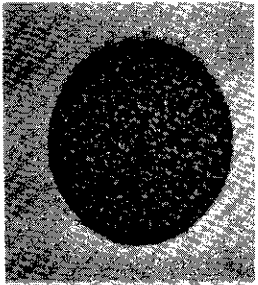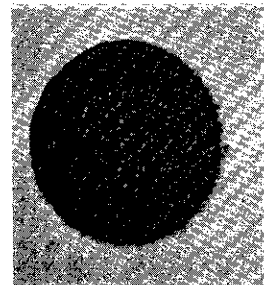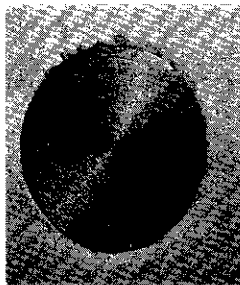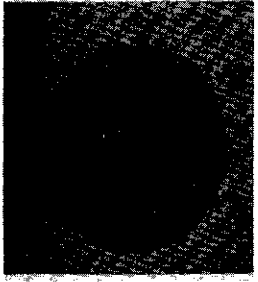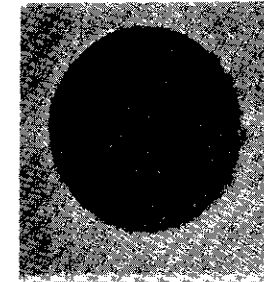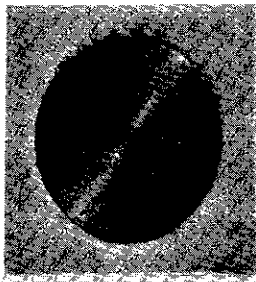
Mo-½Ti (P & W)   Mo-½Ti (P & W)   Mo-½Ti (P & W)
                             12 Hour Exposure   10 Hour Exposure

T-111 (P & W)   T-111 (P & W)   T-111 (P & W)
(Ta-8W-2Hf)   12 Hour Exposure   10 Hour Exposure

Fig. 25.--Specimens subjected to cavitation damage in lead-   1607
bismuth alloy at 500°F and 1500°F.

BEFORE EXPOSURE   500°F.   1500°F.
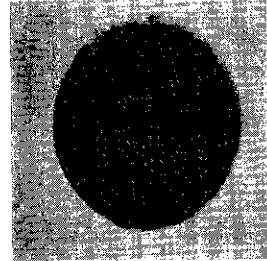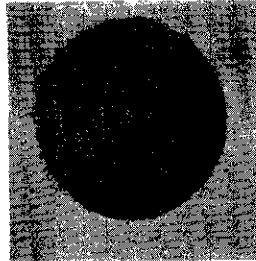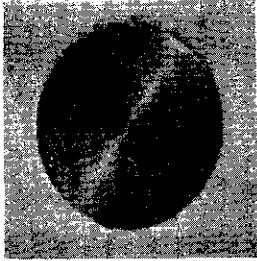
T-222(A) (P & W)   T-222(A) (P & W)   T-222(A) (P & W)
(Ta-9.5W-2.5Hf-.05C)   12 Hour Exposure   10 Hour Exposure
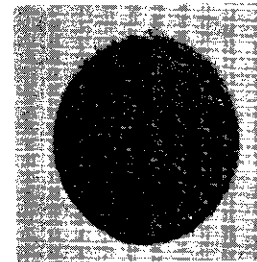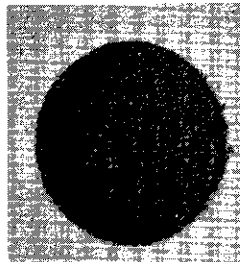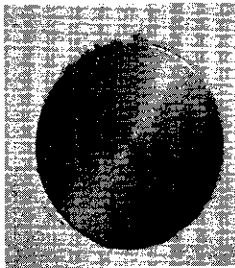
Cb-1Zr (P & W)   Cb-1Zr (P & W)   Cb-1Zr (P & W)
                         12 Hour Exposure   10 Hour Exposure
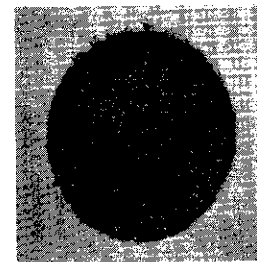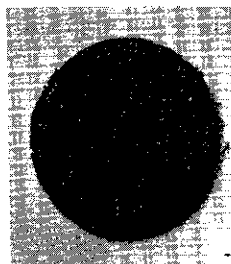
Cb-1Zr(A) (P & W)   Cb-1Zr(A) (P & W)   Cb-1Zr(A) (P & W)
                         8 Hour Exposure   10 Hour Exposure

Fig. 25.--Specimens subjected to cavitation damage in lead-   1608
bismuth alloy at 500°F and 1500°F.

Figure 26 is a plot of accumulative weight loss versus test duration for the seven materials tested, while Figure 27 is the corresponding plot of accumulative MDP versus test duration. The results presented in Table 7 are the slopes of these curves.

On the basis of MDP the refractory alloy T-111 exhibited the greatest resistance to cavitation damage in this experiment. This was also true at 500°F. The T-222(A) and the Mo-1/2Ti were also quite cavitation-resistant relative to the other materials tested. The Cb-1Zr and the 316 stainless steel rated behind the tantalum and molybdenum alloys, while both the Cb-1Zr(A) and the 304 stainless steel exhibited little resistance to cavitation erosion at this temperature. Both were grossly damaged, especially the 304 stainless steel after only 5 hours of testing. It is clear from Figures 26 and 27 that the rate of erosion for each individual material was approximately constant for all the materials tested except perhaps near the start of the test. This behavior was also noted at 500°F.

There is no question that the refractory alloys T-111, T-222(A), Mo-1/2Ti, and Cb-1Zr are far superior to the stainless steels with respect to resistance to cavitation erosion at 1500°F. Such materials are likely choices for components that are subject to cavitation damage in various types of turbomachinery, magnetohydrodynamic devices, etc., which are expected to operate at very high temperatures.

Photographs of the test specimens before exposure and at the conclusion of the cavitation experiments at both 500°F and at 1500°F are

---

temperature and expressions for MDP presumed applicable at this temperature also.
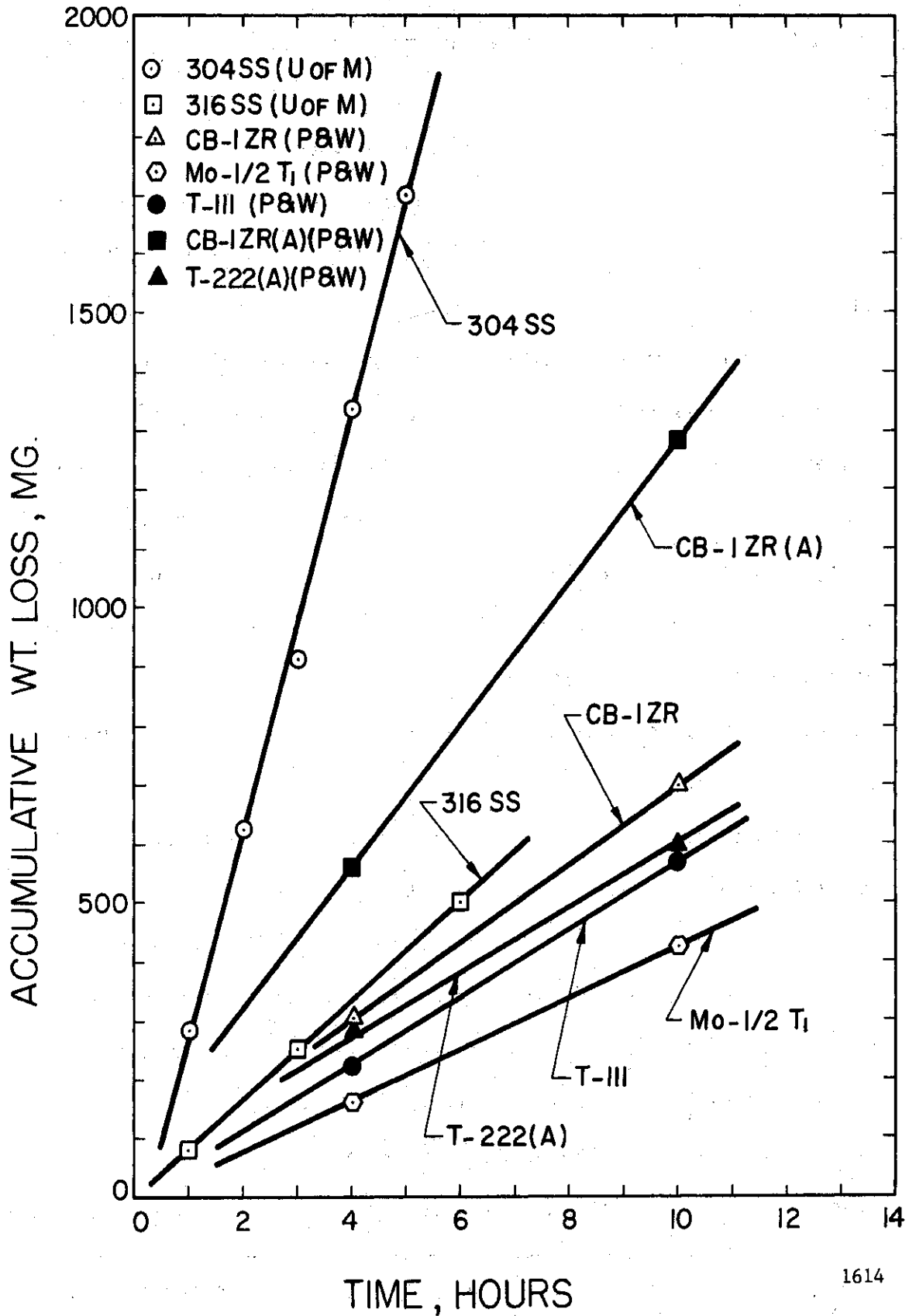
Fig. 26.--Effect of cavitation test duration on weight loss at 1500°F in lead-bismuth alloy.
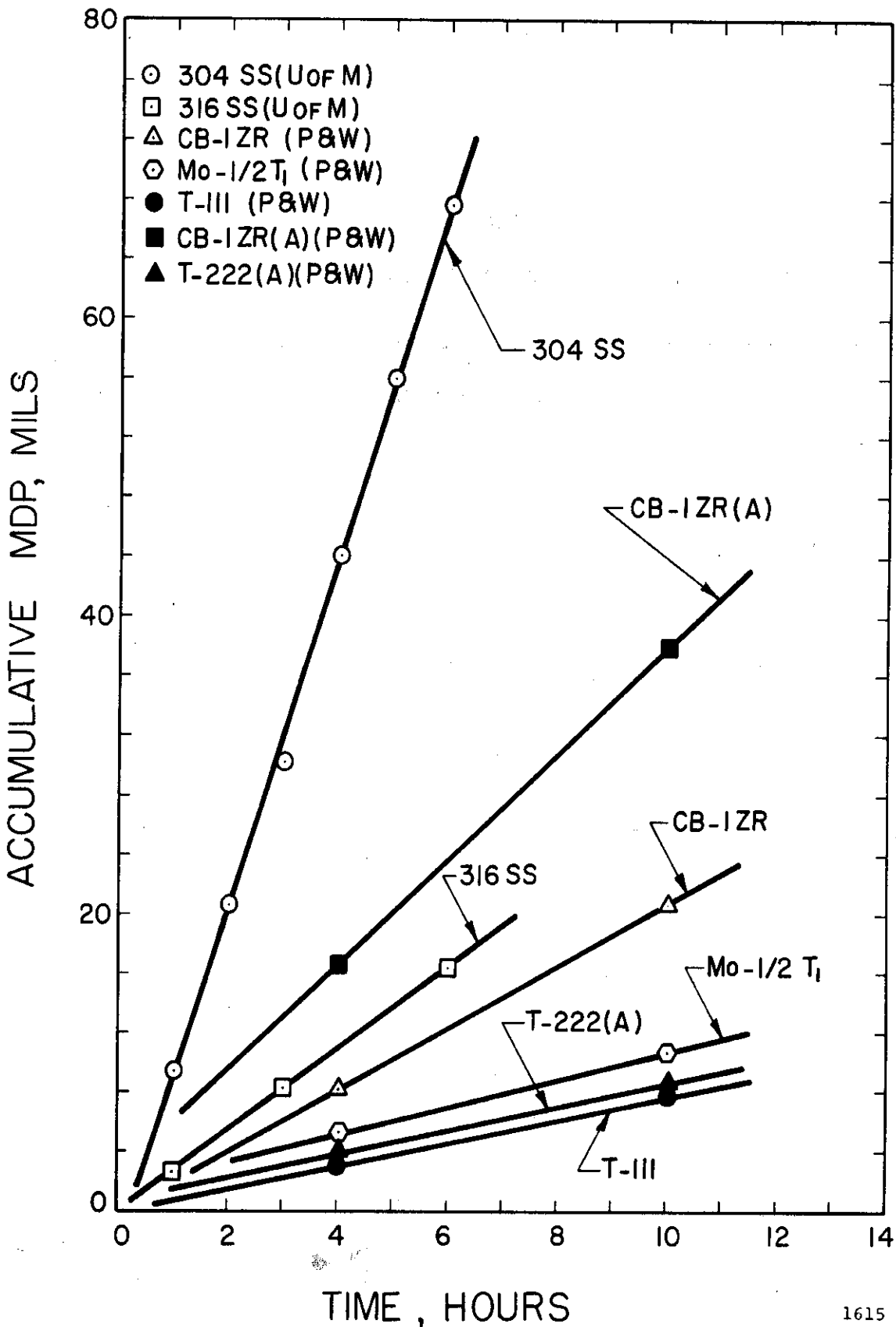
Fig. 27.--Effect of cavitation test duration on MDP at 1500°F in lead-bismuth alloy.

TABLE 7

SUMMARY OF CAVITATION RESULTS IN LEAD-BISMUTH AT 1500°F

Material	Avg. Wt. Loss Rate	Average MDP Rate
T-111 (P & W)	57.1 mg./hr.	.84 mils/hr.
T-222(A) (P & W)	59.9	.88
Mo-1/2Ti (P & W)	42.6	1.08
Cb-1Zr (P & W)	70.0	2.07
316 SS (U-M)	83.3	2.80
Cb-1Zr(A) (P & W)	128.4	3.80
304 SS (U-M)	342.0	11.30

presented in Figure 25 (previously cited) for comparison.

Detailed examination of the 303 stainless steel exponential horn, the 316 stainless steel container vessel, and the sides of the various test specimens, all of which are not subject to cavitation, but are submerged in the test fluid, indicates that corrosion effects in the absence of cavitation in these investigations at both 500°F and 1500°F were negligible. Also, the photomicrographs presented in Figures 20, 21, and 22 (previously discussed) do not show any evidence of intergranular corrosion or corrosion at the surface of the specimen. Figure 20 does show slip lines in the grains near the surface, indicating the mechanical nature of the attack. Hence, one might conclude that the damage suffered by the test specimens in these tests was due almost completely to the mechanical cavitation-erosion process, and not to chemical corrosion.

4. Discussion and Comparison of Results

Table 8 summarizes the cavitation data obtained at 500°F and at 1500°F. The seven materials tested have been rated on the basis of cavitation resistance as determined by MDP, with a rating of "1" indicating the most cavitation resistant material, while a rating of "7" would denote that material most susceptible to cavitation damage.

The tantalum alloys, T-111 and T-222(A), are the most resistant to cavitation at both 500°F and at 1500°F. The Mo-1/2Ti ranks third at both temperatures. It is significant to note the poor performance of the stainless steels at 1500°F after being only 25% less resistant to cavitation at 500°F than the T-111 and the T-222(A). In fact, at 1500°F

TABLE 8

COMPARISON OF CAVITATION RESULTS IN LEAD-BISMUTH
AT 500°F AND 1500°F

Material	500°F (Avg. MDP Rate)	Rating	1500°F (Avg. MDP Rate)	Rating
T-111	.72 mils/hr.	1	.84 mils/hr.	1
T-222(A)	.76	2	.88	2
Mo-1/2Ti	.78	3	1.08	3
316 SS	.88	4	2.80	5
304 SS	.93	5	11.30	7
Cb-1Zr	1.63	6	2.07	4
Cb-1Zr(A)	3.54	7	3.80	6

the 304 stainless steel was damaged grossly after being subjected to the cavitation environment for only 5 hours. A similar comment applies to the Cb-1Zr(A) at 500°F and 1500°F. Figure 25 displays photographs of the specimens before exposure to cavitation and at the conclusion of the tests at 500°F and 1500°F. The differences in the amount of erosion attack on the various specimens and the effect of temperature are readily apparent.

It is important to note that for each material tested the amount of damage sustained by the specimen at 1500°F was greater than that sustained at 500°F for constant testing time.

The effect of temperature on the cavitation results in lead-bismuth alloy is further displayed in Figure 28, which is a plot of average MDP rate versus temperature for the seven materials tested. The effect of temperature on the T-111, T-222(A), and Mo-1/2Ti is almost negligible, while the effect on the stainless steels is quite dramatic, as evidenced by the slopes of the appropriate curves. Later it is noted that this is due primarily to the fact that the mechanical properties of the stainless steels over the range tested are strong functions of temperature, whereas those of the refractories are only slightly affected by it. At the same time the pertinent fluid properties for lead-bismuth alloy at 500°F and 1500°F are nearly identical.

D. Cavitation Studies in Mercury at 70°F and 500°F

1. Experimental Procedure

The eight materials tested in mercury at 500°F were 304 stainless steel (U-M), 316 stainless steel (U-M), hot-rolled carbon
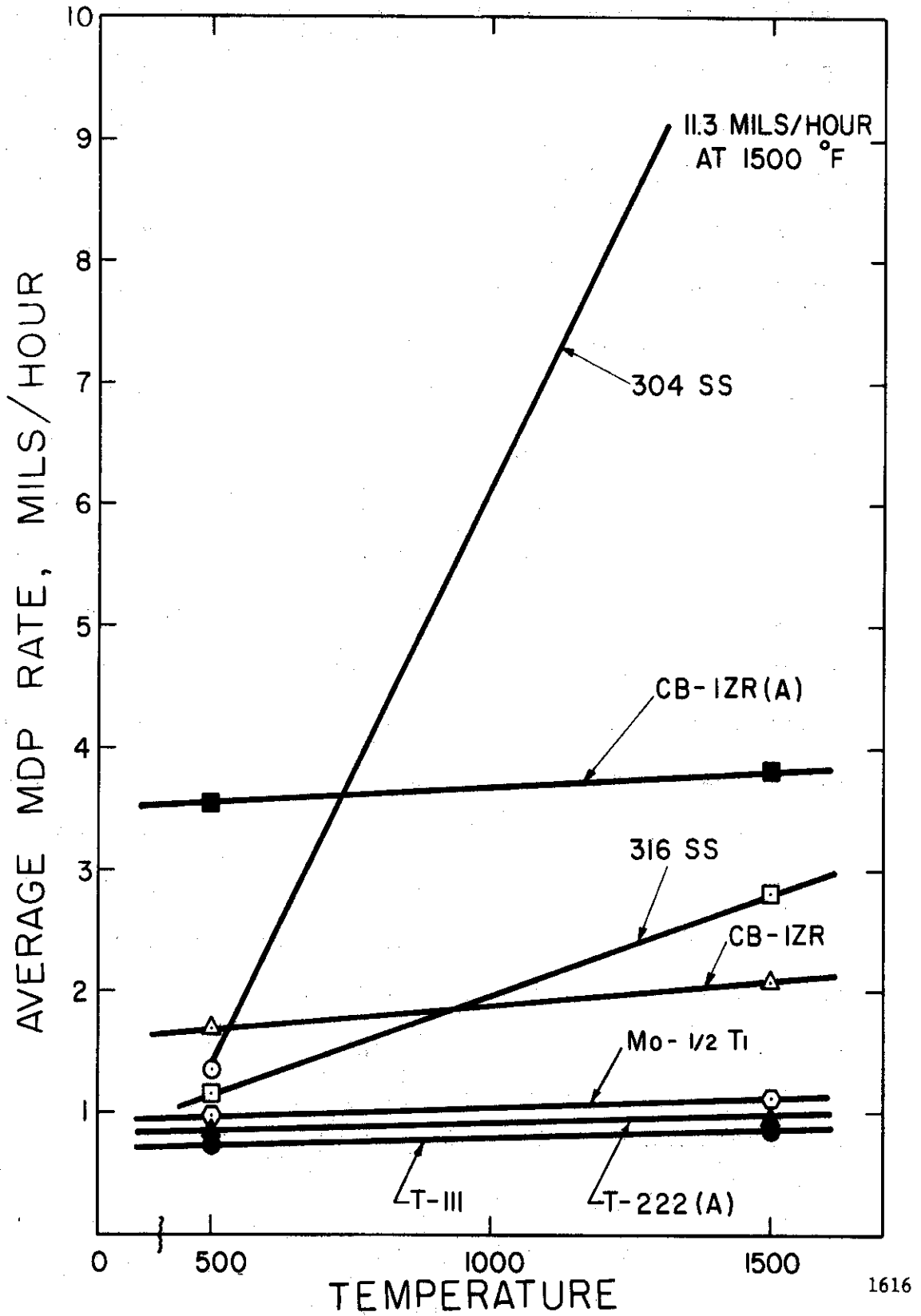
Fig. 28.--Effect of temperature on cavitation resistance in lead-bismuth alloy.

steel (U-M), T-111 (P & W), T-222(A) (P & W), Mo-1/2Ti (P & W), Cb-1Zr
(P & W), and Cb-1Zr(A) (P & W). Standard cavitation test specimens, as
shown in Figure 6, were machined from available bar stock. The required
dimensions "A" and "B" for the eight materials tested are listed in
Table 4. These dimensions provide a standard specimen weight of 9.4 ±
0.1 g.

The materials tested in mercury at 70°F were identical to those
tested at 500°F, and listed previously in Table 2, with the exception of
T-222 which was substituted for T-222(A) due to a shortage of the
annealed bar stock. In addition, Plexiglas was also tested at 70°F
because of availability of cavitation data for this material from the
venturi tests.[20,21,22] Standard cavitation test specimens of T-222 have
the same dimensions as given previously for the annealed stock
(Table 4).

Due to the low density of the Plexiglas (compared to the other
materials tested) and its brittle nature, as previously explained, it
was completely impractical to fabricate standard cavitation test speci-
mens as shown in Figure 6. Hence, the design previously discussed and
shown in Figure 7, consisting of a Plexiglas test specimen with internal
thread and a separate stainless steel mounting stud was adopted and
proved to be satisfactory.

The vapor pressure of mercury at 70°F is completely negligible
in its effect on suppression pressure, while at 500°F it is 1.9 psia.
Thus, the argon cover gas pressure was maintained at a slight overpres-
sure of 0.5 psig throughout the tests at 70°F, and at a pressure of

2.4 psig for the tests at 500°F. This resulted in a suppression pressure of about 15.3 psia at both temperatures, as desired.

At 70°F total test duration varied for the different materials, ranging from 8 to 12 hours, with the exception of the Plexiglas which was tested for only one hour due to mechanical problems. Very fine cracks began to develop within the Plexiglas cylinder after a test duration of approximately one hour which resulted in poor transmission of acoustic energy to the tip of the exponential horn. For all materials frequent inspections and weighings monitored the specimen surface. Prior to each weighing any excess mercury adhering to the specimen surface was removed by heating in a vacuum furnace (except for the Plexiglas) so as to eliminate oxidation of the specimen.

At 500°F the total test duration also varied for the different materials, ranging from 8 to 12 hours, with frequent inspections and weighings monitoring the specimen surface. Prior to each weighing any excess mercury adhering to the specimen surface was removed using the same procedure employed for the 70°F tests.

2. Experimental Results at 70°F

The cavitation results obtained at 70°F in mercury are displayed as accumulative weight loss and also accumulative mean depth of penetration (MDP) versus test duration, as for the lead-bismuth.

Table 9 summarizes the cavitation results obtained in mercury at 70°F. Figure 29 is a plot of accumulative weight loss versus test duration, while Figure 30 is the corresponding plot of accumulative MDP versus test duration for the nine materials tested.

TABLE 9

SUMMARY OF CAVITATION RESULTS IN MERCURY AT 70°F

Material	Avg. Wt. Loss Rate	Average MDP Rate
304 SS (U-M)	9.82 mg./hr.	.32 mils/hr.
316 SS (U-M)	9.88	.33
T-111 (P & W)	23.71	.35
T-222 (P & W)	28.92	.43
Mo-1/2Ti (P & W)	22.58	.57
Cb-1Zr (P & W)	31.04	.92
Carbon Steel (U-M)	31.17	1.03
Cb-1Zr(A) (P & W)	54.22	1.61
Plexiglas (U-M)	19.00	3.99
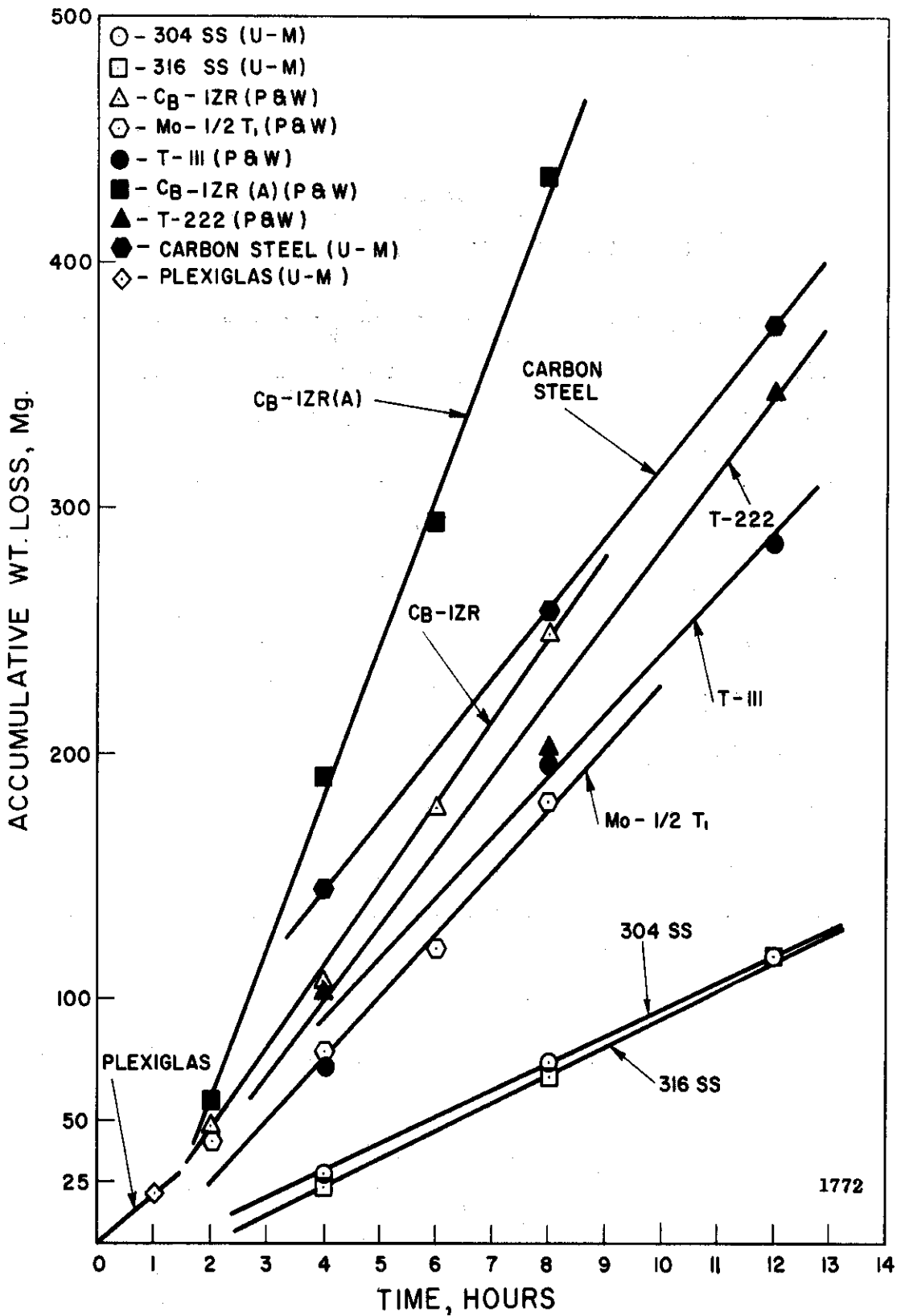
Fig. 29.--Effect of cavitation test duration on weight loss at 70°F in mercury.
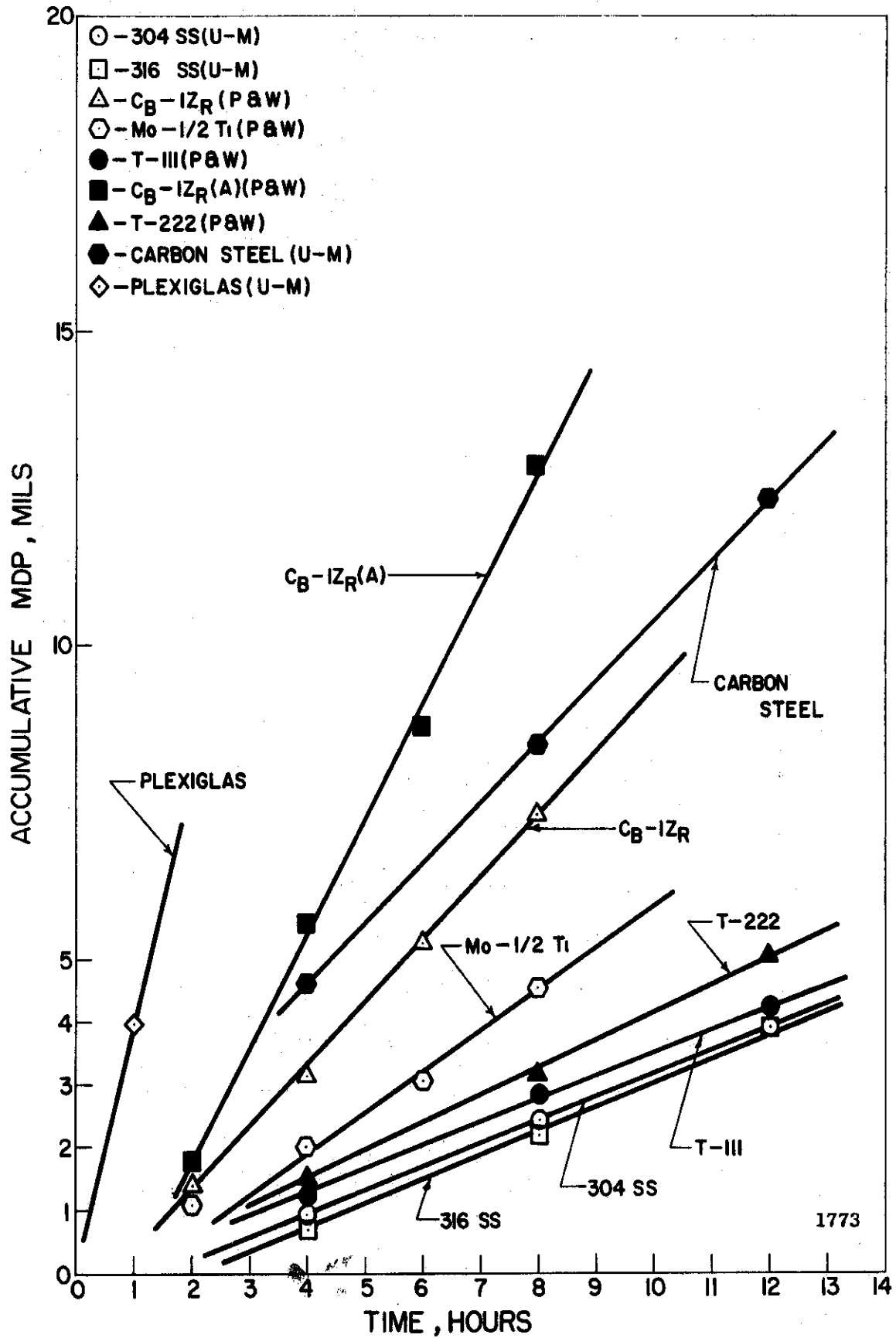
Fig. 30.--Effect of cavitation test duration on MDP at 70°F in mercury.

The 304 stainless steel and 316 stainless steel, differing by only 3%, were the most resistant to cavitation at 70°F based either on average weight loss rate or average MDP rate. These materials exhibited average MDP rates of 0.32 mils/hour and 0.33 mils/hour, respectively. The alloys T-111 and T-222 were 6% and 30% less resistant than the stainless steels, respectively, while the Mo-1/2Ti was 80% less resistant. The Cb-1Zr, hot-rolled carbon steel, and Cb-1Zr(A) all suffered heavy damage in the cavitation environment at 70°F. The MDP rates for these materials were approximately 3 times to 5 times greater than for the stainless steels and the T-111. The Plexiglas suffered the most severe damage in terms of average MDP rate with a value of 3.99 mils/ hour. It is clear from Figures 29 and 30 that the rate of erosion for each individual material is approximately constant for all the materials tested for the duration of the test.

Photographs of the test specimens at the conclusion of the cavitation experiment are presented in Figure 31. The materials are arranged in order of decreasing resistance to cavitation damage. Note the severe pitting of the Cb-1Zr, hot-rolled carbon steel, Cb-1Zr(A), and Plexiglas. In all cases the damage noted is relatively uniform over the specimen face as opposed to individual isolated, deep pitting which, as will be discussed later, was encountered with the low density fluids tested. This was also noted in the lead-bismuth tests at 500°F and 1500°F. It is felt that the approximately constant rate of erosion noted for all the materials tested in both mercury and lead-bismuth is due to this uniform damage pattern, and the fact that the area and
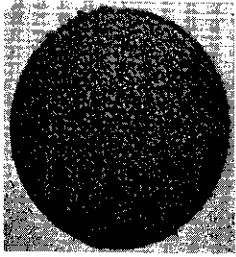
(1) 304 SS(U-M)
12 Hour Exposure
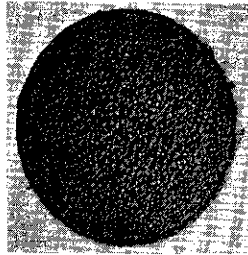
(2) 316 SS(U-M)
12 Hour Exposure
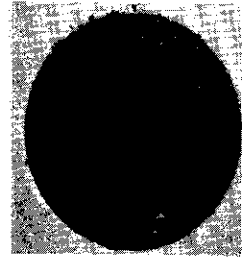
(3) T-111(P & W)
12 Hour Exposure
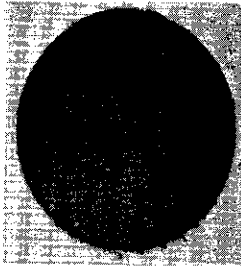
(4) T-222(P & W)
12 Hour Exposure
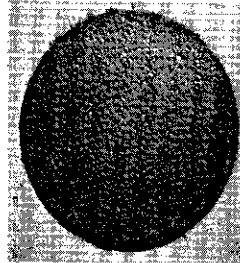
(5) Mo-1/2Ti(P & W)
8 Hour Exposure
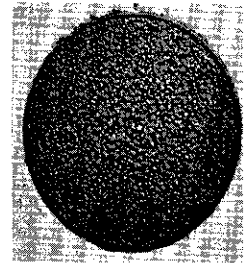
(6) Cb-1Zr(P & W)
8 Hour Exposure
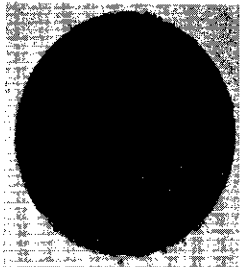
(7) Carbon Steel(U-M)
12 Hour Exposure
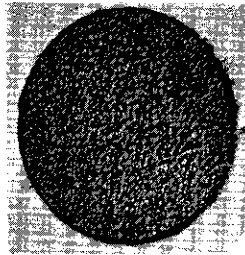
(8) Cb-1Zr(A)(P & W)
8 Hour Exposure
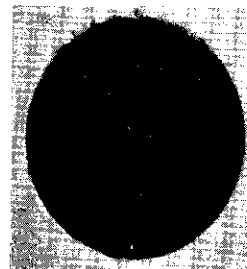
(9) Plexiglas(U-M)
1 Hour Exposure

304 SS(U-M)

Before Exposure

Fig. 31.--Photographs of specimens subjected to cavitation

1774

configuration (i.e., specimens remain approximately flat throughout the test duration) presented to the collapsing bubble cloud is approximately constant for the duration of the test. A photograph of a 304 stainless steel specimen before exposure is included in Figure 31, and serves to indicate a representative initial surface condition for all the specimens tested.

Detailed examination of the 303 stainless steel exponential horn, the 316 stainless steel container vessel, and the sides of the various test specimens, all of which are not subject to cavitation, but are submerged in the test fluid, indicates that corrosion effects in the absence of cavitation in these investigations were negligible, as previously discussed for lead-bismuth.

3. Experimental Results at 500°F

The cavitation results obtained at 500°F in mercury are displayed as accumulative weight loss versus test duration, and also as accumulative mean depth of penetration (MDP) versus test duration. Table 10 summarizes the cavitation results obtained in mercury at 500°F. Figure 32 is a plot of accumulative weight loss versus test duration, while Figure 33 is the corresponding plot of accumulative MDP versus test duration for the eight materials tested.

On the basis of either average weight loss rate or average MDP rate it is clear that the T-111 is the most cavitation resistant of the materials tested, while the T-222(A) is about 7% less resistant. These materials exhibited average MDP rates of 0.43 mils/hour and 0.46 mils/ hour, respectively. The hot-rolled carbon steel, 316 stainless steel,

TABLE 10

SUMMARY OF CAVITATION RESULTS IN MERCURY AT 500°F

Material	Avg. Wt. Loss Rate	Average MDP Rate
T-111 (P & W)	29.48 mg./hr.	.43 mils/hr.
T-222(A) (P & W)	31.52	.46
Carbon Steel (U-M)	18.60	.61
316 SS (U-M)	19.01	.63
304 SS (U-M)	20.83	.69
Mo-1/2Ti (P & W)	43.16	1.09
Cb-1Zr (P & W)	81.85	2.43
Cb-1Zr(A) (P & W)	125.78	3.73
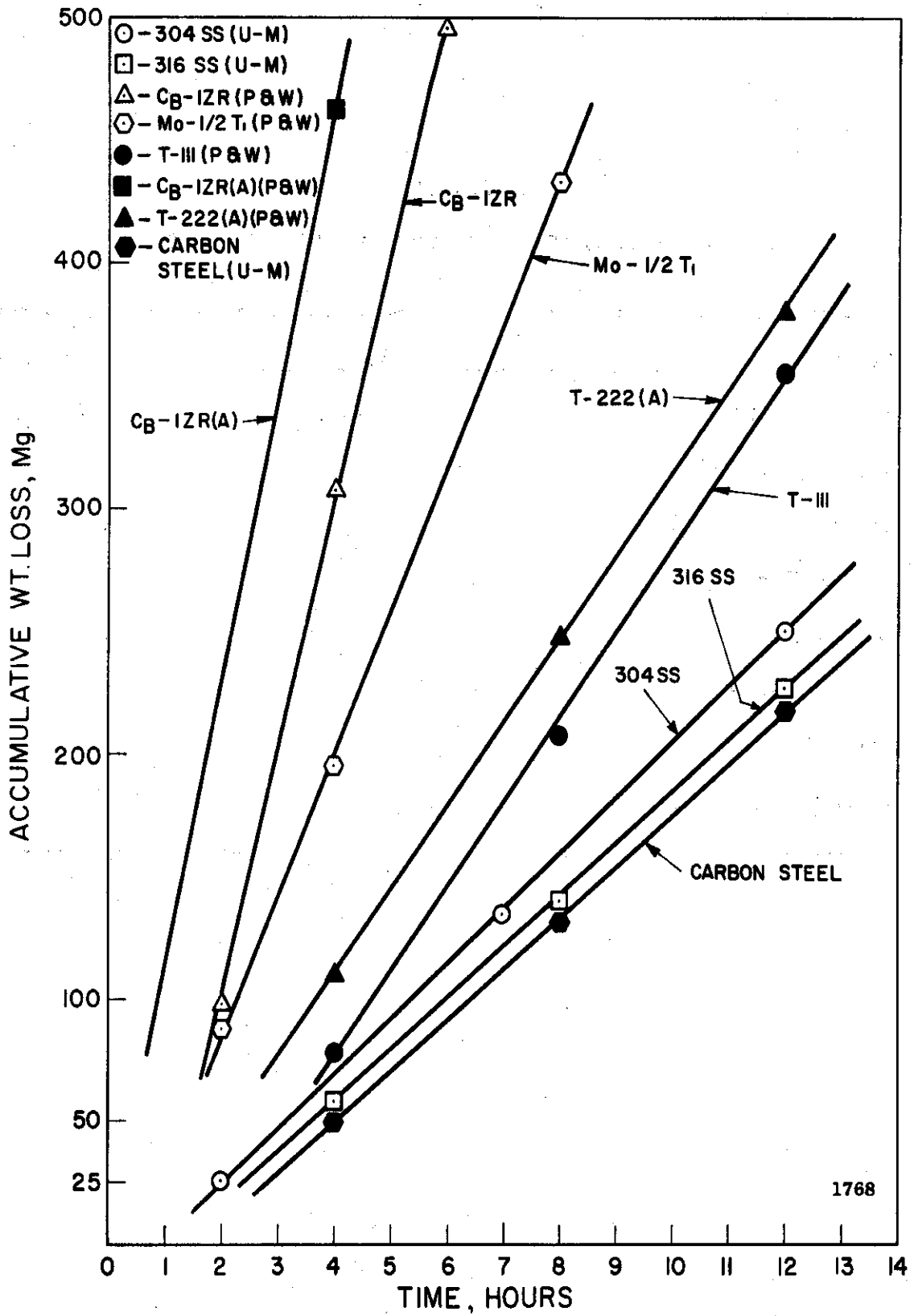
Fig. 32.--Effect of cavitation test duration on weight loss at 500°F in mercury.
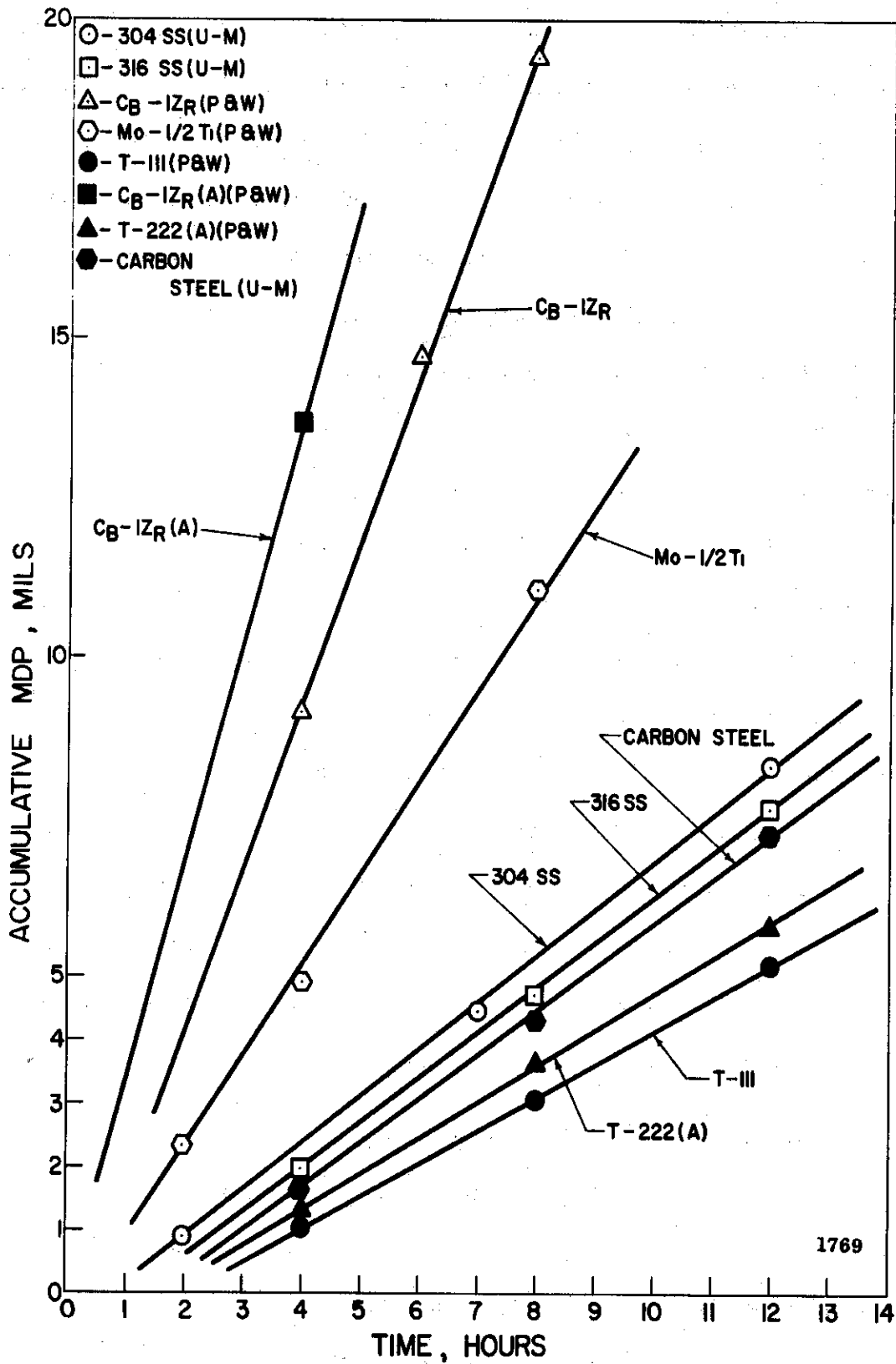
Fig. 33.--Effect of cavitation test duration on MDP at 500°F in mercury.

and 304 stainless steel rank third, fourth, and fifth, respectively, with average MDP rates of 0.61 mils/hour, 0.63 mils/hour, and 0.69 mils/ hour, respectively. Three refractory materials: Mo-1/2Ti, Cb-1Zr, and Cb-1Zr(A) were the least resistant to cavitation damage, with the Cb-1Zr(A) suffering gross damage and ranking last among the materials tested. These three materials suffered damage ranging from 3 times to 8 times greater than that suffered by the tantalum-base alloys, T-111 and T-222(A). It is clear from Figures 32 and 33 that the rate of erosion for each individual material is approximately constant for all the materials tested for the duration of the test.

Photographs of the test specimens at the conclusion of the cavitation experiment are presented in Figure 34. The materials are arranged in order of decreasing resistance to cavitation damage. Note the severe pitting of the Mo-1/2Ti, Cb-1Zr, and Cb-1Zr(A) surfaces. In all cases the damage is again relatively uniform over the specimen face, as was the case for the 70°F tests.

Detailed examination of the exponential horn, container vessel, and the sides of the various test specimens indicates again that corrosion effects in the absence of cavitation in these investigations were negligible.

4. Discussion and Comparison of Results

Table 11 summarizes the cavitation data obtained in mercury at 70°F and 500°F. The eight materials tested at both temperatures have been rated on the basis of cavitation resistance as determined by MDP, with a rating of "1" indicating the most cavitation resistant material,
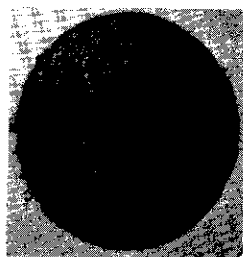
(1) T-111(P & W)
12 Hour Exposure
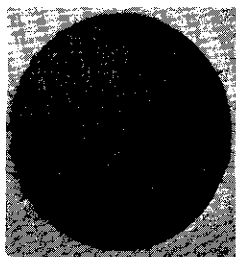
(2) T-222(A)(P & W)
12 Hour Exposure
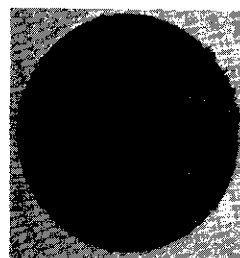
(3) Carbon Steel(U-M)
12 Hour Exposure
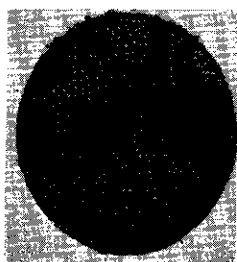
(4) 316 SS(U-M)
12 Hour Exposure
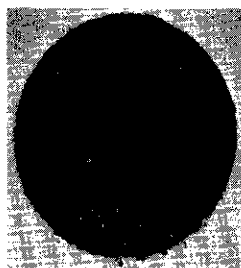
(5) 304 SS(U-M)
12 Hour Exposure
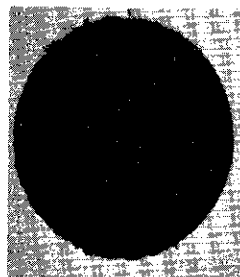
(6) Mo-1/2Ti(P & W)
12 Hour Exposure
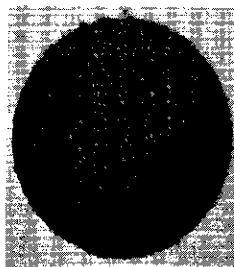
(7) Cb-1Zr(P & W)
8 Hour Exposure
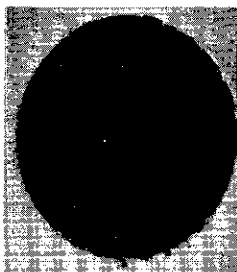
(8) Cb-1Zr(A)(P & W)
8 Hour Exposure
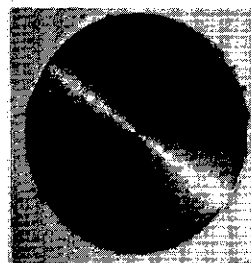
304 SS(U-M)
Before Exposure

Fig. 34.--Photographs of specimens subjected to cavitation
damage in mercury at 500°F.

1770

TABLE 11

COMPARISON OF CAVITATION RESULTS IN MERCURY
AT 70°F AND 500°F

Material	70°F		500°F	
	Avg. MDP Rate	Rating	Avg. MDP Rate	Rating
304 SS	.32 mils/hr.	1	.69 mils/hr.	5
316 SS	.33	2	.63	4
T-111	.35	3	.43	1
T-222*	.43	4	.46*	2
Mo-1/2Ti	.57	5	1.09	6
Cb-1Zr	.92	6	2.43	7
Carbon Steel	1.03	7	.61	3
Cb-1Zr(A)	1.61	8	3.73	8
Plexiglas	3.99	9	--	-

*T-222(A) was tested at 500°F.

while a rating of "8" would denote that material most susceptible to cavitation damage.

The most cavitation-resistant materials at 70°F were the stainless steels with the tantalum-base alloys ranking third and fourth. At 500°F the superior mechanical properties of the tantalum-base alloys at even a very moderate elevated temperature are already evident as the T-111 and T-222(A) rank first and second, respectively. The hot-rolled carbon steel, 316 stainless steel, and 304 stainless steel rank third, fourth, and fifth, respectively, at 500°F. The Mo-1/2Ti, Cb-1Zr, and Cb-1Zr(A) all maintained the same relative position at both test temperatures. The hot-rolled carbon steel which had fared well at 500°F with a rating of "3" was damaged almost 70% more at 70°F. This apparently anomalous behavior is easily explained by the fact that the mechanical properties of the hot-rolled carbon steel such as tensile strength and yield strength are greater at 500°F than at 70°F, which is attributed to "strain aging." As temperature is increased from room temperature, the strength properties pass through a maximum and then decrease. Very few materials possess this rather unique property. The engineering strain energy at 500°F is about 5% greater than at 70°F. However, the true strain energy at 500°F is about 35% less than at 70°F.

It is further noted that with the exception of the hot-rolled carbon steel, all of the materials tested sustained greater damage at 500°F than at 70°F. The stainless steels were damaged about 100% more and the T-111 about 23% more, while the damage rates for the Mo-1/2Ti, Cb-1Zr, and Cb-1Zr(A) were 2 times to 3 times greater at 500°F than at

70°F. No direct comparison is possible in the case of the T-222 and T-222(A), tested at 70°F and 500°F, respectively, as the mechanical properties of these materials differ.

The effect of temperature on the cavitation results in mercury is further displayed in Figure 35, which is a plot of average MDP rate versus temperature for the eight materials tested. The effect of temperature on the T-111 and T-222 is almost negligible (at 500°F the T-222(A) data point is plotted), while the effect on all of the other materials is quite dramatic, as evidenced by the slopes of the appropriate curves. The behavior of the hot-rolled carbon steel is once again noted. Later discussion shows that the temperature-dependent behavior of the cavitation resistance of these materials can be explained on the basis of the variation of mechanical properties with temperature. It is further shown that the mechanical properties of the tantalum-base alloys are weak functions of temperature, whereas those of the other materials vary considerably, even over the range from 70°F to 500°F.

5. **Comparison with Venturi Facility Mercury Results**

It was noted earlier that the utility of acoustic cavitation damage results has been limited because no direct correlation with cavitation in a flowing system was available. However, if such a correlation could be formulated, it might be possible to substitute relatively economical acoustic testing for tests in a tunnel facility. This laboratory has conducted venturi cavitation tests in both water and mercury for the past several years,[20,21,22,58] and has accumulated much useful
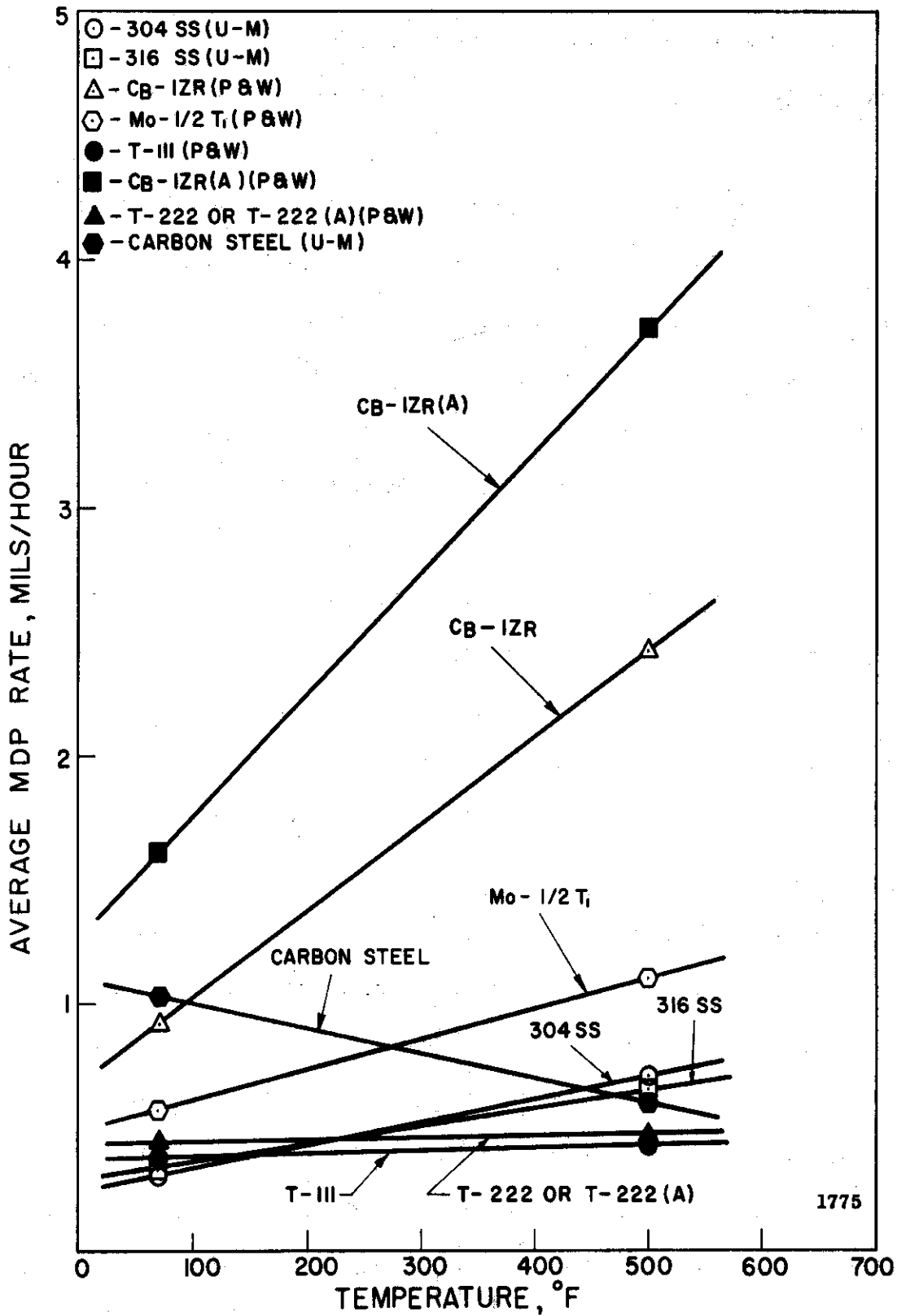
Fig. 35.--Effect of temperature on cavitation resistance in mercury.

data over this period of time. Now that data in mercury at 70°F has been obtained with the ultrasonic (acoustic) facility, it is possible to qualitatively compare the data from both facilities for similar materials.

Table 12 is a tabulation of the available data in mercury at 70°F for the two facilities. The wear in the venturi loop is given in terms of MDP after 50 hours of testing, whereas in the case of the acoustic facility, the average MDP rate is listed. The stainless steels tested in the venturi are similar to the 304 stainless steel and 316 stainless steel tested in the ultrasonic facility, but not identical. The composition of the T-111 is Ta-8W-2Hf, so that the corresponding specimens in both facilities are of the same composition. The composition of the T-222 is Ta-9.5W-2.5Hf-.05C and differs slightly from the Ta-10W tested in the venturi. The carbon steels tested are not identical but have similar carbon content and hardness values. The remainder of the materials investigated in both facilities are nearly identical in composition.

In both facilities the materials have been listed in order of decreasing cavitation resistance, or increasing susceptibility to cavitation-erosion attack. The first five materials have identical rankings in each facility with the stainless steels being the most resistant to cavitation-erosion attack. The Cb-1Zr, carbon steel, and Cb-1Zr(A) occupy the next three places in this qualitative ranking for both facilities, but their rankings do not agree in detail. In the case of the venturi tests the Cb-1Zr ranks eighth, while it ranks sixth in

TABLE 12

COMPARISON OF CAVITATION EROSION DATA IN MERCURY AT 70°F -
VENTURI AND ULTRASONIC FACILITIES

Venturi Data		Ultrasonic Data	
Material	MDP at 50 Hours	Material	Avg. MDP Rate
Stainless Steel	$.28 \times 10^{-2}$ mils	304 SS	.32 mils/hr.
		316 SS	.33
Ta-8W-2Hf	$.85 \times 10^{-2}$	T-111	.35
Ta-10W	1.71×10^{-2}	T-222	.43
Mo-1/2Ti	2.10×10^{-2}	Mo-1/2Ti	.57
Carbon Steel	2.94×10^{-2}	Cb-1Zr	.92
Cb-1Zr(A)	5.87×10^{-2}	Carbon Steel	1.03
Cb-1Zr	29.0×10^{-2}	Cb-1Zr(A)	1.61
Plexiglas	$225 \times 10^{-2*}$	Plexiglas	3.99

*MDP at 25 hours.

the ultrasonic facility. The order of ranking of the carbon steel and Cb-1Zr(A) is preserved in both facilities. It was noted in the venturi investigations that the damage sustained by the Cb-1Zr apparently indicated a thin multi-layer-like (laminated) structure. This could easily lead to greater damage and weight losses since large sections of the Cb-1Zr outer layer were removed in some cases by the cavitation action as opposed to the normal minute pitting mechanism that would be expected. The unusual structure of the Cb-1Zr tested in the venturi, apparently the result of improper heat-treat, probably accounts for the poor showing of this material in that facility. No such observation was made in the case of the acoustic facility. The Plexiglas was the least resistant to cavitation damage by far in both facilities and attained ninth ranking.

It is clear that with the exception of the Cb-1Zr the qualitative rankings of the materials tested in the venturi and ultrasonic facilities agree very well. This agreement offers hope that a quantitative correlation could be developed that would couple the results of the two facilities. Such a correlation must await the generation of more complete data in both facilities for a variety of test fluids and temperatures.

It is interesting to note from Table 12 that the intensity of damage in the acoustic facility is approximately 1000 times greater than that in the venturi loop, and also that the ratios of damage between various materials in the venturi facility is much greater, even though the rankings are almost identical. This latter phenomenon may involve

the fact that corrosion is probably more important in the venturi tests since the exposure time is longer and the intensity of mechanical attack much less. However, the venturi test probably represents typical field conditions much more closely than the vibratory-type test.

E. Cavitation Studies in Water at 70°F

1. Experimental Procedure

The 24 materials tested in water at 70°F are listed in Table 2 (previously cited). The three grades of aluminum and the various heat-treats of Cu, Cu-Zn, Cu-Ni, and Ni were included in the vibratory cavitation program in water because extensive results from the venturi program are available for these materials in water. Standard cavitation test specimens, as shown in Figure 6, were machined from available bar stock of the three grades of aluminum, carbon steel, stainless steels, and refractory alloys. The appropriate "A" and "B" dimensions are given in Table 4.

It was desired to test in the vibratory facility the identical heat-treats of Cu, Cu-Zn, Cu-Ni, and Ni that had been previously tested in the venturi loop facility. Since these materials were available only in sheet stock 1/16 in. thick, it was necessary to design a special specimen consisting of an adaptor of a suitable material and a disk of the desired material. Means of attaching the disk to the adaptor had to be provided so that a firm bond would result. This is necessary so that the ultrasonic energy is efficiently transferred across the interface. Hence, the design previously discussed and shown in Figure 8, consisting

of a brass adaptor and a disk of the desired material, was adopted and

proved to be satisfactory. The disk is fastened to the adaptor with

soft solder. It was not desired to use a stronger higher temperature

solder with these materials since their mechanical properties might be

significantly altered by exposure to the higher temperatures required

to make the joint. Various epoxies and cements were attempted as a

bonding material, but the bond was immediately destroyed upon initia-

tion of the test. The acoustic impedance of the soft solder is on the

order of that of both the brass adaptor and disk materials, while the

epoxies and cements possessed a very low acoustic impedance due to neg-

ligible elastic properties. The arrangement shown in Figure 8 results

in a standard specimen weight of 9.4 ± 0.1 g.

The Plexiglas specimens tested in water were fabricated as per

Figure 7 (previously cited).

The water tests were conducted in a Plexiglas cavitation vessel

whose dimensions are identical to those of the 316 stainless steel con-

tainer previously employed for the lead-bismuth and mercury tests. The

Plexiglas vessel permits visual observation of the bubble cloud and con-

tinuous monitoring of the condition of the specimen surface during a

test. All other equipment is identical to that previously used in the

lead-bismuth and mercury investigations.

The vapor pressure of water at 70°F is approximately 0.4 psia.

Thus, the argon cover gas pressure was maintained at 1.5 psig through-

out the tests to provide the required suppression pressure of 15.3 psia.

Total test duration varied for the different materials, ranging

from 1 hour for the very soft 1100-0 aluminum to 36 hours for the

stainless steels and the refractory materials. The Cu, Cu-Zn, Cu-Ni, and Ni specimens were tested for 6 hours. Frequent inspections and weighings monitored the specimen surface.

2. Experimental Results--Subsets One and Two

The cavitation results obtained in water at 70°F are displayed as for the other fluids, and the appropriate expressions for computing the MDP of the aluminum, Cu, Cu-Zn, Cu-Ni, and Ni alloys are presented in Table 5.

The 24 materials tested in water at 70°F have been divided into three subsets for data display purposes. One subset consists of those materials that were also tested in mercury, lead-bismuth, and lithium; namely: 304 stainless steel, 316 stainless steel, T-111, T-222, Mo-1/2Ti, hot-rolled carbon steel, Cb-1Zr, and Cb-1Zr(A). The second subset consists of the three aluminum alloys and Plexiglas, while the third subset includes the 12 alloys of Cu, Cu-Zn, Cu-Ni, and Ni. The second and third subsets contain materials that have been tested only in water (with the exception of the Plexiglas that was tested in mercury at 70°F).

Table 13 summarizes the cavitation results obtained in water at 70°F for the materials in the first two subsets. Figure 36 is a plot of accumulative weight loss versus test duration, while Figure 37 is the corresponding plot of accumulative MDP versus test duration for the eight materials contained in subset one. Figures 38 and 39 are the corresponding plots for subset two, which consists of the aluminum alloys and the Plexiglas.

TABLE 13

SUMMARY OF CAVITATION RESULTS IN WATER AT 70°F -
SUBSETS ONE AND TWO

Material	Avg. Wt. Loss Rate	Average MDP Rate
T-222 (P & W)	1.05 mg./hr.	.02 mils/hr.
T-111 (P & W)	4.33	.06
Mo-1/2Ti (P & W)	3.49	.09
316 SS (U-M)	2.81	.09
304 SS (U-M)	3.04	.10
Cb-1Zr (P & W)	5.10	.15
Cb-1Zr(A) (P & W)	6.10	.18
Carbon Steel (U-M)	7.08	.23
2024-T351 Al (U-M)	6.13	.57
6061-T651 Al (U-M)	7.73	.72
Plexiglas (U-M)	6.60	1.39
1100-0 Al (U-M)	28.90	2.70
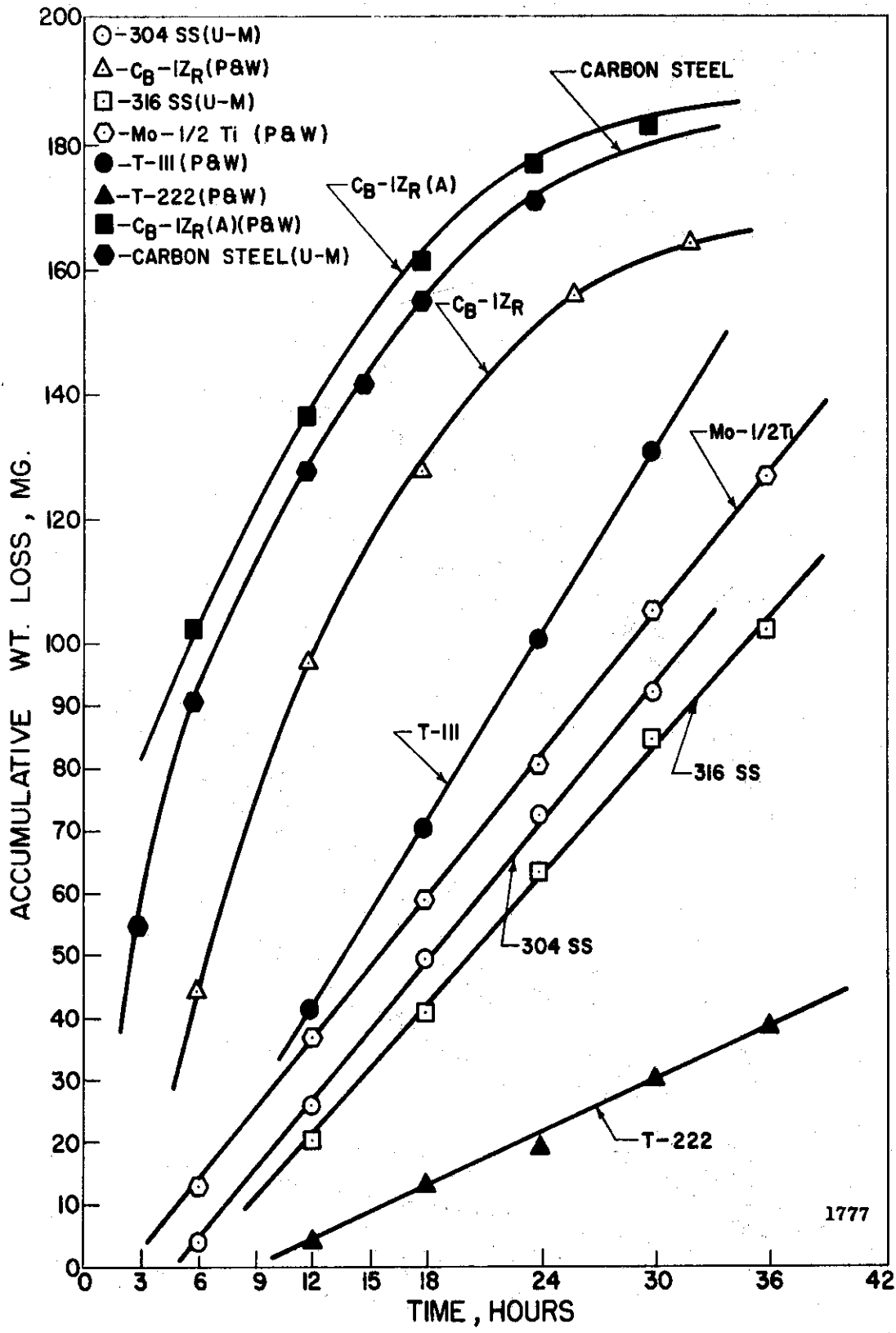
Fig. 36.--Effect of cavitation test duration on weight loss at 70°F in water - subset one.
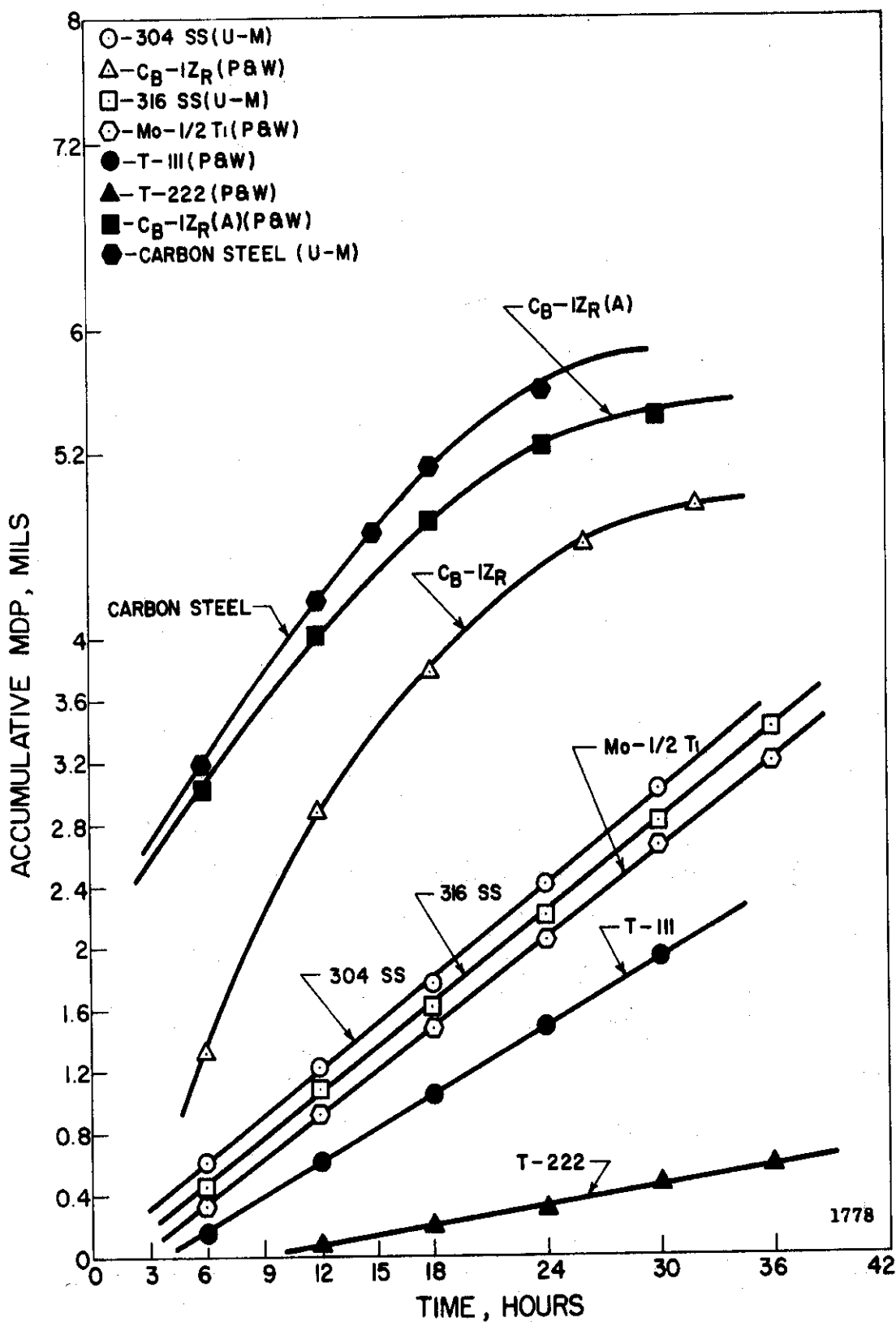
Fig. 37.--Effect of cavitation test duration on MDP at 70°F in water - subset one.
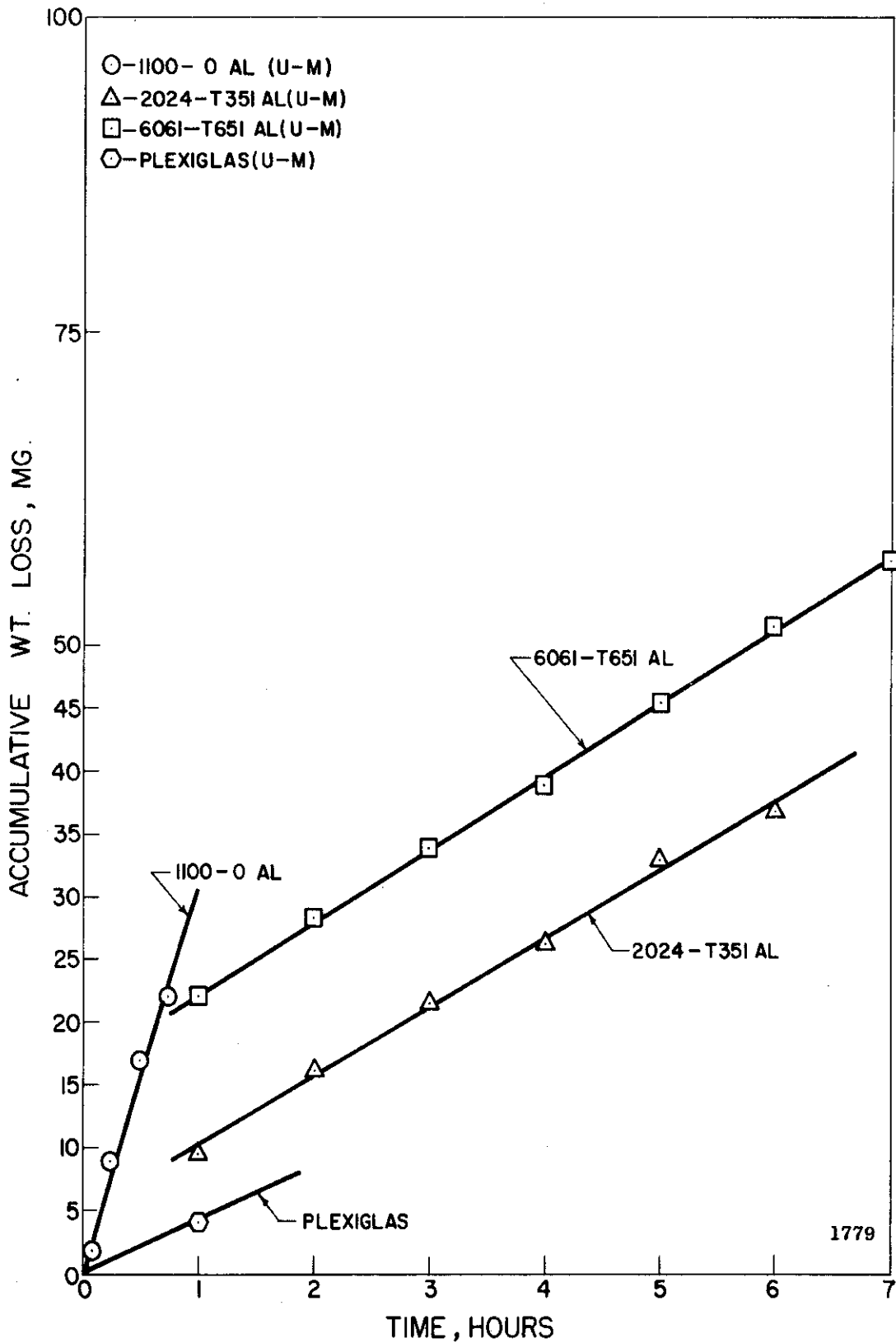
Fig. 38.--Effect of cavitation test duration on weight loss at 70°F in water - subset two.
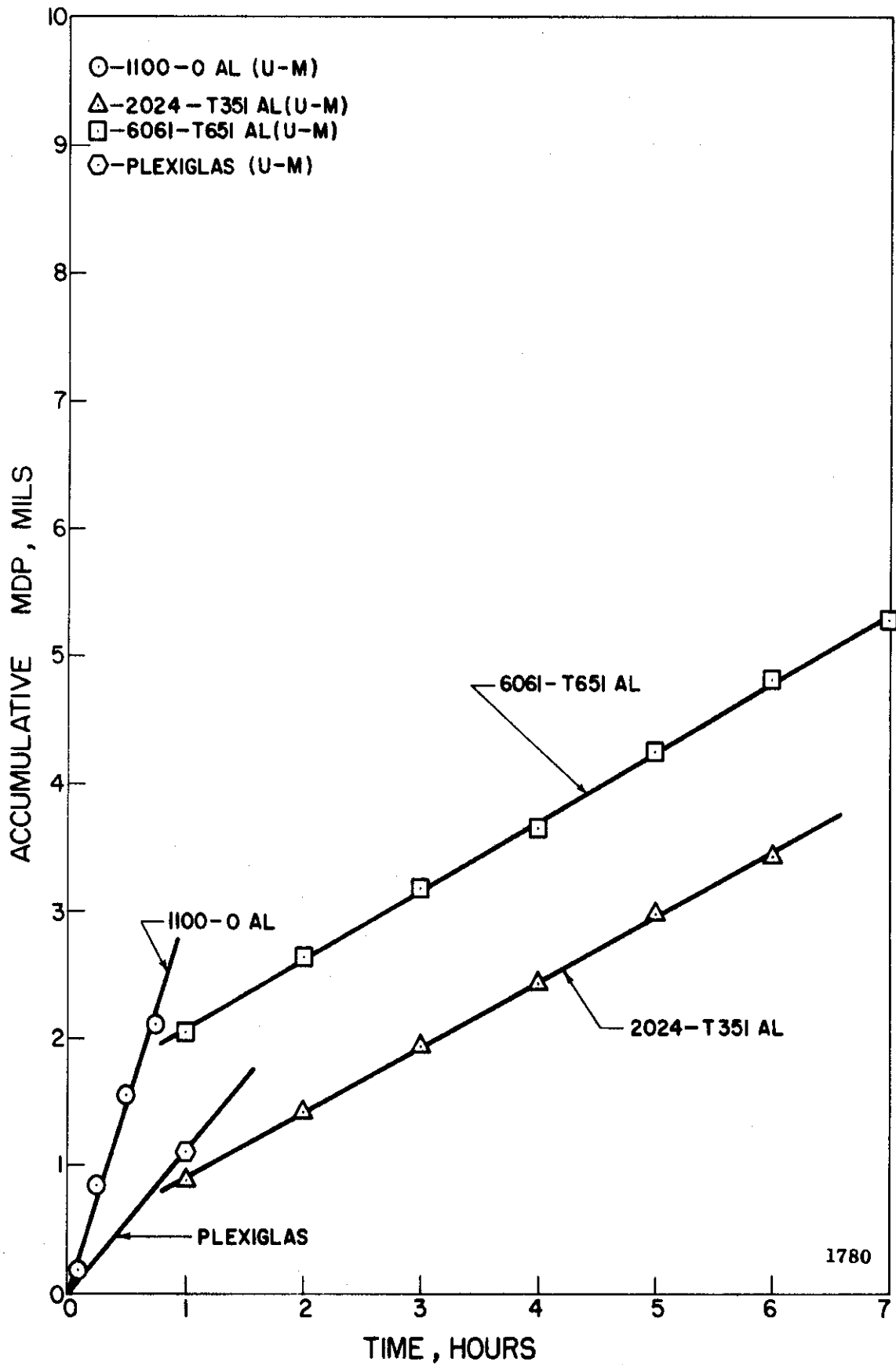
Fig. 37.--Effect of cavitation test duration on MDP at 70°F in water - subset two

On the basis of either average weight loss rate or average MDP rate it is clear that the T-222 is the most cavitation resistant of the materials contained in subsets one and two. The T-111 which ranked second suffered about 3 times more damage than the T-222, while the Mo-1/2Ti and 316 stainless steel were equally damaged and ranked third and fourth. The 304 stainless steel in fifth place sustained 5 times more damage than the T-222. The Cb-base alloys, Cb-1Zr and Cb-1Zr(A), and the hot-rolled carbon steel ranked sixth through eighth, respectively, and suffered damage 7 to 12 times more severe than the T-222, based on average MDP rate. The aluminum alloys and the Plexiglas were the least resistant to cavitation-erosion attack among the materials in subsets one and two. Considering only the three aluminum alloys, the 2024-T351 alloy was the most resistant while the very soft 1100-0 alloy sustained the greatest damage.

An examination of Figures 36 and 37 indicates that the rate of erosion for the T-222, T-111, Mo-1/2Ti, 316 stainless steel, and 304 stainless steel is approximately constant for the duration of the test, while the rate of erosion for the Cb-1Zr, Cb-1Zr(A), and the hot-rolled carbon steel is approximately constant during the early stages of the test and then begins to decrease as the accumulative weight loss and the accumulative MDP increase to larger values. Examination of the specimens generally indicated that those materials showing a linear response rate exhibit a fairly uniform surface damage pattern, whereas those showing a non-linear response are characterized by surface damage consisting primarily of heavy, isolated, deep pitting. This latter pattern

would result in a reduced surface area being presented to the collapsing

bubble cloud since the area surrounding the very deep isolated pits has

been shown to produce relatively few cavitation bubbles.[59] Hence, one

would expect the erosion rate to decrease as the total weight loss or

MDP increased, as clearly pointed out in a recent paper by Plesset and

Devine.[59]

Photographs of the test specimens in subset one at the conclu-

sion of the cavitation experiment are presented in Figure 40. The

materials are arranged in order of decreasing resistance to cavitation

damage. Note the severe pitting of the Cb-1Zr, Cb-1Zr(A), and hot-

rolled carbon steel surfaces.

It is clear from Figures 38 and 39 that the rate of erosion for

the three aluminum alloys is approximately constant for the duration of

the test in spite of the deep, isolated pitting of the type which in the

previous materials corresponded to a non-linear damage rate, at least

when MDP exceeds the order of 4 to 5 mils, i.e., the influence of the

non-uniform wear may not become significant until the volume loss

roughly corresponding to this range of MDP has been reached. As pre-

viously indicated, the specimens tested in high density fluids main-

tained a constant MDP rate out to the order of 50-60 mils. However,

their damage was extremely uniform. Thus, it may be that the rate

remains essentially constant as long as a uniform damage pattern is

maintained, and that the MDP for which uniform damage can be maintained

is a function of the material-fluid combination. The possible reasons

for fluid density effects on damage characteristics are discussed later.
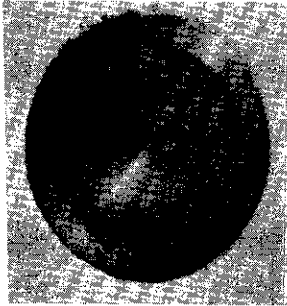
(1) T-222(P & W)

36 Hour Exposure
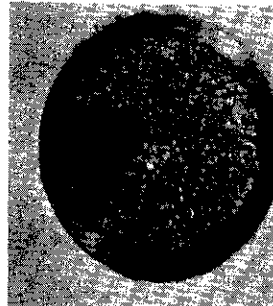
(2) T-111(P & W)

30 Hour Exposure
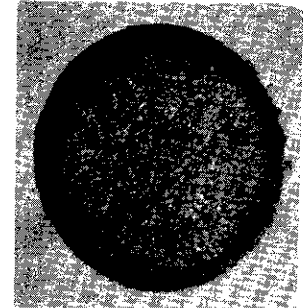
(3) Mo-1/2Ti(P & W)

36 Hour Exposure
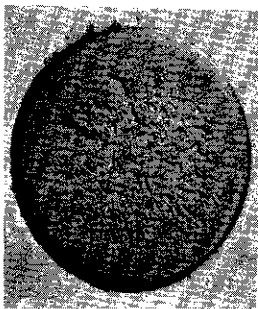
(4) 316 SS(U-M)

36 Hour Exposure
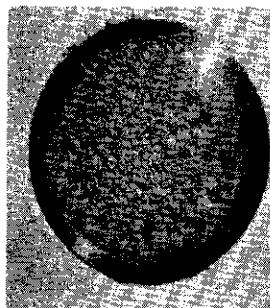
(5) 304 SS(U-M)

30 Hour Exposure

(6) Cb-1Zr(P & W)

32 Hour Exposure
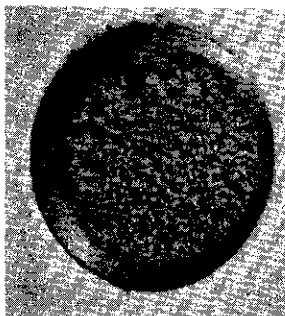
(7) Cb-1Zr(A)(P & W)

30 Hour Exposure
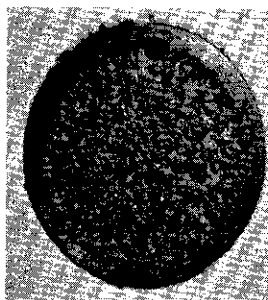
(8) Carbon Steel(U-M)

21 Hour Exposure
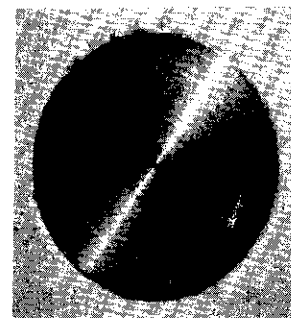
304 SS(U-M)

Before Exposure

Fig. 40.--Photographs of specimens subjected to cavitation
damage in water at 70°F - subset one·

1781

Photographs of the test specimens in subset two at the conclusion of the cavitation experiment are presented in Figure 41. A photograph of a 2024-T351 aluminum specimen before exposure is included for comparison.

3. Experimental Results--Subset Three

Table 14 summarizes the cavitation results obtained in water at 70°F for the materials in subset three, namely the 12 Cu, Cu-Zn, Cu-Ni, and Ni alloys. The various heat-treats of a given material are grouped together for purposes of comparison. Figure 42 is a plot of accumulative weight loss versus test duration, while Figure 43 is the corresponding plot of accumulative MDP versus test duration for the 6 Cu and Ni alloys in subset three. Figures 44 and 45 are the corresponding plots for the 6 Cu-Zn and Cu-Ni alloys in subset three.

On the basis of either average weight loss rate or average MDP rate the Cu-Zn (60% cold-worked) was the most cavitation resistant among the 12 materials contained in subset three with an average MDP rate of 0.38 mils/hour. The Ni (75% cold-worked) ranked second with an average MDP rate of 0.44 mils/hour, while the Cu-Ni (1800°F anneal, 1 hour) and Ni (1600°F anneal, 1 hour) were third and fourth with erosion rates of 0.47 mils/hour and 0.48 mils/hour, respectively. The three copper heat-treats were the least resistant to cavitation damage in subset three with the Cu (900°F anneal, 1 hour) ranking last with an erosion rate of 1.02 mils/hour. This specimen suffered approximately 3 times as much damage as the most resistant material, Cu-Zn (60% cold-worked).

Considering only the three copper specimens tested, the cold-worked material was the most cavitation resistant while the high-
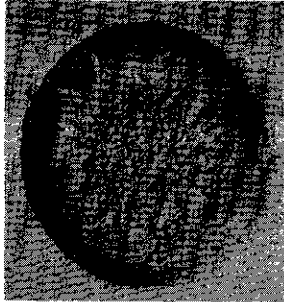
(1) 2024-T351 Al(U-M)
6 Hour Exposure
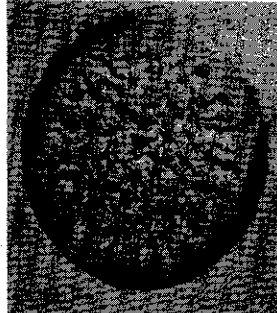
(2) 6061-T651 Al(U-M)
8 Hour Exposure
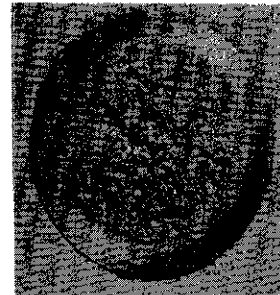
(3) 1100-0 Al(U-M)
45 Minute Exposure
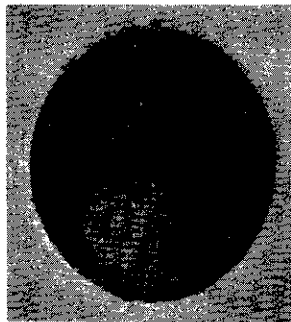
Plexiglas(U-M)
30 Minute Exposure
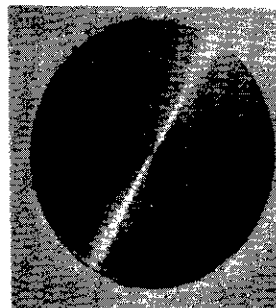
2024-T351 Al(U-M)
Before Exposure

Fig. 41.--Photographs of specimens subjected to cavitation
damage in water at 70°F - subset two.   1782

TABLE 14

SUMMARY OF CAVITATION RESULTS IN WATER AT 70°F -
SUBSET THREE

Material	Avg. Wt. Loss Rate	Average MDP Rate
Cu, cold-worked	32.83 mg./hr.	.95 mils/hr.
Cu, 900°F anneal	35.37	1.02
Cu, 1500°F anneal	33.32	.95
Cu-Ni, cold-worked	24.18	.70
Cu-Ni, 1300°F anneal	21.97	.63
Cu-Ni, 1800°F anneal	16.25	.47
Cu-Zn, cold-worked	12.74	.38
Cu-Zn, 850°F anneal	23.88	.72
Cu-Zn, 1400°F anneal	22.78	.68
Ni, cold-worked	15.27	.44
Ni, 1100°F anneal	20.25	.58
Ni, 1600°F anneal	16.69	.48
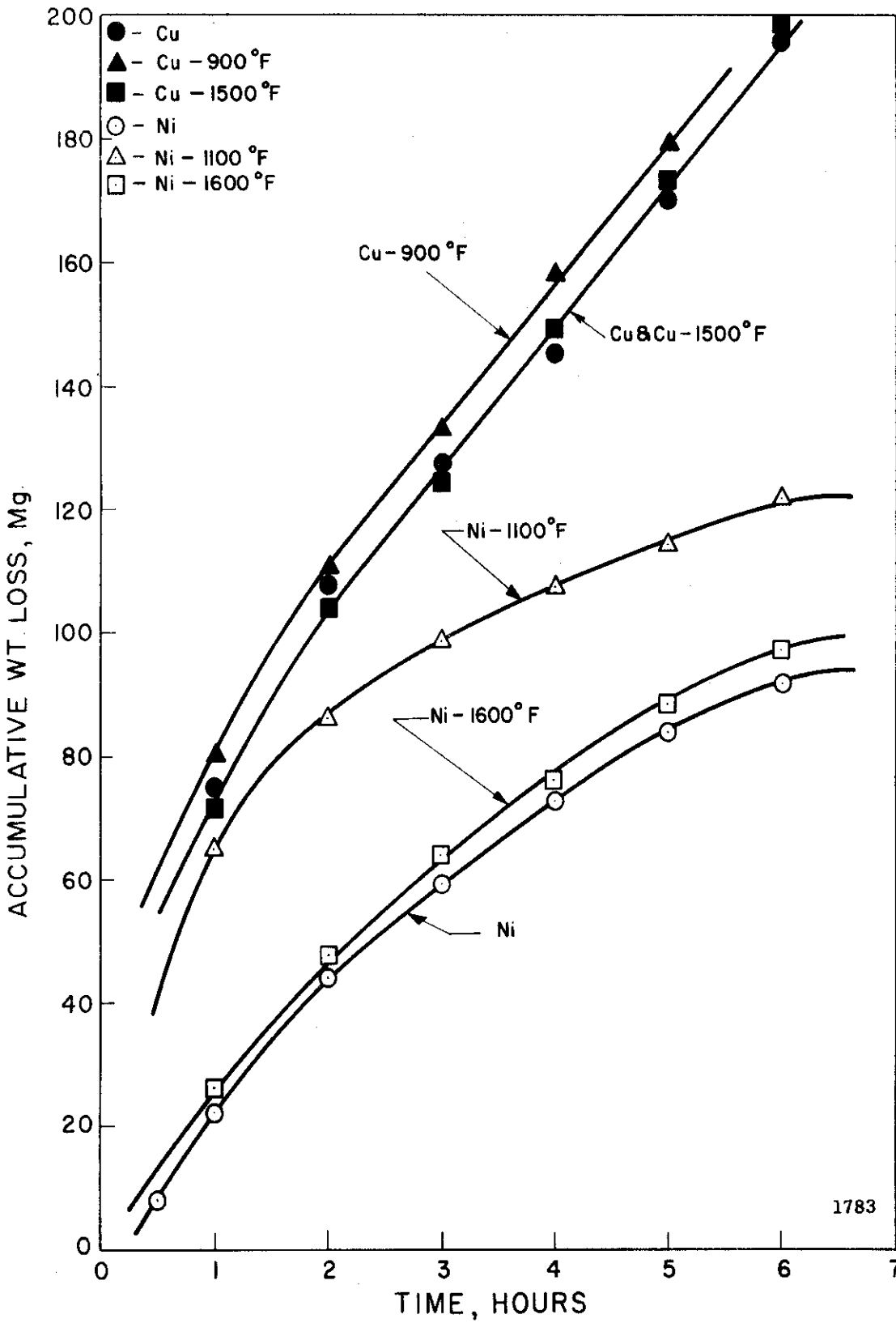
Fig. 42.--Effect of cavitation test duration on weight loss at 70°F in water - Cu and Ni (subset three).
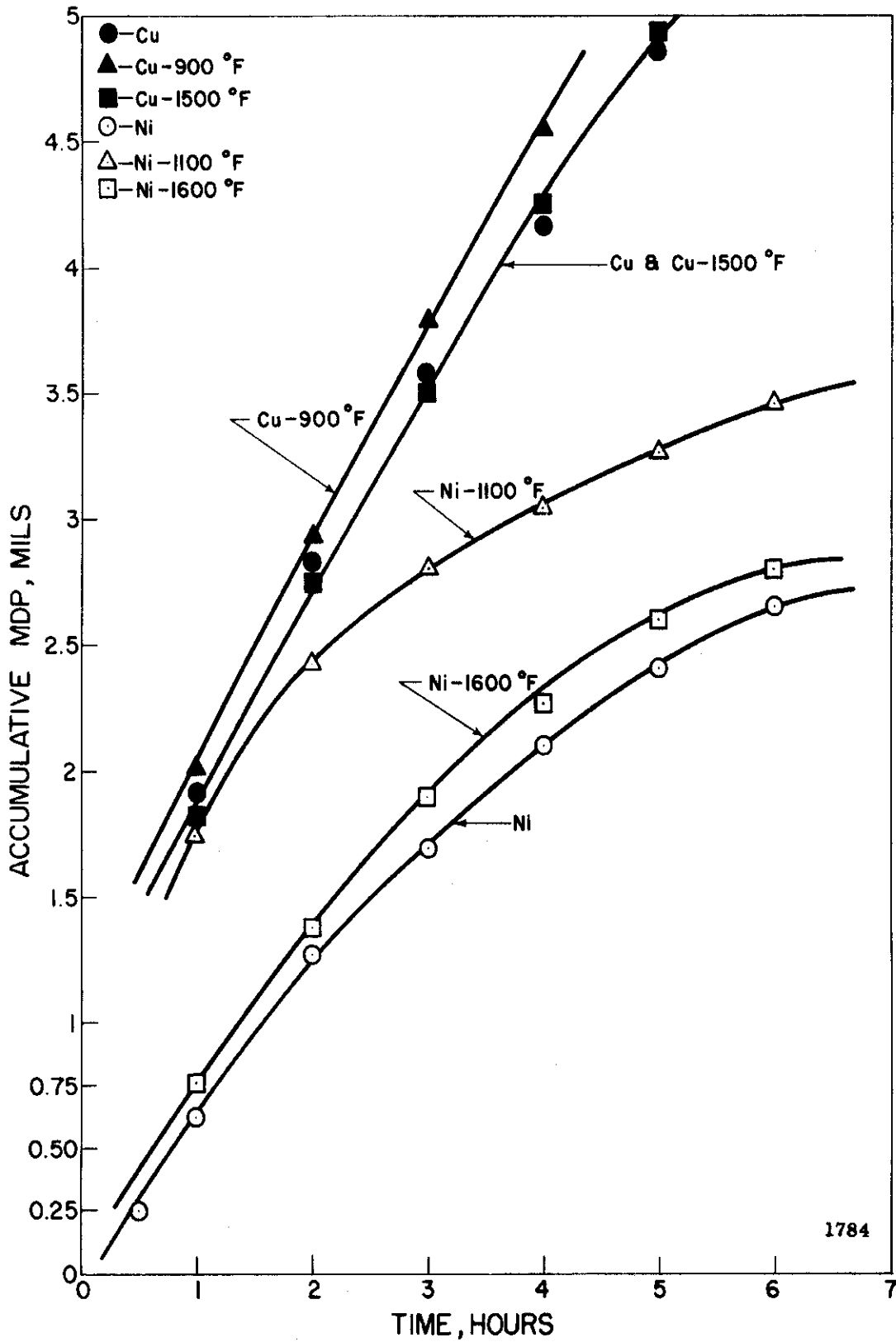
Fig. 43.--Effect of cavitation test duration on MDP at 70°F in water - Cu and Ni (subset three).
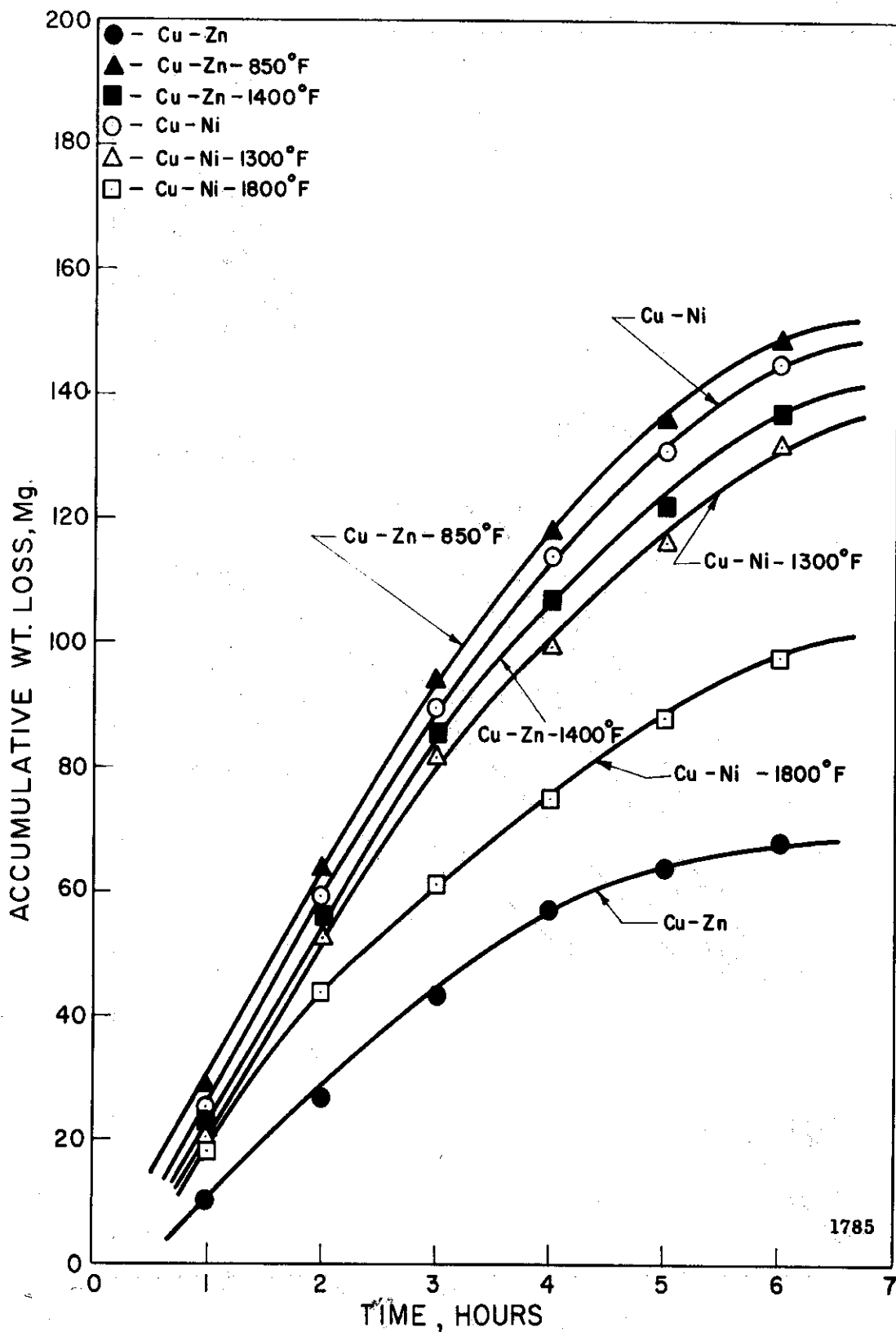
Fig. 44.--Effect of cavitation test duration on weight loss at 70°F in water - Cu-Ni and Cu-Zn (subset three).
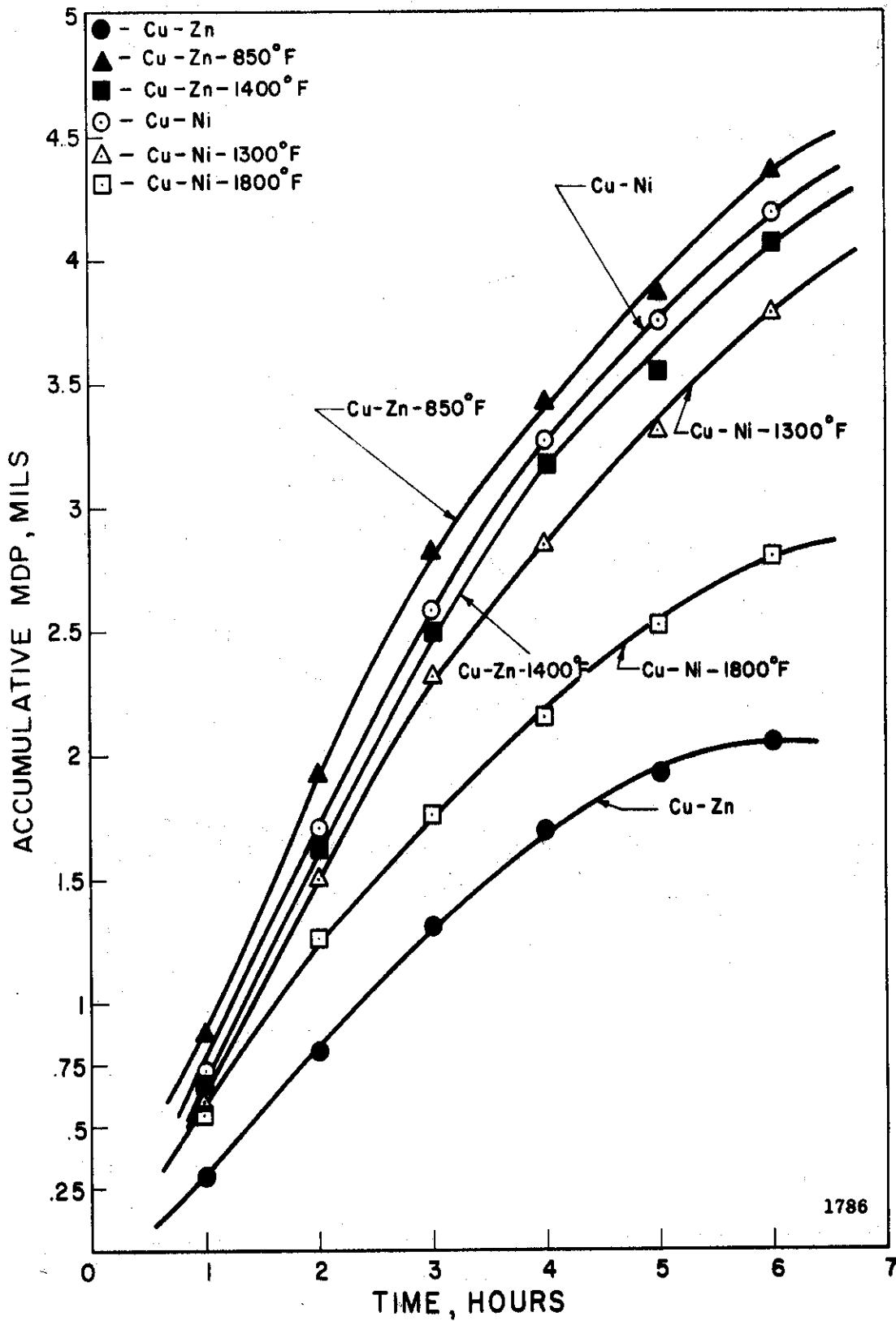
Fig. 45.--Effect of cavitation test duration on MDP at 70°F in water - Cu-Ni and Cu-Zn (subset three).

temperature heat-treat ranked second and the low-temperature heat-treat
was last. Identical rankings apply to the three Cu-Zn specimens and the
three Ni specimens. For Cu-Ni the high-temperature heat-treated speci-
men was the most cavitation resistant followed by the low-temperature
heat-treated material and the cold-worked specimen in that order.

An examination of Figures 42, 43, 44, and 45 indicates that the
rate of erosion for the materials contained in subset three is generally
not constant beyond about 2 mils MDP. This is presumed due to the pat-
tern of the surface damage which is again characterized by heavy, iso-
lated, deep pitting, even very early in the test. This preferential
damage of the surface may be caused by non-uniformity of applicable
mechanical properties. However, it is curious that for materials as
stainless steel, the character of the damage in lead-bismuth or mercury
is a uniform distribution, while in water it is composed of the previ-
ously discussed deep, isolated pitting. This lack of similarity in dam-
age pattern may be due to the fact that the NPSH has not been modeled
between tests, and similarity of "flow regime" would then not occur.
One manifestation of the difference in flow regimes encountered is the
occurrence of a star pattern of bubble cloud as opposed to the uniform
bubble cloud observed on other occasions.[60] No theoretical explanation
for predicting these observed flow patterns yet exists.

Typical photographs of the test specimens in subset three at the
conclusion of the cavitation experiment are presented in Figure 46.
Note the heavy, isolated deep pitting that has developed.

In all of the tests conducted in water, only the hot-rolled
carbon steel specimen showed definite visual indications of having

Cu(60% cold-worked)(U-M)
6 Hour Exposure
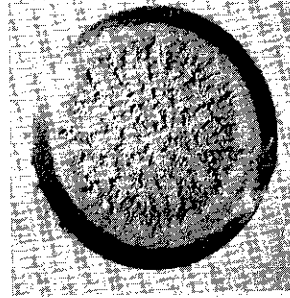
Ni(75% cold-worked)(U-M)
6 Hour Exposure

Cu-Ni(1300°F anneal)(U-M)
6 Hour Exposure
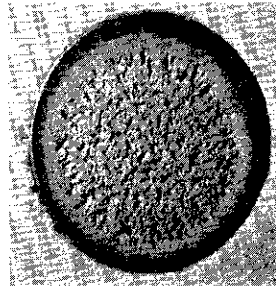
Cu-Zn(1400°F anneal)(U-M)
6 Hour Exposure

Fig. 46.--Photographs of selected specimens subjected to cavitation damage in water at 70°F - subset three.

1787

suffered corrosion damage. Hence, the results quoted for this material reflect damage caused both by the corrosion and erosion components. All other results can be attributed solely to the cavitation-erosion mechanism.

4. Comparison with Venturi Facility Water Results

Cavitation data from the venturi facility operated by this laboratory was previously obtained for all of the materials that were tested in the ultrasonic facility in water. Hence, as was the case in mercury at 70°F, it is now possible to qualitatively compare the data from both facilities and hopefully be able to eventually arrive at a quantitative relationship coupling the results. Table 15 is a tabulation of the data available in water for the two facilities for the materials contained in subsets one and two. Table 16 is a similar tabulation for the materials contained in subset three, namely the Cu, Cu-Ni, Cu-Zn, and Ni alloys. The wear in the venturi loop is given in terms of MDP after 50 hours of testing, whereas in the case of the acoustic facility, the average MDP rate is listed. The stainless steels tested in the two facilities are comparable as are the T-111 and the Ta-8W-2Hf. The T-222 and the Ta-10W are similar as are the carbon steels. The remainder of the materials investigated in both facilities are nearly identical in composition.

In Table 15, the materials have been listed in order of decreasing cavitation resistance, or increasing susceptibility to cavitation erosion attack for both facilities. A certain amount of agreement is

  -148-

TABLE 15

COMPARISON OF CAVITATION EROSION DATA IN WATER AT 70°F -
VENTURI AND ULTRASONIC FACILITIES
(SUBSETS ONE AND TWO)

Venturi Data		Ultrasonic Data	
Material	MDP at 50 Hours	Material	Avg. MDP Rate
Cb-1Zr	3.50×10^{-3} mils	T-222	.02 mils/hr.
Stainless Steel	5.27×10^{-3}	T-111	.06
		Mo-1/2Ti	.09
Ta-8W-2Hf	7.62×10^{-3}	316 SS	.09
Ta-10W	11.11×10^{-3}	304 SS	.10
Cb-1Zr(A)	20.29×10^{-3}	Cb-1Zr	.15
Plexiglas	$67.25 \times 10^{-3*}$	Cb-1Zr(A)	.18
Mo-1/2Ti	99.72×10^{-3}	Carbon Steel	.23
Carbon Steel	769.2×10^{-3}	2024 Al	.57
2024 Al	1618×10^{-3}	6061 Al	.72
6061 Al	1976×10^{-3}	Plexiglas	1.39
1100-0 Al	2451×10^{-3}	1100-0 Al	2.70

*MDP at 4 hours.

TABLE 16

COMPARISON OF CAVITATION EROSION DATA IN WATER AT 70°F -
VENTURI AND ULTRASONIC FACILITIES
(SUBSET THREE)

Material	Venturi MDP at 50 Hours		Ultrasonic MDP Rate	
Cu-Zn	39.77×10^{-3} mils	(12)	.38 mils/hr.	(1)
Ni	14.85×10^{-3}	(5)	.44	(2)
Cu-Ni-1800°F anneal	8.58×10^{-3}	(2)	.47	(3)
Ni-1600°F anneal	4.04×10^{-3}	(1)	.48	(4)
Ni-1100°F anneal	14.63×10^{-3}	(4)	.58	(5)
Cu-Ni-1300°F anneal	13.29×10^{-3}	(3)	.63	(6)
Cu-Zn-1400°F anneal	25.09×10^{-3}	(9)	.68	(7)
Cu-Ni	19.23×10^{-3}	(6)	.70	(8)
Cu-Zn-850°F anneal	25.72×10^{-3}	(10)	.72	(9)
Cu	24.29×10^{-3}	(8)	.95	(10)
Cu-1500°F anneal	27.62×10^{-3}	(11)	.95	(11)
Cu-900°F anneal	23.75×10^{-3}	(7)	1.02	(12)

noted in Table 15. In both facilities the stainless steels, the tanta-lum-base alloys, and the Cb-1Zr are among the most cavitation resistant materials. But the rankings do not agree in detail. Among the least resistant materials, the carbon steel and the three aluminum alloys have identical rankings in both facilities. In was noted in the venturi investigations that the damage sustained by the Cb-1Zr apparently indi-cated a thin laminated structure which could lead to erroneous results in this case. Note also the anomalous position of Plexiglas which is relatively much more resistant in the venturi than in the ultrasonic facility. Also note that the damage rate is about 100 times as great in the ultrasonic facility (water tests) as compared to a factor of about 1000 in the mercury tests, but that the range of difference encountered in the venturi is about 10 times that in the ultrasonic facility (water tests) as compared to a factor of about 100 in the mercury tests. The reasons given in the discussion of the mercury tests are probably also applicable here.

The results presented in Table 16 for the Cu, Cu-Ni, Cu-Zn, and Ni alloys agree only in a few respects. The rather general disagreement noted for this data subset cannot be fully explained at this time. How-ever, it is noted that the damage rates for these materials differ by a much smaller factor than for those previously discussed (only about a factor of 3 for the ultrasonic tests and a factor of 10 for the ven-turi), so that an upsetting of the ranking order would involve much smaller errors in damage rates. For these materials it would be expected that corrosion would play little part in either facility so

that this may have prevented the range between materials from differing

as widely as in the other cases.

F. Cavitation Studies in Lithium at 500°F and 1500°F

1. Experimental Procedure

The seven materials tested in lithium at 500°F and 1500°F

were 304 stainless steel (U-M), 316 stainless steel (U-M), T-111

(P & W), T-222(A) (P & W), Mo-1/2Ti (P & W), Cb-1Zr (P & W), and

Cb-1Zr(A) (P & W). Standard cavitation test specimens, as shown in

Figure 6, were machined from available bar stock. The required dimen-

sions "A" and "B" for the seven materials are listed in Table 4. These

dimensions provide a standard specimen weight of 9.4 ± 0.1 g.

The vapor pressure of lithium at 500°F is approximately zero,

while at 1500°F it is nearly 0.1 psia. As a result, the argon cover gas

was maintained over the molten lithium throughout the tests at an over-

pressure of 1.1 psig for the 500°F tests and at 1.2 psig for the 1500°F

tests. This resulted in the required suppression pressure of 15.3 psia.

At 500°F, the test duration for each material was 10 hours with

the exception of the Cb-1Zr(A) which showed gross erosion after 6 hours

of testing. At frequent intervals the specimens were visually examined,

photographed, and carefully weighed. At 1500°F, total test duration was

10 hours in all cases with the exception of the T-111 which was exposed

for 30 hours. Once again, frequent inspections and weighings were made.

The lithium used in these investigations was obtained from the

Lithium Corporation of America, Inc. (Bessemer City, North Carolina) in

the form of individual ∿ 1/2 pound cylindrical ingots sized to fit into the cavitation vessel and fill it, upon melting, to the desired level. The ingots were packaged and hermetically sealed in individual tin cans, which were easily opened for charging the lithium into the experimental vessel. The solid ingot was first placed in a clean stainless steel beaker which fit snugly into the cavitation vessel and provided for easy removal and disposal at the conclusion of a test. The loading operation was carried out at room temperature (where oxidation would be at a minimum rate) in a glove box under an argon atmosphere. The sealed vessel was then removed from the glove box and placed in the furnace where the lithium was brought to the required test temperature of 500°F or 1500°F. Each test was conducted with a new, fresh lithium ingot in a new, unused stainless steel beaker. This procedure eliminated the need for transferring the molten lithium to and from the experimental vessel and eliminated trace heaters, line heaters, hot traps, cold traps, valves, etc., from the system design. This procedure resulted in a very economical design and kept oxide contamination relatively uniform and at a minimum, since a fresh ingot was used for each test.

At the conclusion of each 500°F investigation, the vessel was removed from the furnace and quickly air-cooled to a temperature of about 375°F, which is slightly above the melting point of 362°F, and below the ignition temperature of 392°F. With the lithium at 375°F, the vessel top plate was unbolted, and the ultrasonic transducer and specimen were quickly removed from the molten lithium while maintaining the argon cover gas over the test fluid. The vessel was then covered

and the lithium allowed to solidify in the stainless steel beaker. The beaker and used ingot were then easily removed from the vessel and discarded. The next run made use of a new clean stainless steel beaker and a fresh lithium ingot.

After solidification, any excess lithium adhering to the test specimen and the exponential horn was easily removed by dipping the end of the transducer into a large container of cold water placed outdoors. The reaction of lithium with water under these conditions was not very vigorous and resulted in complete removal of the excess lithium metal in a few minutes. The test specimen was then removed from the tip of the transducer and weighed.

At the conclusion of a 1500°F test the cavitation vessel remained in the furnace until it had cooled to 500°F. Then it was removed and air-cooled until the lithium temperature reached the required 375°F at which point the specimen was removed.

This complete procedure of ingot loading, unloading, and specimen retrieval was found to be completely safe and was carried out more than 50 times without incident. Personnel wore suitable protective clothing during the unloading and specimen retrieval operations.

2. Experimental Results at 500°F

The cavitation results obtained at 500°F in lithium will be displayed as accumulative weight loss versus test duration, and also as accumulative mean depth of penetration (MDP) versus test duration.

Table 17 summarizes the cavitation results obtained in lithium at 500°F. Figure 47 is a plot of accumulative weight loss versus test

TABLE 17

SUMMARY OF CAVITATION RESULTS IN LITHIUM AT 500°F

Material	Avg. Wt. Loss Rate	Average MDP Rate
T-111 (P & W)	1.70 mg./hr.	0.03 mils/hr.
T-222(A) (P & W)	2.48	0.04
Mo-1/2Ti (P & W)	4.61	0.12
Cb-1Zr (P & W)	5.02	0.15
304 SS (U-M)	10.42	0.34
316 SS (U-M)	10.91	0.36
Cb-1Zr(A) (P & W)	33.70	1.00
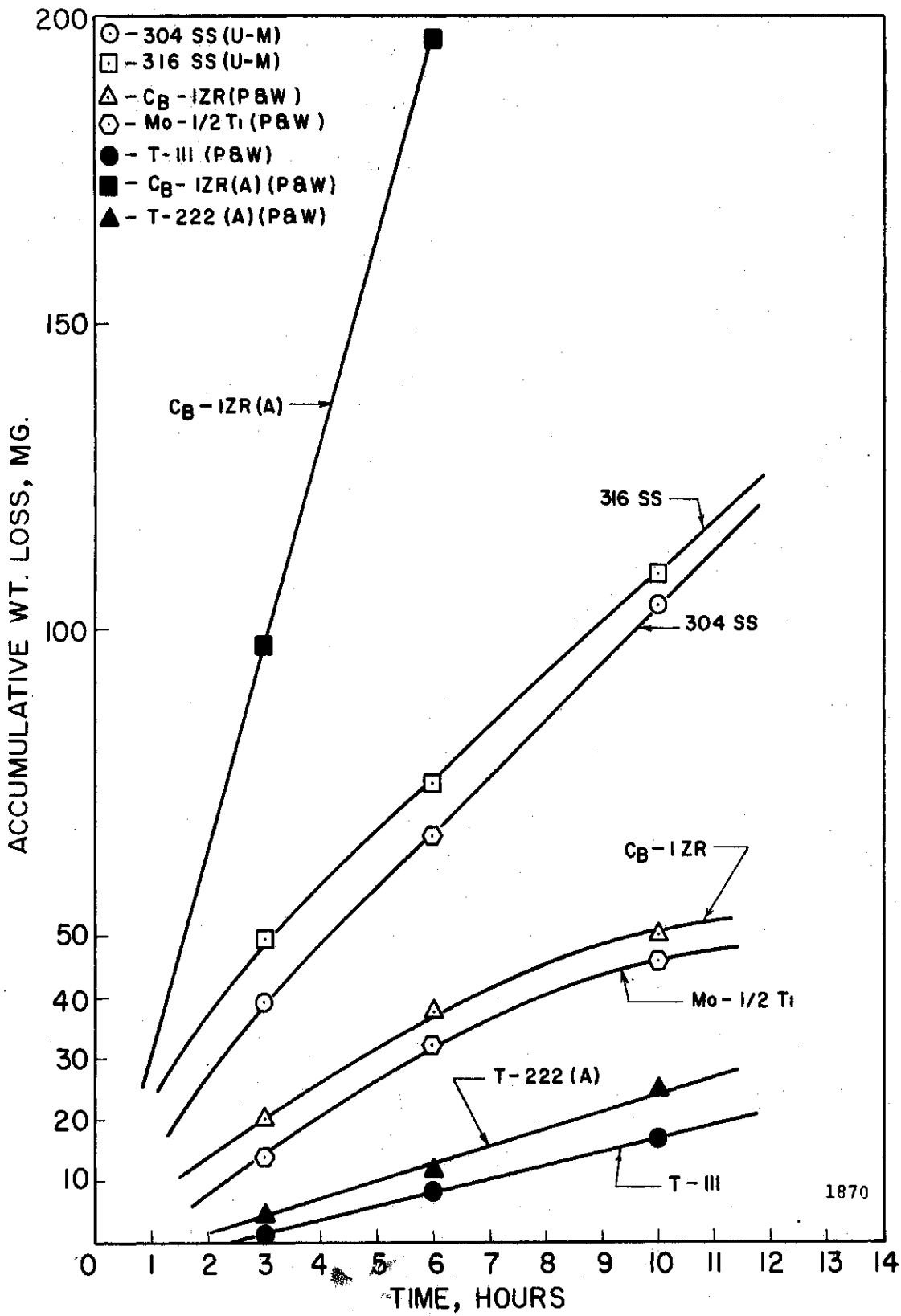
Fig. 47.--Effect of cavitation test duration on weight loss at 500°F in lithium.

duration, while Figure 48 is the corresponding plot of accumulative MDP versus test duration for the seven materials tested.

On the basis of either average weight loss rate or average MDP rate it is clear that the T-111 is the most cavitation resistant of the materials tested, while the T-222(A) is about 30% less resistant. These materials exhibited average MDP rates of 0.03 mils/hour and 0.04 mils/ hour, respectively. The refractory materials, Mo-1/2Ti and Cb-1Zr, rank third and fourth, respectively, with average MDP rates of 0.12 mils/hour and 0.15 mils/hour, respectively. The 304 stainless steel and 316 stainless steel were about equally resistant but suffered 11 times to 12 times the damage incurred by the T-111. The Cb-1Zr(A) was the least resistant to cavitation damage of the materials tested with an average MDP rate of 1.00 mils/hour, approximately 33 times greater than the rate of damage exhibited by the T-111. It is clear from Figures 47 and 48 that the rate of erosion for each individual material is approximately constant for most of the test. In some cases, the rate of damage is not constant in the early part of the test due to lack of temperature equi-librium of the ultrasonic transducer and the smooth surface of the specimen face which appears to prevent maintenance of a stable bubble cloud. In some cases the rate of damage decreases with increasing test duration. This is probably due to a decrease in the number of bubbles generated by some types of roughened surfaces,[59] as has been discussed in relation to the other fluids. Except for Cb-1Zr and Mo-1/2Ti, the rates are fairly constant from about 1 to 4 mils MDP, which is reason-ably consistent with the other low density fluid tested, i.e., water.
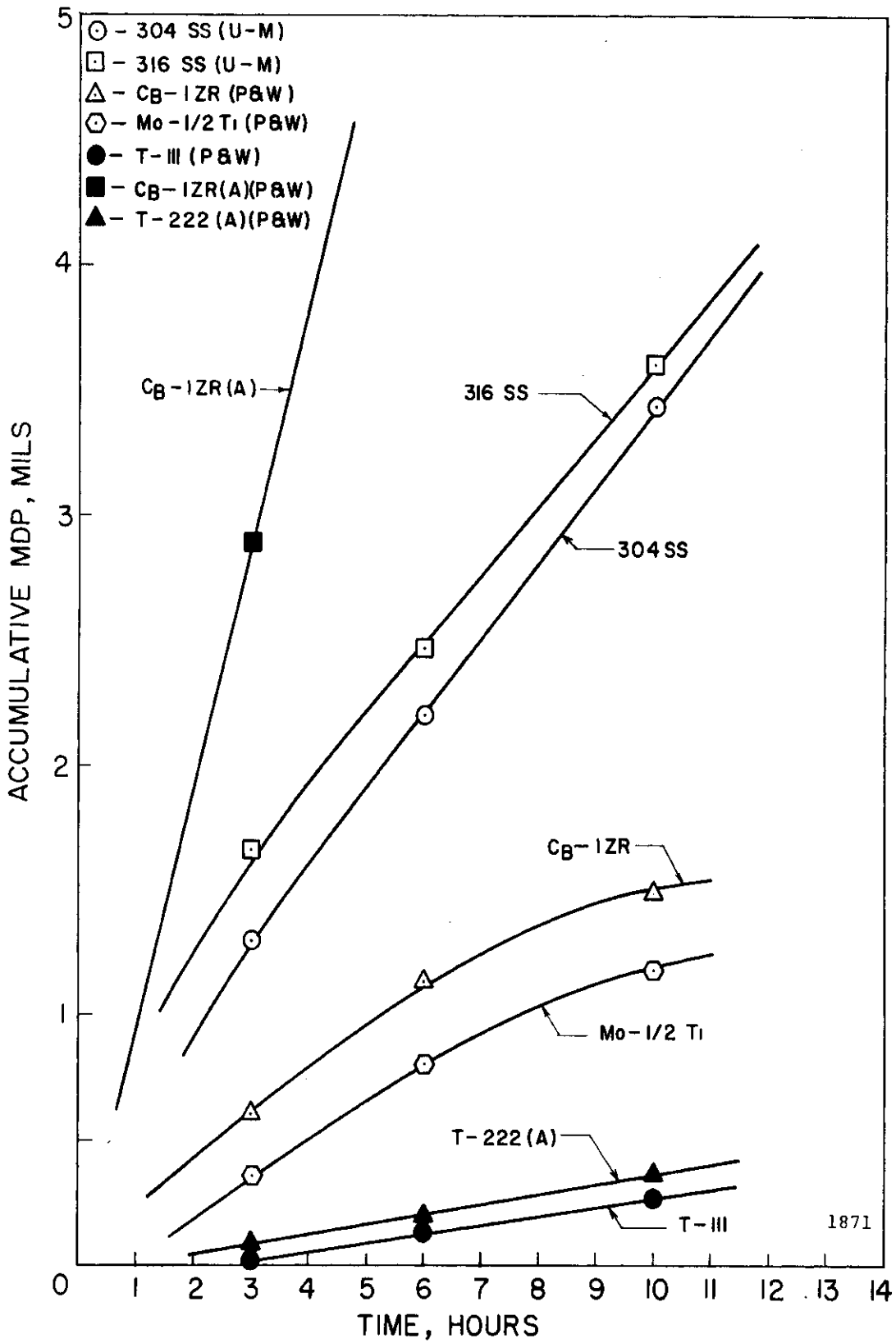
Fig. 48.--Effect of cavitation test duration on MDP at 500°F in lithium.

The high-density fluids showed constant rates over a much greater MDP

range, as was previously mentioned.

Photographs of the test specimens at the conclusion of the cav-

itation experiment are presented in Figure 49. The materials are

arranged in order of decreasing resistance to cavitation damage. Note

the very heavy pitting suffered by the Cb-1Zr(A), 304 stainless steel,

and 316 stainless steel.

As opposed to the other fluids, the damage is substantially con-

centrated at the central portion of the specimen with a large outer rim

nearly undamaged (a small undamaged outer rim has been noted for all

fluids). It is thought that the lack of damage in the outer annular

ring is due to "end effects" which create vortex action[61,62] near the

edge of the vibrating horn. This results in higher pressures adjacent

to the horn in this region and, hence, fewer bubbles. That these con-

ditions are apparently much more pronounced with the lowest density

fluid (lithium) is believed due to the large suppression head (NPSH)

values used for this fluid. The damage suffered by the other specimens

is somewhat more uniform with the exception of the T-111. However, the

undamaged outer rim is present in all cases.

It has been noted in the cavitation tests with different fluids,

all conducted at a constant suppression pressure (lead-bismuth, mercury,

water, and lithium), that the heavier fluids give quite a uniform damage

pattern. The water patterns are intermediate between the heavy liquid

metals and the lithium here observed in that for the lighter fluids the

damage tends to become concentrated toward the center and less
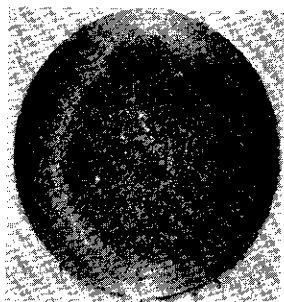
(1) T-111(P & W)

10 Hour Exposure
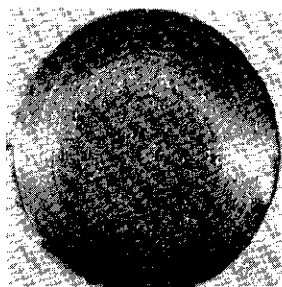
(2) T-222(A)(P & W)

10 Hour Exposure
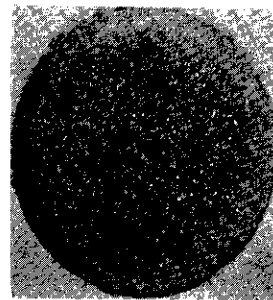
(3) Mo-1/2Ti(P & W)

10 Hour Exposure
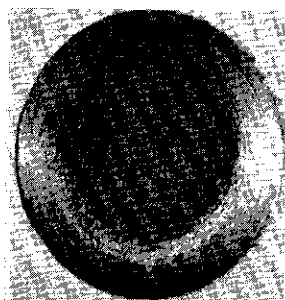
(4) Cb-1Zr(P & W)

10 Hour Exposure
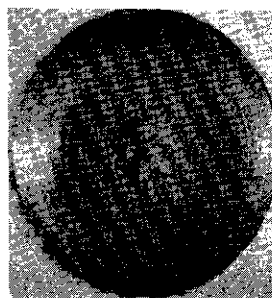
(5) 304 SS(U-M)

10 Hour Exposure
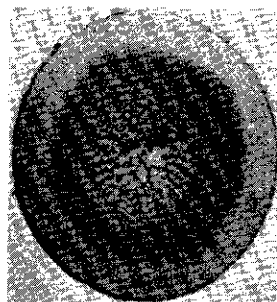
(6) 316 SS(U-M)

10 Hour Exposure
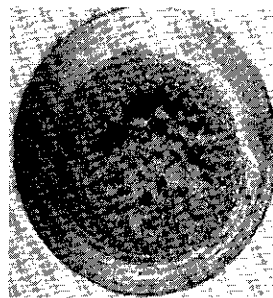
(7) Cb-1Zr(A)(P & W)

6 Hour Exposure

Fig. 49.--Photographs of specimens subjected to cavitation
damage in lithium at 500°F.

1906

pronounced on the outer edge. As mentioned above, this may be due to

the fact that NPSH is much greater for the lighter fluids than for the

heavier, since suppression pressure was constant, i.e., the "flows" are

not properly modeled (due, as already mentioned, to insufficient pres-

sure capability of the high-temperature cavitation vessel design).

Detailed examination of the 303 stainless steel exponential

horn, the 316 stainless steel beaker, and the sides of the various test

specimens, all of which are not subject to cavitation, but are submerged

in the test fluid, indicates that corrosion effects in the absence of

cavitation in these investigations were negligible, as with all the

other fluids tested, as would be expected for the short durations

involved.[63]

3. Experimental Results at 1500°F

The data obtained in lithium at 1500°F will be displayed as

accumulative weight loss versus test duration and also as accumulative

mean depth of penetration (MDP) versus test duration.

Table 18 summarizes the cavitation results obtained in lithium

at 1500°F. Only the 304 stainless steel, 316 stainless steel, T-111,

and Cb-1Zr(A) were tested at this temperature. Figure 50 is a plot of

accumulative weight loss versus test duration for the four materials

tested, while Figure 51 is the corresponding plot of accumulative MDP

versus test duration.

On the basis of either weight loss or MDP the refractory alloy

T-111 exhibited the greatest resistance to cavitation damage at 1500°F.

This was also true at 500°F. The refractory alloy Cb-1Zr(A) which

TABLE 18

SUMMARY OF CAVITATION RESULTS IN LITHIUM AT 1500°F

Material	Avg. Wt. Loss Rate	Average MDP Rate
T-111 (P & W)	0.26 mg./hr.	0.004 mils/hr.
Cb-1Zr(A) (P & W)	0.58	0.017
316 SS (U-M)	0.81	0.027
304 SS (U-M)	1.04	0.034
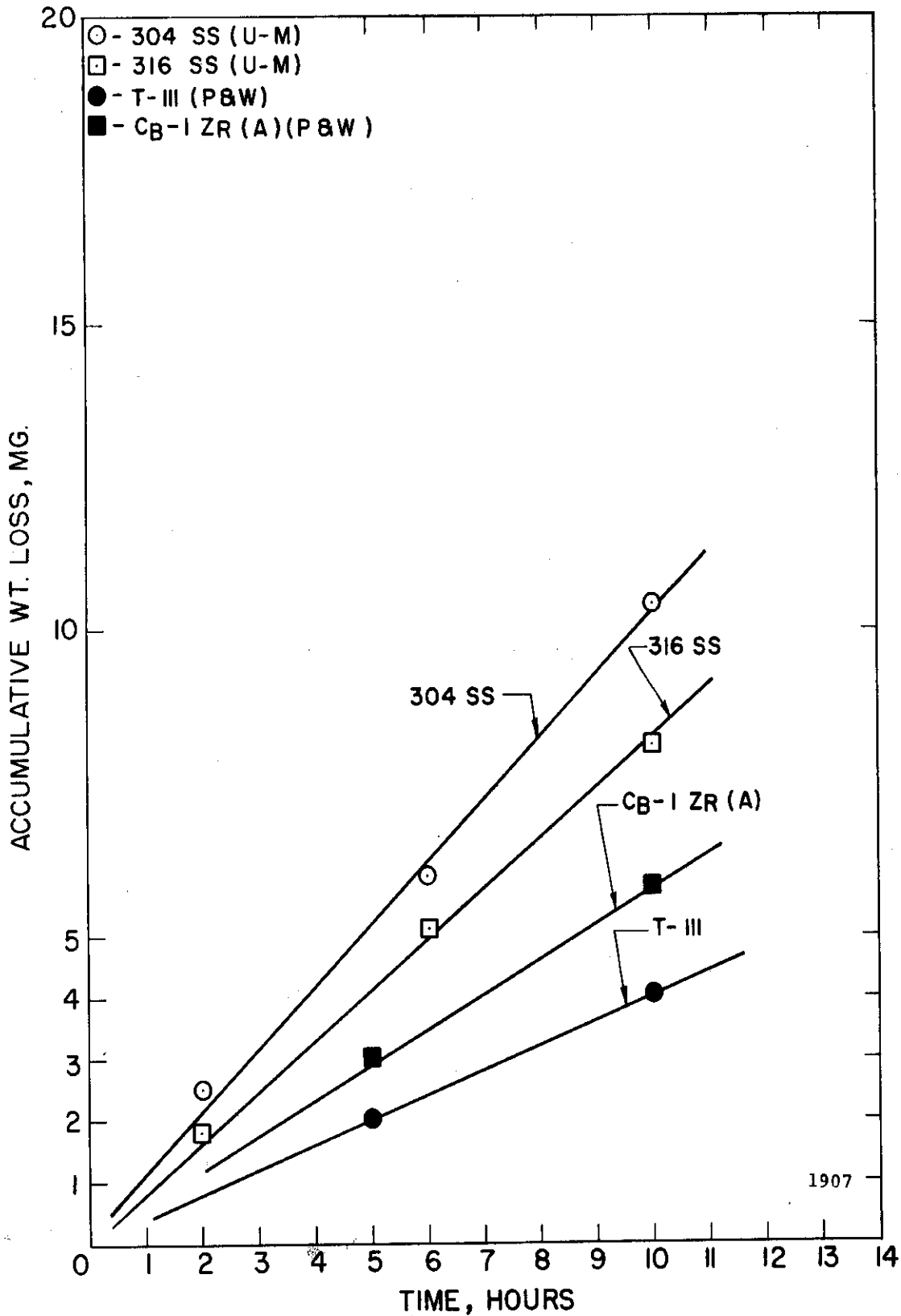
Fig. 50.--Effect of cavitation test duration on weight loss at 1500°F in lithium.
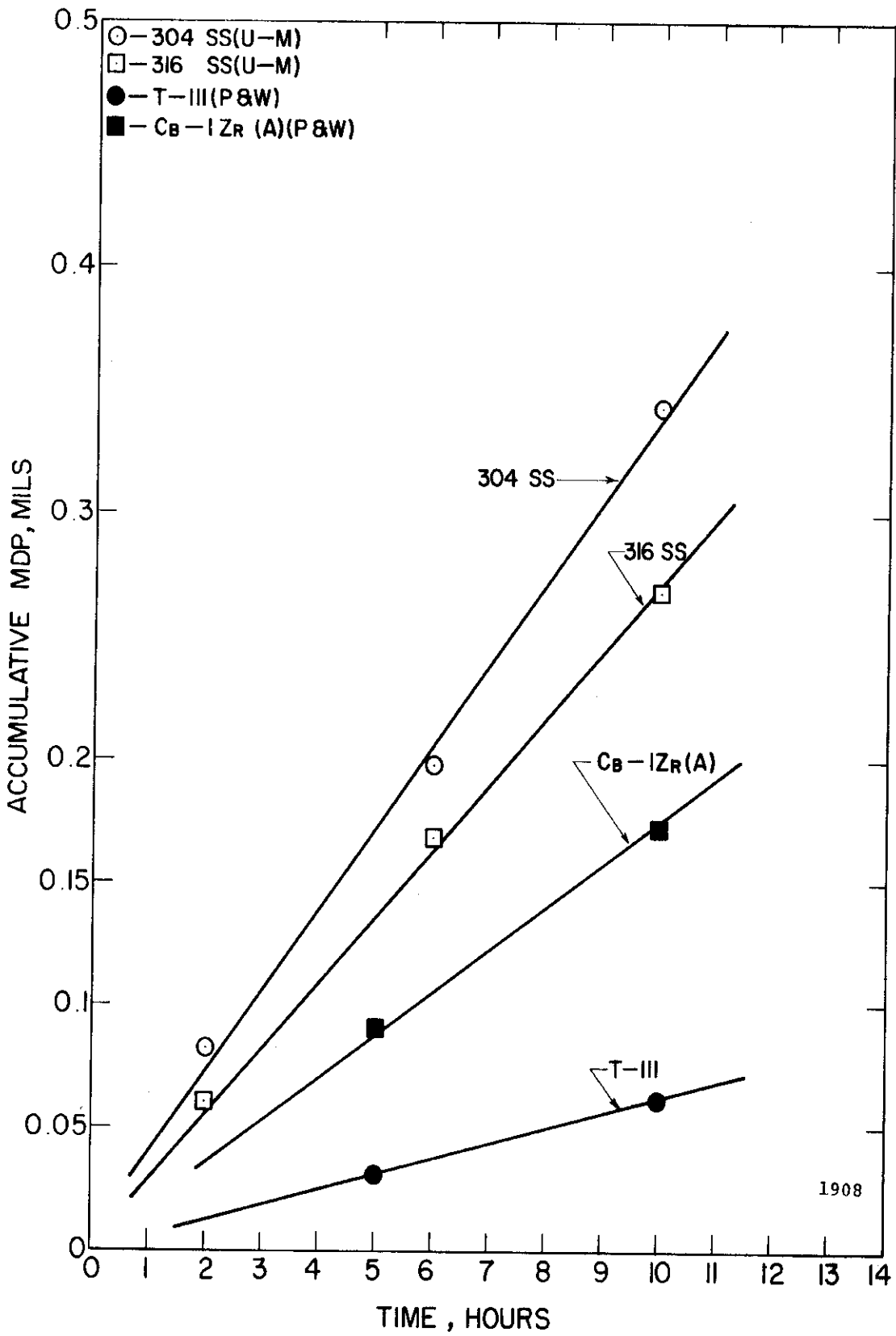
Fig. 51.--Effect of cavitation test duration on MDP at 1500°F in lithium.

suffered gross damage at 500°F and ranked last had an average MDP rate of only 0.017 mils/hour at 1500°F and ranked second. The two stainless steels were the least resistant of the four materials tested at 1500°F, as expected from mechanical properties considerations. The 316 stainless steel sustained 7 times the damage rate of the T-111 (versus a factor of about 4 in the 1500°F lead-bismuth test), whereas the 304 stainless steel exhibited 9 times the damage rate (versus about a factor of 14 in the 1500°F lead-bismuth test). It is clear from Figures 50 and 51 that the rate of erosion for each individual material was approximately constant for all the materials tested during most of the test.

Photographs of the test specimens at the conclusion of the cavitation experiment are presented in Figure 52. The materials are arranged in order of decreasing resistance to cavitation damage. Very little damage is apparent on any of the specimens.

Corrosion effects on the non-cavitated surfaces in the tests at 1500°F were negligible, as was also the case for the 500°F tests.

4. Discussion and Comparison of Results

Table 19 summarizes the cavitation data obtained in lithium at 500°F and 1500°F. The seven materials tested at 500°F and four tested at 1500°F have been rated on the basis of cavitation resistance as determined by MDP, with a rating of "1" indicating the most cavitation resistant material, while a rating of "7" at 500°F and "4" at 1500°F would denote that material most susceptible to cavitation damage at each temperature.
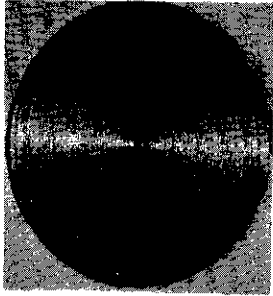
(1) T-111(P & W)

10 Hour Exposure
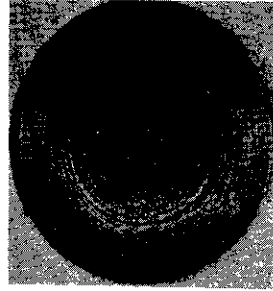
(2) Cb-1Zr(A)(P & W)

10 Hour Exposure
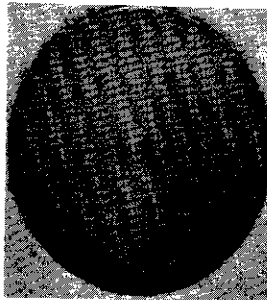
(3) 316 SS(U-M)

10 Hour Exposure
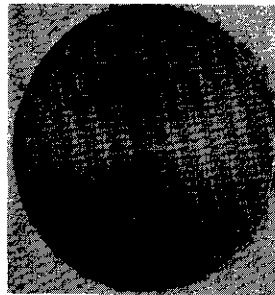
(4) 304 SS(U-M)

10 Hour Exposure

Fig. 52.--Photographs of specimens subjected to cavitation
damage in lithium at 1500°F.

1909

TABLE 19

COMPARISON OF CAVITATION RESULTS IN LITHIUM
AT 500°F AND 1500°F

Material	500°F		1500°F	
	(Avg. MDP Rate)	Rating	(Avg. MDP Rate)	Rating
T-111	0.03 mils/hr.	1	0.004 mils/hr.	1
T-222(A)	0.04	2	..	.
Mo-1/2Ti	0.12	3	..	.
Cb-1Zr	0.15	4	..	.
304 SS	0.34	5	0.034	4
316 SS	0.36	6	0.027	3
Cb-1Zr(A)	1.00	7	0.017	2

The tantalum alloys, T-111 and T-222(A), are the most resistant to cavitation damage at 500°F, while the T-111 is the most resistant at 1500°F, T-222(A) not having been tested at this temperature. The Cb-1Zr(A) which had a rating of "7" at 500°F ranked second among the four materials tested at 1500°F. The 304 and 316 stainless steel were among the least resistant materials at 500°F (although superior to Cb-1Zr(A)), but ranked last at 1500°F. Thus, the expected superior performance of the refractories at the higher temperature, due to their less temperature-dependent mechanical properties, was verified. At both temperatures, the T-111 was approximately 10 times more resistant than the stainless steels.

It is important to note that for each of the four materials tested at both temperatures the amount of damage sustained by the specimen at 1500°F was much less than that sustained at 500°F for constant testing time. The exact opposite behavior was noted in the cavitation tests conducted earlier in lead-bismuth alloy[64] and mercury[42] (and reported earlier in this document) where the damage sustained by a given material at the higher temperature was greater than that measured at the lower temperature. One might expect this latter behavior due to the reduced strength of the materials at the elevated temperature. However, the variation of the fluid properties with temperature is also important and must be considered. A recent paper by Leith[65] presents predictions of cavitation damage in a vibratory facility exposed to atmospheric pressure for liquid metals as a function of temperature for a material possessing constant mechanical properties, i.e., not a function of

temperature. Leith's interpretation of the previously available data is
that the specific gravity, vapor pressure, viscosity, and surface ten-
sion are important fluid properties which affect the amount of damage
sustained as a function of temperature. In the case of NaK, potassium,
lithium, rubidium, cesium, and sodium, Leith concludes that cavitation
damage as a function of temperature reaches a maximum at a temperature
15% to 20% up the melting-boiling range, falling off below and above
this maximum damage temperature. In the case of water, several investi-
gators[32,33,66,67,68] have reported that cavitation damage as a function
of temperature reaches a maximum at a temperature 50% up the melting-
boiling range (50°C or 122°F), falling off below and above this maximum
damage temperature. Our own laboratory has investigated this effect in
water, and the plot of cavitation damage versus temperature is presented
in Figure 53. The maximum occurs at approximately 50°C, or 122°F. The
discrepancy in the position of the maximum cavitation damage may be due
to the following mechanism.[66] In the case of the water, the dissolved
air is an important factor, whereas in the liquid metals, the solubility
of most common gases is nearly zero at all temperatures. At the low
temperatures the dissolved air cushions the bubble collapse and, hence,
the cavitation damage is reduced. As the temperature is increased, the
dissolved air is driven off and this factor becomes unimportant. Then
the effect of vapor pressure becomes predominant. The damage peaks and
then begins to decrease due to the cushioning effect of the vapor which
does not have sufficient time to condense in the vibratory test. We
feel that the cushioning effect of the dissolved air in the water test
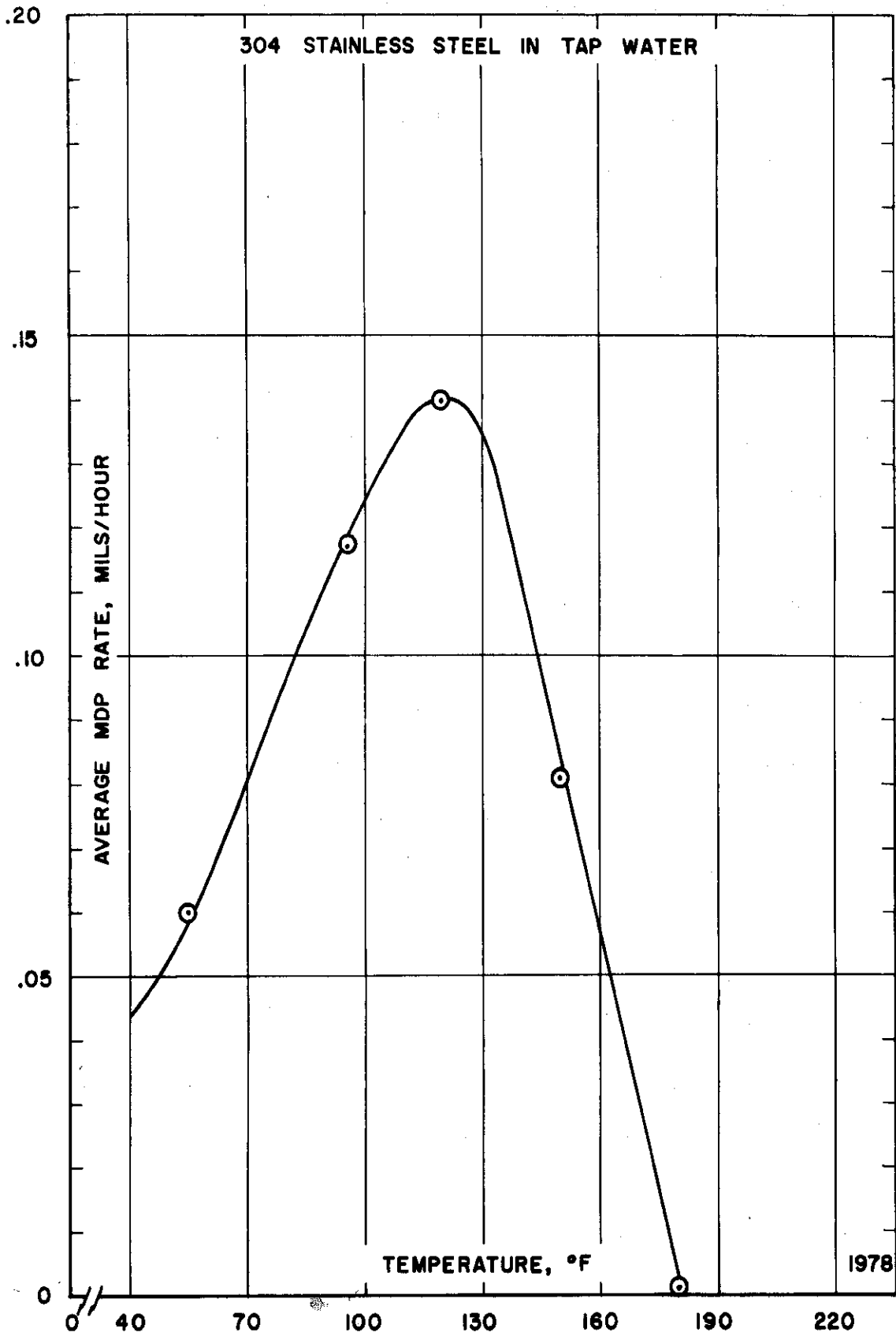
Fig. 53.--Effect of temperature on cavitation damage on water -
type 304 stainless steel specimen.

results in the maximum damage occurring at a temperature further up the melting-boiling range, as opposed to the liquid metal tests where this mechanism is negligible.

The mechanical properties of several refractory alloys, such as T-111, T-222(A), Mo-1/2Ti, and Cb-1Zr, tested in our investigations are very weak functions of temperature, and Leith's analysis would apply more closely to these than to the stainless steels.

It is our present feeling that the trend in the lithium results can be explained primarily on the basis of cavitation "thermodynamic effects," as follows. At 1500°F the vapor pressure of lithium is many times greater than at 500°F. When the cavitation bubbles collapse at the higher temperature, the heat of condensation from the condensing vapor trapped within the bubble must be conducted into the surrounding fluid. If this does not occur rapidly enough, then the uncondensed vapor serves to cushion the bubble collapse with a resultant decrease in collapse pressures and reduced damage to the test specimens. This effect was not operative in the lead-bismuth tests since the vapor pressure was essentially nil even at 1500°F.

5. Temperature Dependence of Cavitation
   Damage in Lithium

As previously mentioned, the damage suffered by all materials tested at 1500°F in lithium was less than the corresponding damage measured at 500°F. To obtain further information on this somewhat surprising result, the temperature dependence of cavitation damage in our vibratory rig in lithium for a few selected materials over the range

from 500°F to 1500°F was investigated. The 304 stainless steel, T-111, and Cb-1Zr(A) were chosen for this purpose. The mechanical properties of the 304 stainless steel vary greatly over this temperature range, and the predictions of Leith[65] would not be expected to apply without introducing corrections for this effect. The mechanical properties of the refractory materials, T-111 and Cb-1Zr(A), are weak functions of temperature, so that their behavior should more clearly illustrate the effects of fluid property changes over this temperature range.

Cavitation damage data for 304 stainless steel was obtained at 400°F, 500°F, 700°F, 900°F, 1100°F, 1300°F, and 1500°F using the experimental procedure previously discussed. Total test duration at each temperature was 10 hours. Table 20 summarizes the data obtained. Figure 54 is a plot of average weight loss rate versus test temperature, while Figure 55 is the corresponding plot of average MDP rate versus test temperature. The damage rate reaches a maximum at approximately 500°F and decreases thereafter, presumably due to the thermodynamic effects mentioned previously. The shape of the curve is similar to Leith's plot[65] of cavitation damage versus percent of the melt-boil range of lithium. Leith's prediction for lithium is shown in Figure 55 as a dashed curve. The difference between Leith's curve and the experimental data between 500°F and 1500°F is in the wrong direction to be explained by his assumption of constant mechanical properties for the test materials.

Similar experimental data was obtained for T-111 and Cb-1Zr(A) at 500°F, 1000°F, and 1500°F. Total test duration at each temperature was 10 hours. Table 21 summarizes the data obtained, while Figures 56

TABLE 20

EFFECT OF TEMPERATURE ON CAVITATION DAMAGE -
304 STAINLESS STEEL

Temperature	Avg. Wt. Loss Rate	Avg. MDP Rate
400°F	7.23 mg./hr.	0.24 mils/hr.
500	10.42	0.34
700	5.39	0.18
900	2.88	0.10
1100	1.50	0.05
1300	1.21	0.04
1500	1.04	0.03
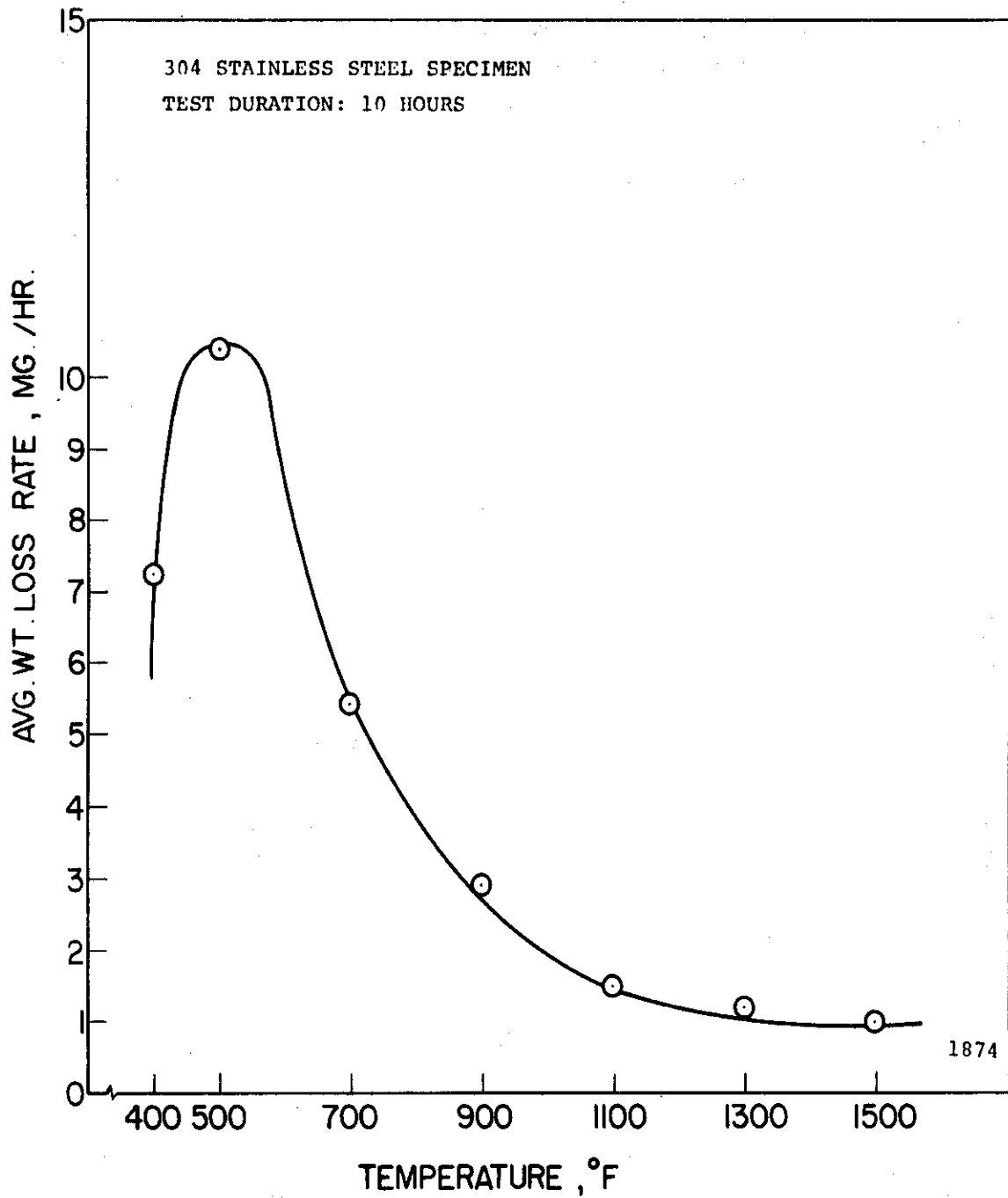
Fig. 54.--Effect of temperature on average weight loss rate for 304 stainless steel.
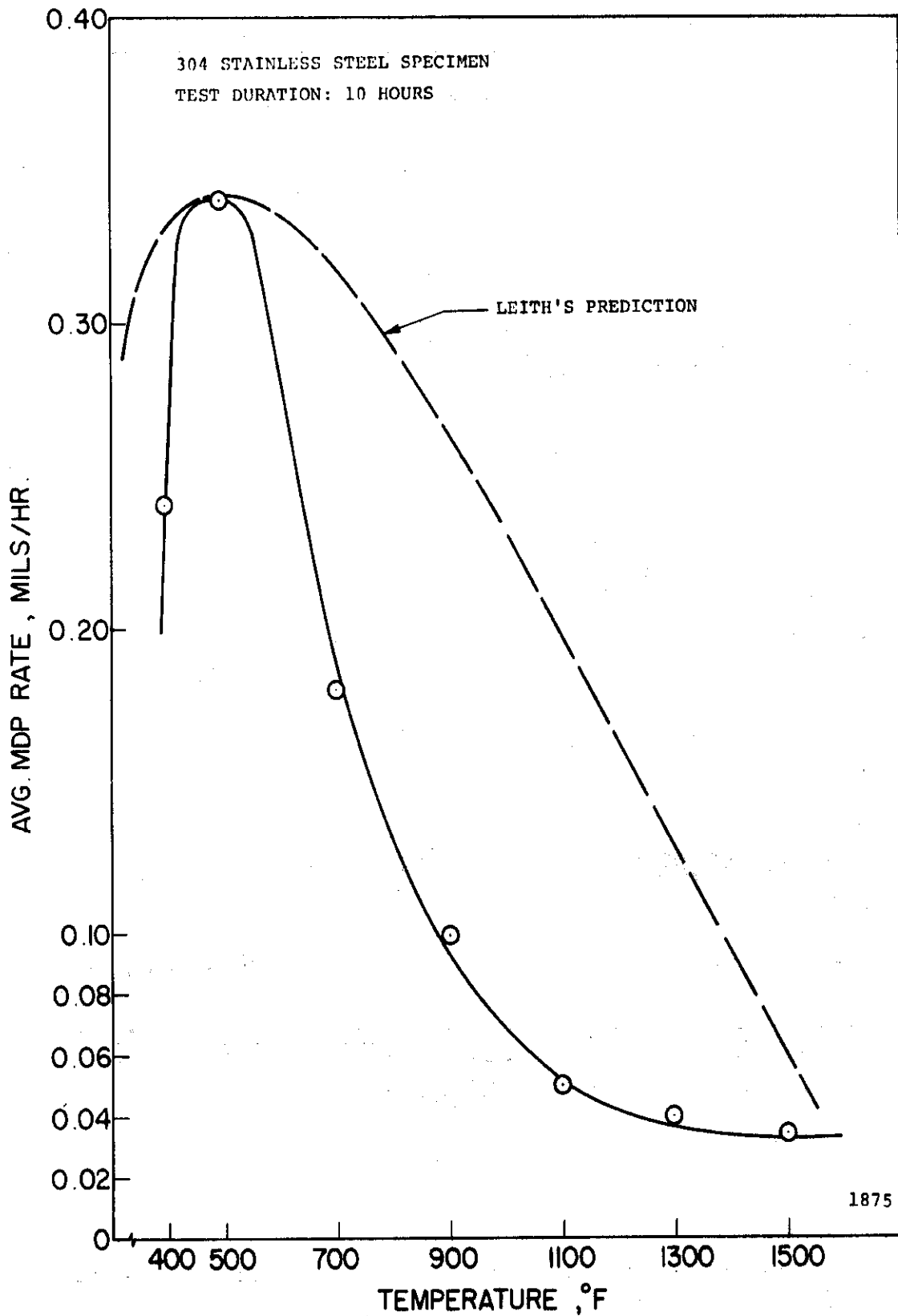
Fig. 55.--Effect of temperature on average MDP rate for 304 stainless steel.

TABLE 21

EFFECT OF TEMPERATURE ON CAVITATION DAMAGE -
T-111 AND Cb-1Zr(A)

Material	Temperature	Avg. Wt. Loss Rate	Avg. MDP Rate
T-111	500°F	1.70 mg./hr.	0.025 mils/hr.
	1000	0.61	0.009
	1500	0.26	0.004
Cb-1Zr(A)	500°F	33.70 mg./hr.	1.00 mils/hr.
	1000	8.10	0.24
	1500	0.58	0.02
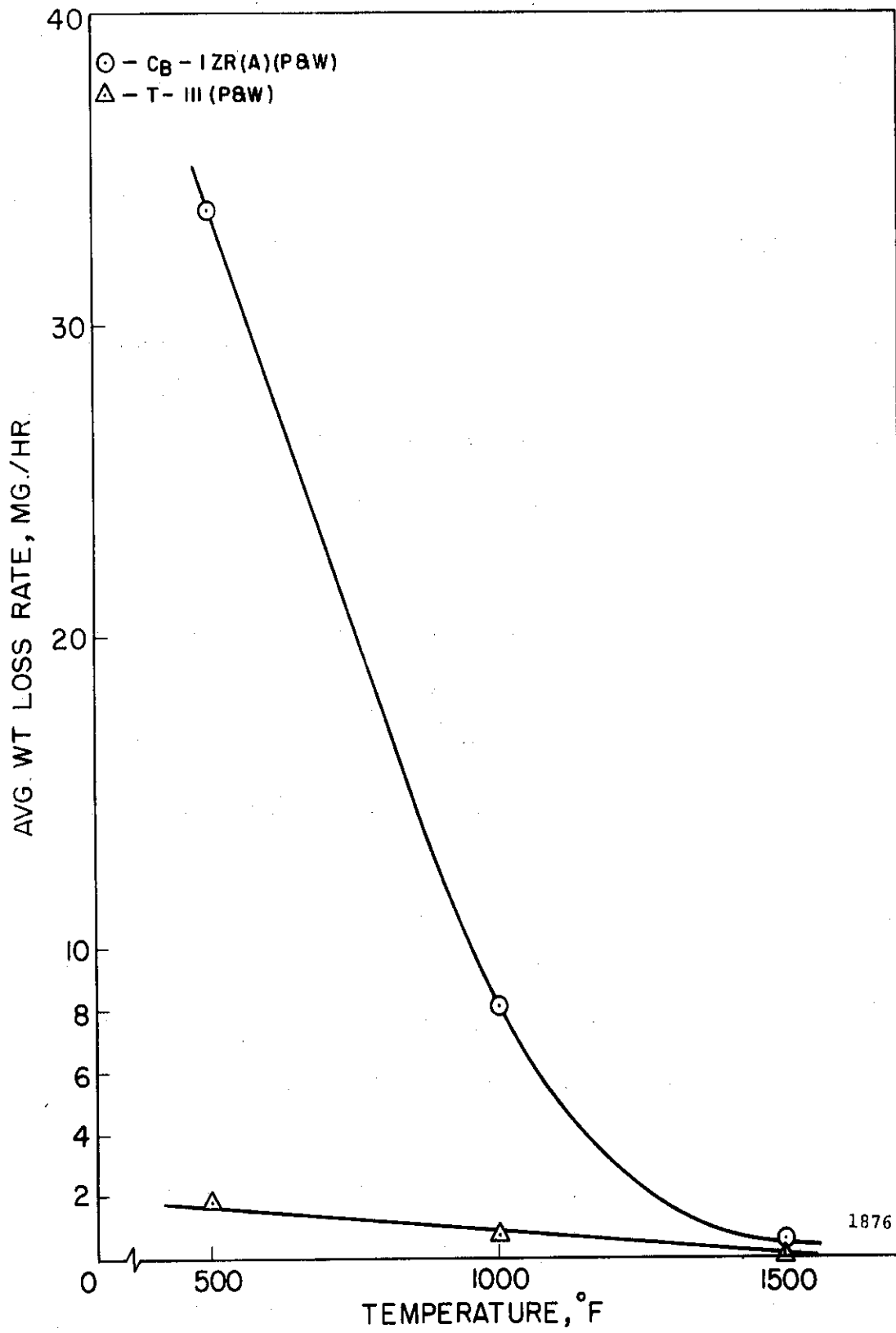
Fig. 56.--Effect of temperature on average weight loss rate for T-111 and Cb-1Zr(A).

and 57 are plots of average weight loss rate versus temperature and average MDP rate versus temperature, respectively, for the T-111 and Cb-1Zr(A). Leith's prediction for lithium is also shown in Figure 57 as a dashed curve. The T-111 damage rate decreases by a factor of 7 from 500°F to 1500°F, while the Cb-1Zr(A) damage rate decreases by a factor of approximately 60 over the same temperature range. A very large decrease in damage in sodium tests in a similar facility over the same temperature range is reported by Hydronautics,[37,38] although in their tests stainless steel appeared very much superior to the refractories at 1500°F. This is, of course, inconsistent with the mechanical properties of these materials (see Chapter IV).

6. Oxygen Analyses

Five lithium ingots were sent to the General Atomic Division of General Dynamics Corp. in San Diego, California, for an analysis of Li_2O in lithium. Each sample was irradiated, along with an oxygen standard, for 10 seconds in a 14 Mev neutron flux of approximately 10^8 neutrons/cm.^{2}-second, and counted for nitrogen-16 induced activity on a single-channel pulse-height analyzer, using a pair of 3" x 3" NaI(Tl) scintillation crystals. The oxygen concentration was determined by comparing the intensity of the 6.13 Mev gamma-ray photopeak of N^{16} from the sample with that from the oxygen standard. Oxygen forms N^{16} by interaction with 14 Mev neutrons via the $O^{16}(n, p)N^{16}$ reaction.

Four of the ingots sent for analysis had been used in cavitation tests at various temperatures, while the fifth was an unopened can of lithium (hermetically sealed) as received from the Lithium Corporation
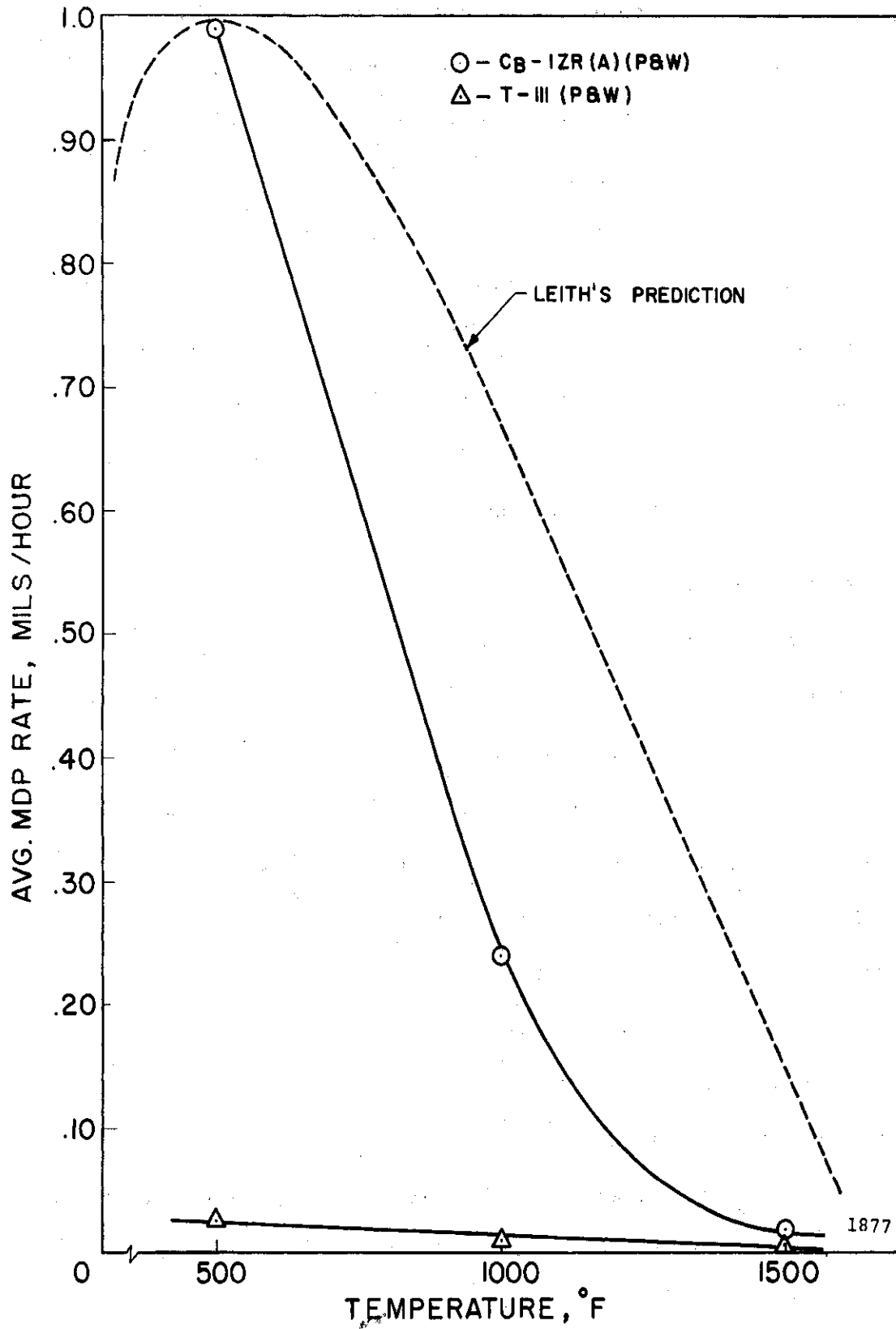
Fig. 57.--Effect of temperature on average MDP rate for T-111 and Cb-1Zr(A).

of America. A sample core was removed by General Atomic from each ingot supplied (cut from the bottom of the ingot) and analyzed. The results of the activation analysis are summarized in Table 22. The plus-or-minus values represent one standard deviation determined from counting statistics only.

The very high oxygen concentration reported for the unopened lithium ingot is quite surprising. Conceivably, it may be due to poor packaging techniques prior to the analysis, rather than a high oxygen content in the lithium as supplied. The oxygen content reported for the ingots which had been used in cavitation tests was greater than the saturation concentration of Li_2O in lithium at the highest temperature experienced by the ingot. This might suggest that excess Li_2O was formed and became entrained in the lithium. Hence, the analysis would detect both oxygen dissolved in the lithium as Li_2O and also the oxygen present in the entrained Li_2O. Alternatively, the high oxygen concentration in the used samples may result from absorption of oxygen by the solid lithium before shipping to General Dynamics, since the solid lithium ingots were exposed to the atmosphere during this period.

Since corrosion effects in the lithium cavitation tests for the short durations involved are apparently negligible,[63] it is felt that the damage rate is only slightly affected by the oxide level. Hence, no further efforts have been made to resolve the above anomalies.

G. Comparison of Mercury and Water Results at 70°F

It is interesting to compare the results obtained in mercury and water at the same test temperature of 70°F in an effort to determine

TABLE 22

SUMMARY OF OXYGEN DETERMINATIONS

Sample	Description	Oxygen Content
#1	Blank--unopened can as received from Lithium Corporation of America	1000 ± 58 PPM
#2	Ingot used in test at 500°F	3850 ± 186 PPM
#3	Ingot used in test at 1000°F	3000 ± 110 PPM
#4	Ingot used in Test at 1500°F	805 ± 110 PPM
#5	Ingot used in test at 500°F	2840 ± 100 PPM

fluid effects on cavitation damage. Table 23 summarizes the cavitation

data obtained in mercury and water at 70°F. The nine materials tested

in both fluids have been rated on the basis of cavitation resistance as

determined by the average MDP rate, with a rating of "1" indicating the

most cavitation resistant material, while a rating of "9" would denote

that material most susceptible to cavitation damage.

The following comments apply to the comparison:

1) There are several differences in the comparative ratings of the

materials in the two fluids. In mercury the stainless steels and the

tantalum-base alloys were the most resistant to cavitation damage at

this temperature and only differed in this respect by about 25%. In the

case of the water the tantalum-base alloys were the most resistant among

the materials tested, while the stainless steels suffered damage 2 times

to 5 times greater than the T-111 and T-222. The Mo-1/2Ti ranked third

in water and fifth in mercury. However, the first five rankings were

occupied by the same materials in both fluids. The Cb-1Zr, carbon

steel, Cb-1Zr(A), and Plexiglas suffered the most damage and had nearly

identical rankings in both fluids.

2) For any given material the damage suffered in mercury was 3

times to 20 times more severe than in water. Note that the comparison

is on the basis of equal static suppression pressures rather than head.

The stainless steels, in particular, suffered about 3 times as much dam-

age in mercury as in water.

3) The stainless steels were the most cavitation resistant materi-

als in mercury, while the tantalum-base alloys, T-111 and T-222, were

TABLE 23

COMPARISON OF CAVITATION RESULTS IN MERCURY AND WATER AT 70°F

Material	Mercury		Water	
	Avg. MDP Rate	Rating	Avg. MDP Rate	Rating
304 SS	.32 mils/hr.	1	.10 mils/hr.	5
316 SS	.33	2	.09	4
T-111	.35	3	.06	2
T-222	.43	4	.02	1
Mo-1/2Ti	.57	5	.09	3
Cb-1Zr	.92	6	.15	6
Carbon Steel	1.03	7	.23	8
Cb-1Zr(A)	1.61	8	.18	7
Plexiglas	3.99	9	1.39	9

far superior in water. The Plexiglas was the least resistant in both fluids, as opposed to the venturi tests where it was quite resistant in water but poor in mercury. This may indicate that materials which rely to some extent on a superior yield deflection range for their protection (as rubberized coatings and also Plexiglas in the present tests) are suitable in relatively low intensity cavitation fields but fail under more intense attack. This observation is consistent with much field experience.

It is felt that the primary cause of the greater damage suffered by all the materials in mercury as opposed to water is its much greater density. The pressure generated by bubble collapse would be proportional to the fluid density if the suppression heads seen by the bubbles were the same, since then collapse velocities would be the same. This may be approximately true in the present case since the major contribution to the suppression head at the start of collapse is the dynamic head caused by the horn motion. This portion would be the same for all tests, assuming horn motion to be unaffected by the test fluid, although the static heads differ by the density ratio since constant static suppression _pressure_ was maintained. A more definite conclusion in this regard will have to await the accumulation of more complete cavitation erosion data in a variety of fluids.

In the venturi results previously presented, it is noted that the stainless steels were the most resistant in mercury at 70°F, as is the case in the ultrasonic facility. In water the venturi results show the Cb-1Zr to be the most resistant, followed by the stainless steels.

H. Comparison of Lead-Bismuth, Mercury, and Lithium Results at 500°F

It is interesting to compare the results obtained in lead-bismuth,[64] mercury,[42] and lithium[43] at the same test temperature of 500°F in a further effort to determine fluid effects on cavitation damage.

Table 24 summarizes the cavitation results obtained at 500°F for the various materials tested in the three fluids in terms of average MDP rate. The following comments apply to the comparison:

1) The tantalum-base alloys, T-111 and T-222(A), are the most resistant in all the fluids, while the Cb-1Zr(A) is the least resistant. In fact, the order of ranking of the various materials based on ability to resist cavitation damage is quite similar for all three fluids, with only minor deviations being noted. Particularly, the stainless steels rank quite low in lithium after being only 20% to 45% less resistant than the best refractories tested in lead-bismuth and mercury.

2) The damage suffered by a given material in lead-bismuth and mercury was of the same order of magnitude for all materials. This is not surprising considering the similarity of the fluid properties. However, the amount of damage sustained in lithium was less than that measured in mercury or lead-bismuth by a factor ranging from 2 to 30. The density of lead-bismuth and mercury is about 25 times that of lithium.

In order to fully determine the effect of various fluid properties on cavitation damage, it will be necessary to conduct computer correlations involving both mechanical properties of the test materials and fluid properties of the test liquid.

TABLE 24

SUMMARY OF CAVITATION RESULTS IN LEAD-BISMUTH,
MERCURY, AND LITHIUM AT 500°F

| Material | Average MDP Rate | | | |
	Lithium	Mercury	Lead-Bismuth	Water - 70°F
T-111	0.03 mils/hr.	0.43 mils/hr.	0.72 mils/hr.	0.06 mils/hr.
T-222(A)	0.04	0.46	0.76	0.02*
Mo-1/2Ti	0.12	1.09	0.78	0.09
Cb-1Zr	0.15	2.43	1.63	0.15
304 SS	0.34	0.69	0.93	0.10
316 SS	0.36	0.63	0.88	0.09
Cb-1Zr(A)	1.00	3.73	3.54	0.18
Carbon Steel	..	0.61	..	0.23

*T-222 was tested in water at 70°F.

Table 24 also includes the cavitation data obtained in water at 70°F. Water at 70°F and lithium at 500°F have the same order of magnitude values of density and vapor pressure. Hence, comparison of the cavitation damage data obtained in the two cases may prove to be instructive. Generally, the damage obtained in lithium at 500°F is somewhat greater than that obtained in water at 70°F (T-111 is the exception), even though the density of lithium is less by a factor of two. Of course, the effect of temperature on material properties must also be considered. This would be negligible for the refractory materials, but would be important for the stainless steels. The data indicates that this is, indeed, the case, as the damage values in the two fluids for the stainless steels are most divergent.

J. Comparison of Lead-Bismuth and Lithium Results at 1500°F

The cavitation results obtained in lead-bismuth alloy and lithium at the same test temperature of 1500°F are summarized in Table 25 for purposes of comparison. Only four materials were tested in lithium at 1500°F. The following comments apply to the comparison:

1) The tantalum-base alloys, T-111 and T-222(A), are the most resistant in lead-bismuth alloy, while the T-111 is the most resistant in lithium (T-222(A) was not tested in lithium at 1500°F). The 304 stainless steel was the least resistant in both fluids.

2) The damage suffered by a given material in lead-bismuth alloy was 100 to 400 times more severe than the damage sustained in lithium. This is undoubtedly due not only to the much greater density of the

TABLE 25

SUMMARY OF CAVITATION RESULTS IN LEAD-BISMUTH
AND LITHIUM AT 1500°F

Material	Average MDP Rate	
	Lithium	Lead-Bismuth
T-111	0.004 mils/hr.	0.84 mils/hr.
T-222(A)	--	0.88
Mo-1/2Ti	--	1.08
Cb-1Zr	--	2.07
304 SS	0.034	11.30
316 SS	0.027	2.80
Cb-1Zr(A)	0.017	3.80

lead-bismuth test fluid but also to thermodynamic effects which are very

important in lithium at 1500°F, but negligible in lead-bismuth at this

temperature.

Again, further analysis is necessary to fully determine the

effect of various fluid properties on cavitation damage.

K. Cavitation Studies of Bearing Materials

1. Introduction

As mentioned previously, it has been shown both experimen-

tally[2] and theoretically[2,6] that damaging cavitation may well occur in

many high-performance bearing applications. This problem is at present

of considerable importance to the designers of the mercury space power-

plant components.[2] The objective of this portion of the present study

is the determination of the cavitation-erosion characteristics of sever-

al selected bearing materials in mercury at 500°F, since this informa-

tion is of considerable present technological value as well as increas-

ing the scope of the general information gathered in this laboratory

relating cavitation damage resistance to material and fluid properties.

It was necessary to conduct some of the investigations at reduced tem-

perature, and in one case to utilize water as the test fluid, due to

various mechanical and compatibility considerations which are discussed

fully later. The materials examined include three heat-treated speci-

mens of the tool steel alloy BG-42 (a modified 440-C stainless steel),

Blue Chip Tool Steel (18-4-1 tool steel), Mo-1/2Ti, Cb-1Zr(A), two

grades of graphitar, single-crystal tungsten, and teflon-coated type 304

stainless steel. Table 3 (previously cited) summarizes the material-fluid-temperature combinations which were studied.

2. Cavitation Studies in Mercury at 500°F

    a. Experimental Procedure

The six materials tested in mercury at 500°F were BG-42 (TRW) in three heat-treated conditions, Blue Chip Tool Steel (TRW), Mo-1/2Ti (P & W), and Cb-1Zr(A) (P & W). The BG-42 in the "as-received" condition was subjected to the heat-treat schedule specified in Table 26 so as to obtain specimens of three distinct hardness ranges, as noted. In Table 27 the heat-treat schedule for the "as-received" Blue Chip Tool Steel is specified. This results in specimens with a hardness of approximately 64 R_c (Rockwell "C"). Prior to any heat treating, standard cavitation test specimens, as shown in Figure 6, were machined from available bar stock. The required dimensions "A" and "B" for the six materials are listed in Table 4. These dimensions provide a standard specimen weight of 9.4 $\pm$ 0.1 g.

The argon cover gas over the mercury was maintained at 2.4 psig throughout the 500°F investigations, resulting in the required suppression pressure of 15.3 psia. Total test duration varied for the different materials, ranging from 8 to 12 hours, with frequent inspections and weighings monitoring the specimen surface. Some specimens were not inspected and weighed as frequently as others due to their brittle nature and the possibility of damaging or breaking the test button during assembly and disassembly. Prior to each weighing any excess mercury

TABLE 26

HEAT TREATMENT FOR BG-42 CAVITATION EROSION SPECIMENS

The following process shall be performed:

1. In a salt bath preheat the part thoroughly at 1400°F to 1450°F.

2. Transfer the part to a salt bath at 2075 to 2100°F. Soak at temperature for 1/2 hour per inch of thickness (20 minutes minimum).

3. Oil quench to room temperature.

4. Temper at 300 to 400°F for one hour.

5. Refrigerate at minus 100°F $\pm$ 10°F for 1/2 hour.

6. After allowing the specimen to warm to room temperature, double temper in a neutral salt bath (preferably chloride) for 2 + 2 hours at one of the following temperatures:

Desired Final Hardness, R_c	Temper Temperature, °F
44-46	1150-1180
53-55	1060-1090
62-64	975-1000

7. Air cool to room temperature in still air after each temper.

TABLE 27

HEAT TREATMENT FOR BLUE CHIP TOOL STEEL
(AMS 5626, T-1, 18-4-1)

For a hardness level of Rockwell C 61-64:

1. In a protective compound, salt, or atmosphere, preheat the
    specimen slowly over a two hour period to 1500°F - 1600°F.

2. Soak at 1500°F - 1600°F for one hour and then transfer the part
    to a controlled atmosphere furnace or salt bath at 2325°F -
    2350°F.

3. Soak at 2325°F - 2350°F for 2 - 5 minutes, the exact time being
    dependent on the size of the part. This soaking time should
    never be overdone.

4. Remove and cool in still air to room temperature.

5. Draw at 1025°F - 1050°F for 2 1/2 hours, then allow to cool
    slowly to room temperature.

6. Re-draw at 700°F - 750°F for two hours, then allow to cool
    slowly to room temperature.

adhering to the specimen surface was removed by heating in a vacuum furnace so as to eliminate oxidation of the specimen.

b. Experimental Results

The cavitation results obtained at 500°F in mercury will be displayed as accumulative weight loss versus test duration, and also as accumulative mean depth of penetration (MDP) versus test duration. The appropriate expressions for computing the MDP of all the materials tested are presented in Table 5.

Table 28 summarizes the cavitation results obtained in mercury at 500°F. Figure 58 is a plot of accumulative weight loss versus test duration, while Figure 59 is the corresponding plot of accumulative MDP versus test duration for the six materials tested.

On the basis of either average weight loss rate or average MDP rate it is clear that the three BG-42 materials and the Blue Chip Tool Steel are far superior to the Mo-1/2Ti and the Cb-1Zr(A). The BG-42 with a hardness of 64 R_c is the most resistant to cavitation based on average weight loss rate while the Blue Chip Tool Steel with identical hardness is about 15% less resistant. Based on average MDP rate these materials exhibit identical resistance to cavitation damage. These two materials are about 10 times more resistant than the tantalum-base alloy, T-111, which was found to be the most resistant in mercury at 500°F among the materials previously tested. The BG-42 specimens with hardnesses of 53 R_c and 47 R_c ranked third and fourth, respectively, among the six materials tested. The Mo-1/2Ti and Cb-1Zr(A) specimens were both much more severely damaged, and exhibited average weight loss

TABLE 28

SUMMARY OF CAVITATION RESULTS IN MERCURY AT 500°F
(BEARING PROGRAM)

Material	Avg. Wt. Loss Rate	Avg. MDP Rate
BG-42 (R_c = 64) (TRW)	1.20 mg./hr.	.04 mils/hr.
Blue Chip Tool Steel (TRW)	1.43	.04
BG-42 (R_c = 53) (TRW)	3.08	.10
BG-42 (R_c = 47) (TRW)	5.88	.19
Mo-1/2Ti (P & W)	43.16	1.09
Cb-1Zr(A) (P & W)	125.78	3.73
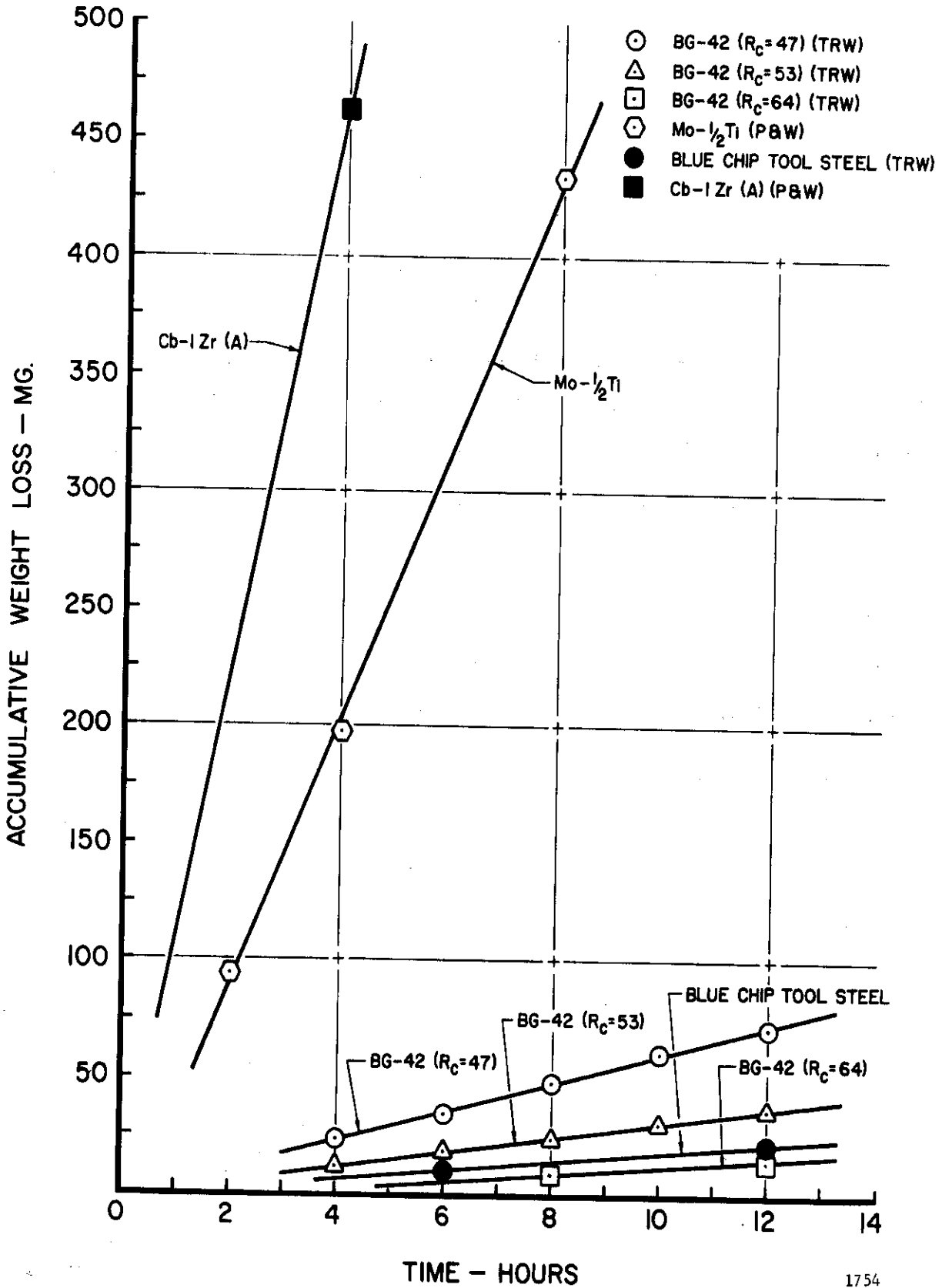
Fig. 58.--Effect of cavitation test duration on weight loss at 500°F in mercury.
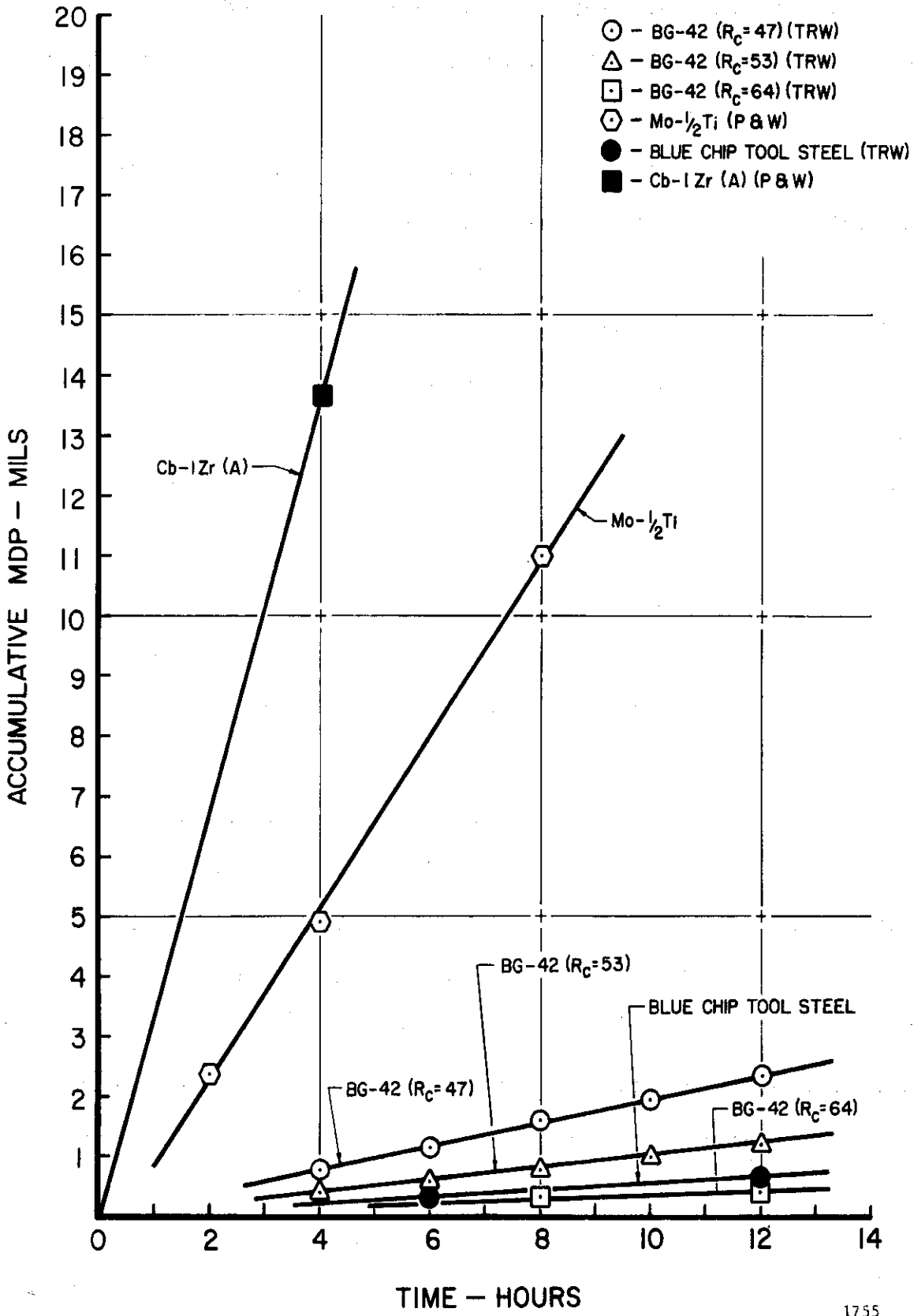
Fig. 59.--Effect of cavitation test duration on MDP at 500°F in mercury.

rates of 43.16 mg./hour and 125.78 mg./hour, respectively. It is interesting to note that the hardest of the BG-42 specimens exhibited the greatest resistance to cavitation damage, while the softest showed least resistance. It is clear from Figures 58 and 59 that the rate of erosion for each individual material is approximately constant for all the materials tested for the duration of the test.

Photographs of the test specimens at the conclusion of the cavitation experiment are presented in Figure 60. Note the severe pitting of the Mo-1/2Ti and the Cb-1Zr(A) surfaces. However, as was previously mentioned for the heavy liquid metal tests, the damage is spread uniformly over the surface. We feel that this results in the uniform damage rates up to the order of 10-15 mils MDP.

Very little damage is noted in the case of the BG-42 (R_c = 64) and the Blue Chip Tool Steel. A photograph of the Cb-1Zr(A) specimen before exposure indicates a representative surface condition for all the specimens tested.

Detailed examination of the stainless steel exponential horn, container vessel, and the sides of the various test specimens, all of which are not subject to cavitation, but are submerged in the test fluid, indicates that corrosion effects in the absence of cavitation in these investigations were negligible. Hence, it seems probable that the damage suffered by the test specimens was due almost completely to the cavitation erosion process and not to chemical corrosion by the mercury test fluid.

-197-
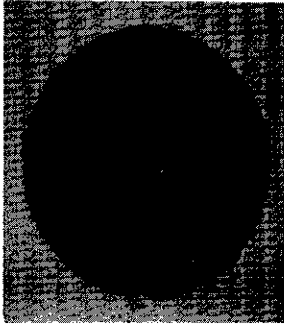
(1) BG-42(R_C = 64)

12 Hour Exposure
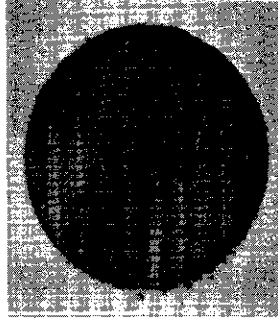
(2) Blue Chip Tool Steel(R_C = 64)
12 Hour Exposure
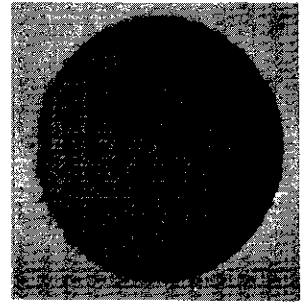
(3) BG-42(R_C = 53)

12 Hour Exposure
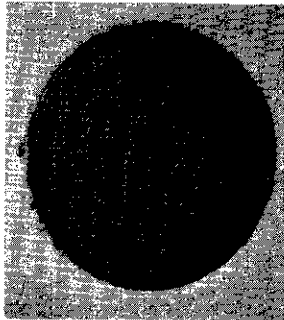
(4) BG-42(R_C = 47)

12 Hour Exposure
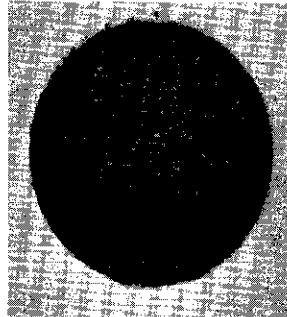
(5) Mo-1/2Ti

12 Hour Exposure
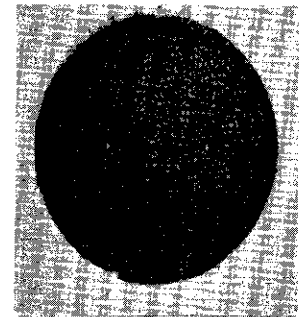
(6) Cb-1Zr(A)

8 Hour Exposure
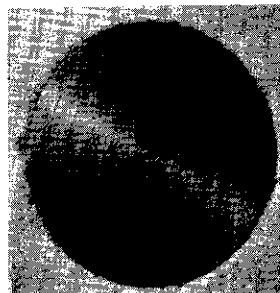
Cb-1Zr(A)

Prior to Exposure

Fig. 60.--Specimens subjected to cavitation damage in mercury at 500°F.   1756

3. Cavitation Studies in Mercury at
   70°F (Graphitar)

   a. Experimental Procedure

   The initial intention was to conduct all of the cavitation-erosion tests of these bearing-type materials at 500°F in mercury, but a variety of mechanical and compatibility problems made this impossible in the case of the graphitar and the single-crystal tungsten. The graphitar materials conceivably could have been tested at 500°F, but it was judged that the changes in mechanical properties from 70°F to 500°F were negligible for this material. Further, testing at 70°F would enable a direct comparison (from a temperature standpoint) with the single-crystal tungsten which had to be tested in water at 70°F, as will be discussed later.

   Graphitar is formed from carbon and graphite powders which are compacted under high unit pressures and then furnaced at temperatures up to 4500°F. A variety of grades are available from The United States Graphite Company and other vendors, and differ in hardness, density, compressive strength, and other mechanical properties. The two grades investigated here are denoted as grades 50 and 80, and were chosen to provide a substantial variation in mechanical properties within the useful range for this material. Applicable mechanical properties are presented in Chapter IV.

   Due to the low density of the graphitar (compared to the other materials tested) and its brittle, porous nature, it was completely impractical to fabricate standard cavitation test specimens as shown in Figure 6. The low density would result in an unusually large "A"

dimension (thus giving the assembly an improper length for resonance) to obtain the required weight, while the brittle, porous nature of the material made it impossible to firmly affix a specimen to the ultrasonic horn without damage to the threaded portion. It is necessary that the specimen be firmly and tightly attached to the horn tip so that the ultrasonic energy is properly transmitted across the interface for efficient operation. Hence the design shown in Figure 7 (also used for Plexiglas), consisting of a graphitar test specimen with internal thread and a separate stainless steel mounting stud was adopted and proved to be satisfactory. The mounting stud results in a firm attachment of the graphitar cylinder to the horn tip without damage to the graphitar internal threads. This design overcomes all of the problems encountered with the standard cavitation test specimen.

The experimental procedure employed for the testing of the graphitar specimens in mercury at 70°F closely parallels that used for the 500°F tests discussed previously. However, for the 70°F tests the argon cover gas pressure was maintained at 0.5 psig throughout the investigations to again provide the same pressure above vapor pressure at the specimen surface. Total test duration for both grades of graphitar was 10 hours, with two specimens of each being run. Frequent inspections and weighings were conducted to monitor the specimen surface. Since the graphitar is very porous and absorbs mercury during the cavitation test, it was necessary to drive off the absorbed mercury by heating in a vacuum furnace before weighing. The vacuum is necessary to eliminate oxidation of the specimen material.

b. Experimental Results

The cavitation results obtained at 70°F for graphitar will

be displayed as accumulative weight loss versus test duration, and also

as accumulative mean depth of penetration (MDP) versus test duration.

Table 29 summarizes the cavitation results obtained in mercury

at 70°F. Figure 61 is a plot of accumulative weight loss versus test

duration, while Figure 62 is the corresponding plot of accumulative MDP

versus test duration for the two grades of graphitar tested. The

response of the graphitar to cavitation-erosion damage was non-linear

for the initial part of the test out to about 50 mils MDP, as opposed to

all the other materials, but a constant rate portion of the curve does

exist from approximately 50 mils MDP out to about 100 mils total MDP.

However, due to the rapid rate of damage obtained, no data points were

obtained below about 25 mils MDP. Hence, there may well have been a

constant rate portion of the curve in the 1-3 mil MDP range used to rate

many other materials which exhibited non-linear tendencies for higher

values of MDP.

On the basis of either average weight loss rate or average MDP

rate the grade 80 variety of graphitar appears to be superior to the

grade 50. However, both grades suffered a total MDP which was on the

order of 100 times as great as that of the Blue Chip Tool Steel and

BG-42 specimens tested at 500°F. In fact, the maximum penetration, as

opposed to mean penetration, of both grades of graphitar was approxi-

mately 1/4 in. (250 mils).

Since the graphitar does not melt at any temperature and begins

to sublime at approximately 6000°F, it is felt that the mechanical

TABLE 29

SUMMARY OF CAVITATION RESULTS AT 70°F
(BEARING PROGRAM)

Material	Avg. Wt. Loss Rate	Avg. MDP Rate
*Graphitar-Grade 50 (U-M)	71.60 mg./hr.	10.90 mils/hr.
*Graphitar-Grade 80 (U-M)	55.30	7.95
**Single-Crystal Tungsten (U-M)	1.55	.025

*Tested in Mercury.

**Tested in Water.
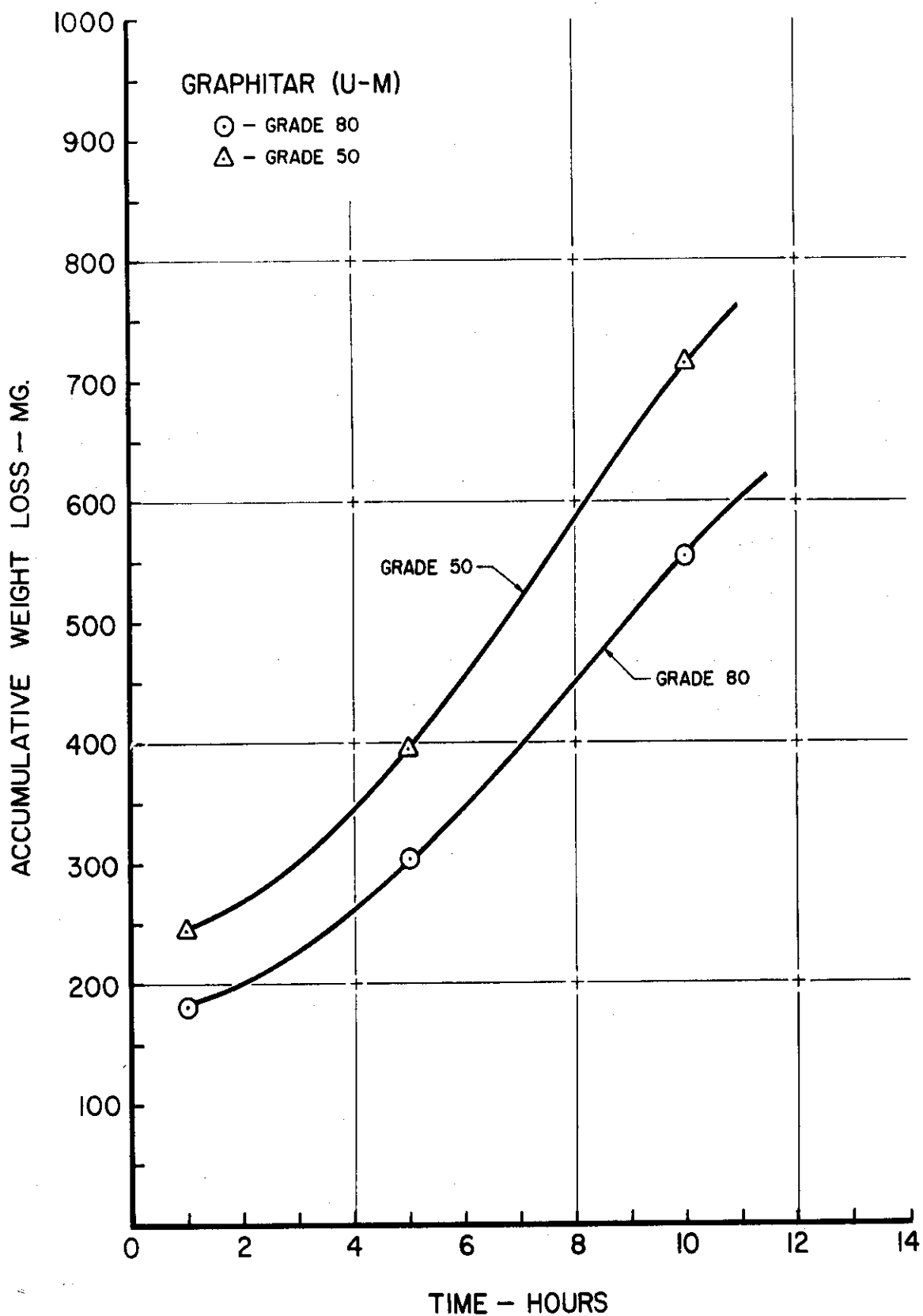
Fig. 61.--Effect of cavitation test duration on weight loss of graphitar at 70°F in mercury.
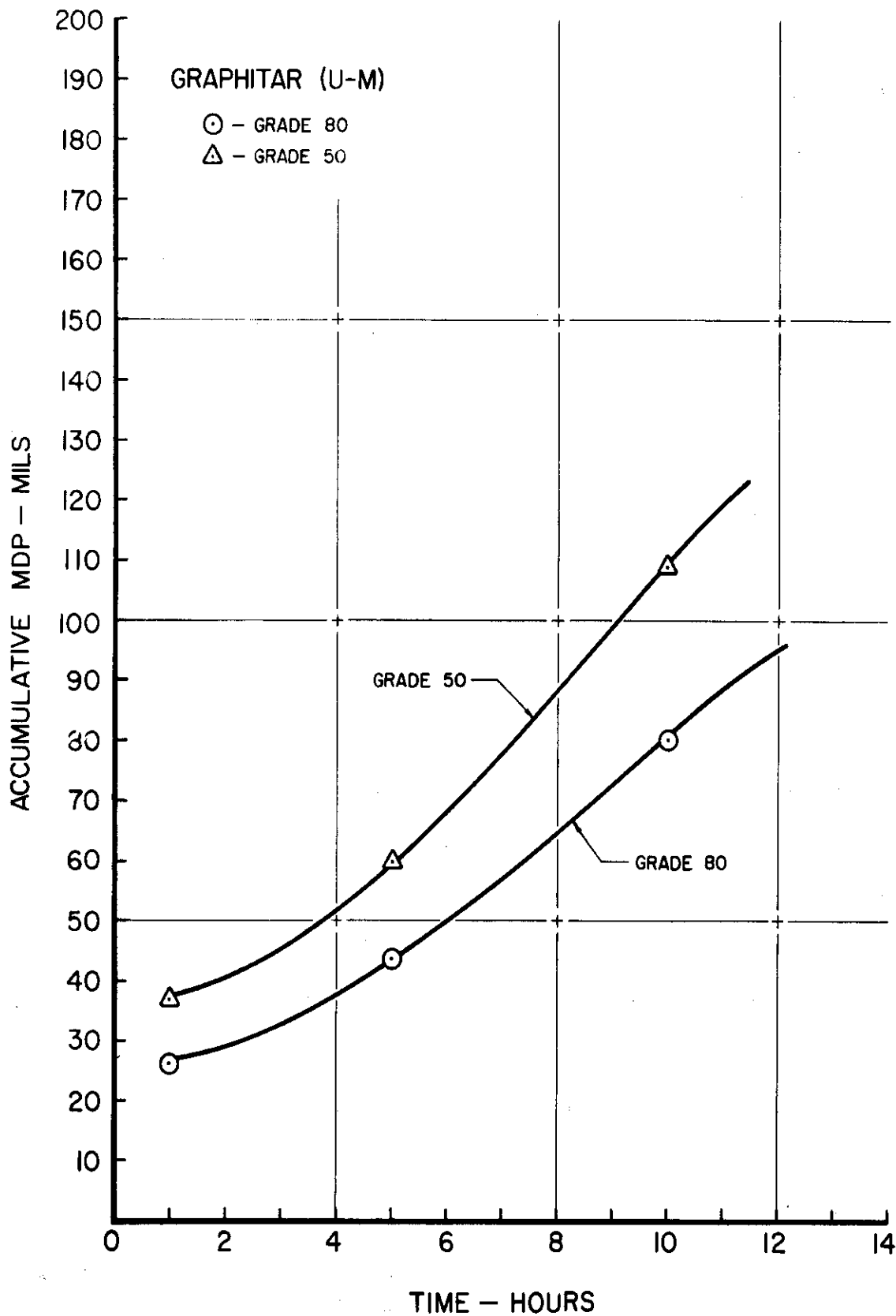
Fig. 62.--Effect of cavitation test duration on MDP of graphitar at 70°F in mercury.

properties of the two grades tested here would not be significantly
affected had the tests been conducted at 500°F. Hence, it is assumed
that the data presented in Table 29 for graphitar is approximately
applicable at 500°F also.

Photographs of the test specimens at the conclusion of the cavi-
tation experiment (10 hours duration) are presented in Figure 63. A
photograph of a typical graphitar cylinder before exposure is included
for comparison. Note the very severe damage suffered by both grades of
graphitar.

4. **Cavitation Studies in Water at 70°F**
   (Single-Crystal Tungsten)

   a. Experimental Procedure

It was intended to test the single-crystal tungsten in mer-
cury at 500°F. However, because of the very great difficulty encoun-
tered in machining a standard cavitation test specimen from this materi-
al, and due to the lack of a suitable grinder for forming the threaded
portion of the specimen, alternate designs were considered. It was
found feasible to produce a simple disk of single-crystal tungsten by
grinding, but it was still necessary to affix the disk firmly to the
ultrasonic horn. Initially, an attempt was made to use epoxy resin to
attach the tungsten disk to a stainless steel adaptor. However, the
epoxy had little elasticity and very low strength in shock so that it
was immediately fractured at the start of the test. Various other
cements provided similar results. Finally, the design shown in Figure 9
was found to be satisfactory. Here a simple disk of single-crystal
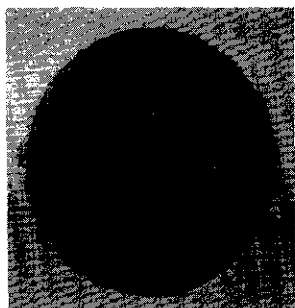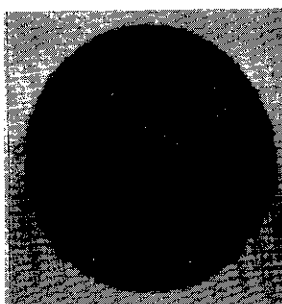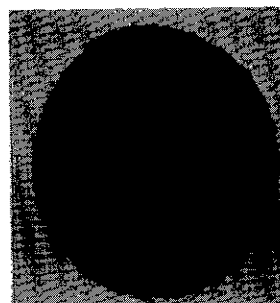
Graphitar	Graphitar	Graphitar
	Grade 80	Grade 50
Before Exposure	10 Hour Exposure	10 Hour Exposure
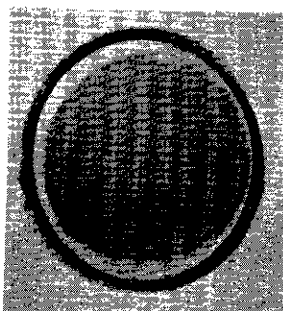
Single Crystal Tungsten

50 Hour Exposure

Fig. 63.--Graphitar and single-crystal tungsten specimens subjected to cavitation damage at 70°F.

1760

tungsten has been attached to a stainless steel adaptor with silver

solder. The use of a high-temperature solder of this type was con-

sidered feasible with tungsten with its very low temperature

sensitivity. The silver solder was found to form a very suitable bond

between the tungsten and stainless steel and resulted in satisfactory

transmission of the ultrasonic energy across the interface. The diam-

eter of the tungsten disk (1/2 in.) was slightly smaller than the diam-

eter of the stainless steel adaptor (.547 in.) due to unavailability of

tungsten in a larger size at the time of the tests. However, it was

felt that errors from this slight dimensional change would not be sig-

nificant within the overall experimental errors.

The silver solder proved to be satisfactory in all respects with

the exception of its compatibility with mercury. Even during a rela-

tively short test in mercury and in spite of the small surface of solder

exposed (merely the edge of the bond), the bond was destroyed. Hence,

it was necessary to test the tungsten in water. Due to pressure limita-

tions of the equipment, a test in water at 500°F was not possible.

Since the properties of tungsten are not significantly temperature

dependent in this range, it was decided that a test in water at 70°F

would suffice to at least obtain some realistic idea of the cavitation

resistance of the material. The single-crystal tungsten used in these

investigations was obtained from Cleveland Tungsten, Inc.

Due to the previously mentioned fabrication difficulties and

lack of ample stock, only one specimen of tungsten was tested. The

tests were conducted at the same frequency, amplitude, and submergence

used in the other tests. The argon cover gas pressure was maintained at

1.5 psig to obtain the same pressure above vapor pressure at the speci-

men surface. The total test duration was 50 hours, with inspections and

weighings being conducted at 10-hour intervals.

b. Experimental Results

Table 29 summarizes the results obtained with the single-

crystal tungsten. Figure 64 is a plot of accumulative weight loss ver-

sus test duration, while Figure 65 is the corresponding plot of accumu-

lative MDP versus test duration for the single-crystal tungsten tested.

The response of the single-crystal tungsten to cavitation-erosion attack

is nearly linear for the duration of the test, at least over the range

of about 0.5 to 1.5 mils MDP. Hence, the characteristics of the damage

rate curve are similar to those of other materials tested.

Clearly, the tungsten tested in water was damaged only slightly

compared to the graphitar tested in mercury at the same temperature. In

fact, the amount of damage incurred by the tungsten is on the order of

that suffered by the Blue Chip Tool Steel and the three BG-42 specimens

tested in mercury at 500°F. Before any true comparison can be made

between these materials, it is necessary to correct the tungsten results

obtained in water at 70°F in an appropriate manner so as to reflect the

expected additional damage that the tungsten would have suffered in mer-

cury at 70°F and 500°F. Cavitation-erosion data obtained for type 304

stainless steel in water at 70°F and in mercury at 70°F and 500°F will

be used for this purpose. Hence, if one assumes that the tungsten and

the stainless steel both suffer the same % increase in damage when
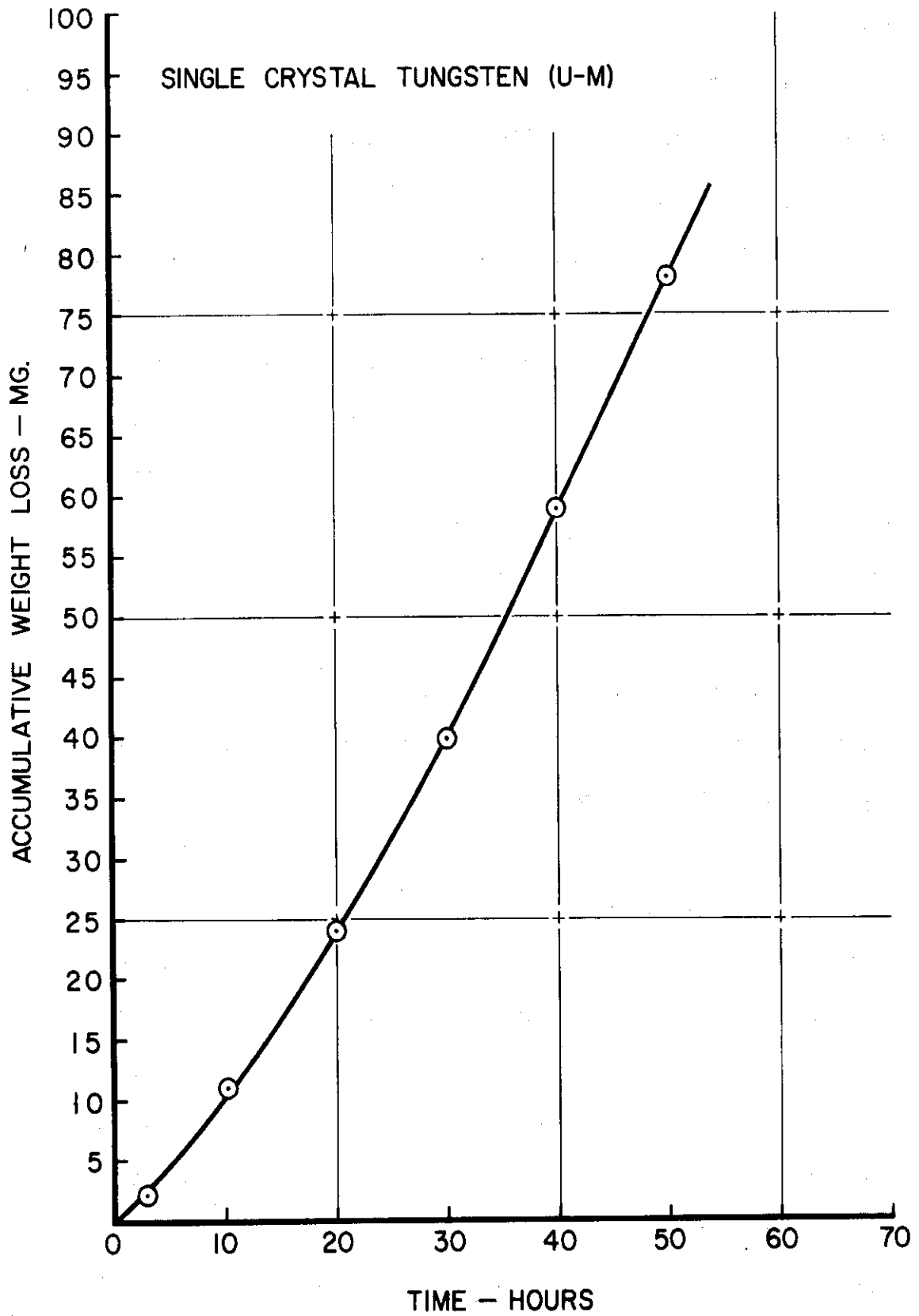
Fig. 64.--Effect of cavitation test duration on weight loss of single-crystal tungsten at 70°F in water.
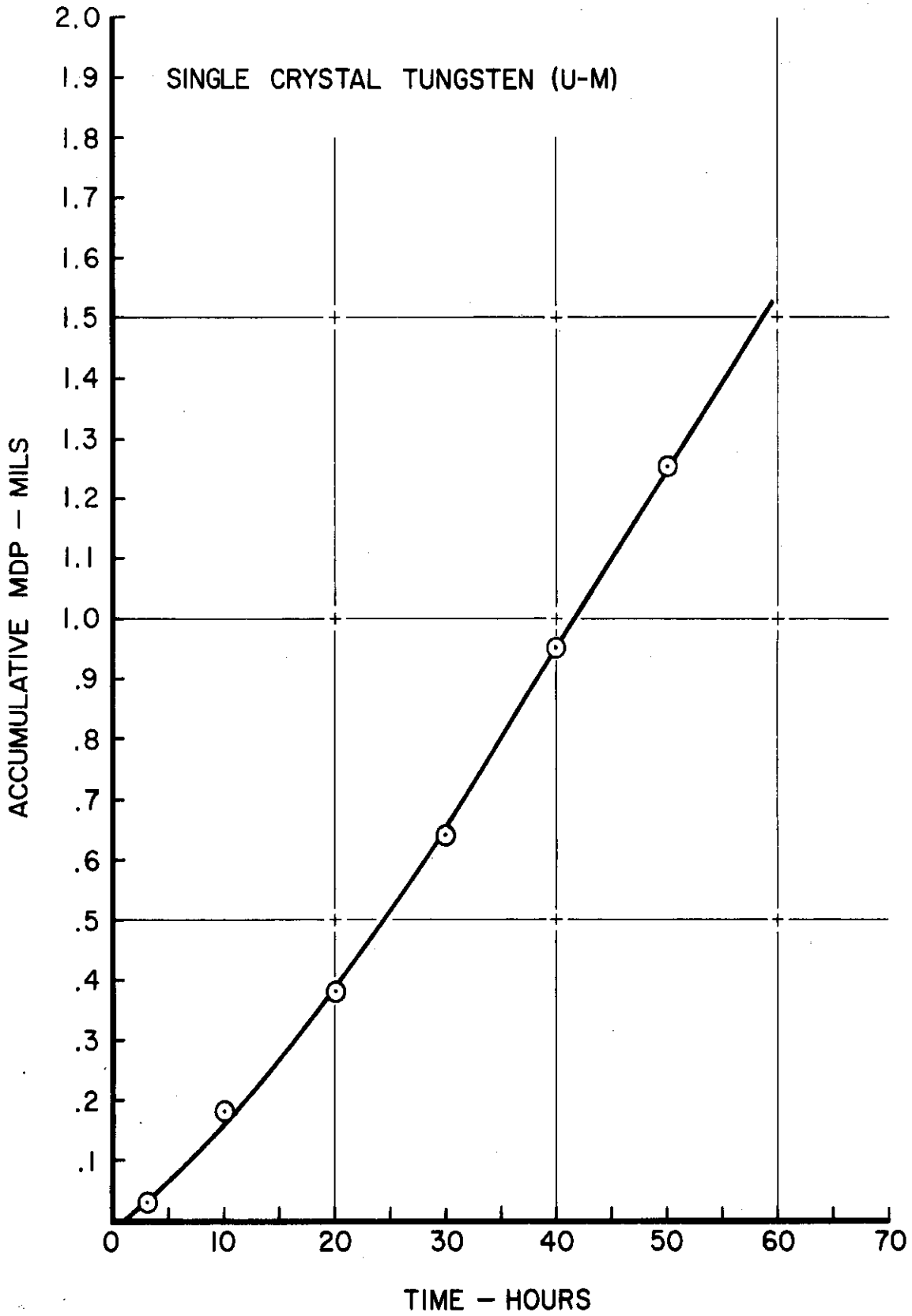
Fig. 65.--Effect of cavitation test duration on MDP of single-crystal tungsten at 70°F in water.

changing the test fluid from water to mercury at 70°F, and when increasing the mercury temperature from 70°F to 500°F, then it is possible to compute projected damage rates for the single-crystal tungsten on the basis of the 304 stainless steel data available. Hence, one might compute the expected rate of damage for single-crystal tungsten in mercury at 70°F as follows:

$$W_{70°F\ Hg} = W_{70°F\ H_2O} \times \frac{304\ SS_{70°F\ Hg}}{304\ SS_{70°F\ H_2O}}$$

$$W_{70°F\ Hg} = (.025\ mils/hr.) \times \frac{.32\ mils/hr.}{.10\ mils/hr.} = 0.08\ mils/hr.$$

where W and 304 SS denote the corresponding MDP rates for tungsten and type 304 stainless steel, respectively. In a similar manner one can estimate the expected rate of damage for the single-crystal tungsten in mercury at 500°F as follows:

$$W_{500°F\ Hg} = W_{70°F\ H_2O} \times \frac{304\ SS_{500°F\ Hg}}{304\ SS_{70°F\ H_2O}}$$

$$W_{500°F\ Hg} = (.025\ mils/hr.) \times \frac{.69\ mils/hr.}{.10\ mils/hr.} = 0.173\ mils/hr.$$

It is felt that the estimate at 500°F is probably conservative, since the mechanical properties of the single-crystal tungsten are only slightly affected by the increase in temperature from 70°F to 500°F as compared with the stainless steel. It is believed that the effects of the change in mercury properties between 70°F and 500°F are probably

small and are in a direction to reduce damage ("thermodynamic effects")[69] if the mechanical properties of the material were constant. Then the MDP rate of 0.08 mils/hour may be more applicable for a test of single-crystal tungsten in mercury at 500°F. Presently, mechanical properties data for the single-crystal tungsten at the two temperatures in question are not available, and this matter will remain in some doubt until such data is obtained.

A photograph of the single-crystal tungsten cavitation specimen at the conclusion of the 50-hour test is included in Figure 63 (previously cited). Very little damage is apparent. The outer dark ring noted in the photograph is not part of the tungsten specimen, but represents a space between the edge of the specimen and the cardboard holder used for photography. However, the lighter ring within this does represent the typical relatively undamaged area around the outside of the specimen.

5. Effect of Teflon Coating on Cavitation-
   Erosion Characteristics

   a. Experimental Procedure

   Several type 304 stainless steel standard cavitation test specimens were coated with liquid teflon obtained from DuPont, Inc., in an attempt to determine its effectiveness as a protective coating against cavitation-erosion attack, since various coatings of this type have sometimes proven effective in water tests. The stainless steel specimens were sand-blasted so as to roughen the surface, and then the liquid teflon was applied with an insecticide sprayer to a thickness of

2.5 mils. The cavitation tests were conducted in mercury at a tempera-
ture of 350°F, which was believed to be about the upper limit of appli-
cability for teflon, at a frequency of approximately 20 Kc./sec. and
double amplitude of approximately 2 mils.

b. Experimental Results

Initially, a teflon-coated 304 stainless steel specimen was
soaked in mercury at 350°F for 15 hours with no cavitation present to
determine whether the teflon coating would adhere to the stainless steel
surface in this environment. Visual examination indicated no damage or
loss of teflon, and precision weighing confirmed this conclusion.

Several teflon-coated 304 stainless steel specimens were then
subjected to cavitation in mercury at 350°F. The rate of weight loss
was essentially the same as that obtained with uncoated 304 stainless
steel tested at 500°F in mercury (agreement within ± 2%). In fact,
after only 5 minutes of testing, it was found that the teflon coating
had been completely removed. Since the teflon coating remained intact
upon exposure to the 350°F non-cavitation environment (i.e., did not
"soak off"), it appears that the teflon coating was ineffective as a
protective measure in the presence of cavitation in mercury at 350°F.

6. Comparison of Cavitation Results
   in Bearing Program

Although it was not possible to test all of the materials in
mercury at 500°F, it is possible to compare all of the results as cor-
rected to 500°F, mercury, as previously discussed. Table 30 summarizes
all of the cavitation data obtained in the bearing program investigation.

TABLE 30

COMPARISON OF CAVITATION RESULTS OBTAINED IN BEARING PROGRAM
(BASED ON 500°F MERCURY OPERATION)

Material	Avg. Wt. Loss Rate	Avg. MDP Rate
BG-42 (R_c = 64) (TRW)	1.20 mg./hr.	.04 mils/hr.
Blue Chip Tool Steel (TRW)	1.43	.04
*Single-Crystal Tungsten (U-M)	4.96	.08
BG-42 (R_c = 53) (TRW)	3.08	.10
BG-42 (R_c = 47) (TRW)	5.88	.19
Mo-1/2Ti (P & W)	43.16	1.09
Cb-1Zr(A) (P & W)	125.78	3.73
*Graphitar-Grade 80 (U-M)	55.30	7.95
*Graphitar-Grade 50 (U-M)	71.60	10.90

*These values estimated from data obtained at 70°F.

The values given for graphitar and single-crystal tungsten are projected

values based on assumptions previously discussed. All of the values for

the other specimens were actually obtained in mercury at 500°F and pre-

viously presented in Table 28.

It is clear from Table 30 that the BG-42 (R_c = 64) and the Blue

Chip Tool Steel are the most resistant to cavitation in mercury at

500°F. The single-crystal tungsten with the estimated MDP rate of

0.08 mils/hour ranks third and the BG-42 (R_c = 53) fourth. The BG-42

(R_c = 47) is about 90% less resistant than the BG-42 (R_c = 53). The

Mo-1/2Ti and Cb-1Zr(A) were both much more heavily damaged and suffered

average MDP rates of 1.09 mils/hour and 3.73 mils/hour, respectively.

The graphitars were both very grossly damaged, exhibiting by far the

least resistance to cavitation attack of the materials tested. It is

interesting to note that the Blue Chip Tool Steel, all three specimens

of BG-42 (varying hardness), and the single-crystal tungsten were all

more resistant to cavitation attack in mercury at 500°F than the refrac-

tory alloy, T-111, which was the most resistant in mercury at 500°F

among the materials previously tested.

Presumably, Table 30 could serve as a materials guide for the

designer of bearings, serving to indicate those materials which exhibit

the greatest resistance to cavitation-erosion attack among those tested

in mercury at 500°F. However, it is believed that final check tests in

a flowing facility similar to the University of Michigan mercury tunnel

or more preferably in a close-clearance space similar to bearing geom-

etry, would be desirable.

Although it has been indicated that considerable difficulty was encountered in fabricating the single-crystal tungsten, it is believed that these difficulties could be overcome with further experimentation so that a test in mercury at 500°F could be accomplished. Since the only specimen of this material which was tested ranked among the best materials, such a continued effort would be desirable to obtain the performance of other closely related materials.

While the teflon coating was unsuccessful, it is known that other coating materials and perhaps more suitable bonding procedures have provided useful materials for cavitation resistance in water in the past. Presumably similar materials could be developed also for fluids, other than water, such as mercury.

CHAPTER IV

MECHANICAL PROPERTIES DATA FOR THE TEST MATERIALS

A. Introduction

In order to obtain a meaningful correlation between the cavita-

tion resistance of the various materials tested, their mechanical prop-

erties, and suitable fluid coupling parameters, it is absolutely essen-

tial that the applicable mechanical properties be measured at the test

temperatures using tensile bars machined from the same bar stock as were

the cavitation specimens. Otherwise the variations between material

lots due to differences in heat-treat, cold work, etc., are too large to

allow useful results. Accordingly, all the cavitation test specimens,

tensile bars, and special hot hardness specimens for each individual

material were machined from the same piece of bar stock. In the case of

the Cu, Cu-Ni, Cu-Zn, and Ni alloys it was desired to use the precise

materials that had been tested in the venturi,[22] and these were avail-

able only in sheet stock. From this sheet stock flat tensile specimens

were fabricated and tested. It was found that handbook values or those

supplied by vendors were not sufficiently accurate to be of use in this

context even for relatively standard materials. It has been the experi-

ence of this laboratory that supposedly identical materials taken from

different heats may have variations in applicable mechanical properties

as great as 50%. Among the properties which may be important are ten-

sile strength (TS), yield strength (YS), engineering strain energy

(ESE), true strain energy (TSE), hardness (H), elongation (ELON), reduc-

tion in area (RA), and elastic modulus (E). Each of these mechanical

properties will be examined with respect to motivation and experimental

evidence pointing to their selection as possible test material correlat-

ing parameters.

B. Mechanical Properties Selection

The mechanical properties of the test materials which were

selected as possible correlating parameters for the experimentally-

determined cavitation damage data are listed above. Qualitative motiva-

tion and experimental evidence supporting their selection as possible

material correlating parameters follow. It is, of course, desired to

find a relation between cavitation damage rate and the conventional

(measurable) mechanical and fluid properties so that cavitation damage

might be predicted in advance.

1. Tensile Strength (TS)

Several investigators have attempted to correlate the cavi-

tation damage resistance of various materials with the tensile strength.

Among these were Mousson,[18] Nowotny,[32] and Plesset and Ellis.[70] In each

case some success was achieved. If one were to generate the engineering

stress-strain curve[71] for a material (based on the original gauge length

and cross-sectional area of the tensile specimen), the maximum stress

experienced by the test specimen as determined from this curve is known

as the ultimate tensile strength. Hence, it seems intuitively reason-

able to include this quantity among the possible material mechanical

properties to be used as correlating parameters.

2. Yield Strength (YS)

Mousson[18] also attempted a correlation with the yield

strength on a limited number of materials. In the case of the engineer-

ing stress-strain curve[71] the yield strength is approximately equal to

the stress beyond which the material passes from the elastic range to

the plastic range. If the cavitation damage mechanism is similar to

fatigue failure, then the yield strength should be an important corre-

lating parameter, since the endurance limit (or fatigue strength) is

usually an approximately fixed proportion of the yield strength rather

than ultimate tensile strength.

3. Engineering Strain Energy (ESE)

Both Shalnev[72] and Thiruvengadam[73,74] have postulated the

use of strain energy concepts with respect to cavitation damage correla-

tions and have reported limited success in their use. The engineering

strain energy[71] (strain energy to failure) is based on the "approximate"

or engineering stress-strain curve and is equal to the area under this

curve. This area is a measure of the work or energy per unit volume

that must be delivered to a tensile specimen in order to completely

fracture it. Hence, it appears that it might be a reasonable correlat-

ing parameter.

4. **True Strain Energy Based on
Elongation (TSEE)**

In an attempt to take into account the elongation and reduction in cross-sectional area experienced by the tensile bar during a test, factors which are neglected in the generation of the approximate, or engineering stress-strain curve, two commonly-used approximations for "true strain energy" will be considered. These are based on approximations of the true stress-strain curve.[71] The first value of true strain energy takes into account elongation of the test specimen in computing the strain, but assumes that necking of the specimen does not occur.

5. **True Strain Energy Based on
Reduction in Area (TSER)**

The second value of true strain energy considered takes into account elongation of the test specimen in computing the strain and also necking of the specimen, i.e., reduction in area after plastic deformation begins, in computing the true breaking stress. Hence, higher values for the breaking stress and strain are obtained in this manner than was the case with the engineering strain energy, since a greater account is taken of the ductility of the material. This may or may not more closely represent the cavitation case which is characterized by very high rates of loading, leading in some cases to apparently brittle fractures. The true strain energy values used in our correlations are only approximations since it is difficult to obtain true stress-strain data beyond the elastic range during a tensile test (except for the values at rupture).

6. Hardness (H)

Hardness has been shown to be an important factor in cavitation damage resistance correlations by many investigators. In general, materials with high hardness values are more resistant to cavitation damage than softer materials. Rheingans[34] showed that the order of resistance generally follows the order of hardness in a series of tests of cast stainless steels using a magnetostriction oscillator. Mousson[18] obtained a similar successful correlation with hardness on materials tested in a venturi apparatus. Plesset and Ellis[70] conducted experiments on a number of different materials and found hardness to be reasonably successful as a correlating parameter. Hence, hardness has been included among the mechanical properties to be used as possible correlating parameters in our investigations.

7. Elongation (ELON)

Since the value of elongation for a particular material is important in determining the true strain energy, it was included in the mechanical properties list.

8. Reduction in Area (RA)

Since the value of reduction in area for a particular material is important in determining the true strain energy, it was included in the mechanical properties list.

9. Elastic Modulus (E)

Plesset and Ellis[70] investigated the use of elastic modulus as a correlating parameter for cavitation damage on a number of

materials ranging from very soft aluminum to stellite and tungsten.

Moderate success was achieved. Early correlations in our own laboratory
with the venturi data[22] showed elastic modulus to be prominent in the
correlating equations. This may not be surprising since it is closely
related to sonic velocity and acoustic impedance, both of which appear
in basic equations involving the stress from an impinging droplet or
jet.

10. Hobbs' Approach

Hobbs[67] suggested the use of still other quantities to cor-
relate cavitation damage. Figure 66 is a schematic diagram of a typical
true stress-strain curve for some material. Hobbs found that the area
under the true stress-strain curve within the elastic region (cross-
hatched in Figure 66) correlated well with some of his data. If one
postulates that when this amount of energy is delivered to the test
specimen (work done on the specimen), i.e., once the yield point is
reached, the collapsing bubbles begin to remove material from the cavi-
tation specimen, then such a quantity is a reasonable correlating param-
eter. This quantity, which Hobbs refers to as the "proof resilience"
(PR), will be examined in our work also. It is seen that it is equal
to:

$$\text{Hobbs' Proof Resilience (PR)} = 1/2 \, (S_{yield}^2/E)$$

where:

$$S_{yield} = \text{yield strength (YS) of the material}$$

$$E = \text{elastic modulus of the material}$$
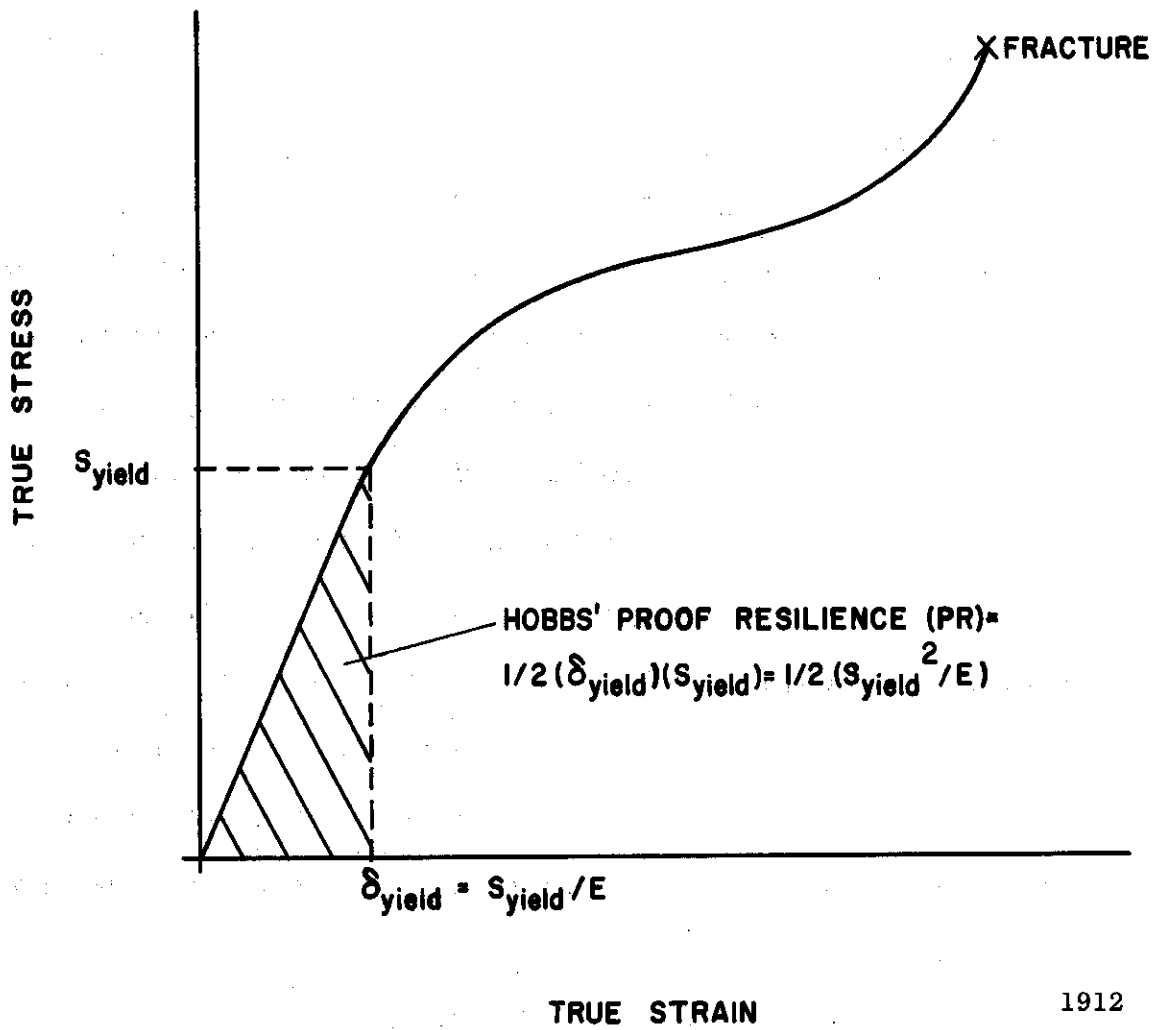
Fig. 66.--True stress-strain curve showing Hobbs' proof resilience concept.

Hobbs found still further that a better correlating parameter for his data was a quantity that he calls the "ultimate resilience" (UR). Figure 67 is another schematic diagram of a typical true stress-strain curve. The cross-hatched area in this figure corresponds to Hobbs' ultimate resilience. Since the process of cavitation represents highly transient loading, Hooke's Law may be valid to fracture as no elongation or reduction in cross-sectional area of the specimen occurs (i.e., brittle fracture occurs). Thus, during the cavitation process, the stress-strain relationship might well be linear up to the point of failure, as suggested in Figure 67. This quantity will also be examined in our work. Hobbs' ultimate resilience can be computed as:

$$\text{Hobbs' Ultimate Resilience (UR)} = 1/2 \ (S_{ultimate}^2/E)$$

where:

$S_{ultimate}$ = true ultimate stress (true breaking stress) of the material

E = elastic modulus of the material

The above mechanical properties were chosen as material correlating parameters for the cavitation damage data obtained in lead-bismuth, mercury, water, and lithium.

C. Tables of Properties at 70°F, 500°F, and 1500°F

The mechanical properties data for the stainless steels and refractory materials were determined at 70°F, 500°F, and 1500°F at Pratt & Whitney Aircraft (CANEL) under the supervision of Mr. Henry P. Leeper, Project Metallurgist. Earlier, Pratt & Whitney Aircraft (CANEL)
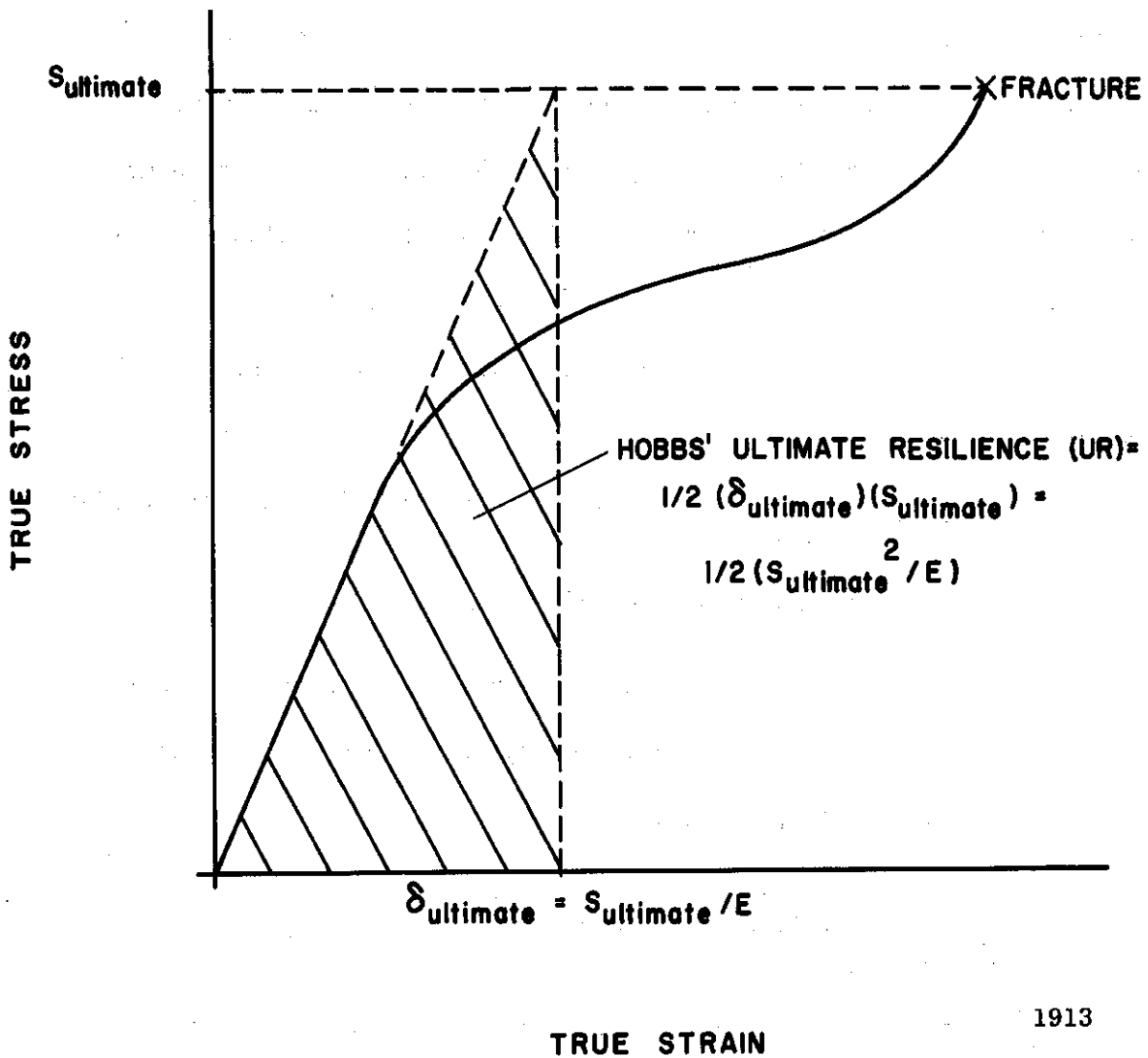
Fig. 67.--True stress-strain curve showing Hobb's ultimate resilience concept.

had supplied generous portions of all of the refractory materials tested
in this program, whereas the stainless steels used were supplied by this
laboratory. The results of the mechanical properties determination pro-
gram were supplied to this laboratory by private communication[75] and
have become an integral part of our cavitation analysis and correlation
effort.

The data supplied by Pratt & Whitney Aircraft (CANEL) at 70°F,
500°F, and 1500°F is tabulated in Tables 31, 32, and 33, respectively.
Three values for strain energy to failure are listed:[71] i.e.,
"engineering strain energy" (ESE) which is based on the "approximate" or
engineering stress-strain curve and is equal to the area under this
curve, and two values for "true strain energy" (TSE), which are based on
approximations of the true stress-strain curve. The first value of true
strain energy listed takes into account elongation of the test specimen
in computing the strain (denoted by TSEE), while the second value takes
into account necking of the specimen (i.e., reduction in area after
plastic deformation begins), and the resulting higher values for the
local true breaking stress and strain in the actual failure region
(denoted by TSER), as previously discussed. The large discrepancies in
some cases, as for highly ductile materials, between these differently-
defined strain energy values indicate the difficulties and uncertainties
incurred in using this parameter. If it occurs that the engineering
strain energy (ESE) proves to be a better correlating parameter than the
true strain energy based on reduction in area (TSER), then this may
indicate that brittle rather than ductile failures are typical of

TABLE 31

MECHANICAL PROPERTIES DATA AT 70°F FROM
PRATT & WHITNEY AIRCRAFT (CANEL)

Material	Tensile Strength psi	Yield Strength psi	Eng. Strain Energy psi	True Strain Energy psi	DPH Hardness 1.1 Kg.	Elonga- tion %	Area Reduction %	Elastic Modulus psi
304 SS	94,500	64,700	57,300	41,300	237	63.8	77.9	29.0×10^6
316 SS	87,200	63,600	48,850	38,200	227	57.8	80.3	29.0×10^6
T-111	131,600	124,900	16,750	16,000	308	14.8	80.4	28.0×10^6
T-222	154,200	154,200	15,250	16,050	338	10.6	55.6	28.0×10^6
T-222(A)	108,900	91,100	23,950	22,180	288	23.1	61.1	28.0×10^6
Mo-1/2Ti	165,800	150,400	21,300	14,570	295	9.3	7.9	45.0×10^6
Cb-1Zr	59,200	59,000	6,650	6,300	151	14.3	88.4	15.0×10^6
Cb-1Zr(A)	36,300	19,200	13,200	7,050	99	41.9	91.4	15.0×10^6

TABLE 32

MECHANICAL PROPERTIES DATA AT 500°F FROM
PRATT & WHITNEY AIRCRAFT (CANEL)

Material	Tensile Strength psi	Yield Strength psi	Eng. Strain Energy psi	True Strain Energy psi	DPH Hardness 1.1 Kg.	Elongation %	Area Reduction %	Elastic Modulus psi
304 SS	92,500	56,700	16,150	37,200	154	30.8	72.9	26.0×10^6
316 SS	72,400	52,300	18,050	38,000	203	30.4	78.2	26.0×10^6
T-111	101,800	100,800	15,100	50,900	218	13.8	86.2	27.0×10^6
T-222	133,800	133,800	12,850	67,800	286	10.9	71.5	27.0×10^6
T-222(A)	92,300	63,400	20,650	42,200	209	23.6	66.9	27.0×10^6
Mo-1/2Ti	84,100	79,700	10,700	44,400	207	15.0	75.9	43.0×10^6
Cb-1Zr	54,700	54,700	6,450	27,700	133	12.7	88.7	14.5×10^6
Cb-1Zr(A)	25,000	11,600	8,100	7,890	71	35.9	92.2	14.5×10^6

TABLE 33

MECHANICAL PROPERTIES DATA AT 1500°F FROM
PRATT & WHITNEY AIRCRAFT (CANEL)

Material	Tensile Strength psi	Yield Strength psi	Eng. Strain Energy psi		True Strain Energy psi	DPH Hardness 1.1 Kg.	Elongation %	Area Reduction %	Elastic Modulus psi
304 SS	21,900	18,400	4,600	1,640	2,410	66	19.7	30.5	18.0×10^6
316 SS	24,200	21,400	7,300	4,160	6,600	74	31.7	55.0	18.0×10^6
T-111	87,300	67,300	15,100	13,400	45,850	161	18.4	79.5	26.0×10^6
T-222	120,700	119,700	16,950	11,960	65,500	257	10.8	75.5	26.0×10^6
T-222(A)	85,500	41,800	16,950	14,030	38,500	140	22.1	72.9	26.0×10^6
Mo-1/2Ti	70,000	61,600	7,950	7,200	32,500	148	13.5	80.4	34.0×10^6
Cb-1Zr	47,600	47,100	5,650	3,460	19,500	106	11.6	84.1	13.5×10^6
Cb-1Zr(A)	28,000	9,700	6,700	2,200	7,050	67	26.5	91.1	13.5×10^6

cavitation damage. The remaining values listed in Tables 31, 32, and 33 are rather commonly reported metallurgical properties which have already been discussed. The hardness values listed were measured with a diamond pyramid indenter and 1.1 Kg. load.

Figures 68, 69, 70, 71, 72, 73, and 74 present plots of ultimate tensile strength, 0.2% yield strength, and hardness of the type 304 stainless steel, type 316 stainless steel, T-111, T-222(A), Mo-1/2Ti, Cb-1Zr, and Cb-1Zr(A), respectively, as a function of temperature. The following observations regarding these mechanical properties are noted:

1) For 304 stainless steel the ultimate tensile strength and the
   0.2% yield strength are nearly constant from room temperature to
   500°F. Then they rapidly deteriorate as the temperature
   increases to 1500°F. The hardness decreases in a relatively
   uniform manner over the temperature range investigated.

2) For 316 stainless steel the ultimate tensile strength, 0.2%
   yield strength, and the hardness all decrease in a fairly uni-
   form fashion as the temperature is increased.

3) For T-111, the ultimate tensile strength and the 0.2% yield
   strength decrease from room temperature to 500°F, but are
   relatively constant thereafter. The same comment applies to
   the variation of the hardness.

4) For T-222(A) the variation of the mechanical properties as shown
   in Figure 71 is similar to that of the T-111. The changes from
   500°F to 1500°F are quite small.

5) For Mo-1/2Ti comments similar to (3) and (4) above apply.
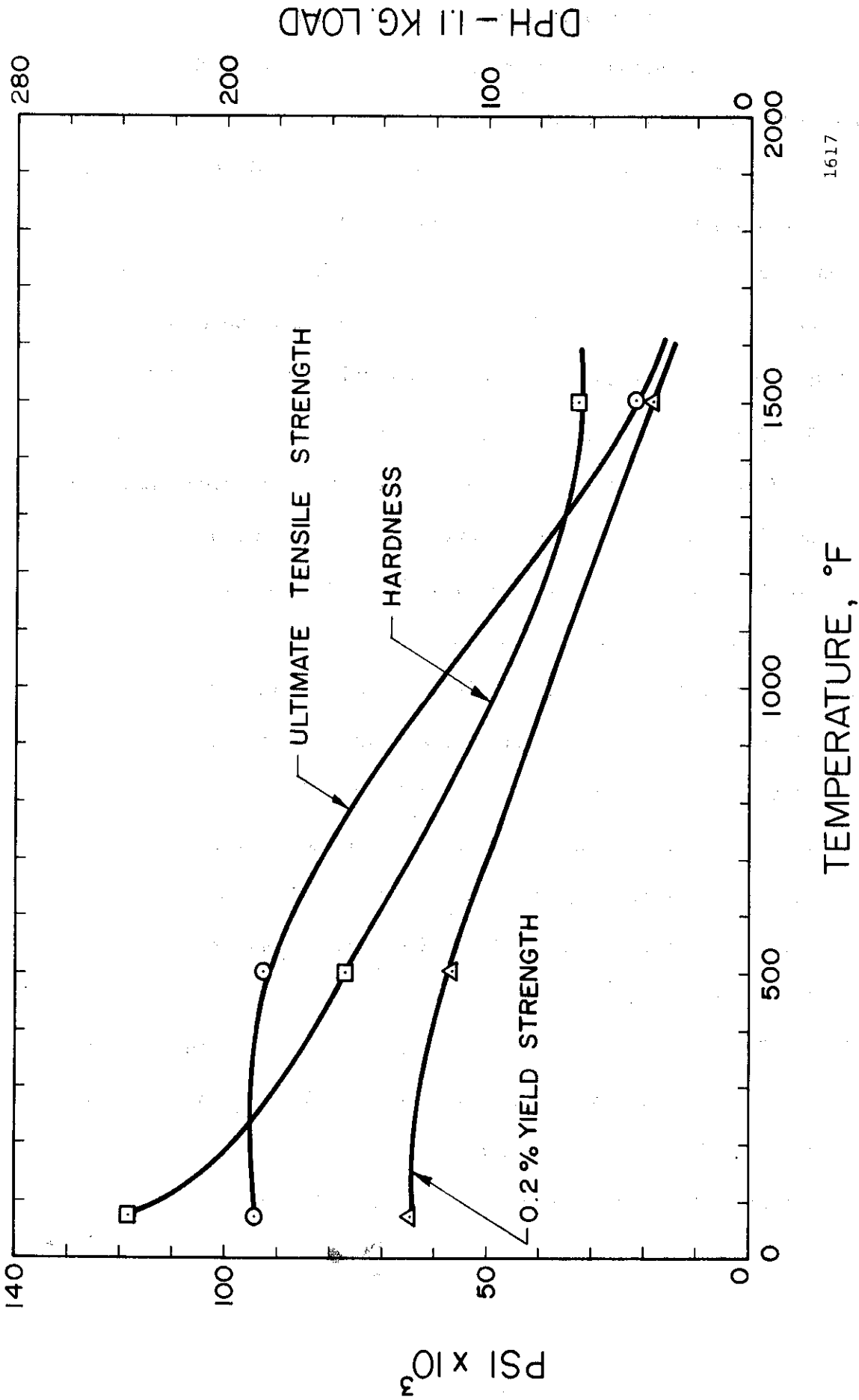
Fig. 68.--Effect of temperature on mechanical properties of type 304 stainless steel.
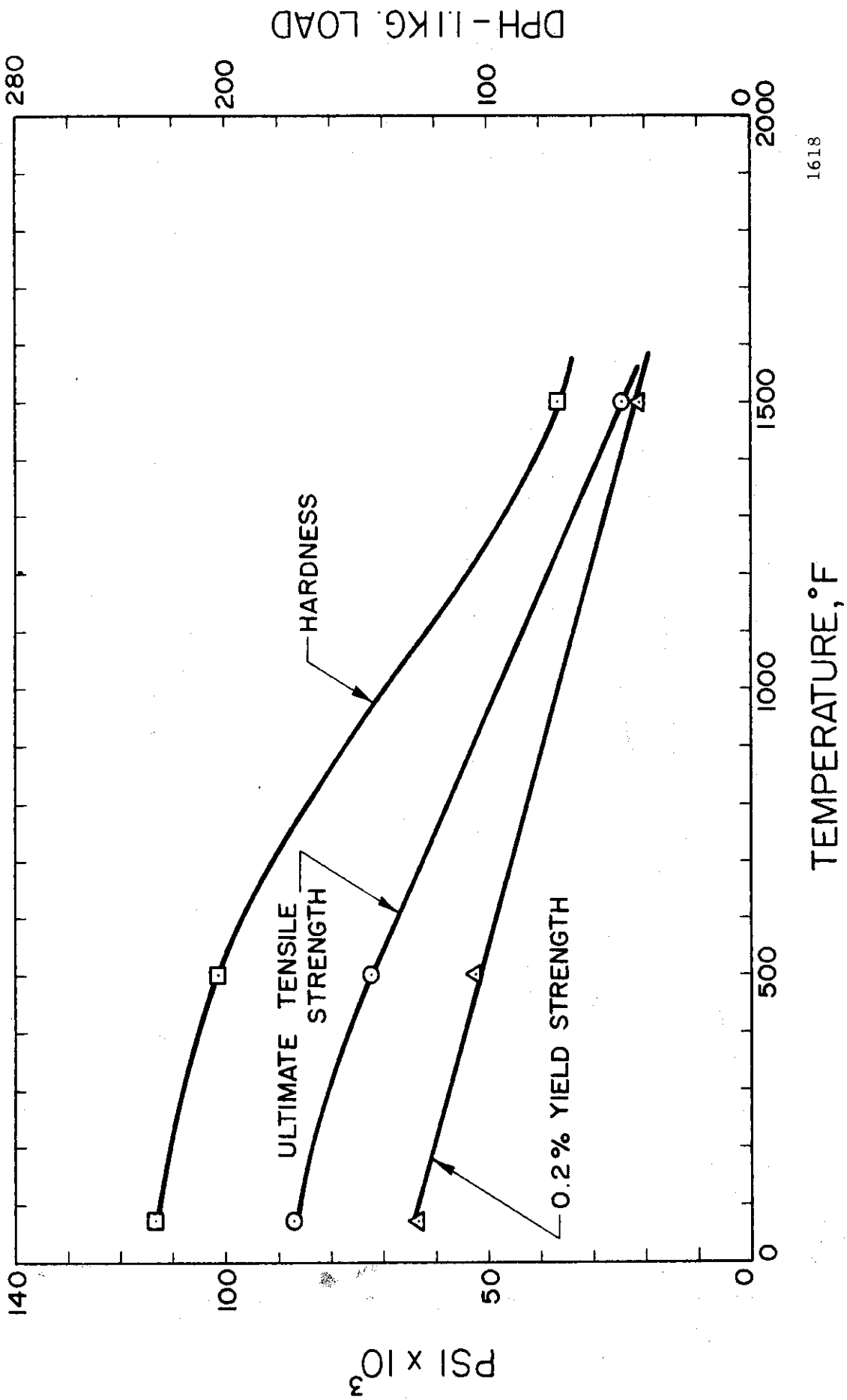
Fig. 69.--Effect of temperature on mechanical properties of type 316 stainless steel.
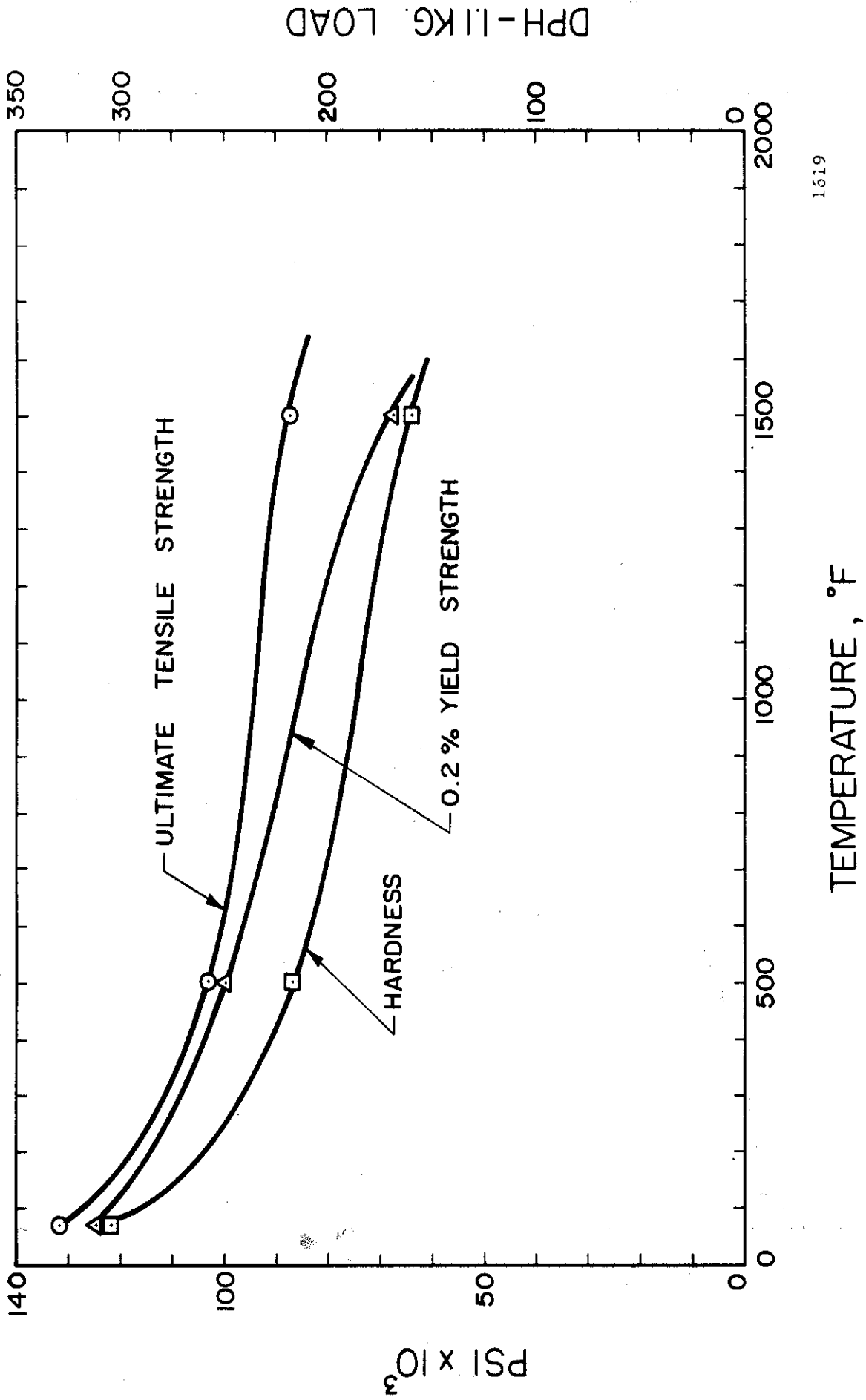
Fig. 70.—Effect of temperature on mechanical properties of T-111.
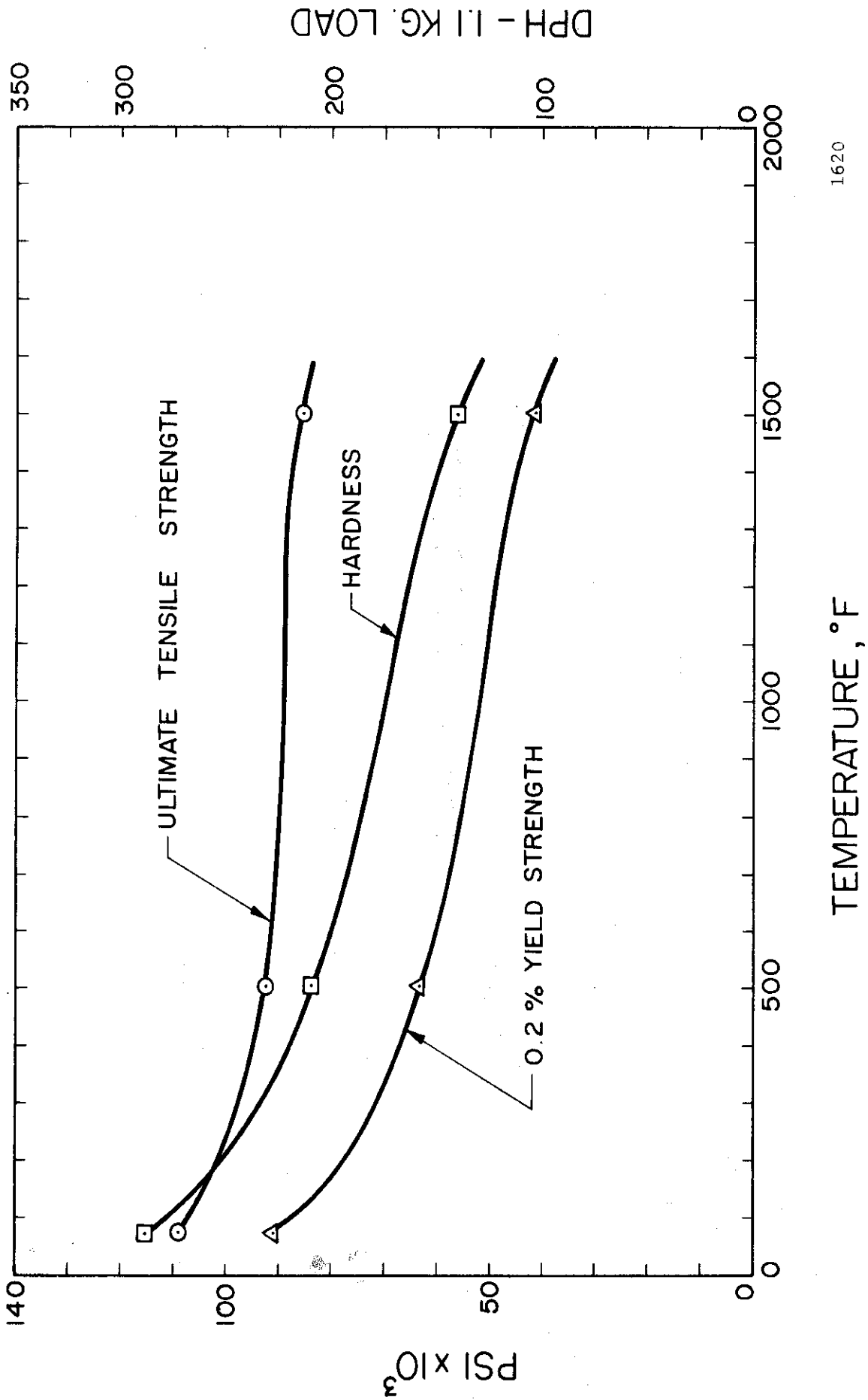
Fig. 71.--Effect of temperature on mechanical properties of T-222(A).
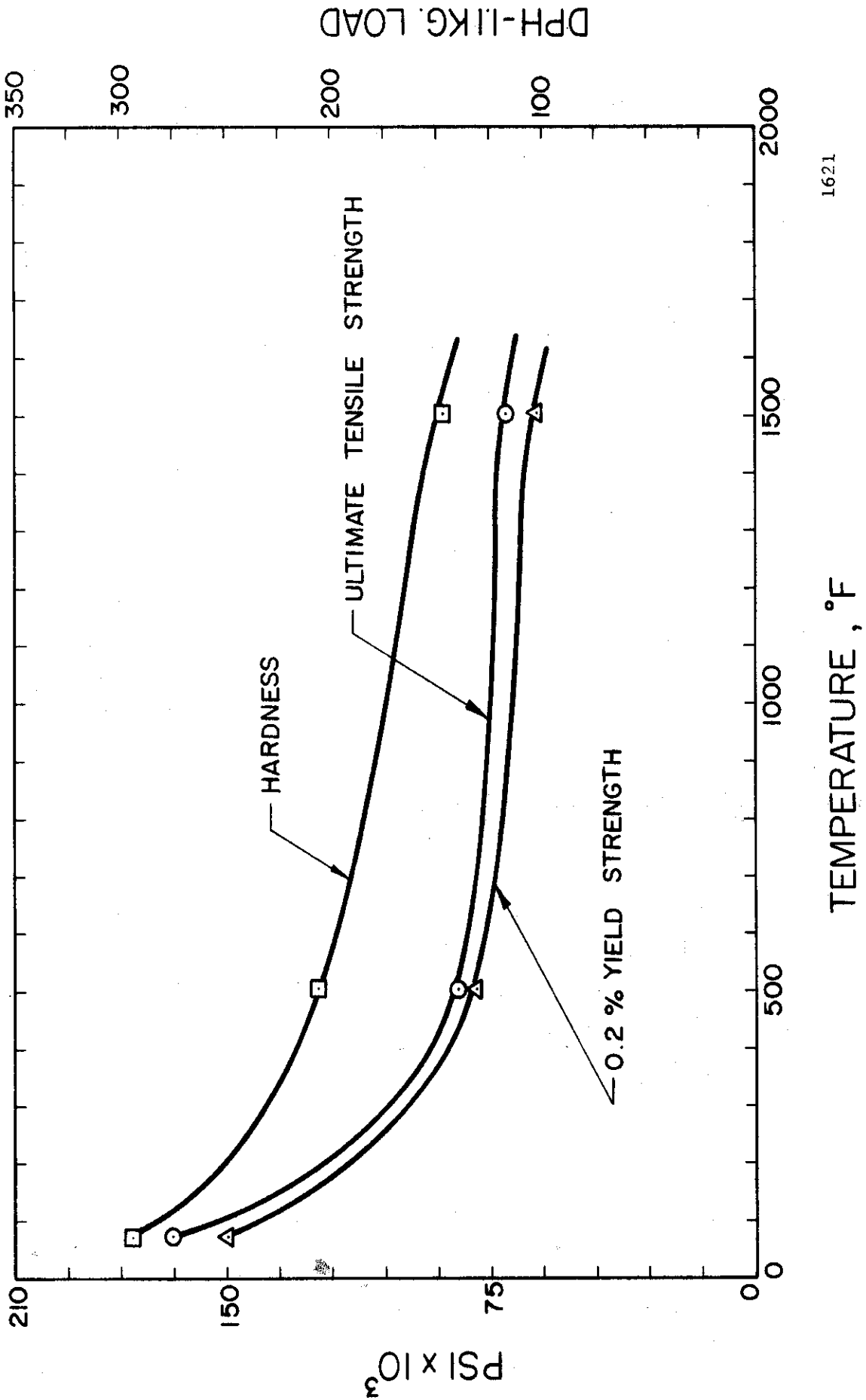
Fig. 72.--Effect of temperature on mechanical properties of Mo-1/2Ti.

1621
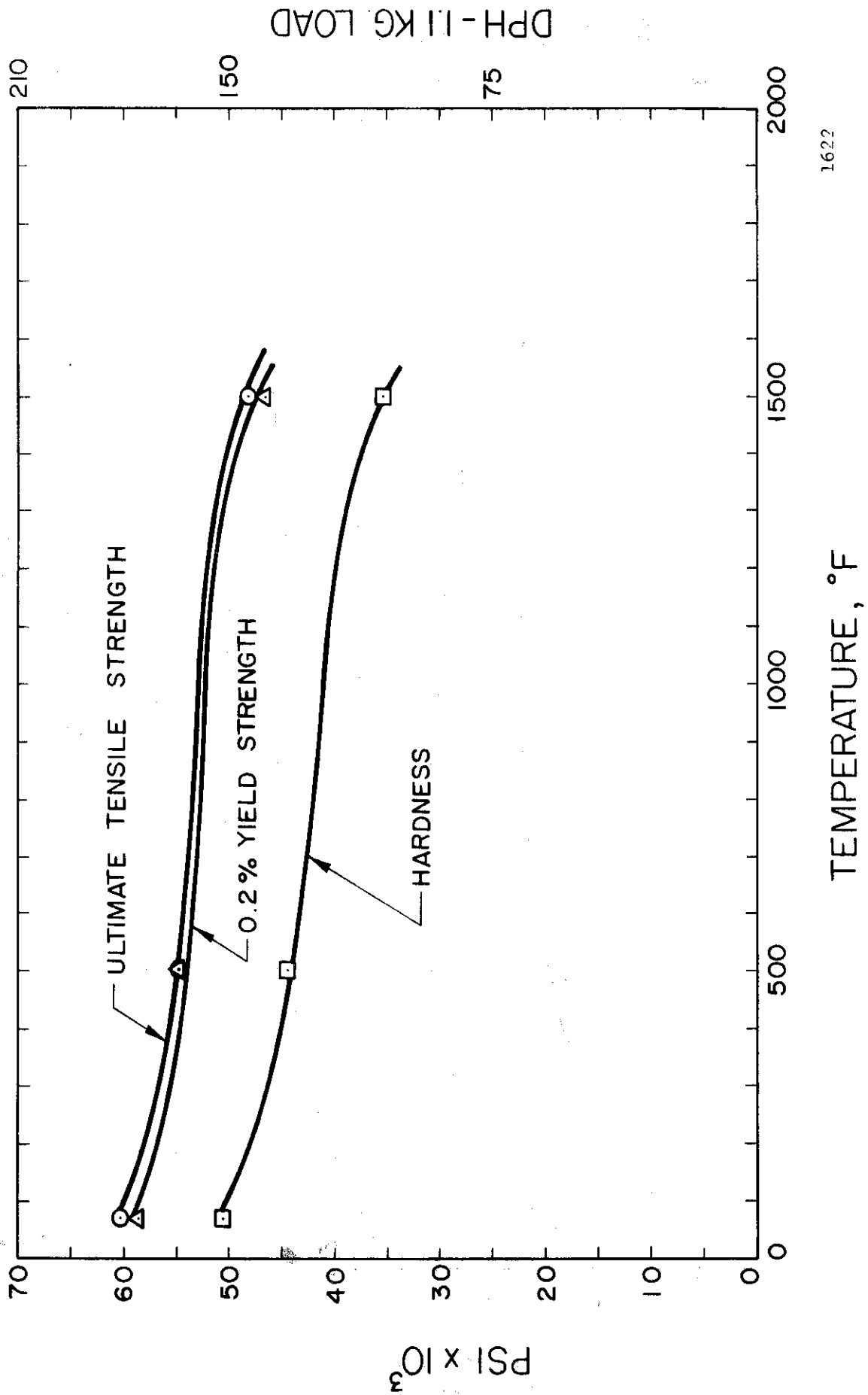
Fig. 73.--Effect of temperature on mechanical properties of Cb-1Zr.

1622
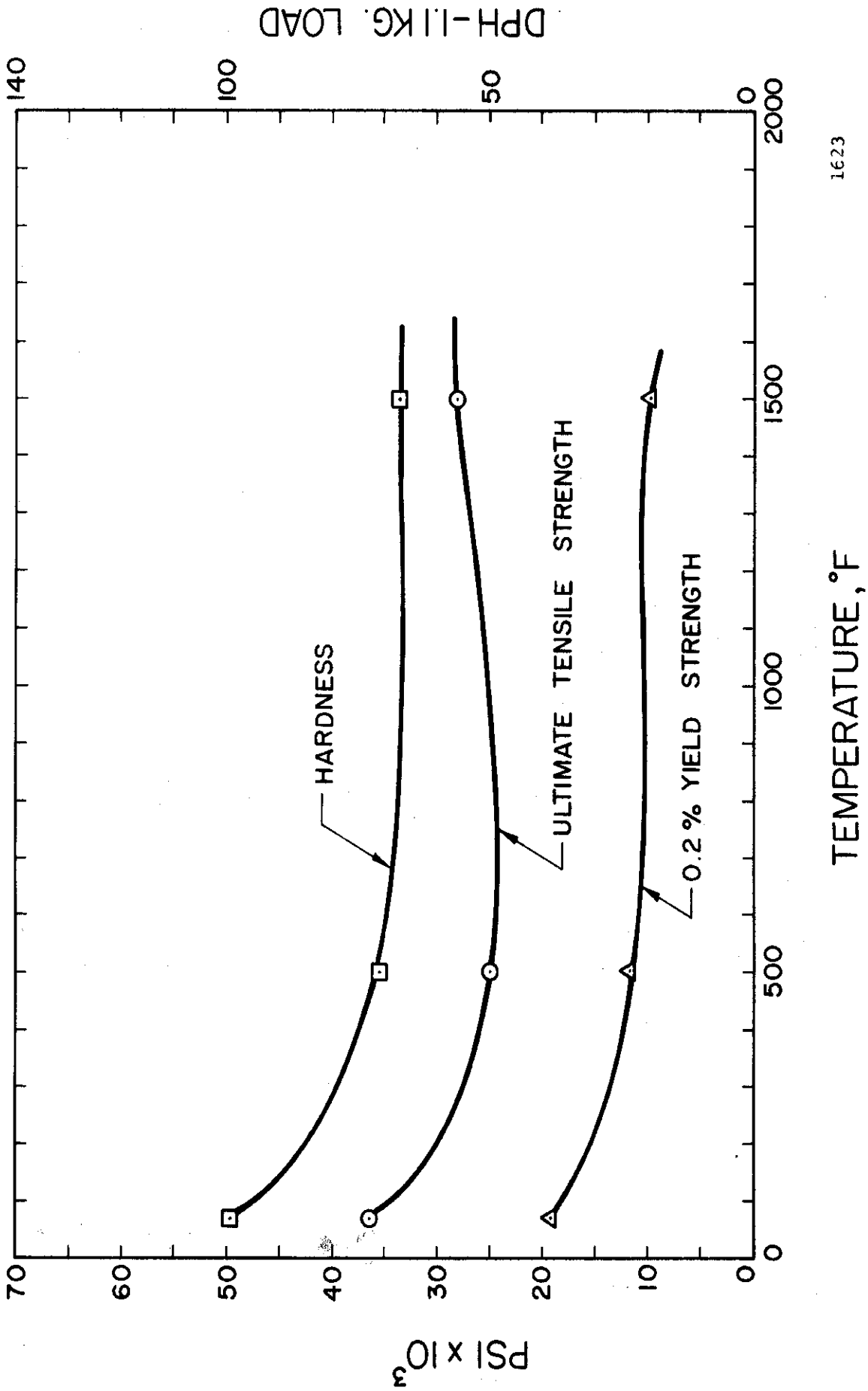
Fig. 74.--Effect of temperature on mechanical properties of Cb-1Zr(A).

1623

6) For Cb-1Zr the variation of the mechanical properties shown in Figure 73 is a very weak function of temperature.

7) For Cb-1Zr(A) there is a decrease in the ultimate tensile strength, 0.2% yield strength, and hardness as the temperature is increased from 70°F to 500°F. Thereafter, the properties are a very weak function of the temperature.

8) At room temperature the tensile strength and yield strength of the stainless steels are about 50% less than the corresponding properties for the T-111, T-222(A), and Mo-1/2Ti.

9) At 500°F the tensile strength and yield strength of the stainless steels are roughly comparable with the corresponding properties of the T-111, T-222(A), and Mo-1/2Ti.

10) At 1500°F the tensile strength and yield strength of the T-111, T-222(A), and Mo-1/2Ti are on the order of 4 times greater than the corresponding properties of the stainless steels.

The strain energy to failure (ESE) was determined by computing the area under the engineering stress-strain curve which was supplied by Pratt & Whitney Aircraft (CANEL). The effect of temperature on the strain energy of the seven materials tested is shown in Figure 75. Again, it is apparent that the strain energy of the stainless steels decreases rapidly with increasing temperature, while the strain energy of the T-111, T-222(A), and Mo-1/2Ti is not greatly affected by temperature. Although the strain energy of the Cb-1Zr and the Cb-1Zr(A) is somewhat insensitive to temperature also, the absolute magnitude of the
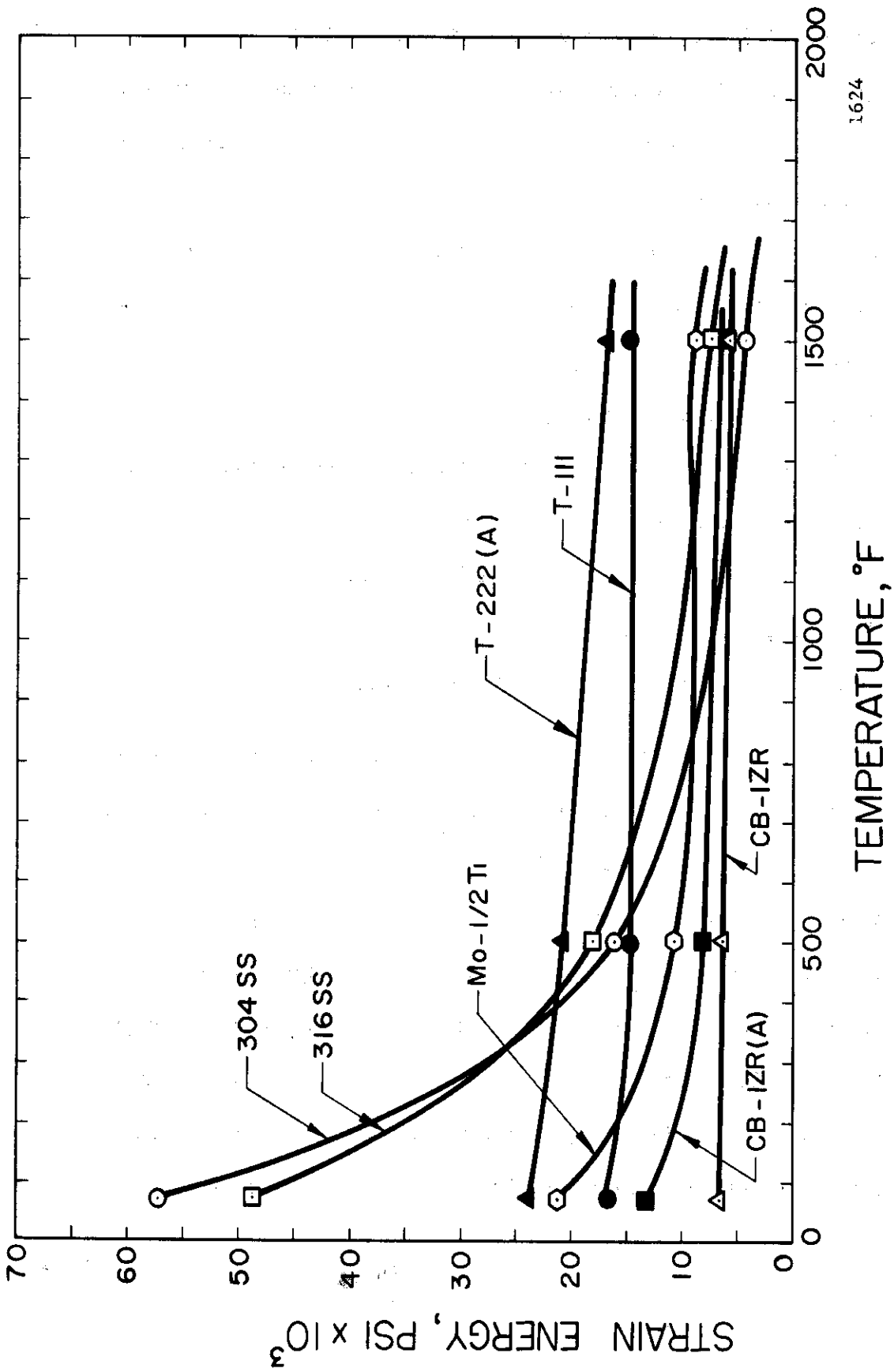
Fig. 75.--Effect of temperature on engineering strain energy
of stainless steels and refractory alloys.

1624

quantity does not compare with that of the other refractory alloys at any temperature.

The mechanical properties data for the aluminum alloys, carbon steel, Plexiglas, and the Cu, Cu-Ni, Cu-Zn, and Ni materials were determined at room temperature in the Department of Chemical and Metallurgical Engineering laboratories at The University of Michigan and are presented in Table 34. The mechanical properties for carbon steel[*] were also determined at 500°F and so noted in Table 34.

Available mechanical properties data for the bearing materials are presented in Table 35. The three BG-42 materials and the Blue Chip Tool Steel were tested at 500°F (stress-strain curve generated and hardness measured) in the Department of Chemical and Metallurgical Engineering laboratories. Hardness data was obtained for all of the bearing materials investigated and is also presented in Table 35.

Examination of the data in Tables 31 through 35 indicates that several of the mechanical properties such as tensile strength, yield strength, strain energy, and hardness decrease in value for a given material as the temperature is increased. Such trends are indicative of the behavior of the cavitation resistance as a function of temperature in some cases, as has been previously discussed. Undoubtedly, it should be possible to correlate the cavitation resistance of the materials tested with the applicable mechanical and fluid properties data at the

---

[*]The hot-rolled carbon steel used in these investigations had a carbon content of 0.05%, silicon content less than 0.05%, and a hardness of Rockwell "B" = 42.

TABLE 34

MECHANICAL PROPERTIES DATA AT 70°F FROM UNIVERSITY OF MICHIGAN LABORATORIES

Material	Tensile Strength psi	Yield Strength psi	Eng. Strain Energy psi	True Strain Energy psi	DPH Hardness 1.1 Kg.	Elongation %	Area Reduction %	Elastic Modulus psi
1100-0 Al	12,250	7,600	4,950	4,320	22,600	27	44.5	85.5	10.0×10^6
2024 Al	72,000	57,900	13,300	13,600	31,050	171	20.0	34.5	10.0×10^6
6061 Al	45,300	40,000	25,800	9,840	38,620	127	19.4	56.7	10.0×10^6
Carbon Steel (70°F)	45,300	41,600	18,440	30,530	111,000	193	46.3	76.1	29.0×10^6
Carbon Steel (500°F)	62,510	18,400	19,225	20,900	66,650	125	37.2	63.6	28.0×10^6
Plexiglas	10,445	1,600	320	320	320	9	4.0	0.0	0.4×10^6
Cu	53,400	49,500	3,100	11,800	11,800	133	6.2	19.8	17.0×10^6
Cu-900°F	31,500	9,500	13,900	26,900	26,900	51	51.3	48.5	17.0×10^6
Cu-1500°F	30,700	5,000	6,100	11,800	11,800	41	32.5	33.2	17.0×10^6
Cu-Zn	93,900	82,000	4,700	55,400	55,400	197	5.3	40.7	16.0×10^6
Cu-Zn-850°F	47,600	20,000	28,600	57,000	57,000	71	62.6	60.9	16.0×10^6
Cu-Zn-1400°F	40,400	11,000	15,300	33,000	33,000	48	58.9	51.7	16.0×10^6
Cu-Ni	87,300	77,000	6,100	13,200	13,200	197	4.5	15.4	22.0×10^6
Cu-Ni-1300°F	57,900	20,000	3,100	36,200	36,200	96	34.9	43.5	22.0×10^6
Cu-Ni-1800°F	53,300	18,000	16,300	21,800	21,800	77	34.4	34.4	22.0×10^6
Ni	93,100	82,000	3,200	8,300	8,300	206	3.9	10.2	30.0×10^6
Ni-1100°F	50,500	13,000	18,300	48,300	48,300	67	43.8	51.6	30.0×10^6
Ni-1600°F	48,700	7,000	16,100	40,500	40,500	59	41.8	49.7	30.0×10^6

TABLE 35

MECHANICAL PROPERTIES DATA FOR BEARING MATERIALS

Material	Tensile Strength psi	Yield Strength psi	Eng. Strain Energy psi	True Strain Energy psi		Hardness	Elonga-tion %	Area Reduction %	Elastic Modulus psi
BG-42(R_c=64)	318,000	273,000	4,840	6,650	7,250	64 R_c(789*)	2.2	2.5	30.0×10^6
BG-42(R_c=53)	251,000	234,000	2,940	3,300	7,940	53 R_c(562*)	1.6	3.2	30.0×10^6
BG-42(R_c=47)	184,000	154,000	3,120	3,810	4,910	47 R_c(471*)	2.3	2.8	30.0×10^6
Blue Chip Tool Steel	340,000	302,000	6,840	7,300	7,800	64 R_c(789*)	2.6	2.5	30.0×10^6
Single-Crystal Tungsten						32 R_c(317*)			
Graphitar-Grade 80	20,000***					54 R_h(80**)			
Graphitar-Grade 50	35,000***					70 R_h(100**)			

*DPH (1.1 Kg. Load).

**Average Shore Scleroscope Hardness.

***Compressive Strength.

test temperatures. However, the conventional mechanical properties as
here described are measured under semi-static conditions and, hence, may
not be fully applicable to the high loading rates typical of cavitation
failure. Applicable fluid properties will now be examined.

CHAPTER V

FLUID PROPERTIES DATA FOR THE TEST FLUIDS

A. Introduction

In order to obtain a meaningful correlation between the cavitation resistance of the various materials tested, their mechanical properties, and suitable fluid coupling parameters, it is important to choose applicable fluid properties for this purpose. Since the dynamics of bubble formation and collapse are controlled by the physical properties of the fluid, it is necessary to account for variations in fluid properties, as the tests were conducted in four different fluids at several test temperatures. Both Plesset[76] and Hammitt and Smith[77] have conducted comprehensive reviews of the dynamics of bubble formation and collapse. The various fluid properties that enter into the appropriate differential equations (and solutions for bubble collapse pressure) describing the growth and collapse of a bubble under different sets of assumptions include the fluid density, surface tension, vapor pressure, net positive suction head, bulk modulus, and kinematic viscosity. In addition, if heat transfer effects[69,76,78] become important in describing the formation and collapse of bubbles, then various thermal properties such as the specific heat, thermal conductivity, heat of

vaporization, thermal diffusivity, and Prandtl Number of the test fluid must be considered.

Initially, the computer correlations of cavitation damage data with applicable mechanical and fluid properties for this study were conducted under the assumption that thermodynamic effects in the formation and collapse of bubbles were negligible. The validity of this assumption has been explored in detail by Florschuetz and Chao,[79] but it is generally true if the fluid temperatures involved are considerably below the ordinary fluid boiling point, i.e., the vapor pressure of the fluid is small. This was not exactly true in all of our investigations. As a result, the thermodynamic effects will be examined separately in a later section.

At this point the fluid properties that have been examined in the computer correlations include the ratio of the acoustic impedances of the test fluid and specimen material, fluid density, surface tension, net positive suction head, compressibility or bulk modulus, and kinematic viscosity. Each of these fluid properties will be examined with respect to theoretical and experimental evidence pointing to their selection as fluid coupling parameters.

B. Fluid Properties Selection

The fluid properties which were selected as coupling parameters for the computer correlations of the experimentally-determined cavitation damage data are listed above. Again, it is emphasized that thermodynamic effects have been neglected in these correlations. From a

theoretical point of view all of these fluid properties have appeared in differential equations describing the formation and collapse of a bubble and the resultant pressure loading on adjacent surfaces, under different sets of assumptions. Hence, it is reasonable to choose such properties as fluid coupling parameters. Detailed comments regarding each of these properties follow.

1. Acoustic Impedance Ratio (AI)

The acoustic impedance ratio is defined as:[52]

$$AI = \frac{\text{Acoustic Impedance of Test Fluid}}{\text{Acoustic Impedance of Test Specimen}} = \frac{R_1}{R_2}$$

$$AI = \frac{(\rho c)_{FLUID}}{(\rho c)_{MATERIAL}}$$

where:

AI = acoustic impedance ratio

ρ = density

c = velocity of sound in medium

R_1 = acoustic impedance of test fluid

R_2 = acoustic impedance of test specimen

The velocity of sound, c, can be expressed as:

$c = (E/\rho)^{1/2}$ (for a solid)

$c = (B/\rho)^{1/2}$ (for a liquid)

where:

E = elastic modulus (for a solid)

B = bulk modulus (for a liquid)

Thus:

$$AI = \frac{(B\rho)^{1/2}_{FLUID}}{(E\rho)^{1/2}_{SOLID}}$$

Physically, the acoustic impedance ratio is related to the ratio of reflected to transmitted energy as liquid shock waves or jets impinge on the solid test material. The transmission coefficient, α_t, which is defined as the fraction of acoustic energy incident upon an interface of two materials possessing dissimilar acoustic impedances that is transmitted across the interface, can be expressed as:[52]

$$\alpha_t = \frac{4\,R_1 R_2}{(R_1+R_2)^2} = \frac{4(R_1/R_2)}{(R_1/R_2)^2 + 2(R_1/R_2) + 1}$$

where in our case R_1 and R_2 are the acoustic impedances of test fluid and test material, respectively. It is seen that as $R_1 \rightarrow R_2$, $\alpha_t \rightarrow 1$, and we have 100% transmission. Further, if a liquid jet is assumed to be the damaging mechanism in cavitation, then according to the most simplified "water-hammer" analysis,[77] R_1/R_2 enters into the expression for the transient pressure generated on the surface by jet impact, i.e.,

$$\Delta P_{impact} = \frac{\rho_1 c_1 v}{1 + R_2/R_1}$$

where:

ΔP_{impact} = pressure increase on surface due to impact

ρ_1 = density of fluid

c_1 = velocity of sound in fluid

v   = velocity of liquid jet

R_1 = acoustic impedance of fluid

R_2 = acoustic impedance of test specimen

In the case of our experiment there are several reasons why one

might select the acoustic impedance ratio as a suitable coupling param-

eter for the comprehensive cavitation damage correlations. First,

acoustic energy in the form of sound waves is transmitted along the

exponential horn assembly to which the test specimen is attached. This

acoustic energy is then propagated from horn to test specimen and from

test specimen into the test fluid, but the amount of energy passing

these two interfaces and into the fluid is determined by the acoustic

impedances of the horn, test specimen, and fluid. Presumably, the form-

ation of a bubble cloud at the specimen face is strongly dependent on

the energy being transmitted into the fluid. Secondly, the bubble col-

lapse gives rise to a shock wave or liquid jet that is propagated

through the fluid. In order for damage to occur at the specimen sur-

face, this energy in the form of the shock wave or liquid jet must be

transmitted across the liquid-solid interface. Hence, one might expect

the amount of damage to the test specimen to be a function of the amount

of energy transmitted across this interface and actually reaching and

being absorbed in the specimen. Here again, the ratio of acoustic

impedances or the transmission coefficient is the determining factor.[80]

Finally, the ratio is involved in the relation for pressure-loading of

the surface in the case of jet impact, as previously stated. Because of

its possible involvement in all these ways the ratio of acoustic

impedances between liquid and specimen was chosen as a possible fluid coupling parameter. It is further postulated that the greater the acoustic impedance ratio, the greater the amount of damage sustained by the test specimen. This is reasonable since as $(R_1/R_2) \to 1, \alpha_t \to 1$, and we have complete transmission of the acoustic energy from transducer tip to fluid, and complete transmission of energy represented by shock waves or liquid jets from fluid to specimen surface, causing maximum damage. In addition, the pressure generated by the impacting jet is also maximized for a given fluid condition.

2. Density (ρ)

The density of the fluid may be a suitable coupling parameter since one would expect the pressure exerted on the specimen surface to be approximately proportional to the density for fixed NPSH, compressibility, kinematic viscosity, etc. Hence, one would expect the damage to increase as the density was increased. Wilson and Graham[81] conducted cavitation tests on silver in a variety of fluids and showed experimentally that this was, indeed, the case, as is also indicated in the present study by comparison of the different fluids used.

3. Surface Tension (σ)

The expected effect of surface tension on cavitation damage, based on the conclusions from dynamics of transient cavities, would be an increase in damage as the surface tension is increased, since collapse pressures would be higher with greater surface tension. This behavior was reported experimentally by Nowotny.[32] However, recent

numerical calculations show that the effect of surface tension in this regard should be quite negligible.[82,83] On the other hand, for a given kinematic situation, high surface tension would inhibit bubble nucleation and thus tend to reduce the bubble population. This, presumably, would result in a reduction of cavitation damage.

4. Net Positive Suction Head (NPSH)

The net positive suction head, NPSH, is defined as:

$$NPSH = \frac{p - p_v}{\rho}$$

where:

p = local pressure of fluid

p_v = vapor pressure of fluid

ρ = density of fluid

It is commonly used as a similarity parameter in turbomachinery design where cavitation is a factor, i.e., to a first approximation, if geometry and NPSH are maintained constant, the cavitating flow regime should remain constant. It was shown by Nowotny[32] that damage was decreased as the vapor pressure increased for tests where p in the above relation was held constant, since the collapsing pressure differential was reduced for a given fluid and, in addition, perhaps the additional vapor served to cushion the collapsing bubbles, as is discussed later under thermodynamic effects. As mentioned previously, the damage rate would be expected to increase as the density increased if the NPSH were held constant. In general, the damage should be inversely related to the NPSH. In our experiments the local static pressure, p, was varied by varying

the argon cover gas pressure so that the difference between local static pressure and vapor pressure, $p - p_v$, was maintained constant. Then;

$$\text{NPSH} \propto 1/\rho$$

for the tests of this study based on steady-state pressure. However, the transient head caused by the vibration of the horn would be the same for all fluids, assuming the fluid density and temperature do not affect the vibrating behavior of the horn (of course, this is not precisely true). Since the transient contribution to the NPSH is probably predominant, these tests may well be closer to a constant NPSH condition than a constant pressure suppression condition. If so, the collapse velocities would be similar for all fluids, and the imposed pressures on the surface would be proportional to the fluid density, so that damage should increase with increased fluid density, as it did. Clearly, more sophisticated and detailed analysis on this point is required to understand the complex relationships involved.

5. <u>Bulk Modulus (B)</u>

The bulk modulus is the inverse of the compressibility. It should be an important coupling parameter, since it strongly affects the pressure exerted on the specimen surface, as shown by numerical analyses.[82,83,84] Hence, one would expect the damage to increase as the bulk modulus increased (compressibility decreased). This behavior was reported from experiments by Wilson and Graham.[81]

6. Kinematic Viscosity (ν)

The kinematic viscosity, ν, is defined as:

$$\nu = \mu/\rho$$

where:

μ = dynamic viscosity of fluid

ρ = density of fluid

Since bubble collapse pressures are theoretically greater[82,83] in fluids of low kinematic viscosity (although the effect is quite small for fluids in the conventional viscosity range), one would expect cavitation damage to be inversely related to this parameter. Since kinematic viscosity is directly involved rather than viscosity, it is chosen at this point. Wilson and Graham[81] reported this effect from their experiments.

It is felt that each of the six quantities discussed above merits consideration as a fluid coupling parameter for the comprehensive lead-bismuth, mercury, water, and lithium correlations to be discussed.

C. Tables of Fluid Properties at 70°F,
   500°F, and 1500°F

Fluid properties data for water, mercury, lead-bismuth alloy, and lithium at the appropriate test temperatures are listed in Table 36. The data was taken from references 65, 85, and 86. The properties include the six coupling parameters that have been discussed previously and which will be used in the comprehensive computer correlations of the cavitation damage data and also the thermal properties which determine the importance of heat transfer effects. These will be described later.

TABLE 36

FLUID PROPERTIES DATA AT VARIOUS TEMPERATURES

(Taken from References 65, 85, and 86)

Fluid Property	Fluid						
	Water 70°F	Mercury 70°F	Mercury 500°F	Pb-Bi 500°F	Pb-Bi 1500°F	Li 500°F	Li 1500°F
Acoustic Impedance (AI) (lbm/ft.²sec.)	0.299×10^6	4.03×10^6	3.85×10^6	3.08×10^6	2.86×10^6	0.149×10^6	0.137×10^6
Density (ρ) (g./cc.)	1.0	13.55	12.98	10.38	9.64	0.50	0.46
Surface Tension (σ) (dynes/cm.)	72.8	465.0	419.0	397.0	367.0	386.0	308.0
Net Positive Suction Head (NPSH) (feet)	36.5	2.7	2.8	3.5	3.8	73.0	79.4
Bulk Modulus (B) (psi)	0.31×10^6	4.11×10^6	3.94×10^6	3.16×10^6	2.92×10^6	0.160×10^6	0.14×10^6
Kinematic Viscosity (ν) (ft.²/hour)	0.039	0.0044	0.0030	0.0064	0.0047	0.035	0.017
Specific Heat (C_p) (cal./g.°C)	1.00	0.033	0.032	0.035	0.035	1.00	1.00
Thermal Conductivity (k) (cal./sec.cm.°C)	1.41×10^{-3}	0.021	0.030	0.025	0.022	0.090	0.090

TABLE 36--Continued

Fluid Property	Water 70°F	Mercury 70°F	Mercury 500°F	Pb-Bi 500°F	Pb-Bi 1500°F	Li 500°F	Li 1500°F
Heat of Vaporization (HV) (cal./g.)	585	69.7	69.7	204	204	4680	4680
Vapor Pressure (p_v) (psi)	0.36	<0.001	1.93	<0.001	<0.001	<0.001	0.1
Thermal Diffusivity (K) (ft.^{2}/hr.)	0.0053	0.169	0.333	0.457	0.522	0.700	0.771
Prandtl Number (Pr) (Dimensionless)	7.31	0.026	0.009	0.014	0.009	0.050	0.022

CHAPTER VI

CORRELATIONS OF CAVITATION DAMAGE DATA WITH

MECHANICAL AND FLUID PROPERTIES

A. Introduction

In order to fully investigate the dependence of cavitation

resistance on the mechanical properties of the test materials and on the

fluid properties, and to obtain a better understanding of the damage

mechanisms involved, it is desirable to subject the experimentally-

determined cavitation data and the appropriate mechanical and fluid

properties data to a least mean squares fit by means of a suitable digi-

tal computer program. For these studies the University of Michigan IBM

7090 digital computer facility has been utilized along with a very

sophisticated least mean squares stepwise regression program which was

first proposed by Westervelt[87] and later revised by Crandall.[88] This

program has been described previously.[42,43,64] However, for the sake of

completeness the detailed explanation is included in Appendix B.

Before the results of the computer correlations are described,

it is instructive to obtain a qualitative feel for those mechanical

properties that might best give some clue as to the cavitation resist-

ance of a particular material. The lead-bismuth data obtained at 500°F

and 1500°F and the data obtained in the bearing program have been examined on a preliminary basis and the results are described below.

B. Preliminary Correlations

1. Lead-Bismuth Data

A preliminary correlation of the lead-bismuth data obtained at 500°F and 1500°F with the ultimate tensile strength, 0.2% yield strength, hardness, and the engineering strain energy was attempted initially. The data at each temperature was analyzed individually. On the basis of the mechanical properties values listed in Tables 32 and 33, it is possible to arrive at several ratings of the materials tested at each temperature. An ultimate tensile strength rating would be obtained by assigning that material with the greatest ultimate tensile strength a value of "1," while "7" would denote that material with the smallest value of this property. In a similar manner the materials can be rated on the basis of the 0.2% yield strength, the hardness, and the engineering strain energy. In each case a rating of "1" would be assigned to that material having the greatest value of the particular property involved, "7" denoting the material with the smallest value. It is intuitively obvious that those materials having greatest tensile strength, yield strength, hardness, and engineering strain energy probably will be the most cavitation resistant also. Based on the four mechanical properties listed above, each material now has four ratings. If one now assumes a weighting factor of unity appropriate for each of these properties, it is possible to obtain a final rating for each of

the materials, namely, the sum of the four ratings already determined. Then the materials can be rated on the basis of the sum of the four individual ratings. The end result is an arrangement of the 7 materials tested with a rating of "1" denoting that material which will probably be most cavitation resistant, predicted on the basis of the mechanical properties listed above. The rating of "7" denotes that material which should be most susceptible to cavitation erosion. It is then possible to compare the final rating of the materials with the rating based on the actual cavitation data obtained in the experiment.

At 500°F the individual ratings of the materials based on mechanical properties, the final rating, and the rating based on the average MDP rate exhibited by the specimens are all summarized in Table 37. It is interesting to note that the experimental rating (based on MDP) agrees almost exactly with the rating based on the mechanical properties data. So, incidentally, does a ranking of hardnesses (which has often been used as a basis for rating cavitation resistance). However, none of the other properties taken singly are successful in this regard. All these results are applicable at 500°F. Although the treatment is very qualitative and may appear naive, it is merely an attempt to generate some feeling for the problem at hand. It does show that, in general, a ranking by either strength or energy properties alone will not suffice. Hardness is a hybrid property in this sense, being neither a pure strength or energy property.

A qualitative correlation was also attempted at 1500°F in the same manner as was indicated at 500°F. The results are summarized in

TABLE 37

PRELIMINARY CORRELATION OF LEAD-BISMUTH DATA WITH
MECHANICAL PROPERTIES DATA AT 500°F

Material	UTS Rating	0.2% YS Rating	ESE Rating	Hardness Rating	Total	Final Rating	MDP Rating
T-111 (P & W)	1	1	4	1	7	1	1
T-222(A) (P & W)	3	3	1	2	9	2	2
Mo-1/2Ti (P & W)	4	2	5	3	14	3	3
316 SS (U-M)	5	6	2	4	17	5	4
304 SS (U-M)	2	4	3	5	14	3	5
Cb-1Zr (P & W)	6	5	7	6	24	6	6
Cb-1Zr(A) (P & W)	7	7	6	7	27	7	7

Table 38. The experimental rating agrees very well with either the final rating based on the mechanical properties data or the hardness rating, as before. Again, only hardness as a single property is reasonably successful in this regard.

2. Bearing Program Data

The only mechanical properties data available for all of the materials tested in the bearing program consists of values for the hardness. However, the complete list of properties used for all the materials and derivable from the stress-strain curve and hardness measurements are available for the various BG-42 materials and the Blue Chip Tool Steel (Table 35). Only fragmentary data is available for both grades of graphitar tested (Table 35).

It is useful to attempt to obtain a qualitative correlation (similar to that presented above for the lead-bismuth data) between the cavitation data obtained in the bearing program and the corresponding hardness data. In Table 39 the materials tested in this study are rated according to their cavitation resistance based on average MDP rate, with the BG-42 (R_c = 64) and the Blue Chip Tool Steel being the most resistant and each having a rating of "1." The graphitar-grade 50 was damaged the most and has a rating of "9." The hardness values for all the materials are also listed along with a rating based on hardness. The material with the greatest value of hardness is given a rating of "1," while the softest is given a rating of "9." There is quite good agreement between the MDP rating and the hardness rating. Only in minor instances is there disagreement. It appears that the cavitation

TABLE 38

PRELIMINARY CORRELATION OF LEAD-BISMUTH DATA WITH
MECHANICAL PROPERTIES DATA AT 1500°F

Material	UTS Rating	0.2% YS Rating	ESE Rating	Hardness Rating	Total	Final Rating	MDP Rating
T-111 (P & W)	1	1	2	1	5	1	1
T-222(A) (P & W)	2	4	1	3	10	2	2
Mo-1/2Ti (P & W)	3	2	3	2	10	2	3
316 SS (U-M)	6	5	4	5	20	5	5
304 SS (U-M)	7	6	7	7	27	7	7
Cb-1Zr (P & W)	4	3	6	4	17	4	4
Cb-1Zr(A) (P & W)	5	7	5	6	23	6	6

TABLE 39

PRELIMINARY CORRELATION OF BEARING PROGRAM
DATA WITH HARDNESS

Material	MDP Rating	Hardness	Hardness Rating	ESE Rating
BG-42 (R_c = 64) (TRW)	1	64 R_c(789*)	1	4
Blue Chip Tool Steel (TRW)	1	64 R_c(789*)	1	3
BG-42 (R_c = 53) (TRW)	4	53 R_c(562*)	3	6
Single-Crystal Tungsten (U-M)	3	32 R_c(317*)	5	-
BG-42 (R_c = 47) (TRW)	5	47 R_c(471*)	4	5
Mo-1/2Ti (P & W)	6	7 R_c(295*)	6	1
Cb-1Zr(A) (P & W)	7	81 R_f(99*)	7	2
Graphitar-Grade 80 (U-M)	8	54 R_h(80**)	9	-
Graphitar-Grade 50 (U-M)	9	70 R_h(100**)	8	-

*DPH (1.1 Kg. Load).

**Average Shore Scleroscope Hardness.

resistance of these materials correlates quite well with hardness on a qualitative basis. Of course, hardness has been selected by many past investigators as the best measure of the ability of a material to resist cavitation-erosion attack. A ranking according to engineering strain energy is also included in Table 39. It is noted that this parameter is low for all the bearing materials as compared to conventional materials, although their cavitation resistance is very high.

The graphitar-grade 50 and graphitar-grade 80 have average compressive strengths of 35,000 psi and 20,000 psi, respectively. However, the grade 80 appears to be the most cavitation resistant of the two, despite having the lower compressive strength, and also the lower hardness.

Obviously, a complete correlation of cavitation data with the applicable mechanical properties data demands full knowledge of the appropriate properties and a suitable digital computer program for analysis. Those materials tested in the bearing program for which complete mechanical properties data is available (all grades of BG-42 and Blue Chip Tool Steel) will be included in the computer correlations to be described at this time.

C. Lead-Bismuth Correlations

1. General

The cavitation data obtained at 500°F and 1500°F in lead-bismuth alloy was all submitted to the least mean squares regression program previously discussed in an attempt to obtain a first-order

interaction correlation that would be applicable at both temperatures and, hence, have the greatest generality allowed by the limited data. Ten mechanical and fluid properties were taken to be the independent variables with the average MDP rate being the dependent variable. The mechanical properties allowed in the analysis were the tensile strength, yield strength, engineering strain energy,[71] true strain energy (two values were considered, as explained before, one taking into account the elongation of the test specimen, and the other the reduction in area),[71] hardness, percentage elongation, percentage reduction in area, modulus of elasticity, and ratio of the acoustic impedances of the test fluid and specimen material.[42] These properties were selected since previous investigators had attempted correlations with them and/or because many of the properties have been involved in hypothesized damage mechanisms, as previously explained.

2. Single Property Correlations

Initially, an attempt was made to correlate the damage data with each mechanical property _individually_ in order to determine the relative importance of each alone with respect to predicting the observed cavitation damage. Table 40 summarizes the results of this effort. The 10 properties considered, the statistically best predicting equations generated by the program for each property, the coefficient of determination (CD)* for the analysis, and the average absolute percent

---

*The coefficient of determination is a statistical quantity that can be interpreted as the proportion of the total variation in the dependent variable that is explained by the predicting equation. Its values range from 0 (no prediction) to 1.0 (perfect prediction).

TABLE 40

SUMMARY OF SINGLE PROPERTY CORRELATIONS - LEAD-BISMUTH ALLOY

Property	Predicting Equation	CD*	AAPD**
1. True Strain Energy (TSER) (Based on Reduction in Area)	Avg. MDP Rate = $0.233 + 2.57 \times 10^4 (TSER)^{-1}$	0.986	0.1
2. True Strain Energy (TSEE) (Based on Elongation)	Avg. MDP Rate = $1.106 + 4.08 \times 10^{10} (TSEE)^{-3}$	0.964	13.8
3. Reduction in Area (RA)	Avg. MDP Rate = $0.937 + 2.89 \times 10^5 (RA)^{-3}$	0.907	37.9
4. Engineering Strain Energy (ESE)	Avg. MDP Rate = $0.324 + 8.77 \times 10^{11} (ESE)^{-3}$	0.878	5.7
5. Tensile Strength (TS)	Avg. MDP Rate = $0.675 + 7.41 \times 10^{13} (TS)^{-3}$	0.847	2.4
6. Hardness (H) (DPH - 1.1 Kg. Load)	Avg. MDP Rate = $0.451 + 1.72 \times 10^6 (H)^{-3}$	0.794	2.9
7. Yield Strength (YS)	Avg. MDP Rate = $-4.139 + 2.14 \times 10^2 (YS)^{-1/3}$	0.632	28.3
8. Acoustic Impedance Ratio (AI)	Avg. MDP Rate = $-2.321 + 12.22 (AI)$	0.546	40.9
9. Elastic Modulus (E)	Avg. MDP Rate = $-0.999 + 6.79 \times 10^7 (E)^{-1}$	0.520	47.2
10. Elongation (ELON)	Avg. MDP Rate = $2.771 - 2.38 \times 10^3 (ELON)^{-3}$	0.434	88.5

*Coefficient of Determination.

**Average Absolute % Deviation.

deviation (AAPD)[*] for the analysis are noted. The predicting equations

are arranged in order of decreasing statistical significance based on

the coefficient of determination. It is seen that true strain energy

based either on the reduction in area or elongation is quite successful

as a single correlating parameter for all of the lead-bismuth data. The

tensile strength, hardness, and engineering strain energy, although hav-

ing much lower values of coefficient of determination, are also success-

ful in this regard, based on the average absolute percent deviation.

The other mechanical properties listed do not suitably account for the

experimental data on an individual basis. It is further noted that the

average MDP rate is inversely proportional to powers of true strain

energy, engineering strain energy, tensile strength, and hardness in

this analysis. Hence, one might conclude that the cavitation resistance

of a group of materials in lead-bismuth alloy could at least be qualita-

tively predicted on the basis of these mechanical properties.

3. Multiple Property Correlations

Further attempts at complete correlations of the experimen-

tal data were conducted in which all ten mechanical properties noted

previously, each raised to any of ten integer or reciprocal integer

exponents, were possible terms in the predicting equation. Hence, a

total of 100 terms plus a pure constant were considered by the program.

Table 41 summarizes the statistically best predicting equations obtained

---

[*]The percent deviations between the experimental and predicted
values of MDP rate are algebraically summed. The average algebraic per-
cent deviation is then the algebraic sum divided by the number of data
points.

TABLE 41

SUMMARY OF BEST CORRELATIONS WITH TEN PROPERTIES CONSIDERED -
LEAD-BISMUTH ALLOY

(1)

$$\text{Avg. MDP Rate} = 0.713 + 3.12 \times 10^4 (\text{TSER})^{-1} - 6.55 \times 10^{-4} (\text{TS})^{-1} + 2.97 \times 10^{21} (\text{E})^{-3}$$

Coefficient of Determination = 0.996

Average Absolute % Deviation = 0.4%

(2)

$$\text{Avg. MDP Rate} = 0.233 + 2.57 \times 10^4 (\text{TSER})^{-1}$$

Coefficient of Determination = 0.986

Average Absolute % Deviation = 0.1%

(3)

$$\text{Avg. MDP Rate} = 0.682 + 3.24 \times 10^{10} (\text{TSEE})^{-3} + 1.09 \times 10^9 (\text{TS})^{-2}$$

Coefficient of Determination = 0.986

Average Absolute % Deviation = 0.8%

under these conditions. The coefficient of determination and average absolute percent deviation are noted for each of the correlations presented. Note that all three equations contain terms involving the true strain energy based either on elongation or reduction in area. The tensile strength is also prominent in two of the equations. These mechanical properties all enter the predicting equations in an inverse manner, as was the case with the single property correlations. The equation with the highest coefficient of determination involves a combination of true strain energy, tensile strength, and elastic modulus, each entering in an inverse relationship.

In the analysis of the lead-bismuth data allowing all ten mechanical properties, the end result is a series of 15 predicting equations or correlations, each with a different statistical accuracy. Obviously, the equation with the greatest statistical accuracy would result in the best fit between the predicted and experimental data. However, for the data submitted for analysis here, namely, the experimental cavitation information obtained at 500°F and 1500°F in lead-bismuth alloy and the corresponding mechanical properties, it was found that the coefficient of determination for all the correlations was never less than 0.98, indicating extremely good agreement between the predicting equation values and the experimental data.

Figure 76 is a plot of the predicted values of average MDP rate based on Equation (1) in Table 41 versus the corresponding experimental points. Deviation from the 45° line noted on the plot is a measure of the error inherent in the correlation. The excellent agreement between the predicted values and experimental points is noted.

AVG. MDP RATE = K_1 + K_2(TSER)$^{-1}$ + K_3(TS)$^{-1}$ + K_4(E)$^{-3}$

COEFFICIENT OF DETERMINATION = 0.996

AVERAGE ABSOLUTE % DEVIATION = 0.4%

1788
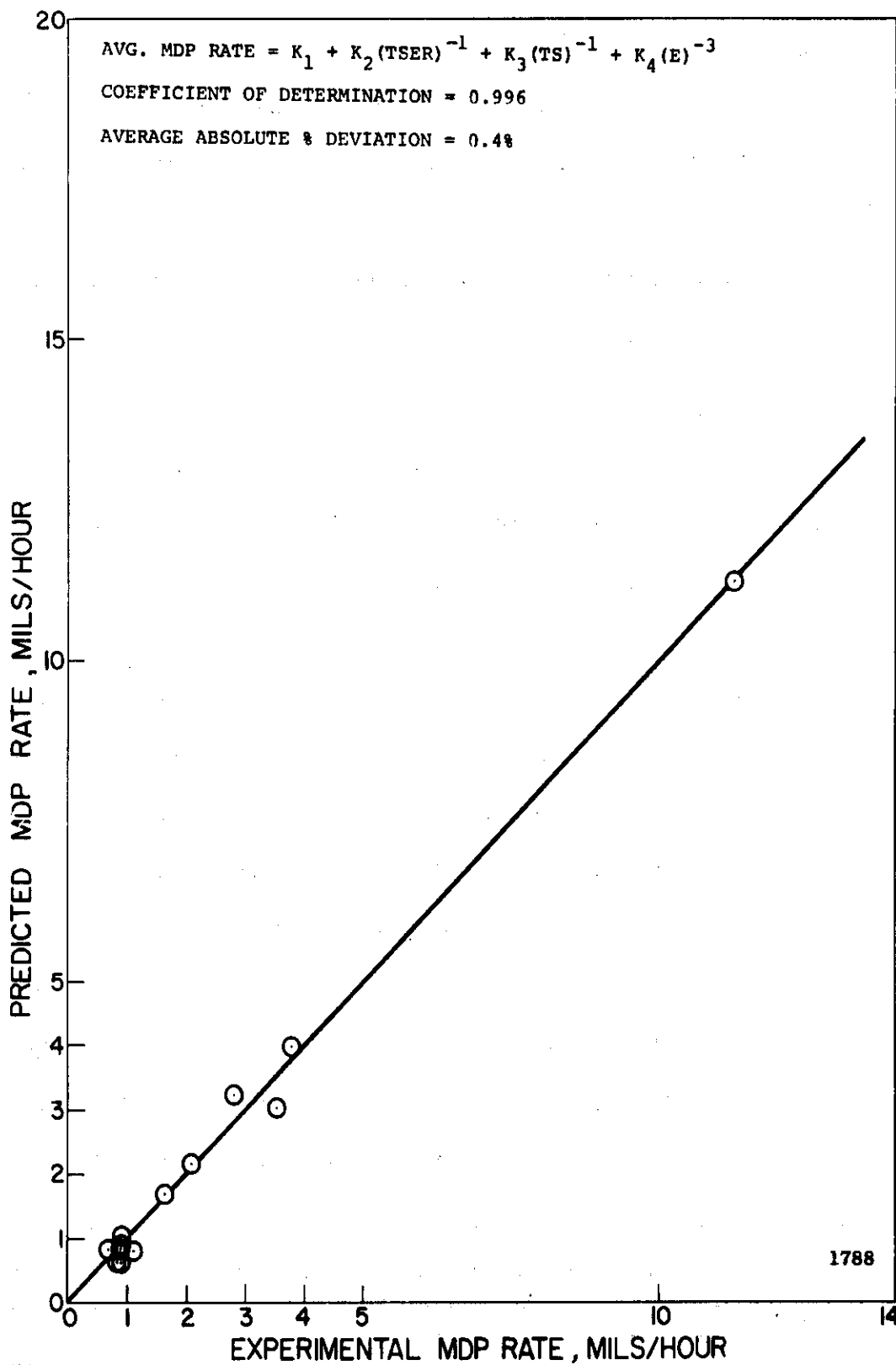
Fig. 76.--Comparison of Predicted MDP rate and experimental MDP rate - lead-bismuth alloy.

D. Mercury Correlations

1. General

The cavitation data obtained at 70°F and 500°F in mercury was also submitted to the least mean squares regression program in an attempt to obtain a first-order interaction correlation that would be applicable at both temperatures. The independent variables were the same as those discussed previously for the lead-bismuth correlations.

2. Single Property Correlations

Initially, an attempt was made to correlate the damage data with each mechanical property individually. Table 42 summarizes the results of this effort. The ten properties considered, the statistically best predicting equation generated by the program for each property, the coefficient of determination for the analysis, and the average absolute percent deviation for the analysis are noted. The predicting equations are arranged in order of decreasing statistical significance based on the coefficient of determination. It is seen that true strain energy based on elongation* and hardness are quite successful as single correlating parameters for all of the mercury data, although the best correlations are significantly worse statistically in terms of either coefficient of determination or percent deviation than those obtained with the lead-bismuth data. Tensile strength, yield strength, and

---

*Note that true strain energy based on reduction in area was a more successful parameter in the lead-bismuth correlations but is quite unsuccessful for the mercury tests. The reason for this disagreement is not known.

TABLE 42

SUMMARY OF SINGLE PROPERTY CORRELATIONS - MERCURY

Property	Predicting Equation	CD*	AAPD**
1. True Strain Energy (TSEE) (Based on Elongation)	Avg. MDP Rate = $0.338 + 4.90 \times 10^7 (TSEE)^{-2}$	0.965	8.5
2. Hardness (H) (DPH - 1.1 Kg. Load)	Avg. MDP Rate = $0.242 + 1.76 \times 10^4 (H)^{-2}$	0.921	15.8
3. Tensile Strength (TS)	Avg. MDP Rate = $-0.385 + 9.59 \times 10^4 (TS)^{-1}$	0.909	14.9
4. Yield Strength (YS)	Avg. MDP Rate = $0.178 + 3.82 \times 10^4 (YS)^{-1}$	0.863	26.5
5. Elastic Modulus (E)	Avg. MDP Rate = $0.269 + 6.16 \times 10^{21} (E)^{-3}$	0.831	18.5
6. True Strain Energy (TSER) (Based on Reduction in Area)	Avg. MDP Rate = $0.657 + 1.40 \times 10^{12} (TSER)^{-3}$	0.824	35.1
7. Engineering Strain Energy (ESE)	Avg. MDP Rate = $-0.179 + 1.58 \times 10^4 (ESE)^{-1}$	0.752	22.3
8. Acoustic Impedance Ratio (AI)	Avg. MDP Rate = $-0.186 + 4.91 (AI)^2$	0.735	34.2
9. Reduction in Area (RA)	Avg. MDP Rate = $-0.237 + 2.52 \times 10^{-6} (RA)$	0.684	49.0
10. Elongation (ELON)	Avg. MDP Rate = $1.091 - 1.96 \times 10^{-6} (ELON)^3$	0.538	64.3

*Coefficient of Determination.

**Average Absolute % Deviation.

elastic modulus are somewhat less successful in this regard. The other

mechanical properties listed do not suitably account for the experimen-

tal data on an individual basis. It is further noted that the average

MDP rate is inversely proportional to some power of true strain energy,

hardness, tensile strength, yield strength, and elastic modulus in this

analysis. Hence, one might conclude that the cavitation resistance of a

group of materials in mercury could at least be qualitatively predicted

on the basis of these mechanical properties.

3. Multiple Property Correlations

Complete correlations in which all ten mechanical properties

were allowed to enter the predicting equation were also conducted with

the mercury data. Table 43 summarizes the statistically best predicting

equations obtained under these conditions. The coefficient of determi-

nation and average absolute percent deviation are noted for each of the

correlations presented. Note that all three equations contain terms

involving the true strain energy based on elongation, whereas, as previ-

ously mentioned, the true strain energy based on reduction in area was

prominent in the lead-bismuth correlations. The hardness and tensile

strength are also prominent. All of these properties are inversely pro-

portional to the average MDP rate and, hence, proportional to cavitation

resistance. The statistically best correlation includes the true strain

energy based on elongation and the hardness.

Figure 77 is a plot of the predicted values of average MDP rate

based on Equation (1) in Table 43 versus the corresponding experimental

data points. The excellent agreement of the predicted values and exper-

imental points is noted.

TABLE 43

SUMMARY OF BEST CORRELATIONS WITH TEN PROPERTIES CONSIDERED - MERCURY

(1)

$$\text{Avg. MDP Rate} = -0.577 + 1.39 \times 10^{11} (\text{TSEE})^{-3} + 16.49 (\text{H})^{-1/2}$$

Coefficient of Determination = 0.966

Average Absolute % Deviation = 10.1%

(2)

$$\text{Avg. MDP Rate} = 0.338 + 4.90 \times 10^{7} (\text{TSEE})^{-2}$$

Coefficient of Determination = 0.965

Average Absolute % Deviation = 8.5%

(3)

$$\text{Avg. MDP Rate} = 0.232 + 1.41 \times 10^{11} (\text{TSEE})^{-3} + 2.89 \times 10^{4} (\text{TS})^{-1}$$

Coefficient of Determination = 0.961

Average Absolute % Deviation = 13.1%
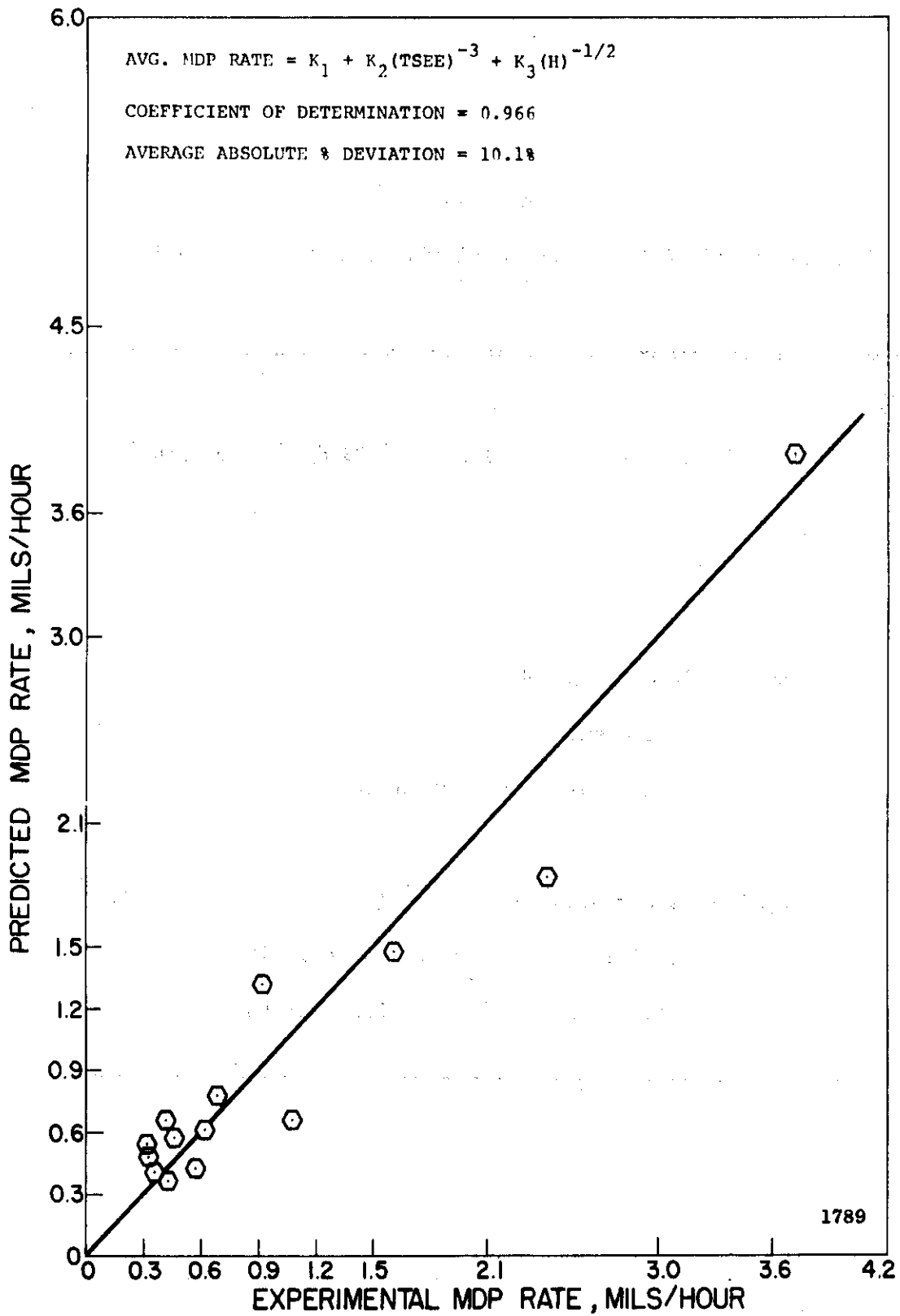
Fig. 77.--Comparison of predicted MDP rate and experimental MDP rate - mercury.

The materials tested in lead-bismuth alloy and mercury were identical with the exception of the carbon steel and Plexiglas which were tested in mercury only. Single property correlations for each of the fluids indicate that a different form of true strain energy is successful as a correlating parameter, each raised to a different exponent. Hardness and tensile strength are also relatively successful in this regard for both fluids. Ten property correlations for each of the fluids show that a form of strain energy and also tensile strength appear in the predicting equations for each fluid. In general, it is seen for both fluids that mechanical properties that successfully correlate the experimental data individually are also prominent in the full ten property predicting equations, as expected.

E. Water Correlations--Subset One

1. General

The cavitation data obtained at 70°F in water was analyzed in a manner similar to that employed for the lead-bismuth and mercury data. Since many more materials were tested in water than in the liquid metals, the materials were divided into three subsets for data analysis, as mentioned previously. Subset one consisted of those materials which were also tested in the liquid metals, whereas subsets two and three were tested in water only. Separate correlations of the cavitation data in subset one, subsets two and three combined, and the full water data set were carried out. Hence, the effects of different fluids on the correlations can be determined by examining the individual correlations

for the lead-bismuth data, mercury data, and subset one of the water data. The materials tested in all three cases were identical. Further, by comparing the correlations of subset one and the full water data set and by examining the correlation of subsets two and three combined, it is possible to determine any significant differences that may exist in correlating parameters for the various subsets of water data.

2. Single Property Correlations

Subset one was first correlated in terms of single properties. Table 44 summarizes the results of this effort. The ten properties considered, the statistically best predicting equation generated by the program for each property, the coefficient of determination for the analysis, and the average absolute percent deviation for the analysis are noted. It is seen that tensile strength, hardness, and yield strength are successful as single correlating parameters for subset one, each appearing in an inverse relationship. Note the extremely low average absolute percent deviation obtained in the tensile strength correlation. The acoustic impedance ratio is partially successful in this regard. The single property correlations of lead-bismuth and mercury data also indicated that tensile strength and hardness were successful correlating parameters. However, the prominence of some form of true strain energy in the lead-bismuth and mercury cases has been reduced considerably in the correlations of the subset one water data. It might also be noted here that the damage obtained in lead-bismuth alloy and mercury was very uniform, as noted previously, whereas the damage

TABLE 44

SUMMARY OF SINGLE PROPERTY CORRELATIONS - WATER - SUBSET ONE

Property	Predicting Equation	CD*	AAPD**
1. Tensile Strength (TS)	Avg. MDP Rate $= 0.006 + 8.38 \times 10^3 (TS)^{-1}$	0.953	0.2
2. Hardness (H) (DPH - 1.1 Kg. Load)	Avg. MDP Rate $= 0.184 - 4.26 \times 10^{-9} (H)^3$	0.934	4.8
3. Yield Strength (YS)	Avg. MDP Rate $= 0.011 + 27.95 (YS)^{-1/2}$	0.922	9.0
4. True Strain Energy (TSER) (Based on Reduction in Area)	Avg. MDP Rate $= 0.108 + 7.50 \times 10^{-17} (TSER)^3$	0.901	15.6
5. Acoustic Impedance Ratio (AI)	Avg. MDP Rate $= 0.038 + 54.55 (AI)^2$	0.897	10.8
6. Elongation (ELON)	Avg. MDP Rate $= 0.147 - 5.62 (ELON)^{-2}$	0.865	17.3
7. True Strain Energy (TSEE) (Based on Elongation)	Avg. MDP Rate $= 0.115 + 1.26 \times 10^{10} (TSEE)^{-3}$	0.860	16.8
8. Reduction in Area (RA)	Avg. MDP Rate $= 0.087 + 7.13 \times 10^{-6} (RA)^2$	0.857	18.3
9. Elastic Modulus (E)	Avg. MDP Rate $= 0.041 + 1.80 \times 10^6 (E)^{-1}$	0.810	3.2
10. Engineering Strain Energy (ESE)	Avg. MDP Rate $= 0.089 + 4.21 \times 10^2 (ESE)^{-1}$	0.782	4.9

*Coefficient of Determination.

**Average Absolute % Deviation.

obtained in water on the materials in subset one was somewhat more
selective and was characterized by some individual, discrete craters.

3. Multiple Property Correlations

Full ten property correlations of the subset one data are
summarized in Table 45 where only the statistically best predicting
equations obtained are listed. We note that each predicting equation
involves only a single mechanical property, namely, tensile strength,
hardness, and acoustic impedance ratio, each of which was successful in
the single property correlations. In fact, the predicting equation
involving the tensile strength is identical to that obtained in the
single property analysis.

Full ten property correlations of the lead-bismuth and mercury
data also showed a strong dependence on tensile strength and hardness.

Figure 78 is a plot of the predicted values of average MDP rate
based on Equation (1) in Table 45 versus the corresponding experimental
data points and serves to indicate the extent of agreement obtained.

F. Water Correlations--Subsets Two and Three

1. Single Property Correlations

The materials contained in subsets two and three (Plexiglas,
aluminum, Cu, Cu-Ni, Cu-Zn, and Ni) were tested in water only. Single
property correlations of the two subsets combined are summarized in
Table 46. Hardness, reduction in area, and tensile strength are most
suitable for correlation purposes, whereas the other properties listed
are less successful in this regard. Tensile strength and hardness were

TABLE 45

SUMMARY OF BEST CORRELATIONS WITH TEN PROPERTIES
CONSIDERED - WATER - SUBSET ONE

(1)

    Avg. MDP Rate = $0.006 + 8.38 \times 10^3 (TS)^{-1}$

        Coefficient of Determination = 0.953

        Average Absolute % Deviation = 0.2%

(2)

    Avg. MDP Rate = $1.83 (H)^{-1/2}$

        Coefficient of Determination = 0.904

        Average Absolute % Deviation = 14.9%

(3)

    Avg. MDP Rate = $72.98 (AI)^2$

        Coefficient of Determination = 0.873

        Average Absolute % Deviation = 28.9%
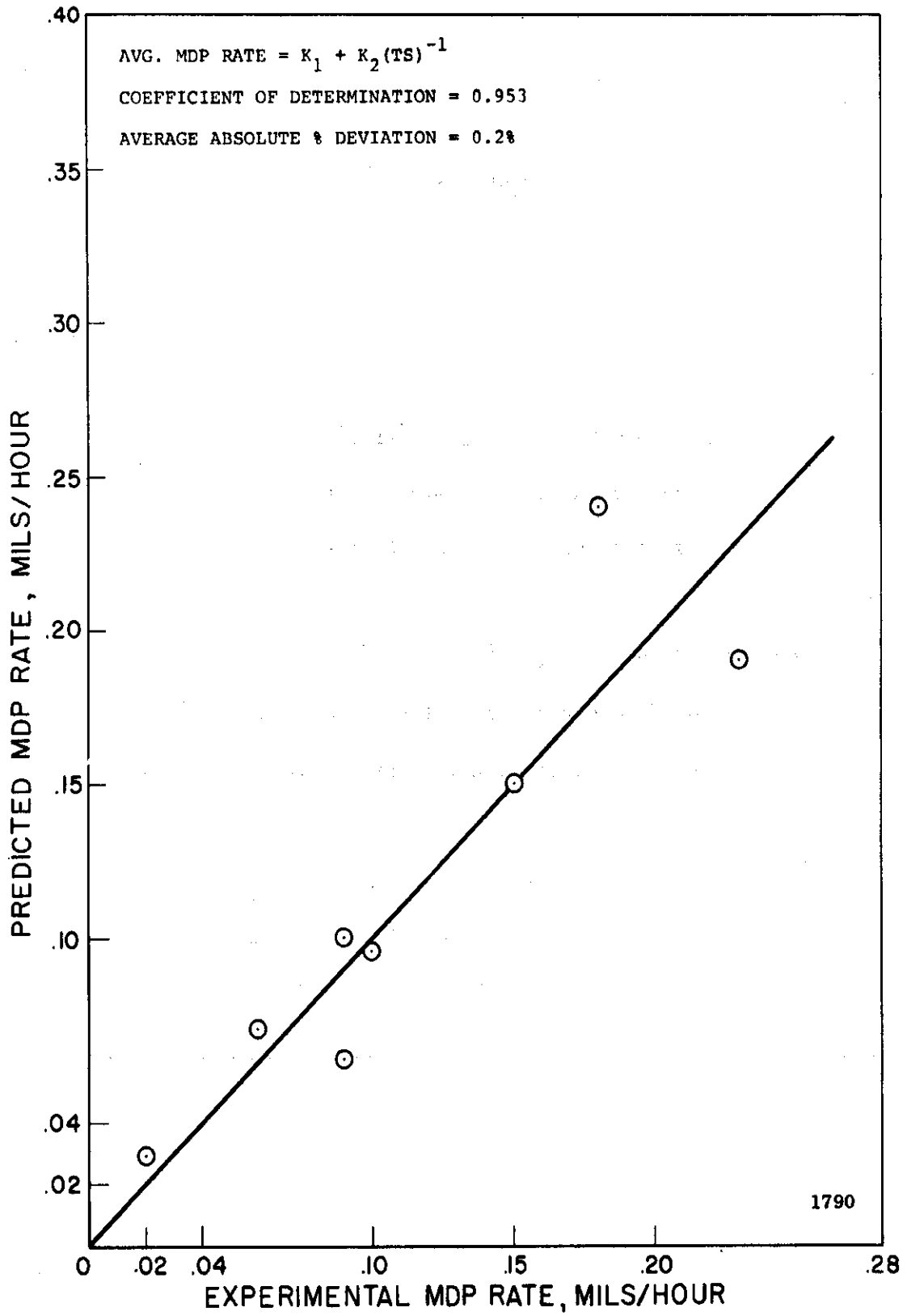
Fig. 78.--Comparison of predicted MDP rate and experimental
MDP rate - water - subset one.

TABLE 46

SUMMARY OF SINGLE PROPERTY CORRELATIONS - WATER - SUBSETS TWO AND THREE

Property	Predicting Equation	CD*	AAPD**
1. Hardness (H) (DPH - 1.1 Kg. Load)	Avg. MDP Rate $= 1.038 - 3.96 \times 10^4 (H)^{-3} - 1.02 \times 10^2 (H)^{-1} + 5.35 \times 10^3 (H)^{-2}$	0.966	6.1
2. Reduction in Area (RA)	Avg. MDP Rate $= 1.383 + 4.54 \times 10^{-6} (RA)^3 - 0.18 (RA)^{1/2}$	0.950	8.0
3. Tensile Strength (TS)	Avg. MDP Rate $= -0.413 + 2.50 \times 10^2 (TS)^{-1/2}$	0.910	5.4
4. Acoustic Impedance Ratio (AI)	Avg. MDP Rate $= 1.505 - 3.31 \times 10^{-2} (AI)^{-1}$	0.794	15.4
5. Elastic Modulus (E)	Avg. MDP Rate $= -0.021 - 1.89 \times 10^6 (E)^{-1} + 3.88 \times 10^3 (E)^{-1/2}$	0.775	19.5
6. Yield Strength (YS)	Avg. MDP Rate $= 0.198 + 15.80 (YS)^{-1/3}$	0.768	17.6
7. True Strain Energy (TSER) (Based on Reduction in Area)	Avg. MDP Rate $= 1.031 - 1.80 \times 10^{-10} (TSER)^2$	0.737	21.2
8. True Strain Energy (TSEE) (Based on Elongation)	Avg. MDP Rate $= 0.447 + 6.91 (TSEE)^{-1/3}$	0.737	21.9
9. Engineering Strain Energy (ESE)	Avg. MDP Rate $= 0.641 + 13.80 (ESE)^{-1/2}$	0.731	22.4
10. Elongation (ELON)	Avg. MDP Rate $= 0.723 + 3.86 \times 10^{-3} (ELON)$	0.709	24.7

*Coefficient of Determination.

**Average Absolute % Deviation.

also successful in the subset one single property correlations, as well as in the corresponding lead-bismuth and mercury analyses, although they did not appear in the same functional relation for the different cases. Note that for water subsets two and three the correlation with any of the forms of strain energy is very poor.

2. Multiple Property Correlations

Full ten property correlations of subsets two and three combined are presented in Table 47. All three expressions listed have very high coefficients of determination and very low average absolute percent deviations, indicating excellent agreement between the experimental and predicted values. Hardness, tensile strength, and yield strength are prominent in these expressions. As noted previously, hardness and tensile strength were also successful as single correlating parameters. Hence, it appears that tensile strength and hardness are the most successful correlating parameters both for the subset one water data and also the combined data in subsets two and three.

Figure 79 is a plot of predicted values of average MDP rate based on Equation (1) in Table 47 versus the corresponding experimental data points and serves to indicate the extent of agreement obtained. In this case the agreement is excellent.

G. Water Correlations--All Water Data

1. Single Property Correlations

Finally, the complete set of water data was subjected to the regression analysis. The single property correlations are summarized in

TABLE 47

SUMMARY OF BEST CORRELATIONS WITH TEN PROPERTIES
CONSIDERED - WATER - SUBSETS TWO AND THREE

---

(1)

$$\text{Avg. MDP Rate} = 0.392 - 12.0(YS)^{-1/3} - 3.82 \times 10^{7}(TSEE)^{-3} + 3.61 \times 10^{4}(TS)^{-1}$$

Coefficient of Determination = 0.991

Average Absolute % Deviation = 2.7%

(2)

$$\text{Avg. MDP Rate} = -0.822 + 6.22 \times 10^{2}(TS)^{-1/2} - 11.45(H)^{-1/2}$$

Coefficient of Determination = 0.985

Average Absolute % Deviation = 1.1%

(3)

$$\text{Avg. MDP Rate} = 0.163 - 3.41 \times 10^{3}(YS)^{-1} + 3.62 \times 10^{4}(TS)^{-1}$$

Coefficient of Determination = 0.984

Average Absolute % Deviation = 3.1%
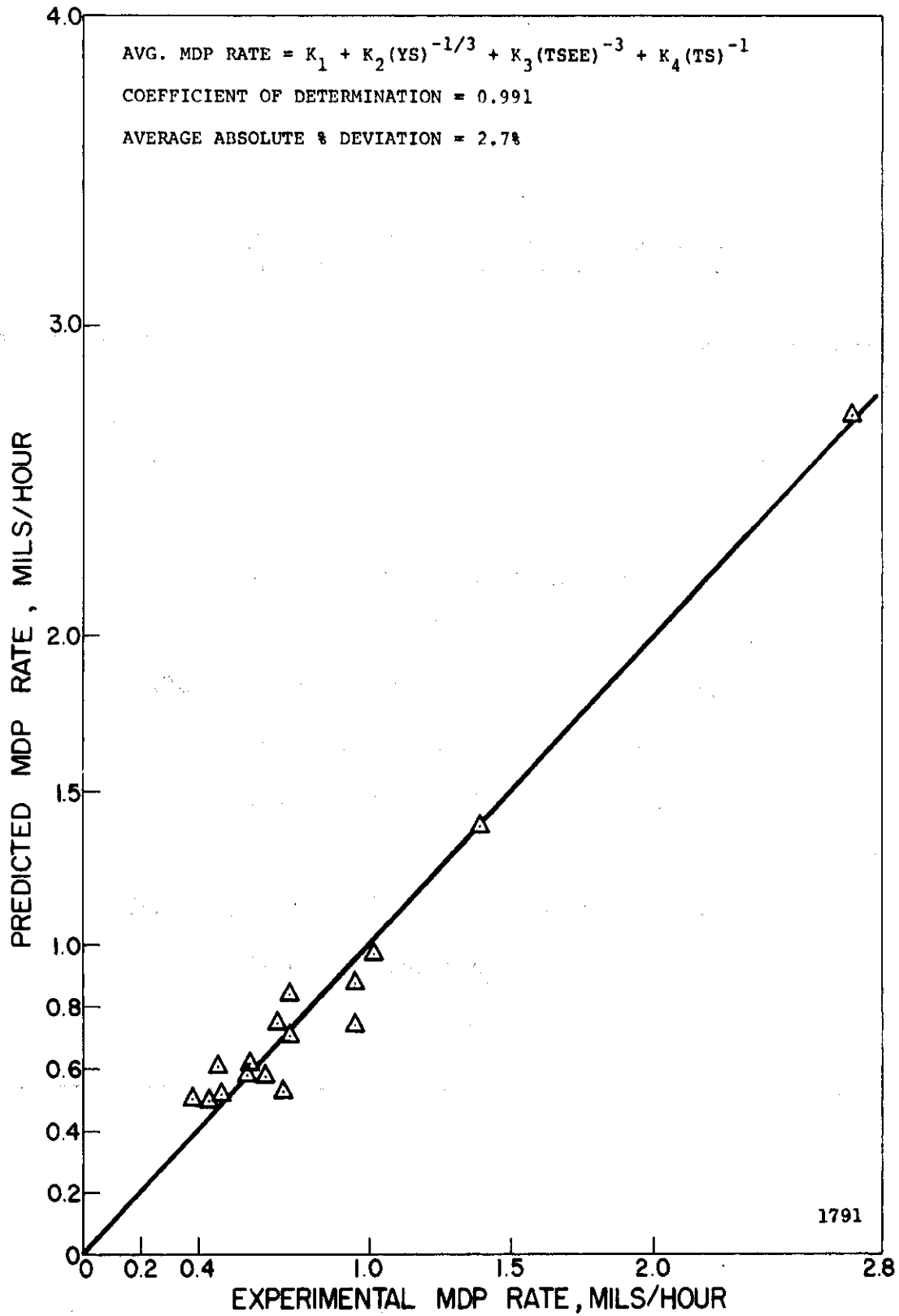
Fig. 79.--Comparison of predicted MDP rate and experimental MDP rate - water - subsets two and three.

Table 48. It is seen that the hardness, tensile strength, and yield strength are the most successful as correlating parameters among the ten properties, as expected. However, only hardness is reasonably successful from a statistical point of view, and then only with a 5 term relation. For the other properties, variations between experimental and predicted values are 40% and greater. This points up the general conclusion that precise correlations between the conventional mechanical properties and large varied sets of cavitation damage data do not apparently exist.

2. Multiple Property Correlations

The statistically best ten property correlations of the water data are summarized in Table 49. Only Equation (1), involving a combination of tensile strength, hardness, and reduction in area, satisfactorily predicts the experimental data.

Figure 80 is a plot of the predicted values of average MDP rate based on Equation (1) in Table 49 versus the corresponding experimental data points and indicates the extent of agreement obtained.

3. Summary

In summary, it is seen that the mechanical properties of hardness, tensile strength, and yield strength adequately predict the experimental water data on a single property basis. This is true either for subset one, subsets two and three combined, or the full water data set. In addition, the elastic modulus is successful as a single correlating parameter for subset one. These same properties are the most prominent in the ten property water correlations. However, for all

TABLE 48

SUMMARY OF SINGLE PROPERTY CORRELATIONS - ALL WATER DATA

Property	Predicting Equation	CD*	AAPD**
1. Hardness (H) (DPH - 1.1 Kg. Load)	Avg. MDP Rate = $-9,023 + 1.30 \times 10^4 (H)^{-2} + 53.63(H)^{-1/3} - 6.17 \times 10^2 (H)^{-1} - 8.00 \times 10^4 (H)^{-3}$	0.946	18.7
2. Tensile Strength (TS)	Avg. MDP Rate = $-0.619 + 2.69 \times 10^2 (TS)^{-1/2}$	0.851	40.7
3. Yield Strength (YS)	Avg. MDP Rate = $-0.193 + 22.4(YS)^{-1/3}$	0.708	62.1
4. Acoustic Impedance Ratio (AI)	Avg. MDP Rate = $1.491 - 3.99 \times 10^{-2} (AI)^{-1}$	0.708	70.8
5. Elastic Modulus (E)	Avg. MDP Rate = $1.832 - 2.79 \times 10^{-4} (E)^{1/2}$	0.695	62.5
6. True Strain Energy (TSEE) (Based on Elongation)	Avg. MDP Rate = $0.053 + 10.70(TSEE)^{-1/3}$	0.627	92.6
7. Engineering Strain Energy (ESE)	Avg. MDP Rate = $0.084 + 10.39(ESE)^{-1/3}$	0.624	91.2
8. True Strain Energy (TSER) (Based on Reduction in Area)	Avg. MDP Rate = $0.295 + 7.95(TSER)^{-1/3}$	0.587	110.9
9. Reduction in Area (RA)	Avg. MDP Rate = $0.829 - 1.51(RA)^{-1/2}$	0.549	124.6
10. Elongation (ELON)	Avg. MDP Rate = $0.557 + 3.28(ELON)^{-2}$	0.538	120.9

*Coefficient of Determination.

**Average Absolute % Deviation.

TABLE 49

SUMMARY OF BEST CORRELATIONS WITH TEN PROPERTIES
CONSIDERED - ALL WATER DATA

(1)

$$\text{Avg. MDP Rate} = -0.068 + 3.07 \times 10^8 (TS)^{-2} - 8.32 \times 10^{-7} (RA)^3$$
$$- 2.03 \times 10^3 (H)^{-3} + 1.49 \times 10^2 (TS)^{-1/2}$$

Coefficient of Determination = 0.976

Average Absolute % Deviation = 0.5%

(2)

$$\text{Avg. MDP Rate} = -2.224 + 19.93 (H)^{-1/3} - 2.22 \times 10^2 (YS)^{-1/2}$$

Coefficient of Determination = 0.864

Average Absolute % Deviation = 28.5%

(3)

$$\text{Avg. MDP Rate} = -0.619 + 2.69 \times 10^2 (TS)^{-1/2}$$

Coefficient of Determination = 0.851

Average Absolute % Deviation = 40.7%
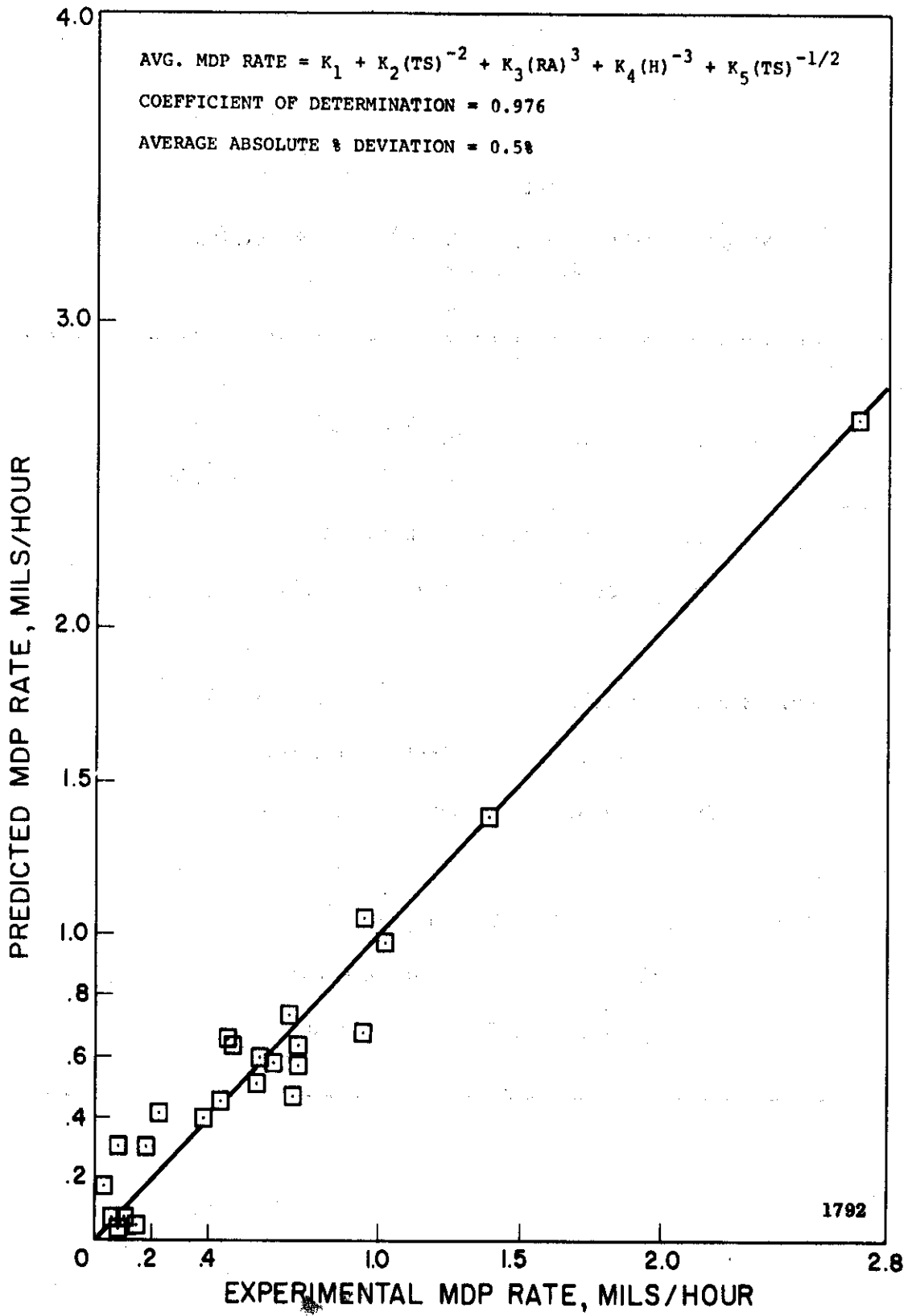
Fig. 80.--Comparison of predicted MDP rate and experimental MDP rate - all water data.

cases different functional forms of the properties are required for good correlation.

In the case of lead-bismuth, tensile strength and hardness were also successful as single property correlating parameters, but the true strain energy was more successful in this respect. A similar comment applies to the single property mercury correlations.

In general, it is concluded that those properties most successful as single correlating parameters in a given fluid are the most prominent in the ten property correlations, as one would expect.

H. Lithium Correlations at 500°F

1. Single Property Correlations

As a first step in the analysis, an attempt was made to correlate the damage data obtained at 500°F with each mechanical property individually to determine the relative importance of each alone with respect to predicting the observed cavitation damage. Table 50 summarizes the results of this effort. The ten properties considered, the statistically best predicting equations generated by the program for each property, the coefficient of determination (CD) for the analysis, and the average absolute percent deviation (AAPD) for the analysis are noted. The predicting equations are arranged in order of decreasing statistical significance based on the coefficient of determination. It is seen that the elongation, yield strength, true strain energy based on reduction in area (TSER), hardness, and tensile strength are quite successful as single correlating parameters. The other mechanical

TABLE 50

SUMMARY OF SINGLE PROPERTY CORRELATIONS - LITHIUM AT 500°F

Property	Predicting Equation	CD*	AAPD**
1. Elongation (ELON)	Avg. MDP Rate = $0.409 - 2.91\times10^{-3}(ELON)^2 + 9.34\times10^{-5}(ELON)^3$	0.992	14.1
2. Yield Strength (YS)	Avg. MDP Rate = $-0.899 + 43.40(YS)^{-1/3}$	0.959	3.2
3. True Strain Energy (TSER) (Based on Reduction in Area)	Avg. MDP Rate = $-0.494 + 1.32\times10^2(TSER)^{-1/2}$	0.929	31.7
4. Hardness (H) (DPH - 1.1 Kg. Load)	Avg. MDP Rate = $0.114 + 3.17\times10^5(H)^{-3}$	0.924	37.3
5. Tensile Strength (TS)	Avg. MDP Rate = $0.143 + 1.34\times10^{13}(TS)^{-3}$	0.920	40.3
6. True Strain Energy (TSEE) (Based on Elongation)	Avg. MDP Rate = $0.129 + 4.17\times10^{10}(TSEE)^{-3}$	0.839	44.2
7. Acoustic Impedance Ratio (AI)	Avg. MDP Rate = $0.028 + 6.36\times10^2(AI)^2$	0.705	33.1
8. Elastic Modulus (E)	Avg. MDP Rate = $0.035 + 1.139\times10^{14}(E)^{-2}$	0.647	73.9
9. Reduction in Area (RA)	Avg. MDP Rate = $-0.244 + 1.01\times10^{-6}(RA)^3$	0.612	25.1
10. Engineering Strain Energy (ESE)	Avg. MDP Rate = $0.055 + 2.74\times10^3(ESE)^{-1}$	0.520	87.3

*Coefficient of Determination.

**Average Absolute % Deviation.

properties listed do not suitably account for the experimental data on an individual basis. Surprisingly, the worst correlation among the ten properties, in terms of either coefficient of determination or average absolute percent deviation, is attained with the engineering strain energy.

It is further noted that the average MDP rate is inversely proportional to powers of yield strength, true strain energy based on reduction in area, hardness, and tensile strength. The dependence of average MDP rate on elongation is not as easily determined, since two terms in the predicting equation are functions of elongation, each contributing to the average MDP rate in an opposite manner. One might conclude that the cavitation resistance of a group of materials in lithium at 500°F could at least be qualitatively predicted on the basis of these five mechanical properties.

2. Multiple Property Correlations

Further attempts at complete correlations of the experimental data were conducted in which all ten mechanical properties noted previously, each raised to ten exponents, were possible terms in the predicting equation. Hence, a total of 100 terms plus a pure constant were considered by the program. Table 51 summarizes the statistically best predicting equations obtained under these conditions. The coefficient of determination and average absolute percent deviation are noted for each of the correlations presented. Note that each equation contains only one mechanical property. In fact, the equations containing the yield strength and the hardness are identical to those obtained in

TABLE 51

SUMMARY OF BEST CORRELATIONS WITH TEN PROPERTIES CONSIDERED -
LITHIUM AT 500°F

(1)

Avg. MDP Rate = -0.899 + 43.40(YS)$^{-1/3}$

Coefficient of Determination = 0.959

Average Absolute % Deviation = 3.2%

(2)

Avg. MDP Rate = -0.039 + 8.21x10^3(TSER)$^{-1}$

Coefficient of Determination = 0.928

Average Absolute % Deviation = 40.6%

(3)

Avg. MDP Rate = 0.114 + 3.17x10^5(H)$^{-3}$

Coefficient of Determination = 0.924

Average Absolute % Deviation = 37.3%

the single property correlations. The true strain energy based on reduction in area enters to the power (-1) in the ten property correlations, while it was present to the power (-1/2) in the single property correlations. However, a comparison between Tables 50 and 51 shows that the correlation to the (-1/2) power was slightly better. The selection of correlating equations which are less suitable than others available is a result of the random selection of the variables by the computer program and the fact that only a small number of random selections were possible within a feasible limitation on machine time. Of course, the mechanical properties involved in the ten property correlations are those that were also quite successful in predicting cavitation damage individually, as expected.

J. Lithium Correlations at 1500°F

Although there are only four experimental points available in lithium at 1500°F, both single and multiple property correlations were carried out on this small body of data. In all of the single property correlations and the multiple property correlations, the same predicting equation was generated by the computer program, namely:

Avg. MDP Rate = 0.0225

Coefficient of Determination = 0.880

Average Absolute Percent Deviation = 21.9%

Thus the predicting equation consisted of only a constant term in all cases. This is a direct result of the lack of a suitable number of data points for a correlation.

K. Correlations of all Lithium Data

The combined lithium data obtained at 500°F and 1500°F was also submitted to the least mean squares regression analysis. One would not expect particularly good predicting equations in this case since only mechanical properties are allowed as independent variables. In fact, it is questionable if a suitable correlation could be obtained even if such fluid properties as the density, surface tension, net positive suction head, bulk modulus, and kinematic viscosity were introduced as independent variables. Thermodynamic effects are apparently quite important in lithium at 1500°F. Hence, a suitable correlation must involve fluid properties of lithium such as specific heat, thermal conductivity, heat of vaporization, thermal diffusivity, Prandtl Number, and vapor pressure. The results of such a study will be presented later. Nevertheless, single property correlations and full ten property correlations of the combined lithium data as a function of mechanical properties only were investigated. It was found in both cases that no suitable predicting equations existed for the combined data, as expected.

L. Summary of Single Fluid Correlations

Thus far, the only property included in the regression analysis that is a function of the fluid has been the ratio of acoustic impedances of the test fluid and specimen material. This quantity did not successfully correlate the lead-bismuth, mercury, or lithium data and did not appear in the ten property correlations. In the case of the

water data the acoustic impedance ratio was more successful as a correlating parameter.

It is noted at this point that whereas energy properties were quite important in the correlation of the data from the tests with high density liquid metals (lead-bismuth alloy and mercury), they are much less significant in the water and lithium tests. On the other hand, the strength properties (including hardness in this category) are predominant in the water and lithium tests. The same observations apply to the venturi tests, although the role of energy terms was not as great for the liquid metal (mercury) venturi tests as for the vibratory liquid metal tests.[22]

Theoretical arguments have been advanced in the past to show that a correlation would involve both energy and strength terms.[58] This argument is reinforced by consideration of the limiting case of a very strong but brittle material. As a hypothetical example, suppose a cavitating flow regime with such a material where the implosions were not capable of imposing stresses on the surface in excess of the "fatigue strength." Then no damage would result, even though the strain energy were very low as it often is for such materials. Data obtained with tool steels and stellite are consistent with this viewpoint. It would be expected that this limiting condition would apply more closely to the water and lithium tests (relatively low density fluids) than to the heavy liquid metal tests, since the stresses imposed are probably roughly proportional to fluid density. Thus this argument is consistent with the present experimental data obtained with these different fluids.

M. Comprehensive Correlations of Lead-Bismuth, Mercury, Water, and Lithium Data

1. General

The major objective of the computer analyses described thus far is to deduce a single comprehensive predicting equation that would suitably explain the lead-bismuth, mercury, water, and lithium data. Such an equation would, of necessity, include at least one fluid coupling parameter to account for the variations in fluid properties for the four fluids considered and the corresponding test temperatures, since it has already been shown that the cavitation resistance of all the materials tested, and their relative rankings, depend on the fluid. The combined lead-bismuth, mercury, water, and lithium data was submitted to the regression program in an attempt to arrive at the required correlation of all experimental data in terms of mechanical and fluid properties. The mechanical properties allowed in these correlations were the same as previously employed: tensile strength, yield strength, engineering strain energy, true strain energy (two values based on elongation and reduction in area), hardness, elongation, reduction in area, and elastic modulus. In addition, each of the six fluid coupling parameters discussed previously, namely, acoustic impedance ratio, density, surface tension, net positive suction head, bulk modulus, and kinematic viscosity, was combined separately with the group of nine mechanical properties. Hence, six comprehensive correlations were attempted, allowing a total of nine mechanical and one fluid property in each. It was hoped that such a procedure would indicate those fluid properties

that were most successful as coupling parameters. The values of the fluid coupling parameters used in these correlations were listed previously in Table 36.

In addition, all of the cavitation data obtained in lead-bismuth, mercury, water, and lithium was correlated in terms of five mechanical properties and five fluid properties. The five mechanical properties chosen for this purpose were the tensile strength, true strain energy based on elongation, true strain energy based on reduction in area, elastic modulus, and hardness. The fluid properties included were the ratio of acoustic impedances of the test fluid and specimen material, fluid density, surface tension, bulk modulus, and kinematic viscosity. Such a correlation indicated those fluid properties which were most successful as coupling parameters.

2. Single Fluid Property Studies

A summary of the results of the six comprehensive correlations (lead-bismuth, mercury, water, and lithium) involving nine mechanical properties and one fluid property follows.

1) Acoustic Impedance Ratio (AI)

When the acoustic impedance ratio is used as the fluid coupling parameter and combined with the nine mechanical properties allowed to enter the predicting equation, the statistically best correlation obtained is:

$$\text{Avg. MDP Rate} = 8.97 - 3.10 \times 10^2 (\text{TSER})^{-1/3} + 4.50 \times 10^4 (\text{TSER})^{-1}$$
$$-0.159 (\text{TSER})^{1/3} - 1.20 \times 10^2 (\text{TSEE})^{-1/2}$$
$$+ 1.71 (\text{AI})^{1/3} - 7.40 \times 10^2 (\text{ESE})^{-1/2}$$

$$- 3.49\text{x}10^9(\text{TSER})^{-3} + 3.22\text{x}10^2(\text{TS})^{-1/2}$$
$$+ 8.88\text{x}10^3(\text{TSEE})^{-1} + 2.32\text{x}10^2(\text{ESE})^{-1/3}$$

Coefficient of Determination = 0.980

Average Absolute % Deviation = 2.7%

Although the equation may appear formidable at first glance, it should be noted that 8 of the 11 terms present involve some form of the strain energy. If the allowable exponents were not restricted to positive and negative integers and their reciprocals, the many strain energy terms, of which all three types are included, could undoubtedly be combined and reduced considerably. The appearance of the tensile strength in an inverse relationship is not surprising since it was successful as a single correlating parameter in each of the four fluids. The acoustic impedance ratio is also included, and it is noted that the damage rate increases as the acoustic impedance ratio increases, as postulated in Chapter V, section B. One might conclude that the acoustic impedance ratio is successful as a fluid coupling parameter in these experiments.

2) Density (ρ)

The density was next combined with the other nine mechanical properties allowed to enter the predicting equation, and the statistically best correlation obtained is:

$$\text{Avg. MDP Rate} = 2.44 - 1.62(\rho)^{-1/3} + 4.82\text{x}10^2(\text{E})^{-1/3}$$
$$+ 2.07\text{x}10^3(\text{TSEE})^{-1} - 1.99\text{x}10^{13}(\text{E})^{-2}$$
$$+ 4.26\text{x}10^4(\text{TSER})^{-1} - 7.35\text{x}10^{-2}(\text{H})^{1/2}$$
$$- 5.48\text{x}10^2(\text{TSER})^{-1/2} + 2.36\text{x}10^8(\text{TS})^{-2}$$

Coefficient of Determination = 0.969

Average Absolute % Deviation = 9.7%

Three of the terms present in the equation involve the true strain energy and two terms are functions of the elastic modulus. The tensile strength and hardness are also present, each indicating that a decrease in damage rate would be expected with increasing tensile strength or hardness. The density also appears as the fluid coupling parameter; and despite the negative exponent, increasing density would result in increased damage, since the coefficient of the term is negative. This is consistent with the observations in our own laboratory, both in the venturi[21,22,58] and vibratory facilities, and has, of course, been postulated by other investigators,[81] as well as being theoretically anticipated through consideration of bubble dynamics or jet impingement equations. However, there is another density effect as will be developed later, in its effect upon NPSH, which in turn affects the configuration of the cavitation flow field.

The fact that density enters to the (-1/3) power is interesting, since yield strength has also been often involved to this power (Tables 40, 46, 47, 48, 50, and 51). According to the simplest bubble collapse or jet impingement calculations, the stress imposed upon the surface is proportional to the density and, hence, it would not be surprising if strength and density entered all relations for volume loss in the same way. Assuming this proportionality between density and stress, it then would follow that volume removed is, very roughly of course, inversely related to the cube root of imposed stress.

3) Surface Tension (σ)

In a similar manner the surface tension was investigated as a possible fluid coupling parameter, and the statistically best predicting equation is:

$$\text{Avg. MDP Rate} = 0.982 - 6.38(RA)^{-1/3} + 2.50\times10^{-6}(\sigma)^2$$
$$- 1.28(ELON)^{-1/2} + 2.36\times10^4(TSER)^{-1}$$
$$+ 4.53\times10^2(ESE)^{-1} + 14.87(TSEE)^{-1/3}$$
$$- 1.28\times10^{13}(E)^{-2}$$

Coefficient of Determination = 0.923

Average Absolute % Deviation = 2.4%

Again, three of the terms involve various forms of the strain energy. The surface tension enters with an exponent of 2, whereas in the previous relations the acoustic impedance ratio and density were each raised to the 1/3 power. The correlation indicates that increasing surface tension results in increased damage. This was reported by Nowotny[32] as a result of his experiments, although his relation between MDP rate and surface tension is nearly linear, rather than squared. However, no variation of MDP rate with surface tension is predicted by numerical analyses of bubble collapse.[82,83] However, the simplified models used may in some way neglect the mechanism here involved.

4) Net Positive Suction Head (NPSH)

Since the local pressure was varied in our experiments so as to maintain the difference between local pressure and vapor pressure constant, the static net positive suction head is inversely proportional

to the density, but the dynamic NPSH applied by the horn is more closely

constant, as already discussed. The correlation was carried out using

the static NPSH values, and the statistically best predicting equation

obtained is:

$$\text{Avg. MDP Rate} = -1.17 \times 10^2 + 5.60 \times 10^{-3} (E)^{1/2} + 1.01 \times 10^7 (TSEE)^{-2}$$
$$- 3.68 \times 10^2 (RA)^{-3} + 1.88 \times 10^3 (TSER)^{-1/2}$$
$$+ 5.81 \times 10^4 (E)^{-1/3} + 2.76 \times 10^4 (TS)^{-1}$$
$$- 2.48 \times 10^{-2} (NPSH) - 45.21 (TSEE)^{-1/2}$$
$$- 5.12 \times 10^2 (TSER)^{-1/3} - 5.17 \times 10^5 (E)^{-1/2}$$

Coefficient of Determination = 0.962

Average Absolute % Deviation = 5.0%

Two terms are functions of each of the forms of true strain

energy used, while three additional terms involve the elastic modulus.

The tensile strength appears in an inverse relationship, as expected,

and the net positive suction head is present in a linear manner, but

with negative coefficient. Hence, increasing net positive suction head

results in a decrease in cavitation damage. However, this probably is

merely the same effect as that previously discussed in relation to den-

sity, since these tests were conducted so that NPSH is always $\propto 1/\rho$.

5) Bulk Modulus (B)

The statistically best predicting equation obtained when

bulk modulus is introduced as the fluid coupling parameter is:

$$\text{Avg. MDP Rate} = 0.665 - 1.66 \times 10^2 (TS)^{-1/2} - 2.59 \times 10^{16} (B)^{-3}$$
$$+ 5.27 \times 10^6 (TSEE)^{-2} + 1.13 \times 10^4 (H)^{-2}$$

$$+ 3.49 \times 10^7 (TSER)^{-2} - 4.53 \times 10^5 (H)^{-3}$$

$$+ 1.99 \times 10^{13} (TS)^{-3} + 9.02 \times 10^6 (E)^{-1}$$

Coefficient of Determination = 0.975

Average Absolute % Deviation = 5.1%

The true strain energy, hardness, and tensile strength are each entered in the equation twice, while the bulk modulus is present with both a negative exponent and negative coefficient. Hence, as the bulk modulus is increased (compressibility decreased), the damage would increase, as expected theoretically,[82,83] and as often observed in field practice where damaging cavitation with petroleum pumps is virtually unknown as compared to water pumps. This trend has also been reported in a previous laboratory investigation using a vibratory facility.[81]

6) Kinematic Viscosity (ν)

The final fluid coupling parameter investigated was the kinematic viscosity, ν . The statistically best predicting equation obtained in this case was:

$$\text{Avg. MDP Rate} = - 0.294 + 6.91 \times 10^2 (E)^{-1/3} - 1.30 \times 10^2 (TSER)^{-1/3}$$

$$+ 3.13 \times 10^4 (H)^{-3} + 25.40 (TSEE)^{-1/3}$$

$$+ 3.76 \times 10^4 (TSER)^{-1} - 5.95 \times 10^{-3} (RA)^{1/2}$$

$$- 6.30 \times 10^2 (\nu)^2 + 0.243 (ELON)^{1/3}$$

$$- 2.54 \times 10^{13} (E)^{-2} + 2.04 \times 10^{-5} (\nu)^{-1}$$

Coefficient of Determination = 0.963

Average Absolute % Deviation = 2.2%

The true strain energy is involved in three terms while the elastic modulus appears in two. The hardness is also prominent in a

strong inverse relationship. The kinematic viscosity, ν , appears in

two terms, such that increasing kinematic viscosity results in a

decrease in cavitation damage, as postulated.

A summary of the statistics applicable to the six comprehensive

damage correlations discussed above are presented in Table 52. The

fluid coupling parameters considered are listed in an order determined

by the coefficient of determination of the corresponding predicting

equation. It is seen that the acoustic impedance ratio results in the

predicting equation with highest coefficient of determination. However,

all fluid properties considered as coupling parameters were quite suc-

cessful in this regard. It should be emphasized that the acoustic

impedance ratio involves both the density and bulk modulus of the fluid,

and, hence, to some extent may also cover effects normally ascribed to

mechanisms associated with these properties. All predicting equations

had a value of coefficient of determination greater than 0.960, except

when the surface tension was employed as the coupling parameter. In

addition, the average absolute percent deviation was less than 10% in

all cases. As a result, it is difficult to make any recommendations as

to an optimum fluid coupling parameter. All fluid properties considered

in this study seem to be successful, and this is not surprising when it

is considered that for a liquid the fluid properties can all be

expressed as smooth functions of temperature alone and, hence, are

smooth functions of each other. The resulting predicting equations show

a strong dependence on strain energy, hardness, tensile strength, and

elastic modulus. In fact, the six predicting equations described above

TABLE 52

SUMMARY OF STATISTICS FOR COMPREHENSIVE DAMAGE CORRELATIONS
(SINGLE FLUID PROPERTY)

Fluid Coupling Parameter	CD*	AAPD**
1. Acoustic Impedance Ratio (AI)	0.980	2.7
2. Bulk Modulus (B)	0.975	5.1
3. Density (ρ)	0.969	9.7
4. Kinematic Viscosity (ν)	0.963	2.2
5. Net Positive Suction Head (NPSH)	0.962	5.0
6. Surface Tension (σ)	0.923	2.4

*Coefficient of Determination.

**Average Absolute % Deviation.

contained terms involving some form of strain energy 23 times (TSER-12, TSEE-8, and ESE-3), elastic modulus 9 times, tensile strength 5 times, hardness 4 times, reduction in area 3 times, and elongation 2 times. Of course, a coupling parameter was present in each equation, although it was by no means forced into the equation, since the program uses a repeated choice and then testing for suitability of the selected terms. It will be recalled that strain energy, tensile strength, and hardness were the most successful properties in the single property correlations of lead-bismuth, mercury, water, and lithium separately (elongation and yield strength were also successful in the lithium correlations). These mechanical properties along with the elastic modulus are also the most prominent in the comprehensive lead-bismuth, mercury, water, and lithium correlations.

The fact that all the forms of strain energy are sometimes involved and that their relative involvement depends on fluid, temperature, material, etc., may indicate that different modes of material failure are involved, depending upon the various test parameters, since it would be expected that TSER would most closely represent resistance to ductile failure, while TSEE or ESE would be most closely involved with brittle failure.

Figure 81 is a plot of the predicted values of average MDP rate, computed using the comprehensive predicting equation with acoustic impedance ratio as the coupling parameter, versus the corresponding experimental data points, and indicates the extent of agreement afforded by this analysis.

AVG. MDP RATE $= K_1 + K_2(\text{TSER})^{-1/3} + K_3(\text{TSER})^{-1} + K_4(\text{TSER})^{1/3} +$

$K_5(\text{TSEE})^{-1/2} + K_6(\text{AI})^{1/3} + K_7(\text{ESE})^{-1/2} +$

$K_8(\text{TSER})^{-3} + K_9(\text{TS})^{-1/2} + K_{10}(\text{TSEE})^{-1} +$

$K_{11}(\text{ESE})^{-1/3}$

COEFFICIENT OF DETERMINATION = 0.980

AVERAGE ABSOLUTE % DEVIATION = 2.7%

1793
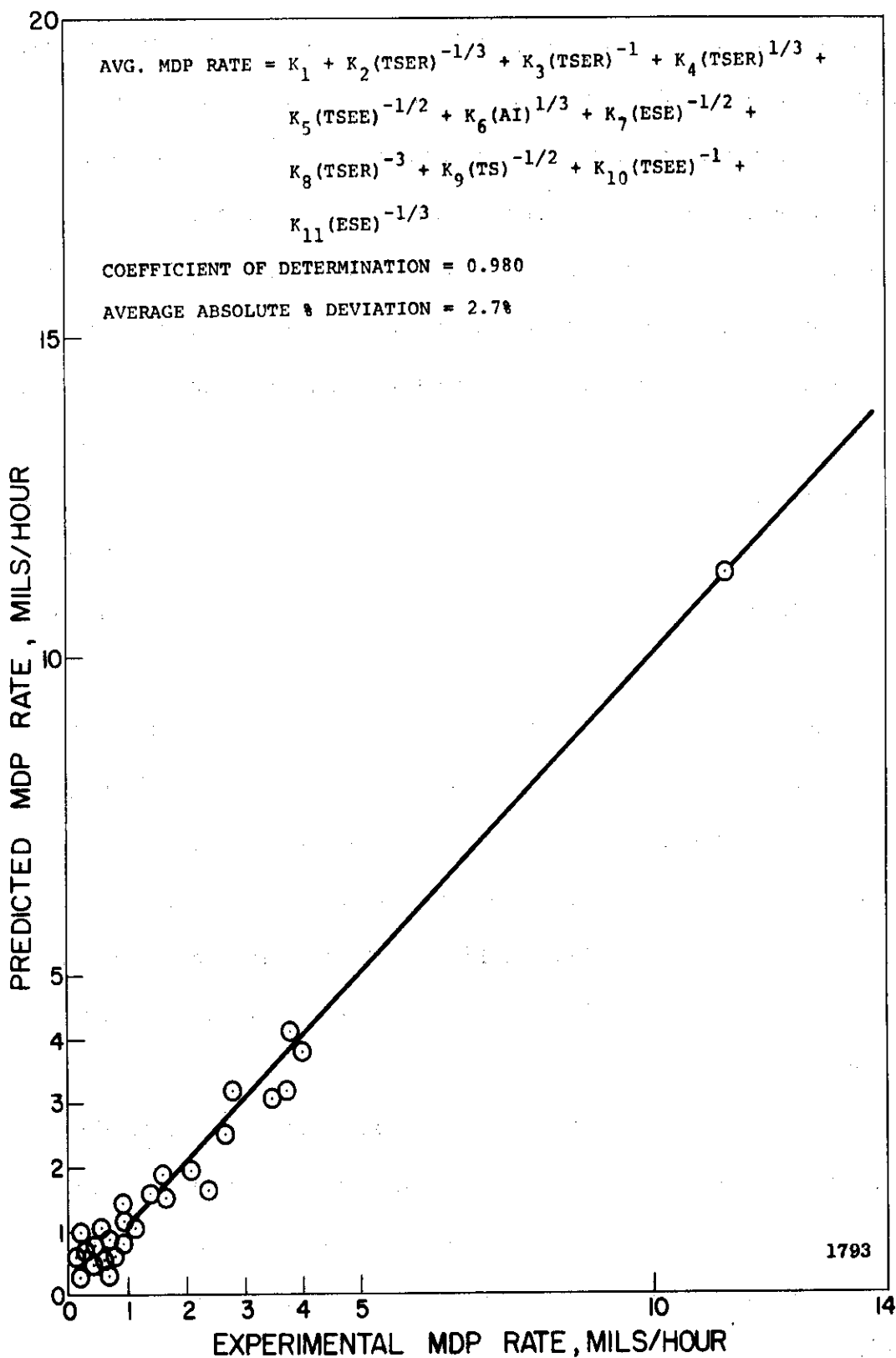
Fig. 81.--Comparison of predicted MDP rate and experimental MDP rate - all lead-bismuth, mercury, water, and lithium data (acoustic impedance ratio is the fluid coupling parameter).

3. Multiple Fluid Property Studies

The previous comprehensive computer correlations have shown that all of the fluid properties considered as coupling parameters were quite successful when considered individually. In order to better determine the most significant fluid coupling parameters for our correlations, five such properties were included in a comprehensive correlation of all the cavitation data. The fluid properties considered were the ratio of acoustic impedances of the test fluid and specimen material, fluid density, surface tension, bulk modulus, and kinematic viscosity. The number of mechanical properties was reduced to five for this study and included the tensile strength, true strain energy based on elongation, true strain energy based on reduction in area, elastic modulus, and hardness. Under these conditions the statistically best correlation obtained is:

$$\text{Avg. MDP Rate} = -2.32 - 1.74(\rho)^{-1} - 4.86 \times 10^5 (\text{TSER})^{-2}$$
$$+ 40.60(\text{TSEE})^{-1/3} + 5.42 \times 10^2 (\text{TS})^{-1/2}$$
$$+ 4.25 \times 10^{-4} (\text{AI})^{-2}$$

Coefficient of Determination = 0.711

Average Absolute % Deviation = 49.5%

It is seen that both the density and the ratio of acoustic impedances appear in the predicting equation. The degree of statistical fit afforded by this equation is not nearly as good as that obtained in the previous comprehensive correlations.

In the 15 correlations obtained when one allows five mechanical and five fluid properties to enter the predicting equation, it was found

that the fluid density and bulk modulus appeared in these equations seven times each, while the ratio of acoustic impedances and the kinematic viscosity each appeared two times. The surface tension did not appear in any of the correlations, and this is consistent with theoretical expectations, as previously discussed.

If this analysis is carried out after omitting the 4 data points obtained in lithium at 1500°F (these points are obviously influenced by thermodynamic effects), then under these conditions the statistically best correlation obtained is:

$$
\begin{aligned}
\text{Avg. MDP Rate} = {} & 10.45 - 2.82 \times 10^2 (\text{TSER})^{-1/3} - 0.11 (\text{TSER})^{1/3} \\
& + 5.13 \times 10^4 (\text{TSER})^{-1} + 2.98 (\text{AI})^{1/3} + 54.68 (\text{H})^{-1} \\
& - 3.95 \times 10^9 (\text{TSER})^{-3} - 3.38 \times 10^{-2} (\text{TSEE})^{1/3} \\
& - 3.23 \times 10^{-4} (\text{B})^{1/2}
\end{aligned}
$$

Coefficient of Determination = 0.965

Average Absolute % Deviation = 1.1%

It is seen that the bulk modulus enters the predicting equation as the fluid coupling parameter. This equation is far superior statistically to that obtained above when the lithium data at 1500°F was retained in the full data set.

4. Second-Order Interaction Correlation

As previously mentioned, the least mean squares regression computer program used for these studies includes the option of a second-order interaction correlation, i.e., cross-products of the independent variables are allowed to appear in the predicting equation. This, of course, increases greatly the number of possible terms that may appear

in the predicting equation as compared to a first-order interaction cor-relation involving the same mechanical and fluid properties. In this preliminary study the five mechanical and five fluid properties previ-ously employed in the multiple fluid property correlations were retained for the second-order interaction study. Clearly, large amounts of com-puter time will be necessary if one is to complete a detailed analysis of the cavitation data under these conditions. The preliminary correla-tions, consuming considerable computer time, did not indicate any parti-cular combinations or products of independent variables appearing con-sistently in the many predicting equations generated in this study.

5. Hobbs' Energy Concepts

Hobbs' proof resilience and ultimate resilience concepts were previously discussed. In order to determine if either would be prominent in explaining our own cavitation data, a comprehensive correla-tion was carried out in which all the mechanical properties previously mentioned were allowed to appear in the predicting equation with the exception of the engineering strain energy (ESE) which was replaced first by Hobbs' proof resilience (PR) and then by Hobbs' ultimate resil-ience (UR). In both cases the fluid density was also included as the fluid coupling parameter as this fluid property had been very prominent in the multiple fluid property correlations.

Under these conditions it was found that Hobbs' proof resilience did not appear in any of the correlations generated in the study. How-ever, Hobbs' ultimate resilience was very successful as a correlating parameter as it appeared in every equation generated. The

statistically best correlation obtained in this case was:

Avg. MDP Rate = 0.510 + 6.045(UR)$^{-1/2}$ - 0.471(ρ)$^{-2}$

Coefficient of Determination = 0.658

Average Absolute % Deviation = 54.5%

Although it is not statistically impressive, the equation is very com-
pact and involves only one mechanical property and one fluid property.
Further, it is seen that damage decreases with increasing ultimate
energy, and increases with increasing density, as expected.

When the data obtained at 1500°F in lithium is removed from the
total data set because of the thermodynamic effects previously men-
tioned, Hobbs' proof resilience still did not appear in any of the pre-
dicting equations generated by the program. However, in the analysis
involving Hobbs' ultimate resilience without the 1500°F lithium data,
the statistically best correlation obtained in this case was:

Avg. MDP Rate = 0.193 + 8.243(UR)$^{-1/2}$ - 0.536(ρ)$^{-1}$

Coefficient of Determination = 0.762

Average Absolute % Deviation = 26.7%

It is seen that the dependence on density has been reduced from an expo-
nent of (-2) to (-1). The coefficient of determination has been
increased considerably and the average absolute percent deviation has
been significantly reduced. The equation is of a very simple form in
that only two properties are involved, one material and one fluid prop-
erty. The dependence on ultimate resilience is the same regardless of
the inclusion or exclusion of the 1500°F lithium data. Note also that

the coefficients of the terms involving the ultimate resilience and the density are not much different in the two cases. Such a simple equation as this, suitably accounting for the complete body of cavitation data (with the exception of the 1500°F lithium data), would be of value to the designer of components susceptible to cavitation damage.

N. Comparison with Venturi Facility
Correlations

Previously,[22] computer correlations of cavitation damage data generated in this laboratory's mercury and water venturi facilities were carried out and reported. It was found that no good correlation existed between any single mechanical property and the cavitation damage in the mercury tests. However, true breaking stress exhibits the best fit. The ten property correlation of the mercury data showed that a combination of true breaking stress and tensile strength was significant. In the case of the corresponding ultrasonic investigations described above, true strain energy (based on elongation), hardness, and tensile strength were successful in the single property correlations. These same properties dominated the ten property correlations.

In the single property correlations of the full set of water data obtained in the venturi facility, it was found that the acoustic impedance ratio and the elastic modulus resulted in the best fit statistical expressions. The corresponding ultrasonic studies showed the hardness and tensile strength to be the most suitable.

Single property correlations of the subset of water data involving materials also tested in mercury was also carried out for the

venturi facility. These materials correspond to subset one of the acoustic results. It was found that elastic modulus and reduction in area result in good fits individually. Subset one of the water data in the ultrasonic facility was correlated well in terms of tensile strength, hardness, yield strength, or elastic modulus. Here, there is some agreement among the two facilities.

The analysis of the remainder of the venturi data (i.e., those materials tested in water only) on a single property basis shows that the correlation with elastic modulus and acoustic impedance ratio again is very good. This was also true with the full set of water data. These materials correspond to subsets two and three of the acoustic water data where hardness, tensile strength, and reduction in area were successful as single correlating parameters.

The multiple property correlation of the full set of venturi water data and the two subsets individually resulted in predicting equations where the acoustic impedance ratio, elastic modulus, tensile strength, and true breaking stress were the most prominent properties. The corresponding ultrasonic studies showed the tensile strength, hardness, and yield strength to be the predominant terms.

Correlations of the combined water and mercury venturi damage results are not yet available for comparison with the corresponding ultrasonic analysis.

In general, it is seen that the venturi results are best correlated in terms of tensile strength, elastic modulus, true breaking stress, and acoustic impedance ratio. The ultrasonic results correlate

best in terms of tensile strength, elastic modulus, hardness, and strain energy. However, the functional relations involving any of the terms are generally not the same between the two facilities or for subsets within the same facility. There is no explanation at this time as to the differences that exist. Undoubtedly, they are due to differences in the damaging mechanism itself in the two facilities.

P. Graphical Single Property Correlations

For the sake of completeness it was decided to graphically investigate the ability of the tensile strength, yield strength, engineering strain energy, true strain energy (based on reduction in area), hardness, and ultimate resilience to correlate cavitation damage individually in each of the fluids tested. These mechanical properties were chosen since they had been the most successful in earlier computer correlations. The lithium data obtained at 500°F and 1500°F was treated separately due to the thermodynamic effects that are important in lithium at 1500°F.

Thus, for lead-bismuth, mercury, water, lithium at 500°F, and lithium at 1500°F, the experimentally-determined cavitation data was normalized to the data obtained for type 304 stainless steel. In lead-bismuth the data was normalized to the type 304 stainless steel data obtained at 500°F, while in mercury the data was normalized to the type 304 stainless steel data point obtained at 70°F. Plots of normalized inverse cavitation damage versus each of the six mechanical properties listed above were made. The best straight line was drawn through the

data points. The specimen materials have been categorized as refractory alloys, ferrous metals, Plexiglas, and a group including aluminum, copper, nickel, Cu-Ni, and Cu-Zn. Thus, it is possible to distinguish from the plots the types of materials whose cavitation resistance (proportional to normalized inverse cavitation damage) may be adequately correlated in terms of a single mechanical property.

The 30 plots prepared for this study are included in Appendix C as Figures 88 through 117.

CHAPTER VII

THERMODYNAMIC EFFECTS

A. Introduction

The cavitation results obtained in lithium (Chapter III) indicated that the amount of damage sustained by a given material at 1500°F was considerably less than that sustained at 500°F for constant testing time. The exact opposite behavior was noted in the cavitation tests conducted in lead-bismuth alloy and mercury as part of this overall investigation. In these two fluids the damage sustained by a given material at the higher temperature was greater than that measured at the lower temperature. One might expect this latter behavior due to the reduced strength of the materials at the elevated temperature. However, the variation of the fluid properties with temperature is also important and must be considered. A recent paper by Leith[65] presents predictions of cavitation damage in a vibratory facility exposed to atmospheric pressure for liquid metals as a function of temperature for a material possessing constant mechanical properties, i.e., not a function of temperature. Leith's interpretation of the previously available data indicates that the specific gravity, vapor pressure, viscosity, and surface tension are important fluid properties which affect the amount of damage

-313-

sustained as a function of temperature. In the case of NaK, potassium,

lithium, rubidium, cesium, and sodium, Leith concludes that cavitation

damage as a function of temperature reaches a maximum at a temperature

15% to 20% up the melting-boiling range, falling off below and above

this maximum damage temperature.

It is our present feeling that the trend in the lithium results

can be explained primarily on the basis of cavitation "thermodynamic

effects," as follows. At 1500°F the vapor pressure of lithium is many

times greater than at 500°F. When the cavitation bubbles collapse at

the higher temperature, the heat of condensation from the condensing

vapor trapped within the bubble must be conducted into the surrounding

fluid. Since the vapor pressure is much higher at the higher tempera-

ture, there is more vapor present within a given bubble and, hence, more

heat must be conducted into the surrounding fluid. If this does not

occur rapidly enough (during the vibratory half-cycle corresponding to

horn insertion), then the temperature and pressure of the uncondensed

vapor are raised, thus arresting the bubble collapse. This uncondensed

vapor serves to cushion the bubble collapse with a resultant decrease in

collapse pressures and reduced damage to the test specimens.

Such thermodynamic effects have been studied in great detail by

many investigators.[65,69,76,77,78,79,82,83,84,89 through 96] These stud-

ies generally have resulted in the derivation of some "thermodynamic

parameter" which could be used to characterize cavitation bubble col-

lapse in a given fluid-temperature environment as being controlled

either by liquid inertia effects or the heat transfer effects discussed

above. Of course, in some cases both effects would influence bubble collapse. A simple model for bubble formation and collapse will now be examined.

B. Calculation of Thermodynamic Parameters

Very qualitatively, if the local pressure is reduced below the vapor pressure in a fluid, the phenomenon of cavitation occurs. The vapor bubbles that are formed when the local pressure is reduced below the vapor pressure depend upon the surrounding liquid for the required heat of vaporization. The heat of vaporization is drawn from a thin liquid film adjacent to the cavity.[76,78,79,84,91 through 95] The basic heat balance between the heat required for vaporization that occurs during cavitation and the heat drawn from a thin liquid film adjacent to the cavity is simply stated as:

$$\rho_V V_V L = \rho_L V_L C_L (\Delta T)$$

where:

ρ_V = vapor density, lbm./ft.^{3}

V_V = vapor volume in bubble, ft.^{3}

L = latent heat of vaporization, Btu/lbm.

ρ_L = liquid density, lbm./ft.^{3}

V_L = liquid volume of film surrounding bubble from which heat can be drawn within the allowed time, ft.^{3}

C_L = specific heat of the liquid, Btu/lbm.°F

ΔT = temperature drop in liquid film due to vaporization,°F

The ratio of vapor volume formed to liquid volume supplying the necessary heat of vaporization is:

$$\frac{V_v}{V_L} = \frac{\rho_L \, c_L \, \Delta T}{\rho_v \, L} = J_a$$

where J_a = Jakob Number.

Generally, for a spherical bubble, the liquid volume, V_L, is expressed as:

$$V_L = A \cdot h$$

where:

    A = liquid film area (vapor-liquid interface)

    h = average thickness of cooled liquid film

The ratio of vapor volume to liquid volume has been called the thermodynamic parameter, B, by several investigators.[69,78,79,95] It seems more physically meaningful to speak in terms of the ratio of the vapor volume formed to the liquid volume supplying the necessary heat of vaporization per decrease in net positive suction head, Δ H. Thus, Hammitt[78] defined the thermodynamic parameter, B, as follows, although various other related definitions are to be found in the literature:[69,79,91,92]

$$B = \frac{\rho_L \, c_L \, \Delta T}{\rho_v \, L \, \Delta H} = \frac{J_a}{\Delta H}$$

where:

Δ H = decrease in net positive suction head corresponding to a decrease Δ T in liquid temperature

This is the form of the thermodynamic parameter that will be initially

considered in this analysis.

Since:

$$\Delta H = \frac{\Delta p}{\rho_L}$$

we have:

$$B = \frac{\rho_L^2 \, c_L \, \Delta T}{\rho_v \, L \, \Delta p}$$

From the Clausius-Clapeyron equation,[97,98] we can express $\Delta p / \Delta T$

as:

$$\frac{\Delta p}{\Delta T} = \frac{\rho_v \, L}{T}$$

Thus, the expression for B becomes:

$$B = \left(\frac{\rho_L}{\rho_v \, L} \right)^2 c_L \, T$$

Hence, B can be computed for a given fluid-temperature combination,

knowing the liquid density, vapor density, heat of vaporization, and

specific heat of the liquid. The thermodynamic parameter, B, above has

been evaluated for water at 55°F, 95°F, 120°F, 150°F, and 180°F, for

mercury at 70°F and 500°F, lithium at 500°F and 1500°F, lead-bismuth at

500°F and 1500°F, and sodium at 500°F and 1500°F. Values of ρ_L,

ρ_v, and B are tabulated in Table 53 for these various fluid-tempera-

ture combinations. ρ_v is computed from the ideal gas law.

TABLE 53

VALUES OF THERMODYNAMIC PARAMETERS FOR VARIOUS FLUID-TEMPERATURE COMBINATIONS

Fluid & Temperature	ρ_L lbm./ft.³	ρ_V lbm./ft.³	B	J_a	J_a^2	C	$B_{eff.}$
Water - 55°F	62.5	6.98×10^{-4}	4.69×10^3	4.69×10^3	2.20×10^7	1.60×10^{10}	174.0
Water - 95°F	62.2	2.48×10^{-3}	413.0	413.0	1.71×10^5	1.60×10^{10}	1.35
Water - 120°F	61.7	4.92×10^{-3}	111.1	111.1	1.24×10^4	1.57×10^{10}	0.10
Water - 150°F	61.1	1.03×10^{-2}	27.4	27.4	729.0	1.54×10^{10}	0.006
Water - 180°F	60.5	1.99×10^{-2}	7.7	7.7	60.0	1.51×10^{10}	0.0005
Mercury - 70°F	845.0	5.56×10^{-7}	3.28×10^{12}	3.28×10^{12}	1.08×10^{25}	1.58×10^7	2.72×10^{21}
Mercury - 500°F	808.0	3.80×10^{-2}	1.14×10^3	1.14×10^3	1.30×10^6	4.06×10^6	644.0
Lithium - 500°F	31.2	1.96×10^{-10}	4.41×10^{14}	4.41×10^{14}	1.94×10^{29}	9.20×10^5	2.02×10^{26}
Lithium - 1500°F	28.7	3.76×10^{-4}	206.0	206.0	4.25×10^4	7.56×10^5	48.9
Lead-Bismuth--500°F	648.0	1.63×10^{-13}	5.04×10^{24}	5.04×10^{24}	2.54×10^{49}	2.15×10^6	1.73×10^{46}
Lead-Bismuth--1500°F	600.0	8.44×10^{-6}	3.30×10^9	3.30×10^9	1.09×10^{19}	1.65×10^6	8.49×10^{15}
Sodium - 500°F	55.3	7.54×10^{-7}	5.42×10^8	5.42×10^8	2.94×10^{17}	6.88×10^4	1.12×10^{15}
Sodium - 1500°F	49.0	1.61×10^{-2}	2.04	2.04	4.16	9.54×10^4	0.01

The formulation of the thermodynamic parameter, B, above neglected the rate of bubble formation and bubble collapse. Hence, the very effect we are most interested in investigating, i.e., the rate of heat transfer, has not been taken into account. Florschuetz and Chao,[79] in a very comprehensive paper dealing with the mechanics of vapor bubble growth and collapse, show that the effective thermodynamic parameter, $B_{eff.}$, which does take into account heat transfer effects, can be expressed as:

$$B_{eff.} = \frac{J_a^2}{C^{1/2}} = \left(\frac{\rho_L c_L \Delta T}{\rho_v L}\right)^2 \frac{K_L}{R_0} \left(\frac{\rho_L}{\Delta P}\right)^{1/2}$$

where:

J_a = Jakob Number (dimensionless)

C = C-number (dimensionless)

K_L = thermal diffusivity of the liquid, ft.^{2}/hr., = $k_L / \rho_L c_L$

k_L = thermal conductivity of the liquid, Btu/hr.ft.°F

R_0 = equilibrium bubble radius, ft.

The Jakob Number, J_a, can be expressed as:

$$J_a = B \cdot NPSH$$

where B is the thermodynamic parameter introduced previously which does not take account of the heat transfer effects. As a result, $B_{eff.}$ can be expressed in terms of B, as:

$$B_{eff.} = B^2 \frac{K_L}{R_0} (NPSH)^{3/2}$$

Florschuetz and Chao[79] show that for low $B_{eff.}$ bubble growth and collapse is heat transfer controlled, whereas for high $B_{eff.}$, it is liquid inertia controlled.

The Jakob Number, J_a, has been computed for the various fluid-temperature combinations listed in Table 53 for a constant NPSH of 1 foot. The values are tabulated in Table 53. The value of 1 foot was selected arbitrarily, but it is reasonable to conclude that the effective NPSH controlling bubble formation and collapse in our experiments was constant, since it is the dynamic NPSH caused by the rapid insertion and withdrawal of the ultrasonic horn that is applicable. This is approximately constant for all the fluid-temperature combinations investigated. The C-number was also computed, assuming an equilibrium bubble radius of 1 cm. This value was also arbitrarily chosen, but it is reasonable to assume that the bubble radius was constant for all the cases considered since the dynamic NPSH was constant in all cases. Values of C and $B_{eff.}$ computed under these assumptions are tabulated in Table 53. Since, as they are used herein, only ratios of these quantities are required, the use of arbitrary constants for R_0 and NPSH is permissible. The values of C and $B_{eff.}$ for other values of R_0 and NPSH can be obtained easily from Table 53 by suitable ratios, if so desired.

In the case of the liquid metals it is seen that $B_{eff.}$ is a minimum for sodium at 1500°F. The value for lithium at 1500°F is also quite small. As the value of $B_{eff.}$ is decreased, this would indicate a greater ratio of vapor volume formed to liquid volume supplying the necessary heat for a given drop in NPSH. Low values of thermal

diffusivity, indicating that the fluid is a poor thermal conductor, would further reduce the value of $B_{eff.}$. Hence, it is clearly seen that as $B_{eff.}$ is reduced, the heat transfer effects become important, i.e., more vapor is available for condensation and/or the heat of condensation cannot be conducted into the surrounding fluid sufficiently rapidly in the horn half-cycle available for bubble collapse because of poor thermal conductivity. Thus, in this case, the uncondensed vapor serves to cushion the bubble collapse as its temperature and pressure are raised by the heat not conducted to the surrounding fluid. In the case of mercury at 70°F, lithium at 500°F, and lead-bismuth at 500°F and 1500°F, the values of $B_{eff.}$ are very large. In these cases bubble collapse was not heat transfer controlled, as demonstrated by the cavitation damage results. Rather, it is controlled by liquid inertia effects. Bubble collapse in mercury at 500°F appears to be influenced by both factors, as will be seen later. The values of $B_{eff.}$ for water are all quite low. However, even at 55°F the vapor density of water is appreciable. It appears that heat transfer effects may be important in bubble collapse in water at all the temperatures considered, especially at the highest temperature of 180°F, which is very near the boiling point. Sodium at 1500°F is also near the boiling point, and the value of $B_{eff.}$ is very small, as expected. In the comprehensive analysis of Florschuetz and Chao[79] in water, it is concluded that for values of $B_{eff.}$ less than 0.05, heat transfer effects control bubble collapse, whereas for $B_{eff.}$ greater than 10, the liquid inertia is controlling. For intermediate values of $B_{eff.}$ both effects are important. Applying these criteria to

our water data, it is seen from Table 53 that the bubble collapse at

55°F and 95°F appears to be controlled by the liquid inertia, while at

150°F and 180°F the heat transfer effects are controlling. At 120°F

both effects are apparently important.

It would be instructive to determine in a more quantitative

manner those fluid-temperature combinations considered in this investi-

gation that are influenced by heat transfer effects in bubble collapse.

In Table 54 is listed the experimental data obtained for type 304 stain-

less steel in the various fluids at several temperatures in terms of MDP

rate. Data for type 316 stainless steel tested in sodium was taken from

references 37 and 38. The data obtained in each individual fluid was

normalized to a given data point in that fluid. Hence, the water data

was normalized to the data point obtained at 120°F, the mercury data to

70°F, the lithium data to 500°F, the lead-bismuth data to 500°F, and the

sodium data to 500°F. The resulting normalized MDP rates are also

included in Table 54. This data was next corrected for differences in

temperature which would change the mechanical properties of the test

material and, hence, influence cavitation damage. The correction

applied was proportional to $(UR)^{-1/2}$, where UR denotes Hobbs' ultimate

resilience, which was previously discussed. The form of the correction

was taken from a predicting equation discussed in Chapter VI, which

suitably accounted for the complete body of cavitation data. The tem-

perature corrections are noted in Table 54, and also the corrected nor-

malized MDP rates, which are computed by simply multiplying the normal-

ized MDP rate by the temperature correction factor. It is noted that in

TABLE 54

EXPERIMENTAL CAVITATION DATA -
TYPE 304 STAINLESS STEEL

Fluid & Temperature	MDP Rate	Norm. MDP Rate	Material Temperature Correction	Corr. Norm. MDP Rate	B_eff.**
Water - 55°F	0.06 mils/hr.	0.43	1.0	0.43	174.0
Water - 95°F	0.11	0.79	1.0	0.79	1.35
Water - 120°F	0.14	1.0	1.0	1.0	0.10
Water - 150°F	0.08	0.57	1.0	0.57	0.006
Water - 180°F	0.001	0.007	1.0	0.007	0.0005
Mercury - 70°F	0.32	1.0	1.0	1.0	2.72×10^{21}
Mercury - 500°F	0.69	2.2	0.81	1.78	644.0
Lithium - 500°F	0.34	1.0	1.0	1.0	2.02×10^{26}
Lithium - 1500°F	0.034	0.1	0.129	0.0129	48.9
Lead-Bismuth--500°F	0.93	1.0	1.0	1.0	1.73×10^{46}
Lead-Bismuth--1500°F	11.30	12.2	0.129	1.57	8.49×10^{15}
Sodium - 500°F	0.53*	1.0	1.0	1.0	1.12×10^{15}
Sodium - 1500°F	0.00033*	0.0006	0.126	0.000076	0.01

*Type 316 stainless steel tested by Hydronautics, Inc. (References 37 and 38).

**Taken from Table 53.

the case of mercury and lead-bismuth the corrected normalized MDP rate is greater at 1500°F than at 500°F. This could be due to the decreased fluid viscosity at the higher temperature. If all effects were precisely accounted for, the corrected normalized MDP rates would be identical at both temperatures. In the case of the lithium and the sodium the corrected normalized MDP rate is much smaller at 1500°F than at 500°F. This is unquestionably due to the heat transfer effects previously discussed that are in a direction to reduce cavitation damage at the higher temperature.

In Figure 82 the Log Corrected Normalized MDP Rate is plotted versus Log B_{eff} for the liquid metals. The water data is not included on this plot due to the additional complicating factor of dissolved gas which affects cavitation damage in water, but is a negligible effect in liquid metals, as previously discussed, since their solubility for any of the common gases is negligible. Any value of corrected normalized MDP rate greater than 1.0 in Table 54 was plotted as a value of 1.0 in Figure 82. This is due to the fact that there is no known physical mechanism that could account for values greater than 1.0 other than data scatter and the minor effect of fluid viscosity or surface tension mentioned previously. Numerical calculations[82,83] show that these effects are apparently quite negligible. Of course, the mechanical property temperature correction applied to the data, $(UR)^{-1/2}$, is only approximate, and this could result in the discrepancy. The data in Table 54 indicates that bubble collapse only in lithium and sodium at 1500°F, of the several cases considered, is subject to heat transfer effects. The
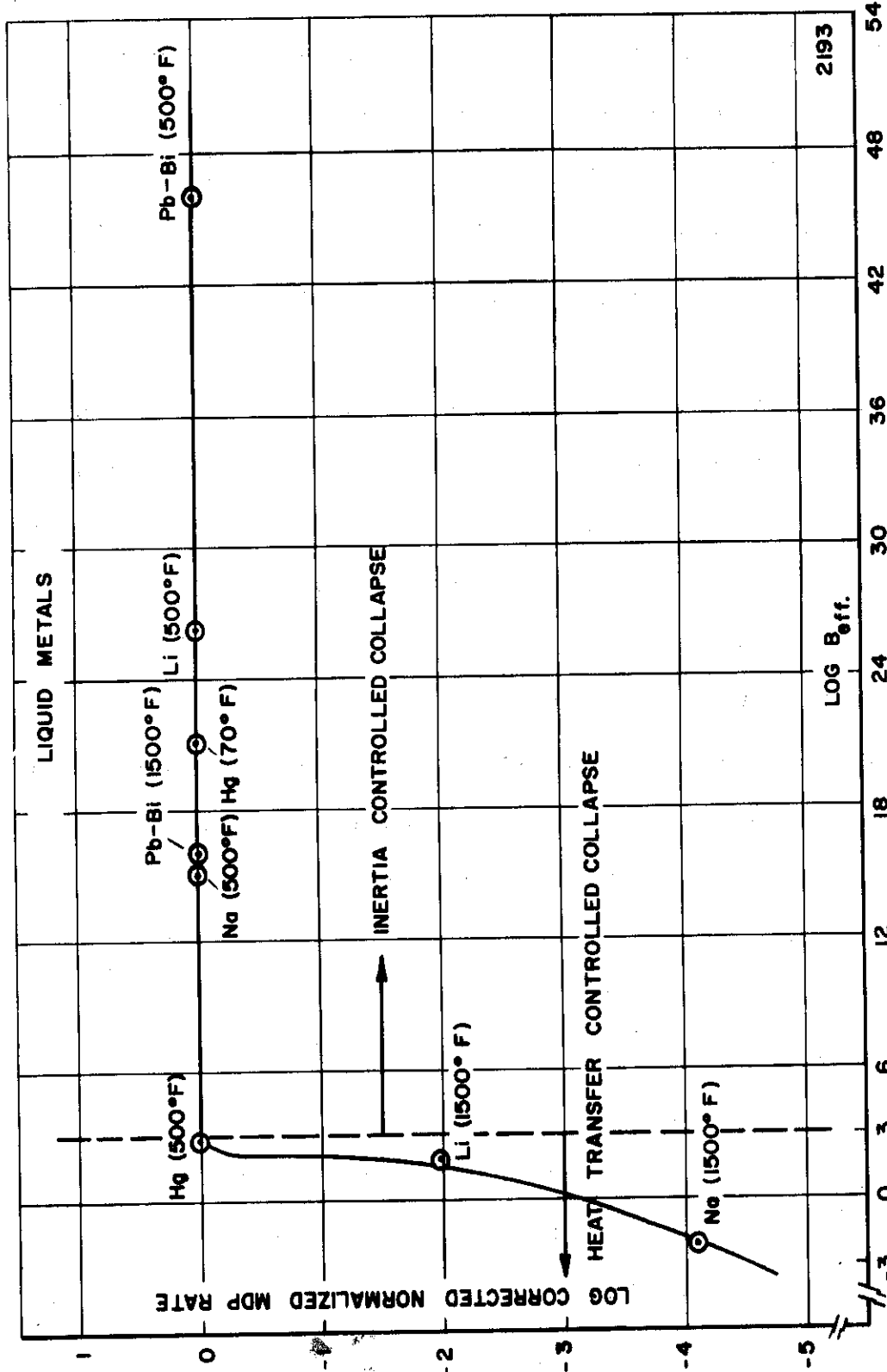
Fig. 82.--Effect of thermodynamic parameter on cavitation
damage - liquid metals.

situation with respect to mercury at 500°F is not nearly as clear, although the corrected normalized cavitation data for mercury at 70°F and 500°F would seem to indicate that heat transfer effects are negligible at 500°F. In the case of the other fluid-temperature combinations, bubble collapse is controlled by liquid inertia only. In Figure 82 a dashed vertical line has been arbitrarily placed on the curve, passing through a value of $B_{eff.}$ = 1000. It is in this range of $B_{eff.}$ that heat transfer effects apparently become important in bubble collapse in liquid metals.

In Figure 83 the corrected normalized MDP rate is plotted versus Log $B_{eff.}$ for the water data. The reduced values of corrected normalized MDP rate noted at 55°F and 95°F are most probably due to effects of dissolved gas,[66] increasing at low temperature due to increased solubility, which serve to cushion the bubble collapse. The dissolved gas is reduced substantially as the temperature is increased. Its proportionate effect is also reduced as the vapor pressure increases with temperature. The reduced damage rate noted at 150°F and 180°F in water is presumably due to the heat transfer effects previously discussed. The dashed curve in Figure 83 serves to indicate the probable behavior of the damage rate as a function of $B_{eff.}$ if the effect of dissolved gas were negligible.

In Figure 84 Log $B_{eff.}$ is plotted versus the fluid temperature for each of the 5 fluids considered. Again, an arbitrary dashed horizontal line is drawn corresponding to a value of $B_{eff.}$ = 1000. Generally, values of $B_{eff.}$ greater than 1000 would denote fluid-temperature
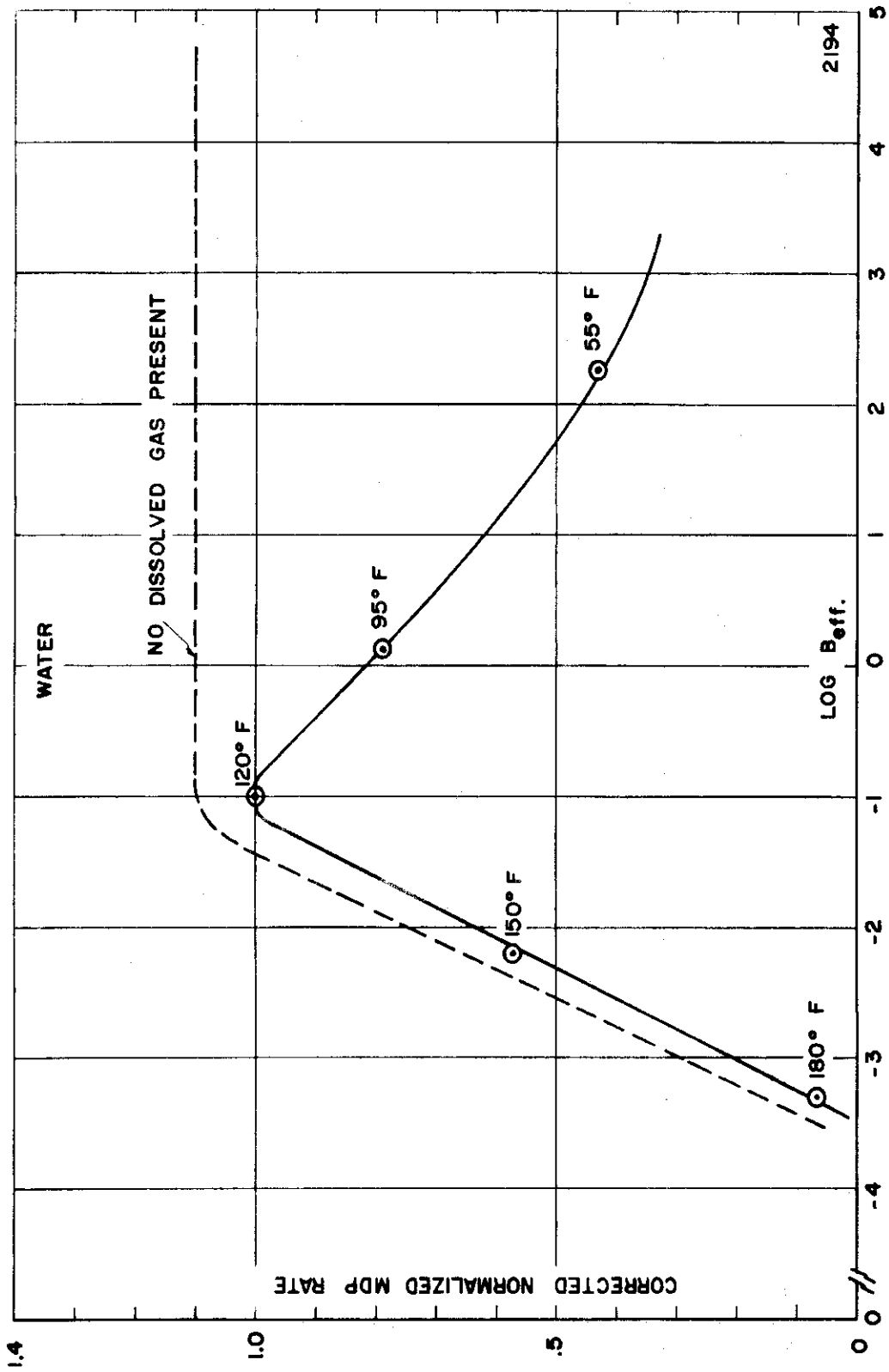
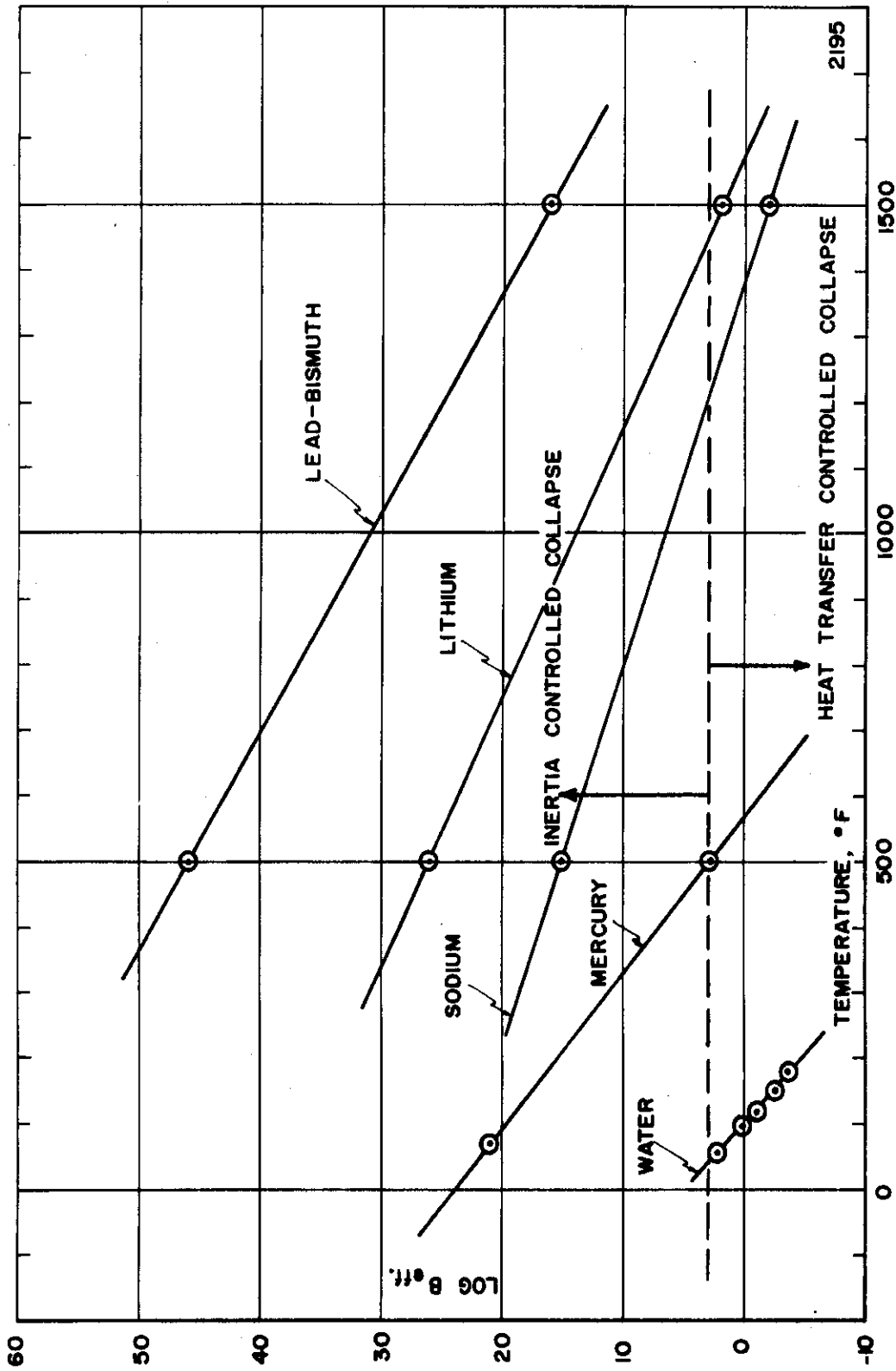Fig. 83.--Effect of thermodynamic parameter on cavitation damage - water.

Fig. 84.--Effect of temperature on the thermodynamic parameter -
liquid metals and water.

combinations where bubble collapse is liquid inertia controlled. Values of $B_{eff.}$ below 1000 would denote fluid-temperature combinations where bubble collapse is heat transfer controlled. Of course, there is an intermediate range of values of $B_{eff.}$ where both effects are operative.

Figures 82, 83, and 84 could be used by the designers of equipment which is susceptible to cavitation damage in order to approximate the change in damage corresponding to a change in operating conditions from one temperature to another in a given fluid if NPSH and degree of cavitation were maintained constant.

C. Final Predicting Equation

Comprehensive computer correlations of experimentally-determined cavitation damage data with applicable mechanical and fluid properties were discussed in Chapter VI. The cavitation damage data used in these correlations was raw experimental data. There are at least two corrections that should be applied to certain sections of the complete data set involving four different fluids and a variety of test materials. The "thermodynamic effects" were discussed in detail, and it was seen that for certain fluid-temperature combinations this mechanism results in a reduction in cavitation damage. Clearly, the damage data obtained in lithium at 1500°F was significantly reduced because of these "thermodynamic effects." The same comment applies to the water data obtained at 70°F, although in this case the effect is believed primarily due to dissolved gas effects. These thermodynamic effects were not operable in the other fluid-temperature combinations considered in this study. The

correction for "thermodynamic effects" that should be applied to the lithium data at 1500°F is merely the ratio of the corrected normalized MDP rates for lithium at 500°F and 1500°F listed in Table 54. This ratio is 1/0.0129 = 77.5. In the case of the water data at 70°F the appropriate correction factor is not so easily obtained because of the complicating factor of dissolved gas, previously discussed. However, part of the error can be accounted for by correcting the data to the maximum point observed in Figure 83 ($\sim$ 120°F). This ratio is 14/11 = 1.27. Hence, the lithium data at 1500°F and the water data at 70°F should be increased by the appropriate factors to take account of the reduced damage due to "thermodynamic effects."

The second correction that should be applied to the cavitation damage data is concerned with the large variation in static net positive suction head (NPSH) between the various fluids. The suppression pressure was maintained constant at 15.3 psia throughout all the tests in all the fluids at all temperatures. It was not possible to maintain constant NPSH in these tests due to the pressure limitations of the experimental equipment. Hence, static NPSH varied by about a factor of 30 between mercury and lithium. As previously discussed, the dynamic portion of the NPSH due to the vibrating horn is approximately constant for all the fluid-temperature combinations. Since this quantity is large compared to the static portion, it controls bubble collapse and no correction is required on this account. However, the static NPSH controls the bubble regime (size of bubble cloud and bubble population) and, hence, it also influences the amount of damage. Variations in

static NPSH obviously lead, then, to improper modeling between fluids.

It was noted that the surfaces of the specimens tested in mercury and

lead-bismuth (minimum NPSH) were almost completely and uniformly covered

with damage, while the specimens tested in water and lithium (maximum

NPSH) were only selectively damaged. Particularly, in the case of the

lithium the damage was concentrated in a small region near the center

of the specimen. It is believed that the difference in these damage

patterns is due to improper flow modeling and the fact that a bubble

cloud does not cover the entire face of the specimen in the case of the

water and lithium tests. From experimental observations it is estimated

that on the average the damaged area noted for a specimen tested in

water was approximately 1/2 the damaged area noted for the same material

tested in mercury. This variation is attributed to the variation in

static NPSH. Thence, an appropriate correction factor is deduced from

this data for all of the fluids. Adopting the mercury test fluid as the

standard (correction factor $= 1.0$), one may compute the correction fac-

tor for water in the following manner:

$$\left[\frac{(NPSH)_{H_2O}}{(NPSH)_{Hg}} \right]^n = 2 = \text{Ratio of damaged areas}$$

i.e., it is postulated that the NPSH ratio between the two fluids,

raised to an appropriate power, is inversely proportional to the corres-

ponding ratio of damaged areas noted in the two fluids, and to the ratio

of bubble populations. Then, we have:

$$\left[(35.3)/(2.60) \right]^n = 2$$

Solving for n, we find that n = 0.266. We further postulate that this

constant is approximately applicable for all of the fluids tested.

Thus, the correction factor for lithium is easily computed as:

$$\left[\frac{(NPSH)_{Li}}{(NPSH)_{Hg}}\right]^{0.266} = X$$

$$\left[(70.6)/(2.60)\right]^{0.266} = X = 2.41$$

The correction factor for lead-bismuth is:

$$\left[\frac{(NPSH)_{Pb-Bi}}{(NPSH)_{Hg}}\right]^{0.266} = X$$

$$\left[(3.40)/(2.60)\right]^{0.266} = X = 1.075$$

Thus, the cavitation damage data obtained in water, lithium, and lead-

bismuth should be increased by the appropriate factors to take account

of the variation in bubble population due to the variation in static

NPSH.

Both the correction for "thermodynamic effects" and the correc-

tion for variation in static NPSH were applied to the complete body of

cavitation data. This corrected data was then submitted to a final com-

puter correlation where only Hobbs' ultimate resilience and the fluid

density were allowed as material and fluid correlating parameters,

respectively. The ultimate resilience and density were chosen since a

combination of these two properties had previously correlated the uncor-

rected data very satisfactorily, whereas simple combinations of other

mechanical and fluid properties were non-existent in this respect. In

the present correlation the allowable exponents were ± 1, ± 2, $\pm 1/2$, ± 3,

and $\pm 1/3$, as was the case with all of the previous correlations. Hence,

a total of 10 exponents per independent variable were allowed and only 2

independent variables. Thus, a total of 20 possible terms could enter

the predicting equation under these circumstances. The statistically-

best predicting equation generated in this case was as follows:

Avg. MDP Rate $\approx 0.142 + 8.918(UR)^{-1/2}$

Coefficient of Determination $= 0.780$

Average Absolute % Deviation $= 51.3\%$

Note that this equation is a function of the ultimate resilience only,

while the fluid density does not appear. This is undoubtedly due to the

fact that the correction for variation in static NPSH that was applied

to the full data set is a function of the fluid density only, since the

suppression pressure was held constant in all cases. Hence, the indi-

vidual effects of density and NPSH cannot be separated in these experi-

ments. Additional tests under different conditions, e.g., variable

suppression pressure and constant density, or constant NPSH and variable

density, would be required in order to assess the separate contribution

of each of these effects to the damage mechanism. However, this present

correction for NPSH would indicate a dependence on the density only to

the extent of $(\rho)^{-0.266}$, whereas previously the density had entered as

$(\rho)^{-2}$ (all data and no corrections of any kind applied) and as $(\rho)^{-1}$

(lithium data at 1500°F excluded from the full data set and no correc-

tions of any kind applied).

When only the correction for "thermodynamic effects" is applied to the full data set, the statistically-best predicting equation generated in this case was as follows:

Avg. MDP Rate $= 0.284 + 7.254(UR)^{-1/2} - 0.331(\rho)^{-2}$

Coefficient of Determination $= 0.744$

Average Absolute % Deviation $= 49.5\%$

Here both the ultimate resilience and the density enter into the predicting equation. In all cases studied the ultimate resilience enters to the power (-1/2), whereas the dependence on density varies.

When neither the correction for "thermodynamic effects" nor the correction for variation in static NPSH is applied to the full data set, the statistically-best predicting equation obtained was as follows:

Avg. MDP Rate $= 0.510 + 6.045(UR)^{-1/2} - 0.471(\rho)^{-2}$

Coefficient of Determination $= 0.658$

Average Absolute % Deviation $= 54.5\%$

This was precisely the predicting equation obtained in Chapter VI when a multiple mechanical and fluid properties correlation was carried out on the full body of cavitation data, and serves as a check on the overall procedure.

The various correlations are somewhat consistent in that the dependence on the ultimate resilience is identical and the dependence on density is either to the power (-1) or (-2) in all cases considered.

In summary, if the designer of equipment susceptible to cavitation damage were to make use of these results in choosing appropriate

cavitation-resistant materials for use in a given fluid-temperature
environment, the recommended equation for computing the relative
expected damage rate is as follows:

1) Avg. MDP Rate $= C_1 \cdot C_2 [0.142 + 8.918(UR)^{-1/2}]$

where:

C_1 = correction for "thermodynamic effects" $(0 \leq C_1 \leq 1)$

C_2 = correction for variation in NPSH $(0 \leq C_2 \leq 1)$

C_1 is precisely the corrected normalized MDP rate, previously discussed,
and plotted in Figures 82 and 83 as a function of the thermodynamic
parameter, $B_{eff.}$. Figure 82 is valid for tests in liquid metals and
Figure 83 for tests in water. Hence, one must first compute the value
of $B_{eff.}$ for the fluid-temperature combination of interest and then
determine the corresponding value of C_1 (corrected normalized MDP rate)
from Figure 82 or 83. Figure 84 could be used for determining $B_{eff.}$ if
the fluid-temperature combination of interest to the designer is dis-
played. Hence, C_1, is easily determined. Note that Figures 82 and 83
are plots of Log Corrected Normalized MDP Rate versus Log $B_{eff.}$ and that
the correction for "thermodynamic effects," C_1, is equal to the cor-
rected normalized MDP rate, not log corrected normalized MDP rate.

C_2 can be easily expressed as:

$$C_2 = 1.29(NPSH)^{-0.266}$$

where NPSH corresponds to the net positive suction head (expressed in
feet) for the fluid-temperature combination of interest. Thus, both C_1
and C_2 result in a reduction of the relative expected damage rate,
except when $C_1 = C_2 = 1$.

If the tests are to be conducted at constant NPSH, then the recommended equation for computing the relative expected damage rate is as follows:

2) Avg. MDP Rate $= C_1[0.284 + 7.254(UR)^{-1/2} - 0.331(\rho)^{-2}]$

where C_1 is determined from Figures 82 or 83, as before. In all cases the ultimate resilience (UR) is expressed in units of in.lbf./in.^{3}, or psi, while the density is expressed in units of g./cc.

CHAPTER VIII

SUMMARY AND CONCLUSIONS

Ultrasonic-induced cavitation studies have been conducted in lead-bismuth alloy at 500°F and 1500°F, in mercury at 70°F and 500°F, in water at 70°F, and in lithium at 500°F and 1500°F for a wide variety of materials including refractory alloys, steels, aluminum, brasses, copper, nickel, tool steels, plastics, etc. The detailed results for the various fluid-material-temperature combinations are listed in the appropriate sections of the report. Various salient features include the following:

1) The ultrasonic cavitation facility which was developed as part of this dissertation is capable of operation at temperatures up to 1500°F in fluids including reactive liquid metals, and provides a sealed, inert atmosphere for these tests at pressures up to about 50 psig.

2) The tantalum-base alloys, T-111 and T-222(A), were the most cavitation resistant of the materials tested in lead-bismuth alloy at 500°F and 1500°F, in mercury at 500°F, in water at 70°F, and in lithium at 500°F and 1500°F. Thus, the superiority of these refractory alloys at elevated temperature has been

-337-

demonstrated. The stainless steels were the most resistant in mercury at 70°F. In the bearing program the tool steel alloys BG-42 (R_c = 64) and Blue Chip Tool Steel were the most resistant. The cavitation resistance of these alloys correlated well with hardness. These tool steels were approximately ten times more resistant than the T-111 and T-222 in mercury at 500°F.

3) The refractory alloy, Cb-1Zr(A), was the least resistant of the materials tested in lead-bismuth alloy, mercury, and lithium at 500°F. Type 304 stainless steel was the least resistant in lead-bismuth alloy and lithium at 1500°F, while Plexiglas (tested only at room temperature) was least resistant in mercury at 70°F, and type 1100-0 aluminum least resistant in water at 70°F. In the bearing program the two grades of graphitar tested were found to be the least resistant of the materials used.

4) As would be expected, all materials tested in lead-bismuth sustained greater damage at 1500°F than at 500°F. All materials tested in mercury sustained greater damage at 500°F than at 70°F with the exception of the hot-rolled carbon steel. This can be explained by the superior mechanical properties of this material at the higher temperature. In lithium the damage suffered by all materials tested at 1500°F was much less than that at 500°F. This is believed due to thermodynamic effects which are very important in lithium at 1500°F. This effect was not operative in the lead-bismuth tests since the vapor pressure was nearly zero even at 1500°F.

5) For the tests at 500°F, wherein the applied static pressure
above vapor pressure was held constant for the different tests,
the amount of damage sustained by a given material in lithium
was less than that measured in mercury or lead-bismuth by a fac-
tor ranging from 2 to 30. The large variation in this ratio
indicates that coupling parameters between fluid and materials
are necessary to obtain a comprehensive correlation. The amount
of damage sustained in lithium at 500°F and in water at 70°F was
of the same order of magnitude. Damage rates with mercury were
3 to 20 times greater than for water at the same temperature
(70°F). No corresponding direct comparison was possible in the
venturi tests,[22] although generally damage with mercury was
greater. The damage noted in lead-bismuth and mercury at 500°F
was about the same.

6) Plexiglas was relatively less cavitation resistant in mercury
than in water, and in fact there are numerous substantial dif-
ferences in rankings between materials in different fluids at
the same temperature. Thus, clearly, any equation to predict
cavitation damage must consider fluid as well as material prop-
erties in such a way as to achieve a coupling between the two.
The acoustic impedance ratio between fluid and test specimen
could serve in this capacity. These observations are consistent
with previous venturi test results from this laboratory.

7) Detailed examination of the wetted but non-cavitated parts of
the equipment and test specimens indicates that corrosion

effects in the absence of cavitation were insignificant in these investigations. Photomicrographs have not indicated intergranular corrosion in any of the tests.

8) In general, the damage rate was approximately constant throughout the tests for the liquid metal tests and for most of the water tests. However, in some of the water tests, the damage rate decreased markedly during the test. It is felt that this is a result of the very deep, isolated pitting encountered in these tests. Generally, water and lithium tests differed from the heavy liquid metal tests in that quite uniform and relatively fine damage was encountered in the heavy liquid metal tests as opposed to the water and lithium tests on the same materials. This difference may be a result of the improper modeling of the fluid flow regime between the two fluids, as indicated by the large difference in static NPSH between tests. It is indicated that the volume loss rate remains approximately constant as long as the damage covers the surface uniformly. This condition persists to different accumulated MDP for different material-fluid combinations. It persisted to the order of at least 50-100 mils accumulated MDP for the heavy liquid metal tests (lead-bismuth and mercury), but in some cases only to $\sim$ 3 mils MDP for the water and lithium tests. In these tests a useful constant rate persisted between about 1 and 3 mils accumulated MDP, and this rate could be used to rank the materials. Since the initial rate is less than the constant

rate achieved, this constant rate is a maximum "plateau" rate.

After the plateau portion of the rate curve, there is usually a

continuous decrease of damage rate. In this respect, the water

tests and the data recently reported by Hobbs[67] and Plesset and

Devine,[59] using a similar facility, are in close agreement. As

was observed in one of the present lead-bismuth tests carried to

very high total MDP, the volume loss rate increased again from a

minimum which followed a first maximum. The test was concluded

before it was possible to determine whether or not a second max-

imum would occur. This plot of MDP rate versus MDP for two type

304 stainless steel specimens tested in lead-bismuth alloy at

1500°F is shown in Figure 85. This type of rate curve has also

been noted in the venturi tests,[99] and a recent theoretical

study[100] based on the statistics of the fatigue process shows

that all of the experimentally observed damage rate curves can

be justified assuming a fatigue mechanism. They can also be

justified on the basis of the feedback between flow regime and

accumulated damage.[101] The difference in extent of the

"plateau" rate between heavy liquid metals on the one hand and

water and lithium on the other is thought to be due to the lack

of proper flow modeling due to a large variation in NPSH.

9) Direct comparison of venturi and vibratory results from this

laboratory shows that the rankings of materials for cavitation

damage are quite similar, and particularly so for the mercury

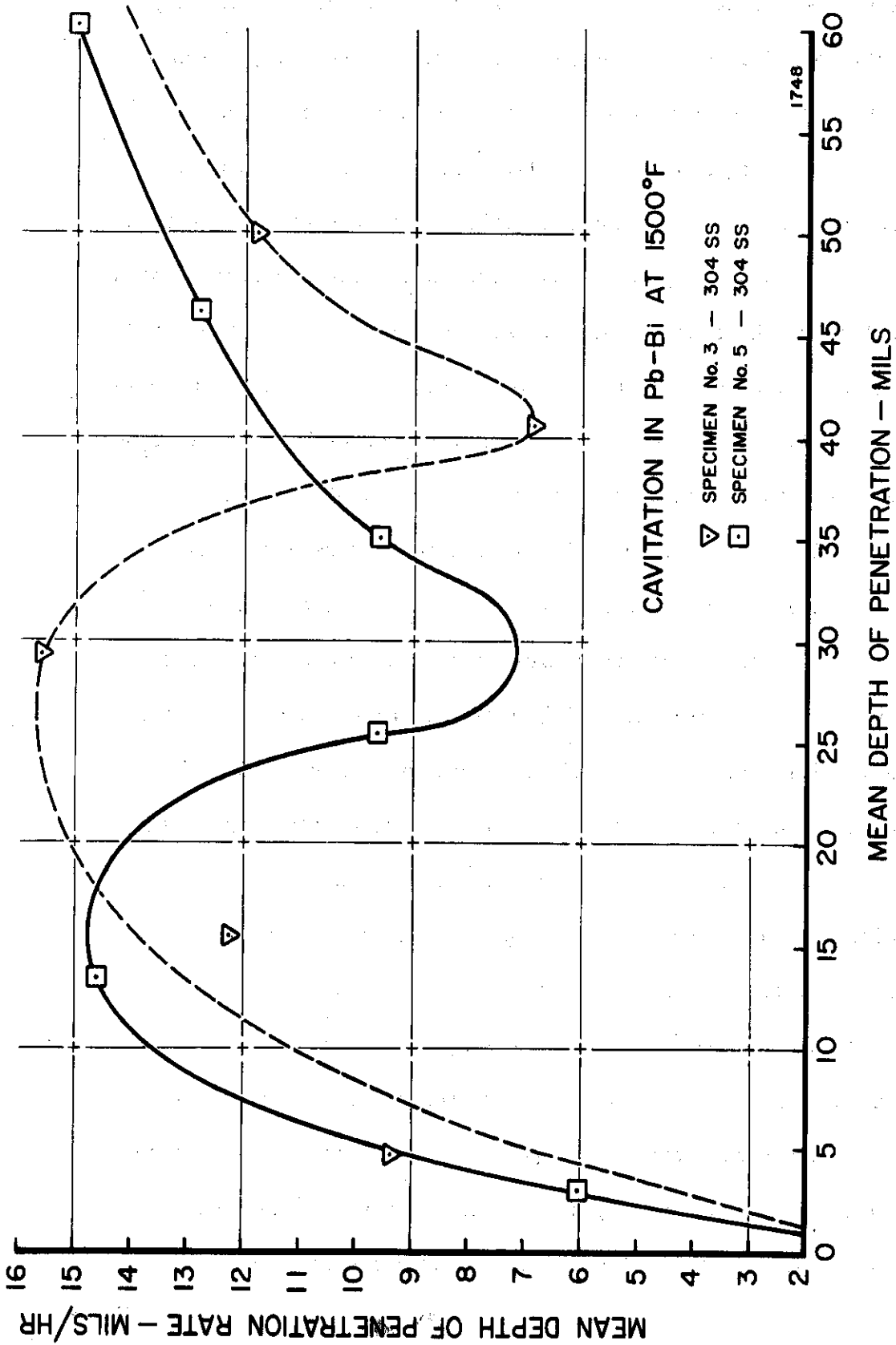tests, but that the relative ratios between different materials

Fig. 85.--Effect of mean depth of penetration on mean depth of penetration rate - type 304 stainless steel in lead-bismuth alloy at 1500°F.

are much greater in the venturi facility. The damage rates in the vibratory tests are of the order of 10^3 times those in the venturi, so that corrosive effects are much less important in the vibratory tests. This factor may be responsible for the much larger range between materials in the venturi test as well as some of the discrepancies in ranking of some materials from these two facilities. To investigate the possible influence of corrosion in the liquid metal tests, a further step would be the use of the pulsing technique pioneered by Plesset.[48]

Computer correlations of the cavitation damage data with applicable mechanical and fluid properties indicate the following important conclusions:

1) There is no single material mechanical property which can be used to correlate the damage with good precision, even if coupling parameters to account for fluid property changes are included in the correlation. However, the "ultimate resilience" suggested by Hobbs[67] seems best in this respect, as discussed below.

2) In general, the best correlations include one or more energy-type mechanical properties, one or more strength-type properties, and one or more fluid coupling parameters if the fluid properties are varied in the data set.

3) The energy-type properties are more predominant in the tests with the high-density liquid metals, while the strength-type

properties predominate for the water and lithium tests. This is consistent with theoretical expectations.

4) In the comprehensive correlations involving data obtained in all four fluids at various temperatures, the fluid density and bulk modulus were the most significant fluid coupling parameters.

5) It was found that a predicting equation involving only Hobbs' ultimate resilience parameter and the fluid density partially accounted for all the cavitation damage data obtained in the four fluids at the various temperatures. This suggests that Hobbs' parameter may be quite significant in predicting cavitation damage.

6) Thermodynamic effects are very important in lithium at 1500°F, reducing the damage by an order of magnitude for the vibratory-type test conducted. This requires that fluid thermal properties such as the specific heat, heat of vaporization, thermal conductivity, and thermal diffusivity, be introduced into the comprehensive computer correlations.

7) No relatively simple single comprehensive correlating equation applies well to all the data. If sufficient terms are allowed, of course, any degree of fit can be obtained. This lack of a single simple correlating equation may indicate that all important mechanisms in cavitation damage may not have been considered. For example, it may not be possible to explain cavitation damage in terms of properties which are determined under semi-static conditions, as are the conventional mechanical and

fluid properties. Also, the contribution of corrosion in the presence of cavitation may be important in some cases, even though it is negligible in the absence of cavitation.

8) For the designer of equipment susceptible to cavitation damage, the recommended equation for computing the relative expected damage rate of potentially useful cavitation-resistant materials for use in a given fluid-temperature environment is as follows:

$$\text{Avg. MDP Rate} = C_1 \cdot C_2 [0.142 + 8.918(\text{UR})^{-1/2}]$$

where C_1 and C_2 are corrections for "thermodynamic effects" and for variation in NPSH, respectively (C_1 and C_2 are both ≤ 1), and are easily determined. If the designer is dealing with a constant NPSH condition, the recommended equation for computing the relative expected damage rate is as follows:

$$\text{Avg. MDP Rate} = C_1 [0.284 + 7.254(\text{UR})^{-1/2} - 0.331(\rho)^{-2}]$$

APPENDIX A

HEAT TRANSFER CALCULATIONS[55]

It is essential that the crystal temperature be kept below the critical value known as the Curie point. For the lead zirconate-titanate crystals used, this is about 150°F. Heat could be transferred to the crystals from the test fluid by two distinct conductive paths. These are:

1) From the test fluid to the cylindrical vessel walls, thence to the flange cone, flange, top plate, transducer horn, and crystals.

2) From the test fluid to the transducer horn tip, thence to the remainder of the transducer horn and the crystals.

In order to maintain the crystal temperature below the Curie point, it is necessary to provide some means of cooling the top plate. Calculations have been made to indicate the extent of cooling which is required. As discussed in the report, 1/2 in. copper tubing is seated in a groove provided in the top of the top plate and brazed into position. Tap water can be continuously circulated through this tubing. The problem is now one of computing the heat flux reaching the top plate by means of the two paths noted above to see if such cooling is adequate. We consider the two paths for heat flow separately.

A. Heat Transferred From the Test Fluid to the Top Plate Via the Cylindrical Vessel Walls, Flange Cone, and Flange

It is first necessary to determine the temperature distribution within the flange cone section before the heat flux conducted to the top plate can be computed. Refer to Figures 10 and 86, which clearly indicate the sections of the cavitation vessel involved and the necessary dimensions. The flange cone section is in the shape of an annular disk, and the differential equation relating the temperature as a function of position is Bessel's equation. For the required boundary conditions the worst conditions (i.e., those which will give maximum heat transfer from the cylindrical vessel to the top plate) will be assumed. Major assumptions and simplifications are listed below:

1) A steady-state condition prevails.

2) The material of which the disk is composed is homogeneous and isotropic.

3) There are no heat sources within the disk itself.

4) The natural convective heat transfer from the exposed surface at any point is proportional to the difference in temperature between the disk and its surroundings. This is a conservative assumption compared to the usual relation that natural convection heat flux is proportional to $(\Delta T)^{4/3}$.

5) The thermal conductivity, k, and heat transfer coefficient, h, are not functions of temperature.

6) The temperature of the surrounding medium is uniform.

FLANGE CONE (TOP VIEW)
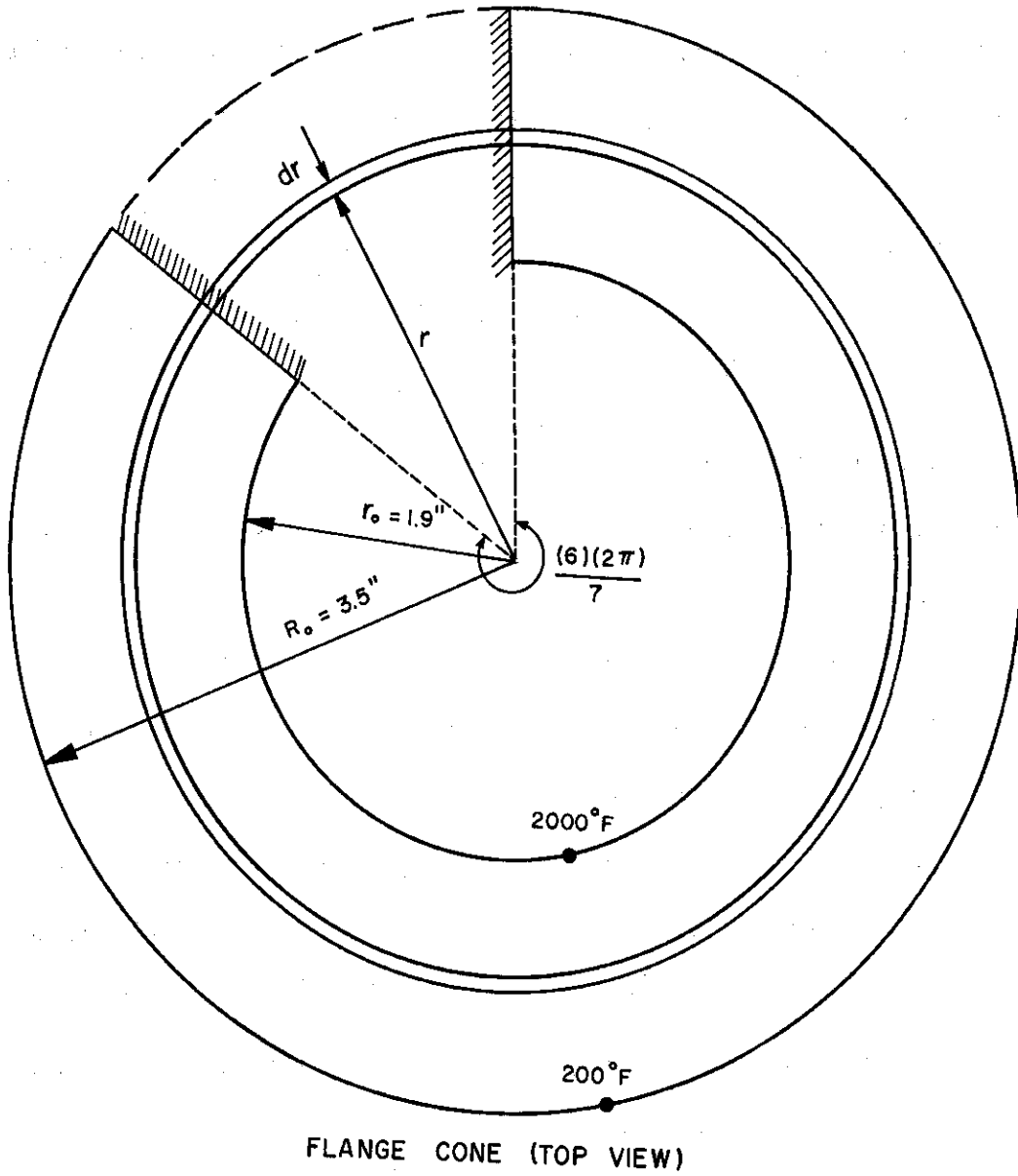
Fig. 86.--Flange cone.

1486

7) There prevails a condition of symmetry of heat flow about the center.

8) The temperature at the base of the cone is assumed to be 2000°F (actual maximum fluid temperature to be used is only 1500°F, so this too is highly conservative).

9) The temperature at the top of the cone is assumed to be 200°F.

10) No heat loss from the inner surface of the cone was assumed, thus introducing an additional safety factor.

11) Since the wall thickness is relatively small compared to the other dimensions, we can consider the system two-dimensional.

The details of the heat transfer calculation can be found in reference 55. However, the major results and procedures will be summarized here. The appropriate heat balance for the flange cone section results in a differential equation (Bessel's equation) relating the temperature of the flange cone as a function of position. The solution is thus well known. After applying the appropriate boundary conditions, the arbitrary constants are evaluated. Hence, the solution for flange cone temperature as a function of position is determined. It is then possible to compute the heat flux into the flange cone from the cylindrical vessel walls by conduction. It is found that heat is being transferred to the flange cone from the vessel walls by conduction at a rate of 2860 Btu/hour. Of this amount, 60 Btu/hour are lost to the atmosphere by the flange cone due to convection and radiation. Hence, 2800 Btu/hour are transferred from the flange cone to the top plate.

B. Heat Transferred from the Test Fluid
   to the Top Plate Via the Transducer
   Horn

It is first necessary to determine the temperature distribution within the transducer horn before the heat flux conducted to the top plate via this path can be computed. Refer to Figure 87, which schematically indicates the transducer horn. After determining the temperature distribution in the transducer horn, it will be possible to compute the heat flux transferred from the tip of the horn to the base of the horn. As a conservative measure, it will be assumed that this heat flux reaches the top plate. Again, the appropriate heat balance for the system yields the required differential equation, giving the temperature of the horn as a function of position. The general solution is determined, the proper boundary conditions are applied, and the temperature distribution is computed. Then, it is possible to determine the heat transferred from the tip of the horn to the base section, which is found to be 109 Btu/hour. This is only a fraction of the heat flux conducted to the top plate via the cylindrical vessel walls, flange cone, and flange (2800 Btu/hour).

C. Total Heat to be Dissipated from Vessel

The heat reaching the top plate, i.e., the conductive heat flux from the vessel walls and from the transducer horn, is to be removed by means of a copper cooling coil through which cold water will be circulated. In the steady-state, the heat removed by the cold water will equal the heat reaching the top plate. Thus, the total amount of heat
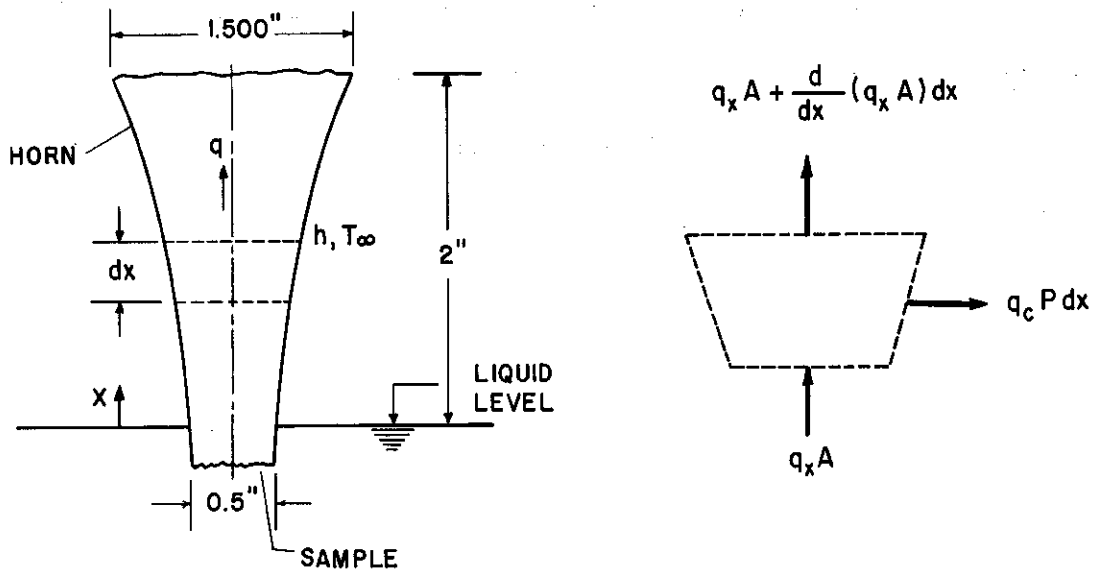
Fig. 87.--Schematic of heat transfer by horn.

to be removed by the cooling water is 2800 Btu/hour + 109 Btu/hour =

2909 Btu/hour = 48.5 Btu/min. ($\sim$ 850 watts).* The copper tubing pro-

vided to remove this heat is 1/2 in. O.D. x .430 in. I.D. #20 (.035 in.

wall) tubing. Considering the normal pressure supplied in the city

water mains, a flow rate of approximately 1 gpm would be achieved in

this tubing. This would result in a steady-state water outlet tempera-

ture of 6°F above the inlet temperature. Such a facility should be able

to easily remove the heat conducted to the top plate.

All the stress calculations pertinent to the design of the high-

temperature cavitation vessel are contained in reference 55.

---

*The electrical input to the crystals is about 200 watts, and,
hence, not of great importance compared to the heat flow from the high-
temperature fluid.

APPENDIX B

COMPUTER REGRESSION ANALYSIS OF CAVITATION DATA[87],[88]

A least mean squares stepwise regression computer program was used to correlate the cavitation damage data with mechanical properties. Using the first-order interaction form of the program, the problem at hand can be simply stated as follows: it is required to determine the appropriate coefficients and exponents in a predicting equation of the form:

$$Y = C_0 + C_1 X_1^a + C_2 X_2^b + C_3 X_3^c + C_4 X_4^d + \ldots\ldots\ldots + C_n X_n^q$$

where C_0, C_1, C_2, C_3, C_4, $\ldots\ldots\ldots\ldots$, C_n are constant coefficients; a, b, c, d, $\ldots\ldots\ldots$, q are constant exponents; the X's are the independent variables, in this case the mechanical properties of the materials and the fluid properties; and Y is the dependent variable, the average MDP rate. The independent variables are allowed to appear in the predicting equation any number of times, each time raised to a different value of exponent and multiplied by an appropriate coefficient. The program allows great latitude on the possible exponents for the independent variables. The form of the program used in this investigation allows any or all of the independent variables to be raised to the following exponents: ± 1, ± 2, $\pm 1/2$, ± 3, $\pm 1/3$.

-353-

A predicting equation of the type noted above would be obtained

by allowing only a "first-order interaction" of the possible terms,

i.e., terms involving products of the independent variables would not be

allowed. The program, however, does allow the option of a "second-order

interaction," i.e., allows terms involving products of different inde-

pendent variables. The choice must be made by the individual

programmer.

In the present analysis (permitting only first-order interac-

tion) the allowable mechanical properties (independent variables) were

taken to be the tensile strength, yield strength, engineering strain

energy,[71] true strain energy,[71] hardness, percentage elongation, per-

centage reduction in area, and modulus of elasticity. In addition the

ratio of acoustic impedances[42] of test fluid and specimen material was

also included among the independent variables for all the correlations

involving only a single fluid. In the comprehensive correlations

involving all four fluids one fluid property was included among the

independent variables for all the correlations as a fluid coupling

parameter to explain differences in cavitation resistance of a given

material in different fluids. The fluid coupling parameters that were

investigated included the ratio of acoustic impedances of test fluid and

specimen material, density of fluid, surface tension, net positive suc-

tion head (NPSH), bulk modulus, and kinematic viscosity. Additional

comprehensive correlations involved a combination of five mechanical

properties and five fluid properties. Hence, in a given correlation

there were 10 independent variables and 10 possible exponents for each

independent variable. As a result a total of 100 terms are possible

candidates for inclusion in the predicting equation plus a pure con-

stant. From a physical point of view, it is hoped that a good statisti-

cal correlation will be possible with a minimum number of terms so that

the predicting equation may hopefully be justified on physical grounds.

This possibility would be unlikely if more than 5 or 6 terms were needed

for the correlation.

A brief outline will be given here of the mechanics of the pro-

gram. The interested reader is referred to the literature previously

cited for the details. The major features of the program are as

follows:

1) Of the 100 possible terms that are candidates for inclusion in

   the predicting equation, the program randomly selects a subset

   of 40 terms to be analyzed.

2) A correlation coefficient is computed for each of the 40 terms.

   The correlation coefficient is a measure of the ability of each

   term to individually explain the experimental data, i.e., pre-

   dict the average MDP rate.

3) The term with the greatest correlation coefficient is then

   included in the predicting equation, which at this point is of

   the form:

$$Y = C_0 + C_1 X_1^a$$

   where C_0 and C_1 are constants to be determined.

4) The constants C_0 and C_1 are computed using the least mean

   squares criterion.

5) The initial 40 terms are then sorted into 2 subsets, those that are included in the predicting equation at this point, and those that are not.

6) An importance factor is computed for each term now in the equation. The importance factor is a measure of the total contribution made by each term in explaining the experimental data.

7) The importance factors of the terms in the equation are compared to a minimum level of importance set by the user. A typical range of values is 1% to 5%.

8) Terms having an importance factor less than the minimum level are deleted from the equation.

9) A potential importance factor is computed for each term not in the equation. The potential importance factor is a measure of the ability of each term not in the equation to explain the presently existing variance between the experimental data and the predicted data.

10) The potential importance factors of the terms not in the equation are compared to a minimum level of importance set by the user. A typical range of values is 1% to 5%.

11) Terms not in the equation having a potential importance factor greater than the minimum level are entered into the equation.

This procedure is used to examine the subset of 40 terms chosen randomly and is terminated either when all qualified terms have been entered into the equation or when certain statistical criteria (such as the coefficient of determination and standard error in the dependent

variable) set by the user have been satisfied. Whenever a new term is entered into the equation, the least mean squares criterion is used to compute a new set of coefficients. For a given problem it is possible to analyze several subsets of 40 terms, each chosen randomly from the set of 100 possible terms available. Such a procedure is advisable in that it increases the probability that the most significant terms contained in the initial set of 100 terms will enter the predicting equation.

The output from the program includes the terms in the predicting equation along with the appropriate exponents and coefficients, predicted MDP rates based on the correlation, experimental MDP rates, percent deviations, standard error in the dependent variable, coefficient of determination for the analysis, average absolute percent deviation for the analysis, etc. As a result, it is possible to show graphically the statistical accuracy of the predicting equation by plotting the predicted MDP values versus the experimental points and noting the deviation from a 45° line which would signify a perfect fit.

APPENDIX C

PLOTS OF NORMALIZED INVERSE CAVITATION DAMAGE VERSUS SINGLE MECHANICAL PROPERTIES--LEAD-BISMUTH ALLOY, MERCURY, WATER, LITHIUM AT 500°F, AND LITHIUM AT 1500°F
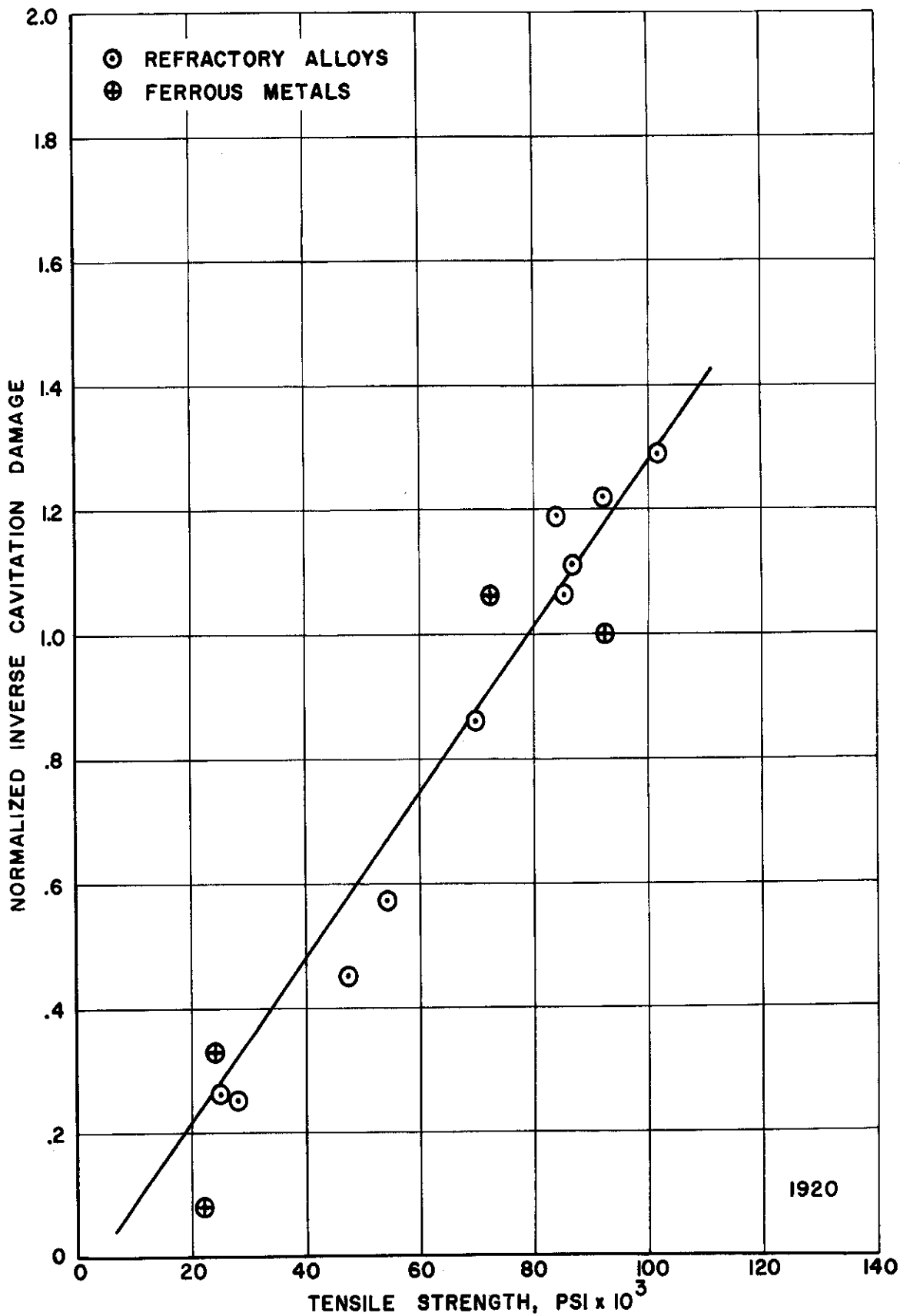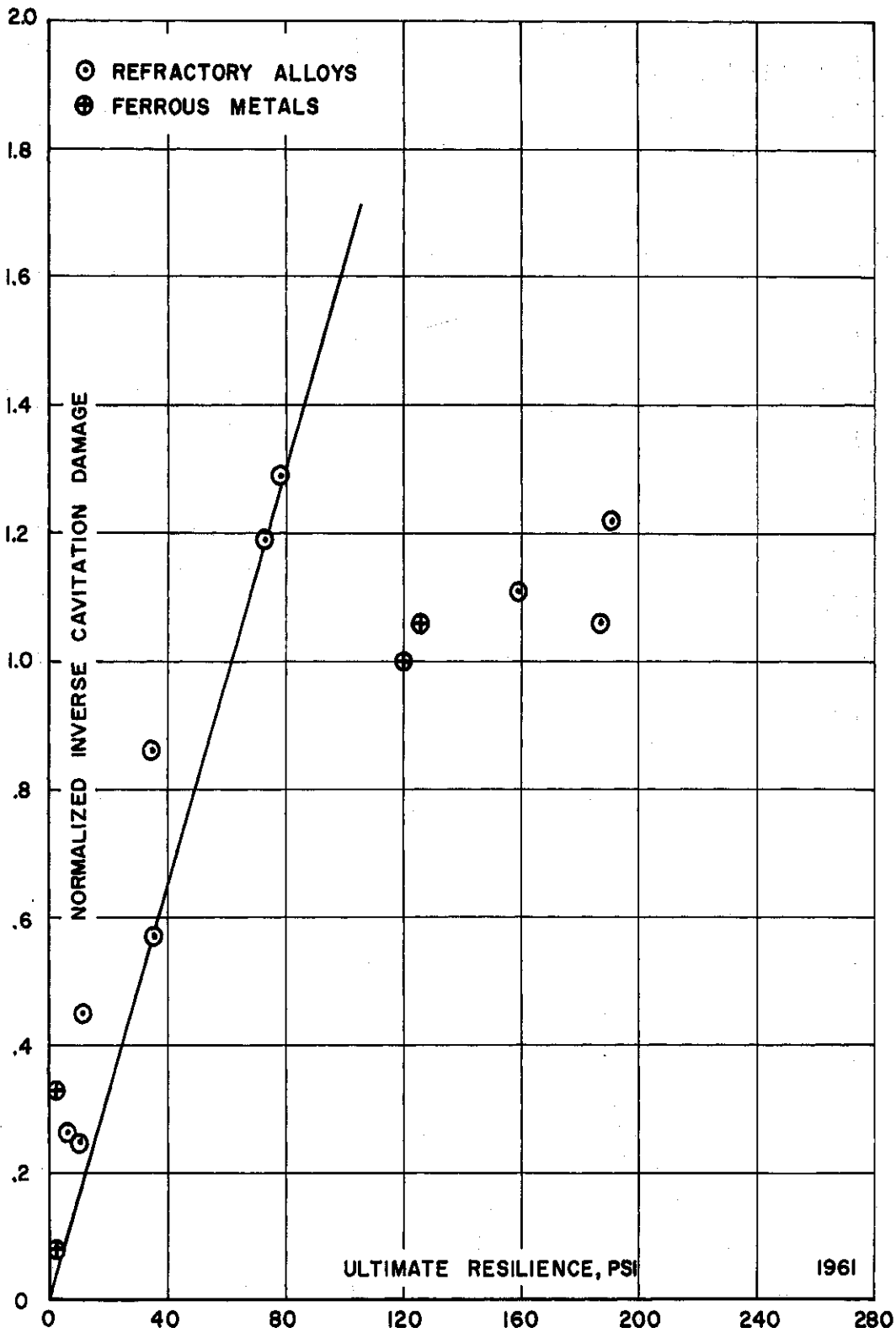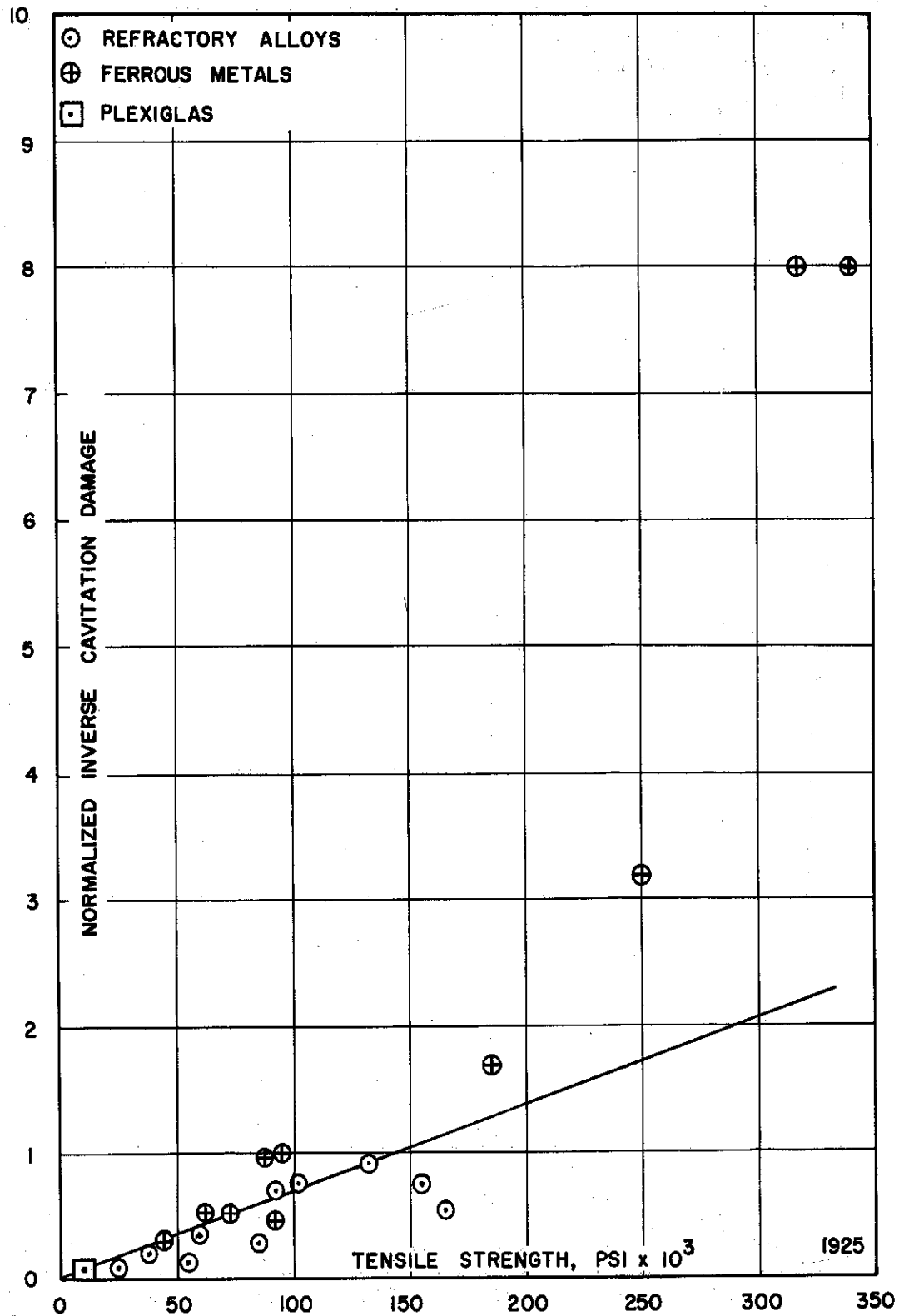
Fig. 88.--Normalized inverse cavitation damage versus tensile strength - lead-bismuth alloy.
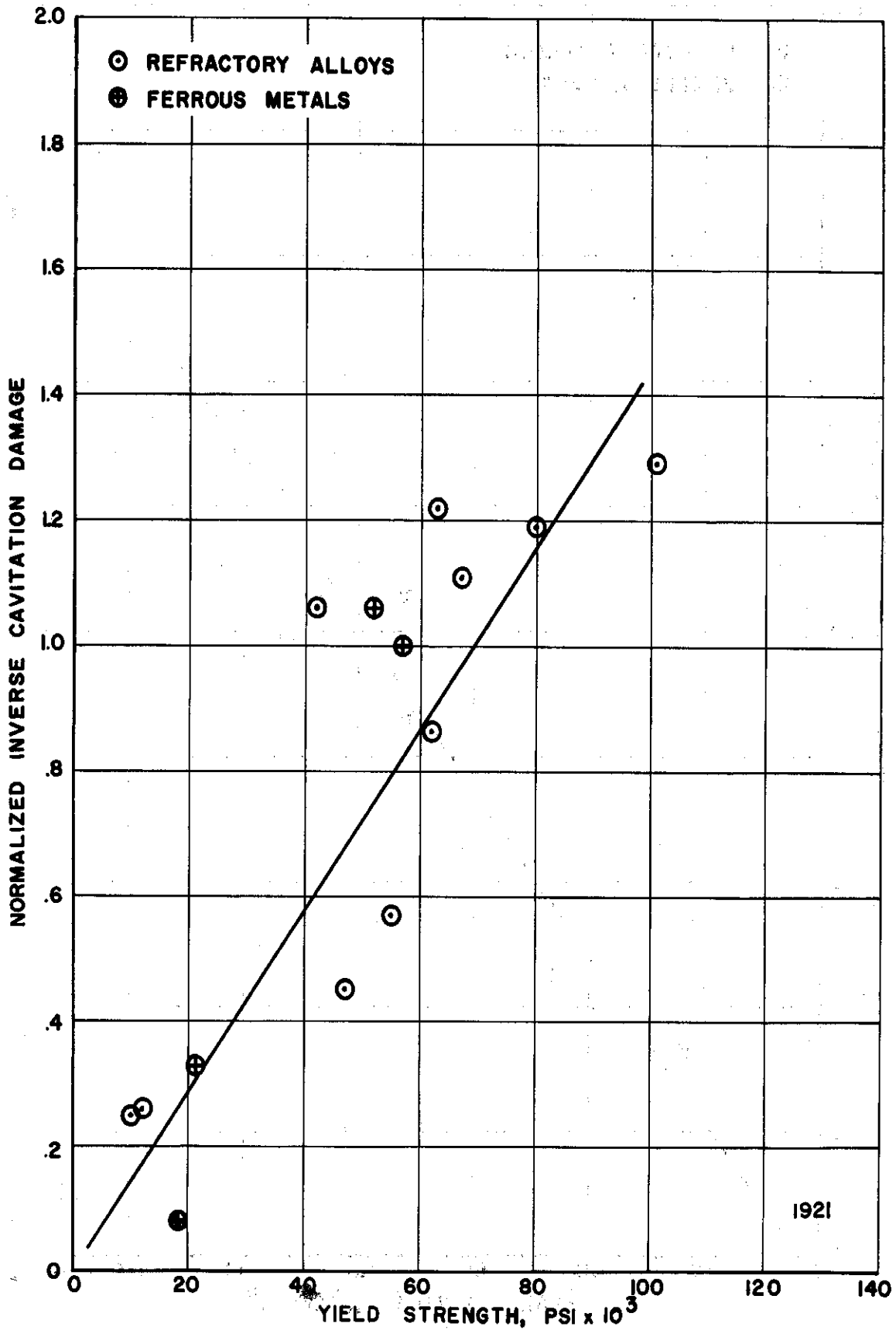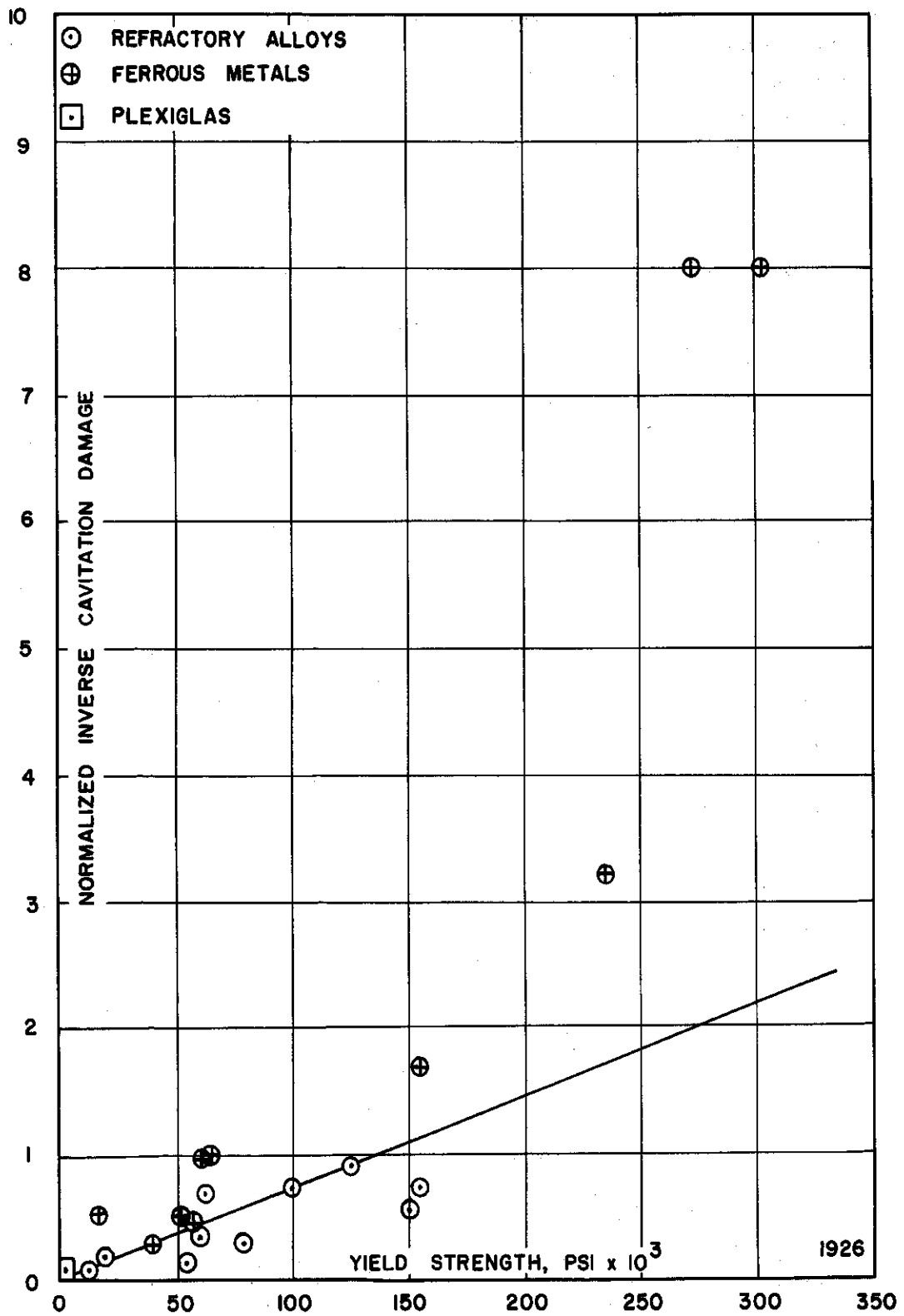
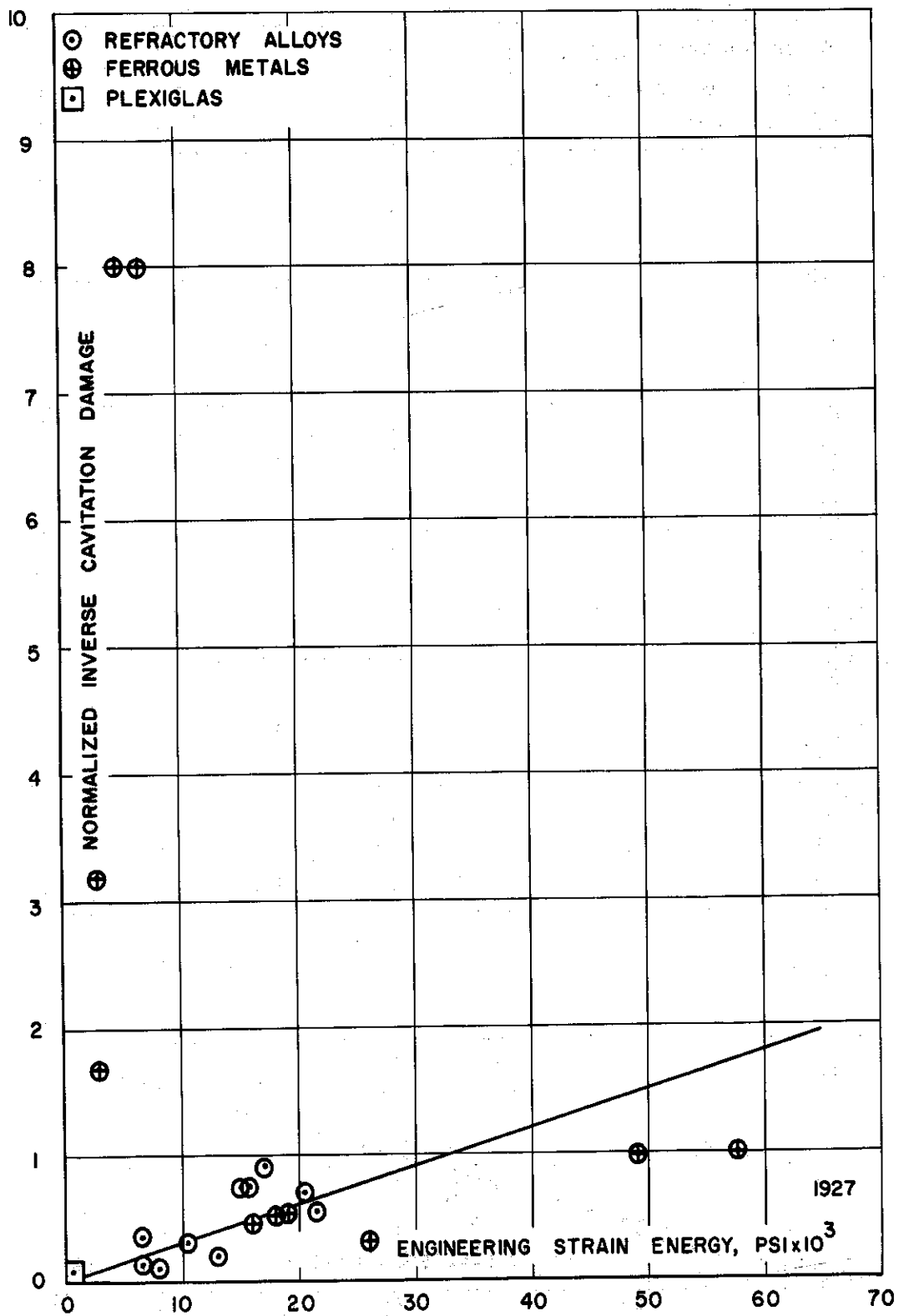Fig. 89.--Normalized inverse cavitation damage versus yield
strength - lead-bismuth alloy.
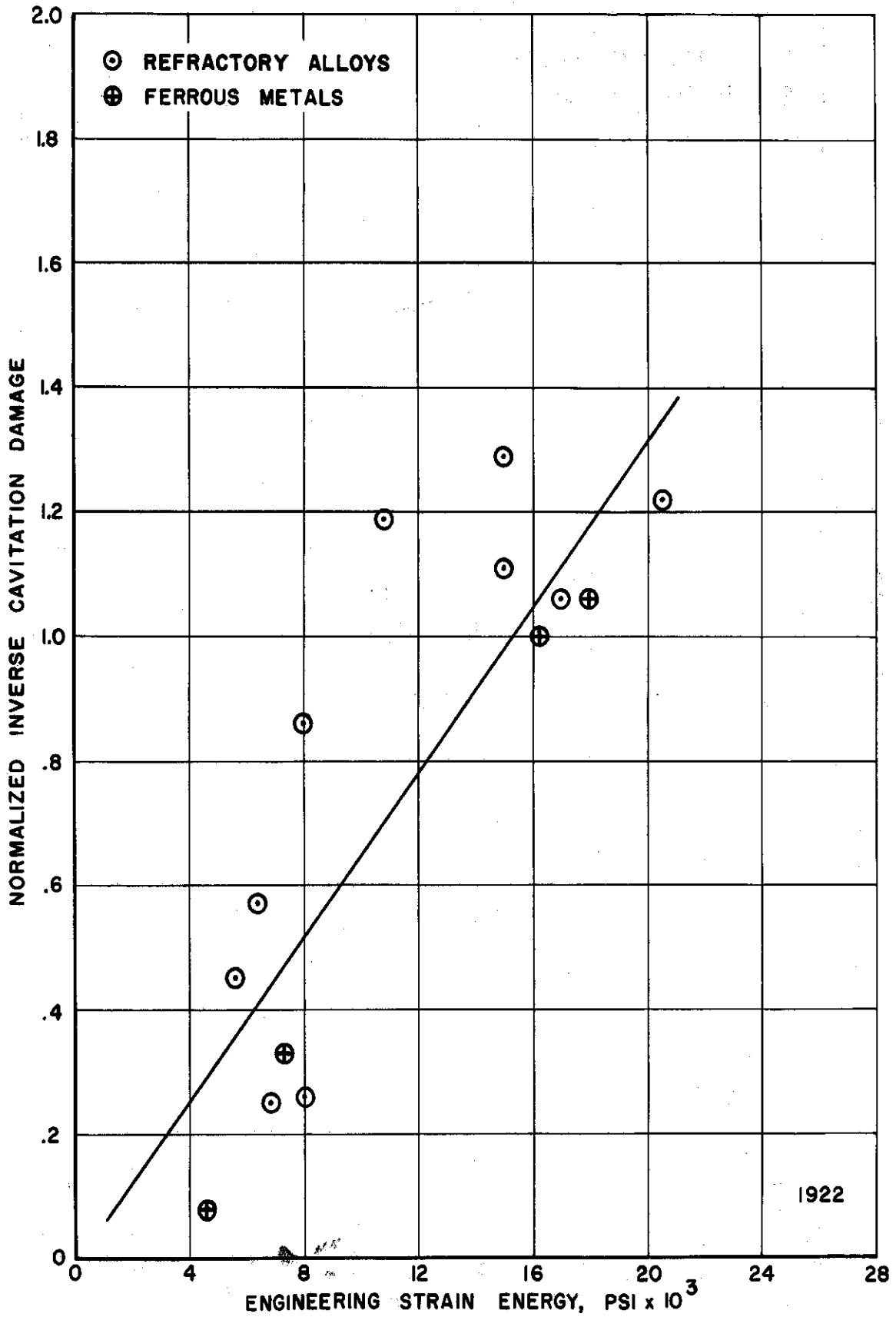
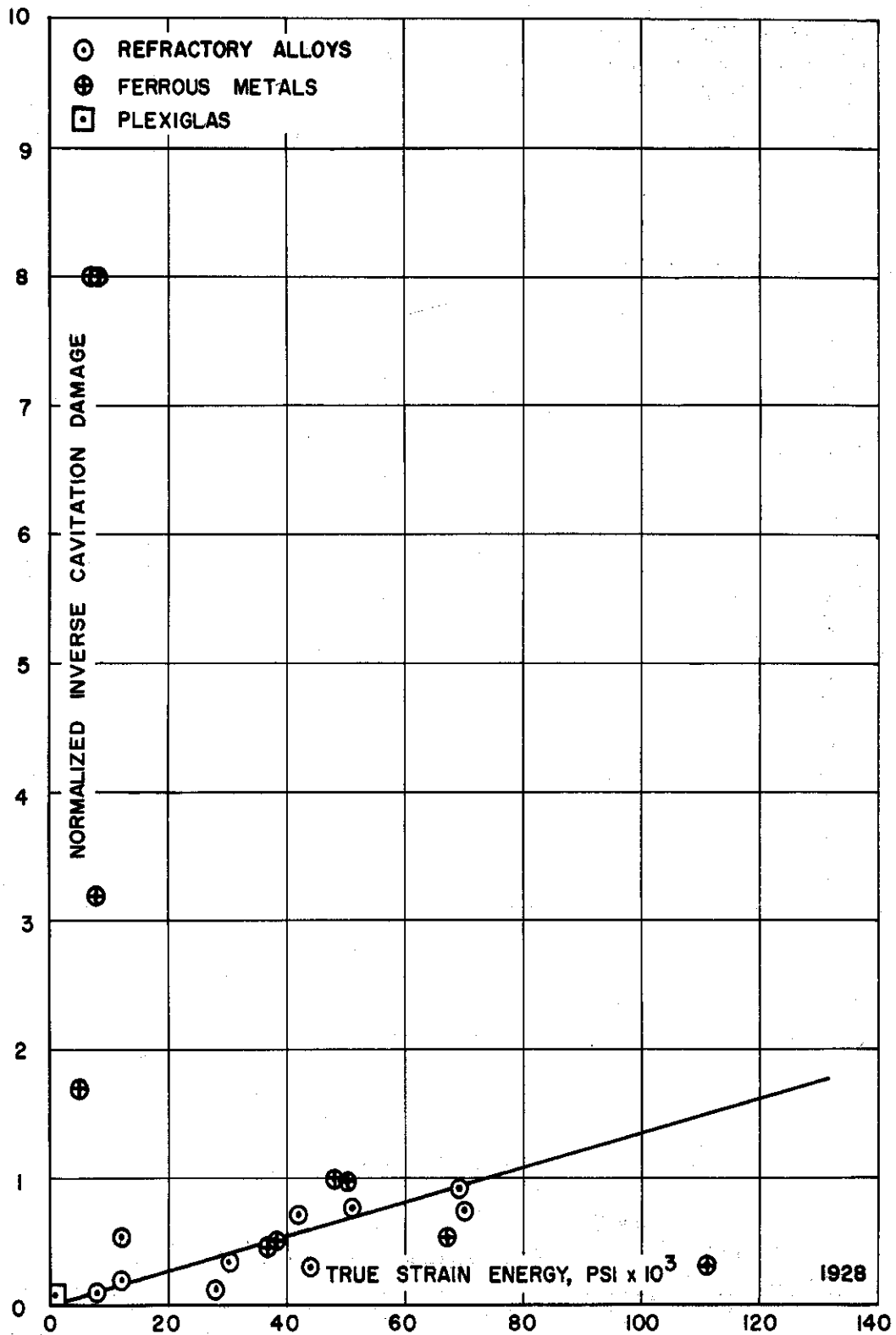Fig. 90.--Normalized inverse cavitation damage versus engineering strain energy - lead-bismuth alloy.
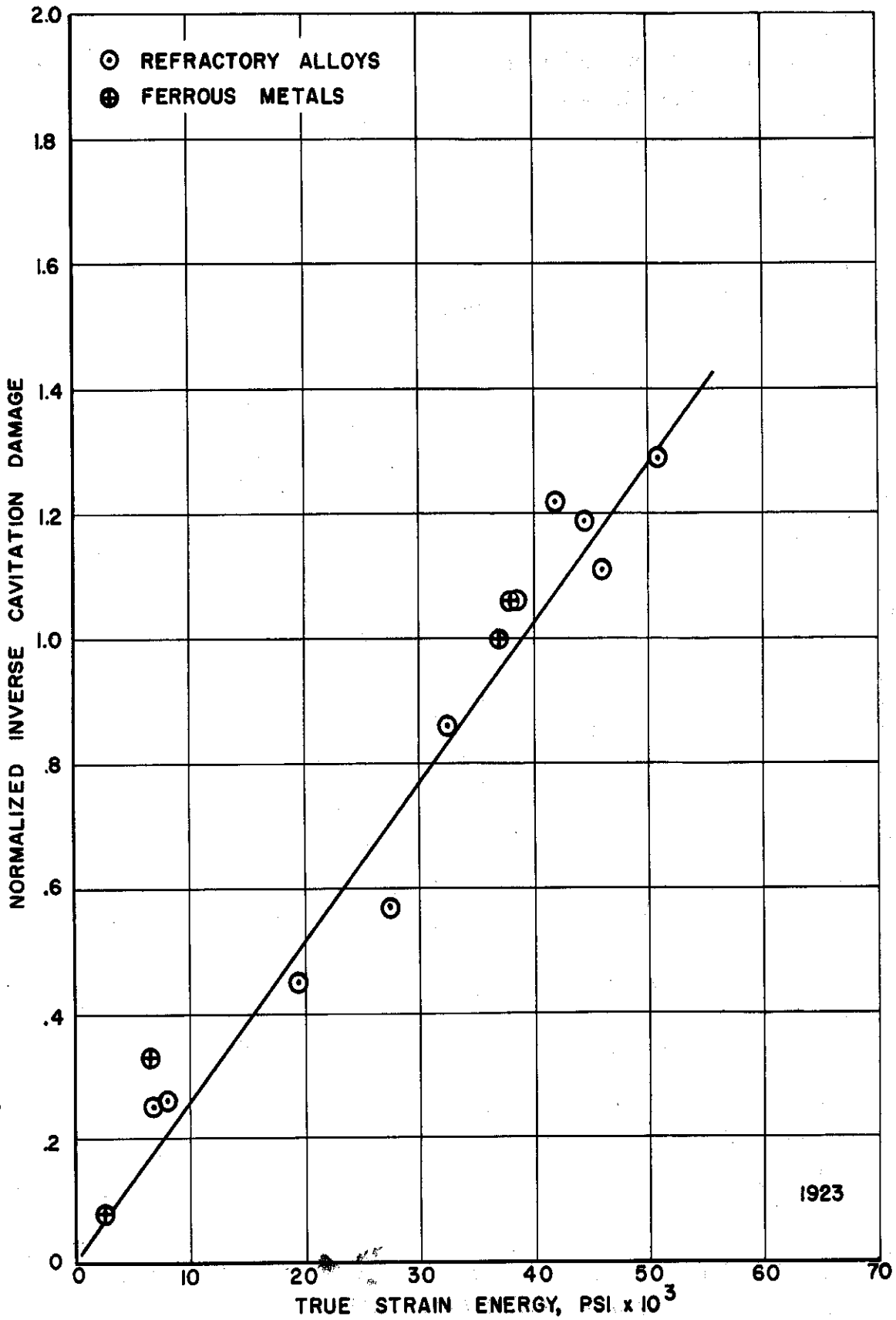
Fig. 91.--Normalized inverse cavitation damage versus true
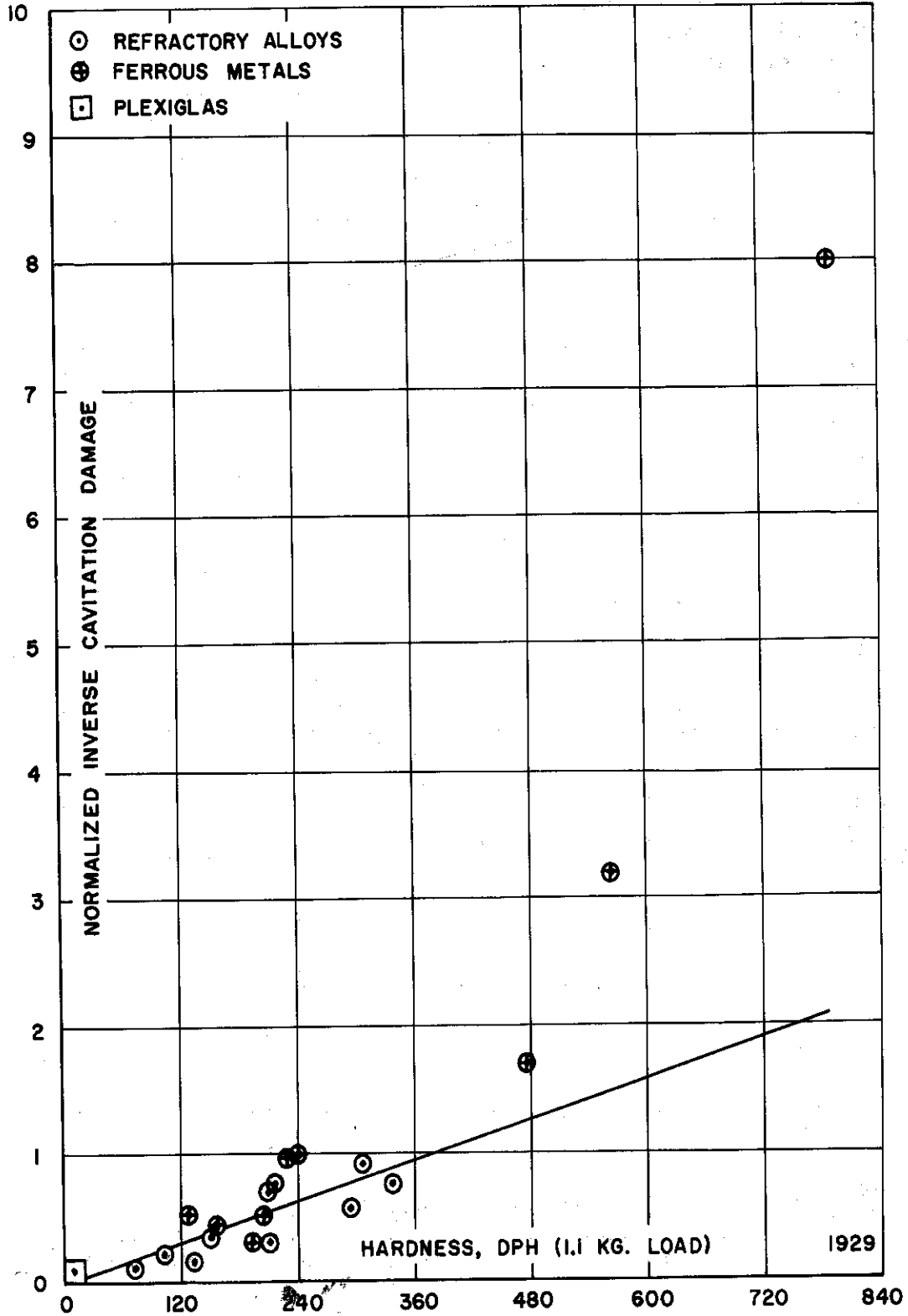strain energy - lead-bismuth alloy.
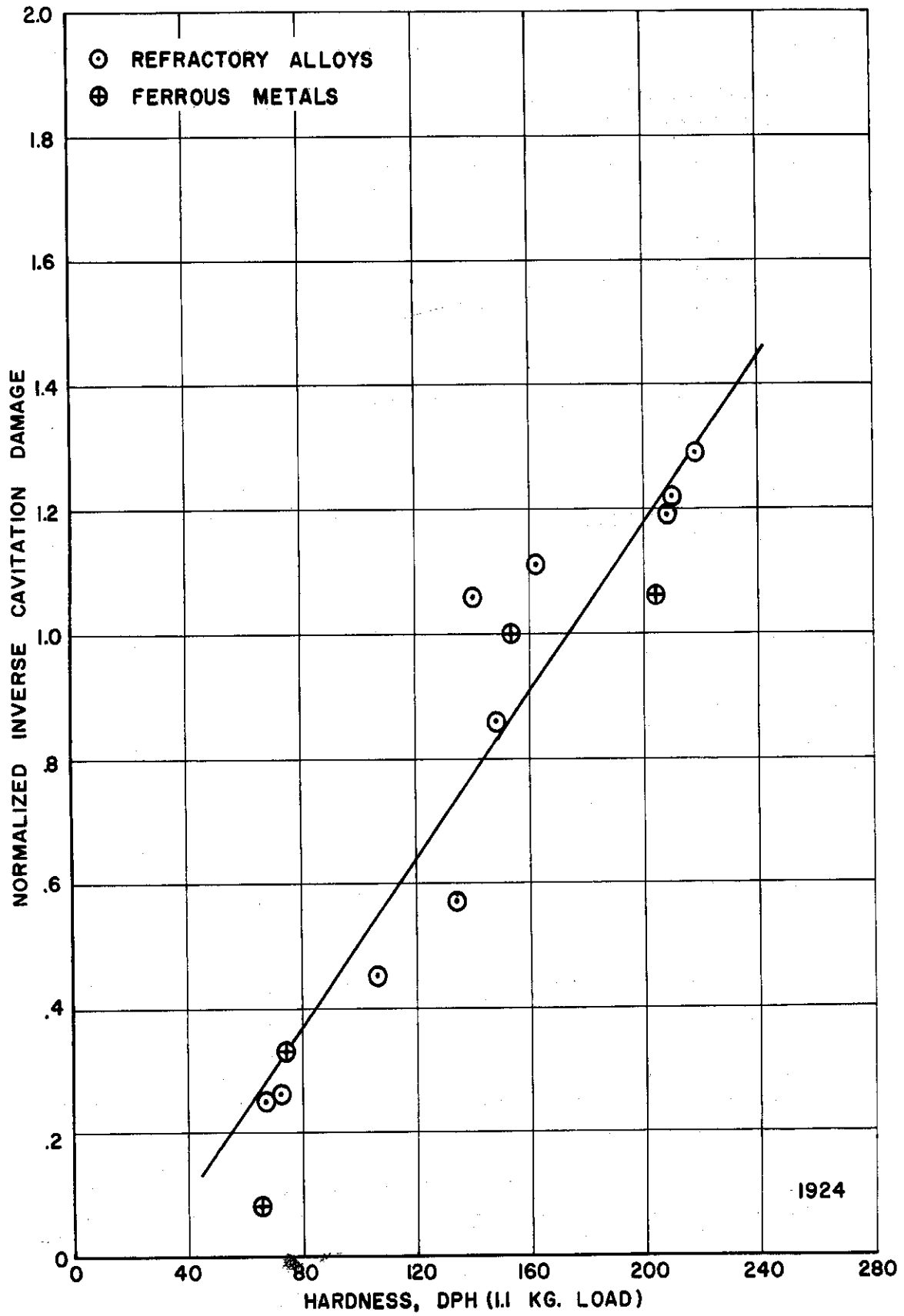
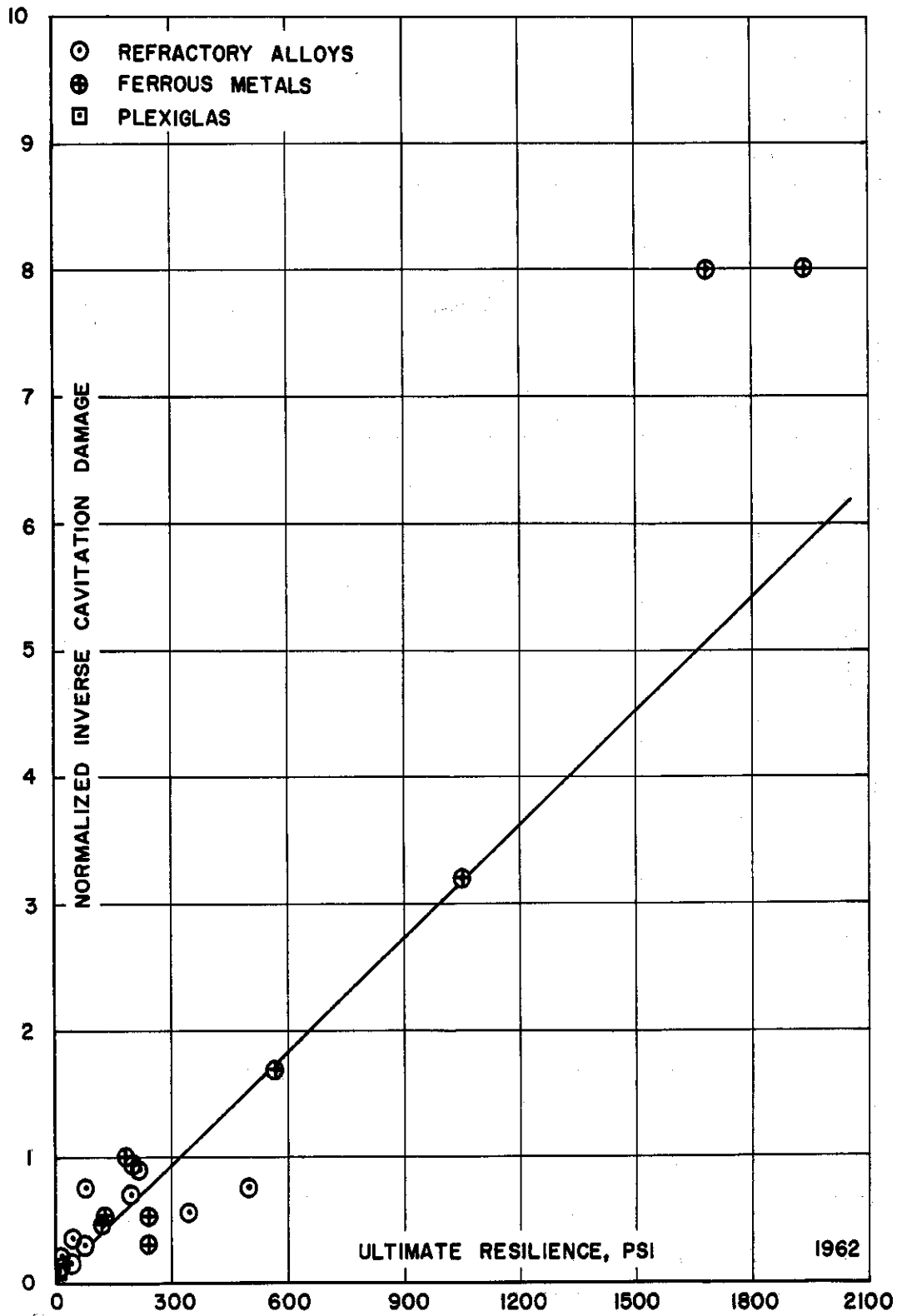Fig. 92.--Normalized inverse cavitation damage versus hardness - lead-bismuth alloy.

Fig. 93.--Normalized inverse cavitation damage versus ultimate resilience - lead-bismuth alloy.
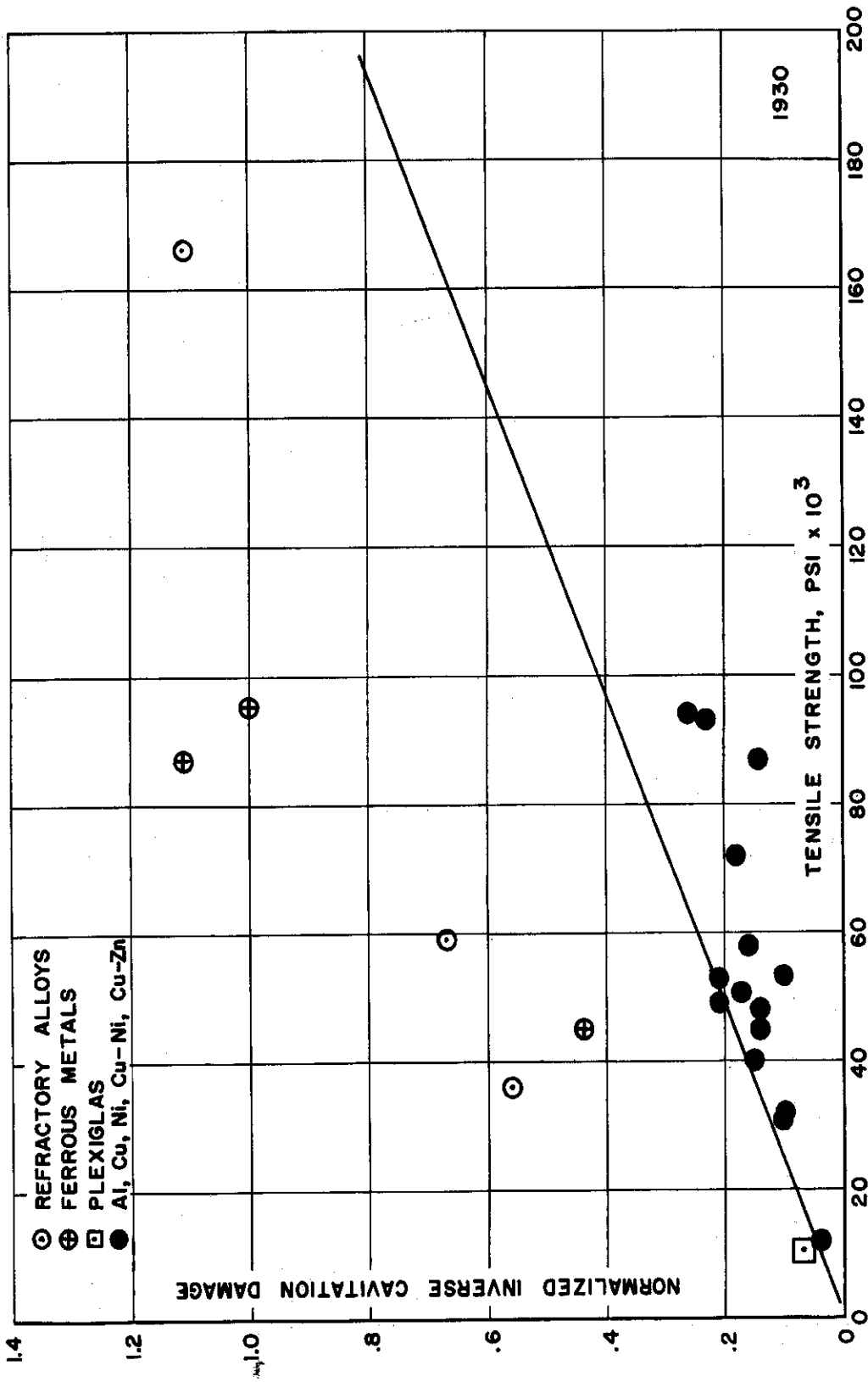
Fig. 94.--Normalized inverse cavitation damage versus tensile strength - mercury.

Fig. 95.--Normalized inverse cavitation damage versus yield strength - mercury.

Fig. 96.--Normalized inverse cavitation damage versus engineering strain energy - mercury.

Fig. 97.--Normalized inverse cavitation damage versus true strain energy - mercury.

Fig. 98.--Normalized inverse cavitation damage versus hardness - mercury.

Fig. 99.--Normalized inverse cavitation damage versus ultimate resilience - mercury.

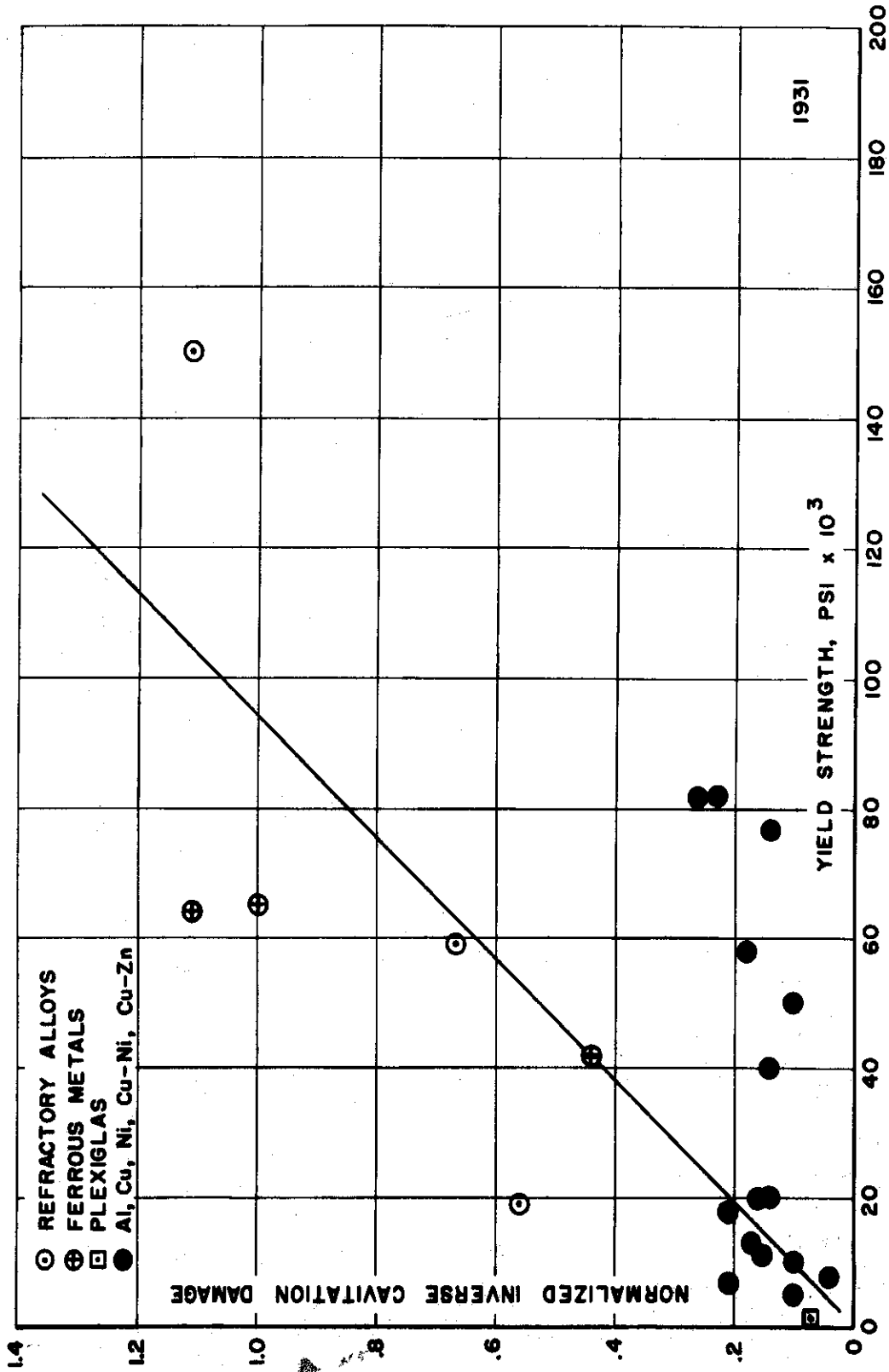Fig. 100.--Normalized inverse cavitation damage versus tensile strength - water.

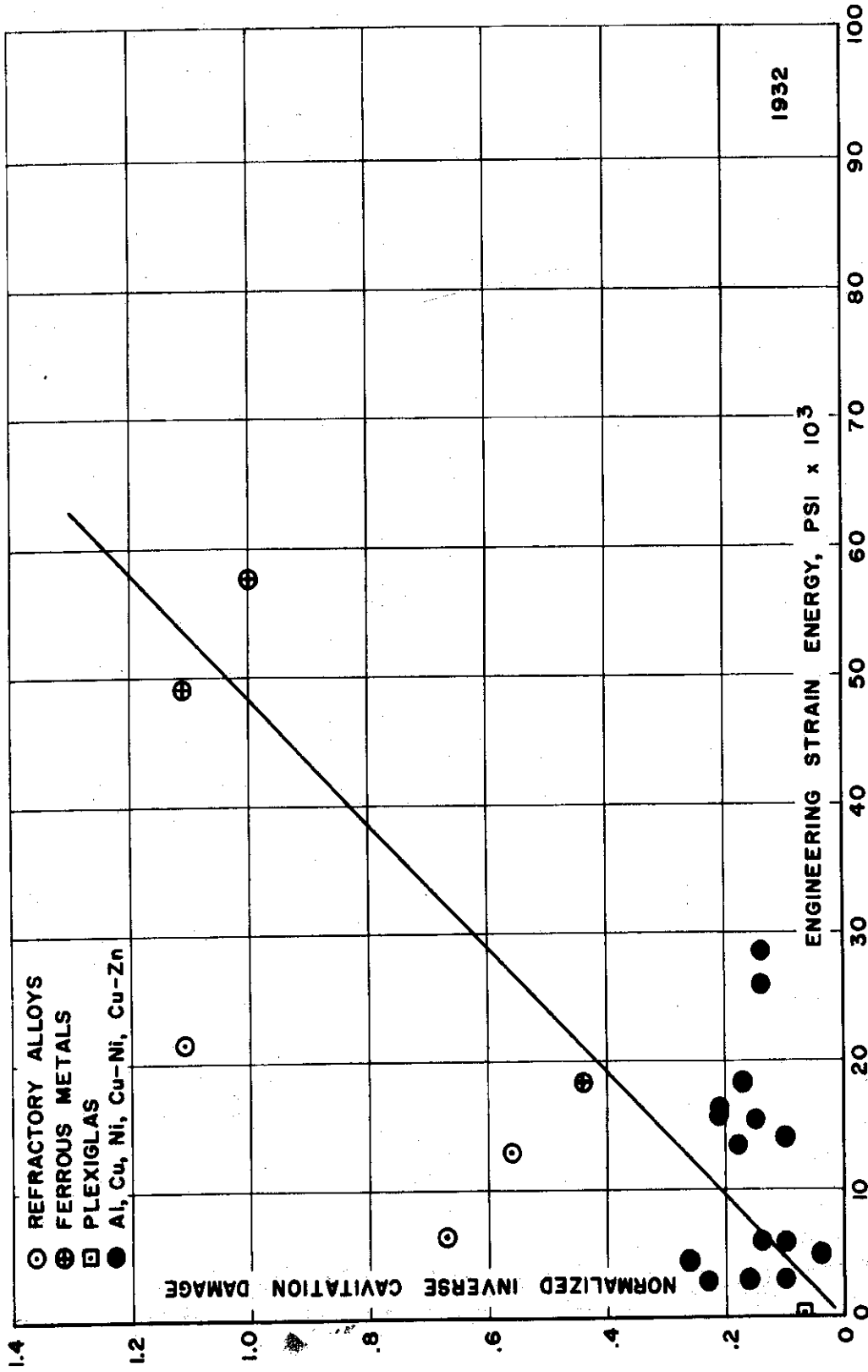Fig. 101.--Normalized inverse cavitation damage versus yield
strength - water.

Fig. 102.--Normalized inverse cavitation damage versus engineer-
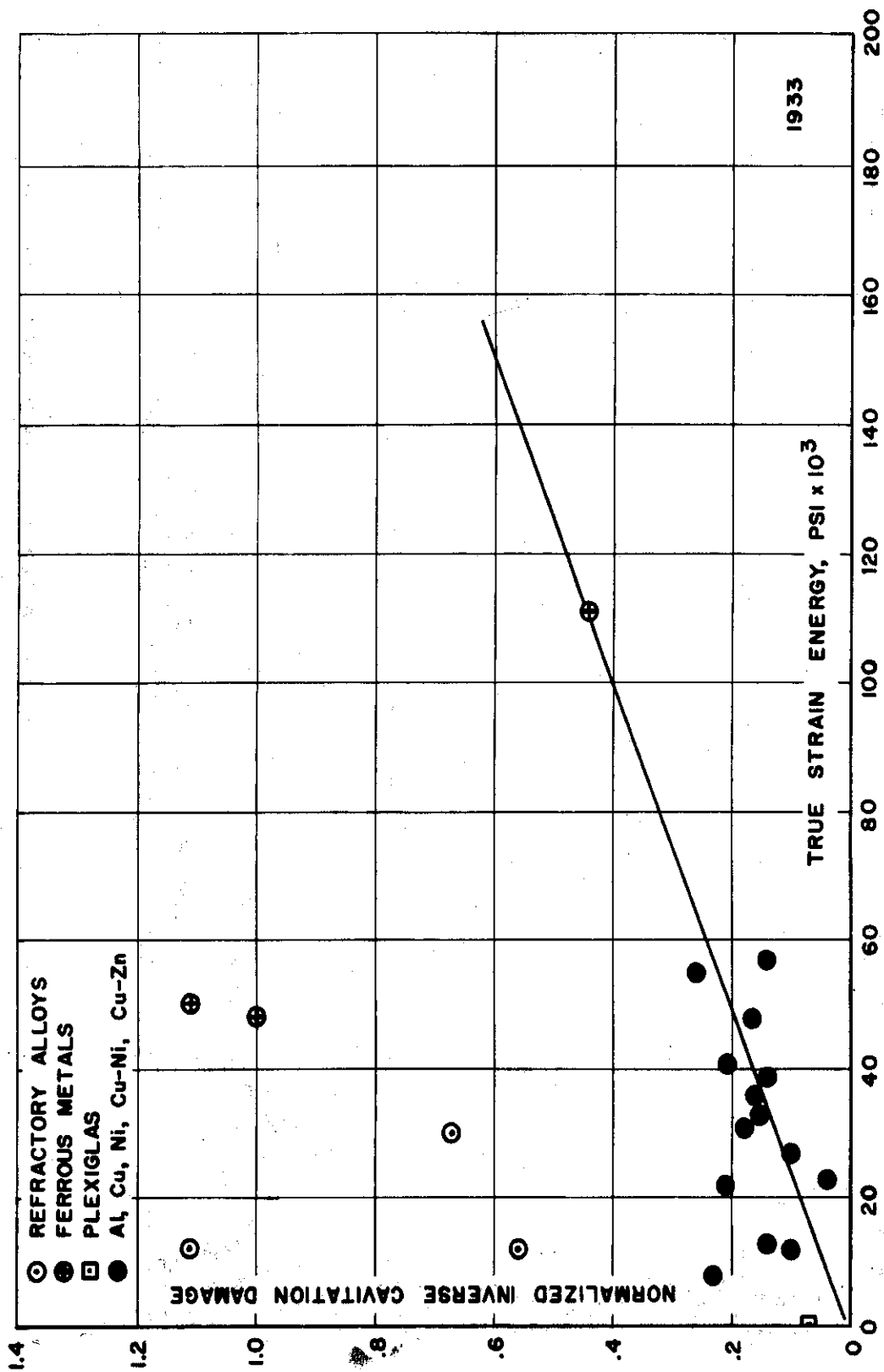ing strain energy - water.

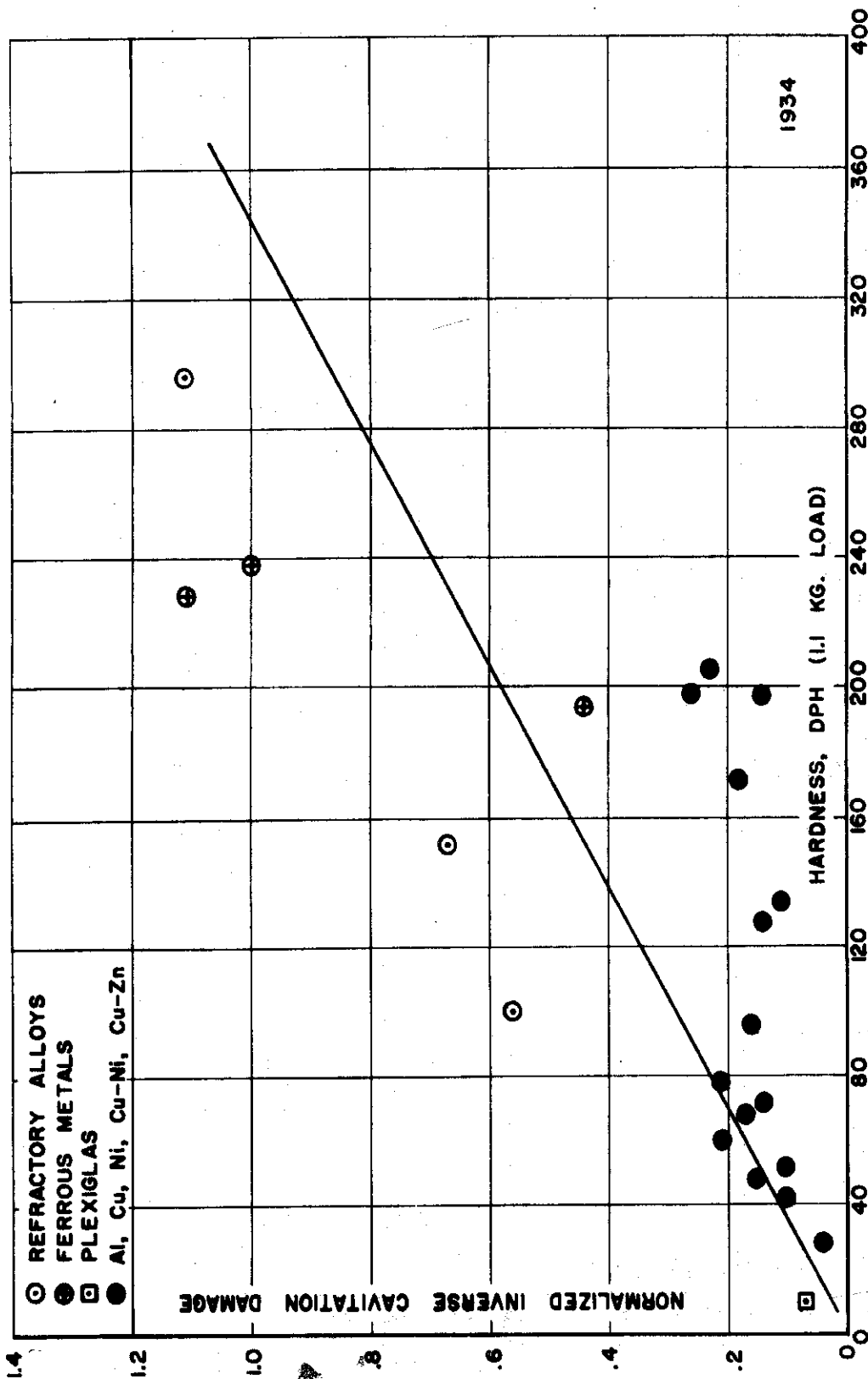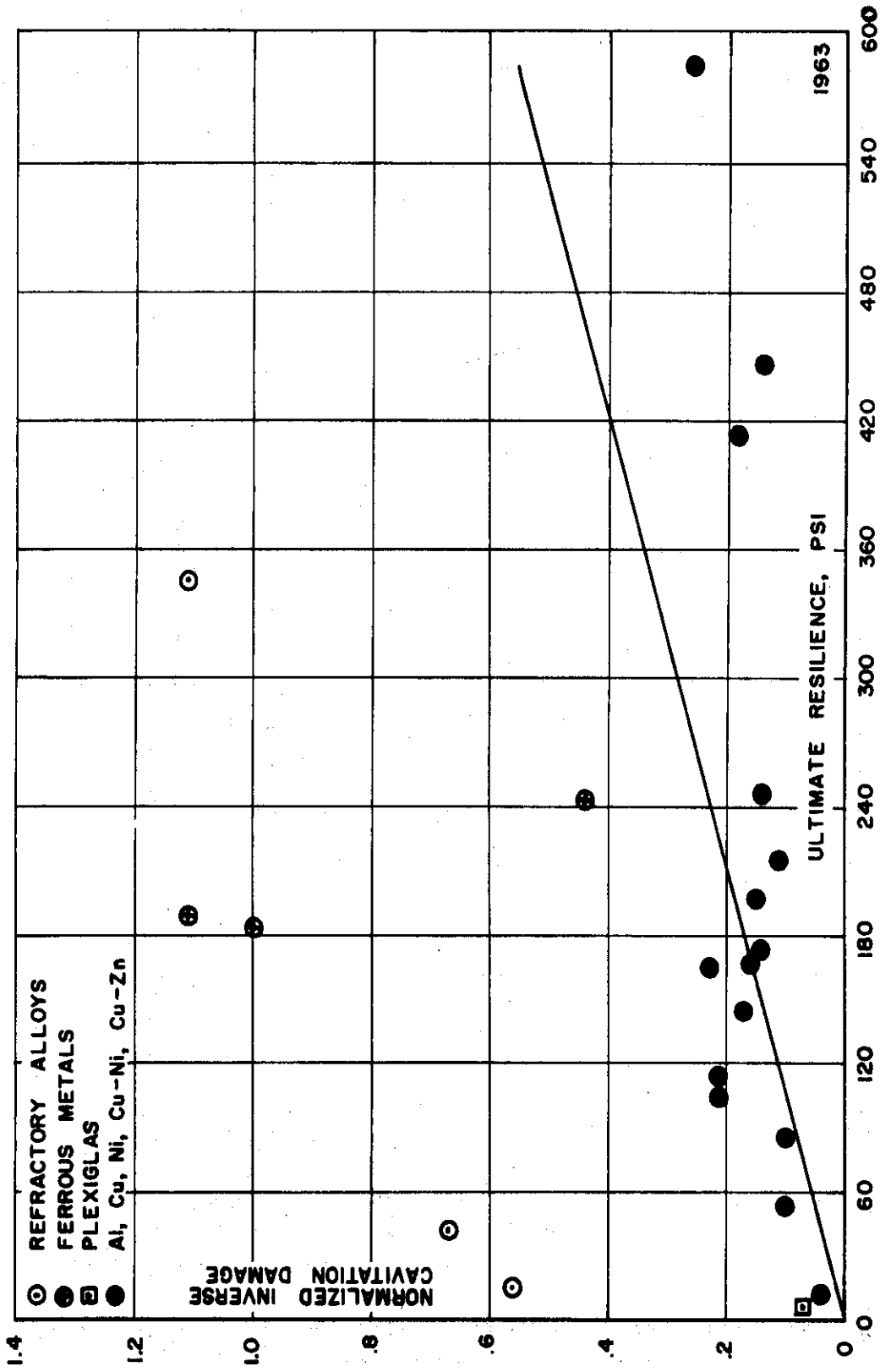Fig. 103.--Normalized inverse cavitation damage versus true
strain energy - water.

Fig. 104.--Normalized inverse cavitation damage versus hardness - water.

Fig. 105.--Normalized inverse cavitation damage versus ultimate resilience - water.
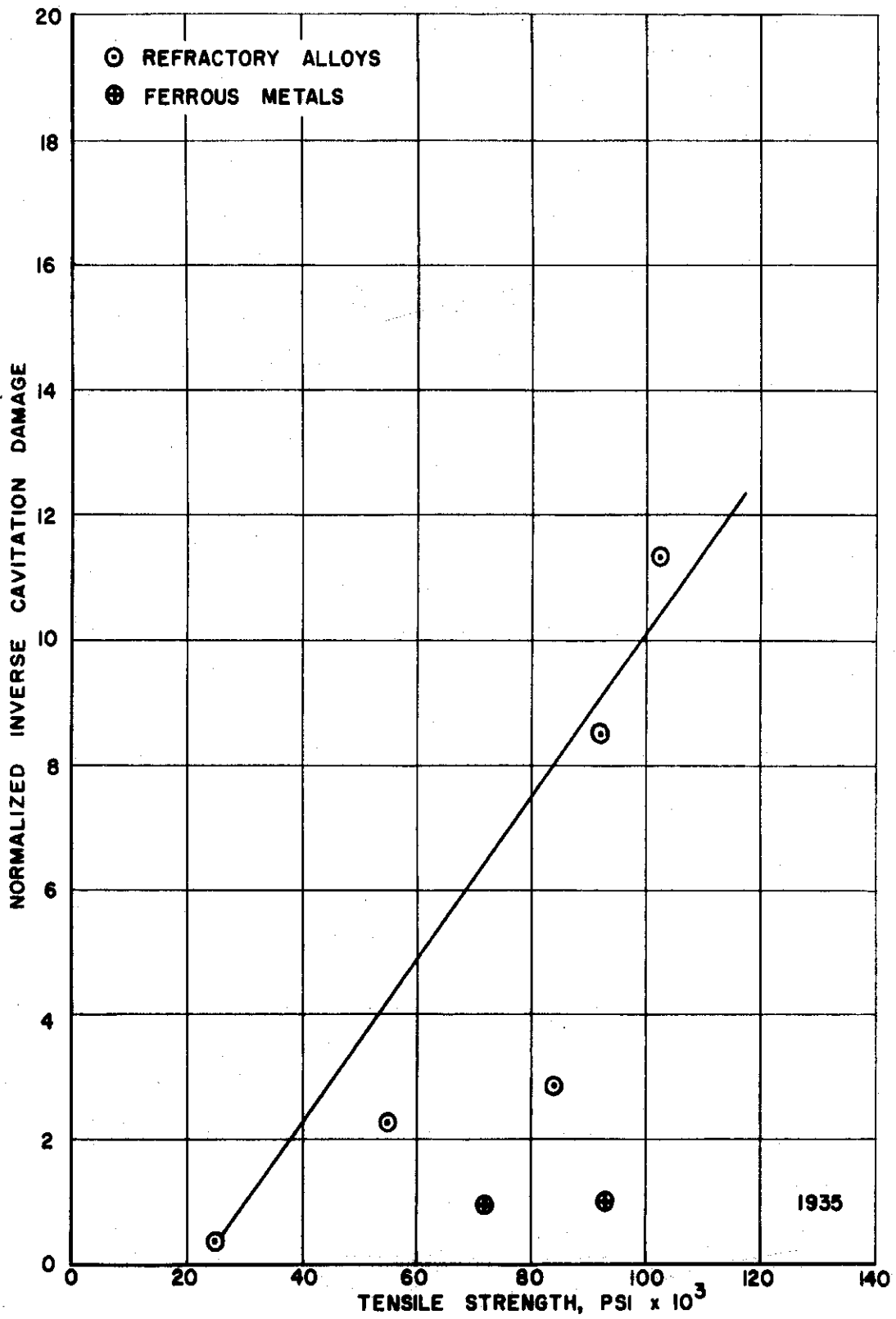
Fig. 106.--Normalized inverse cavitation damage versus tensile strength - lithium at 500°F.

Fig. 107.--Normalized inverse cavitation damage versus yield
strength - lithium at 500°F.

Fig. 108.--Normalized inverse cavitation damage versus engineering strain energy - lithium at 500°F.

Fig. 109.--Normalized inverse cavitation damage versus true strain energy - lithium at 500°F.

Fig. 110.--Normalized inverse cavitation damage versus
hardness - lithium at 500°F.

Fig. 111.--Normalized inverse cavitation damage versus ultimate
resilience - lithium at 500°F.

Fig. 112.--Normalized inverse cavitation damage versus tensile strength - lithium at 1500°F.
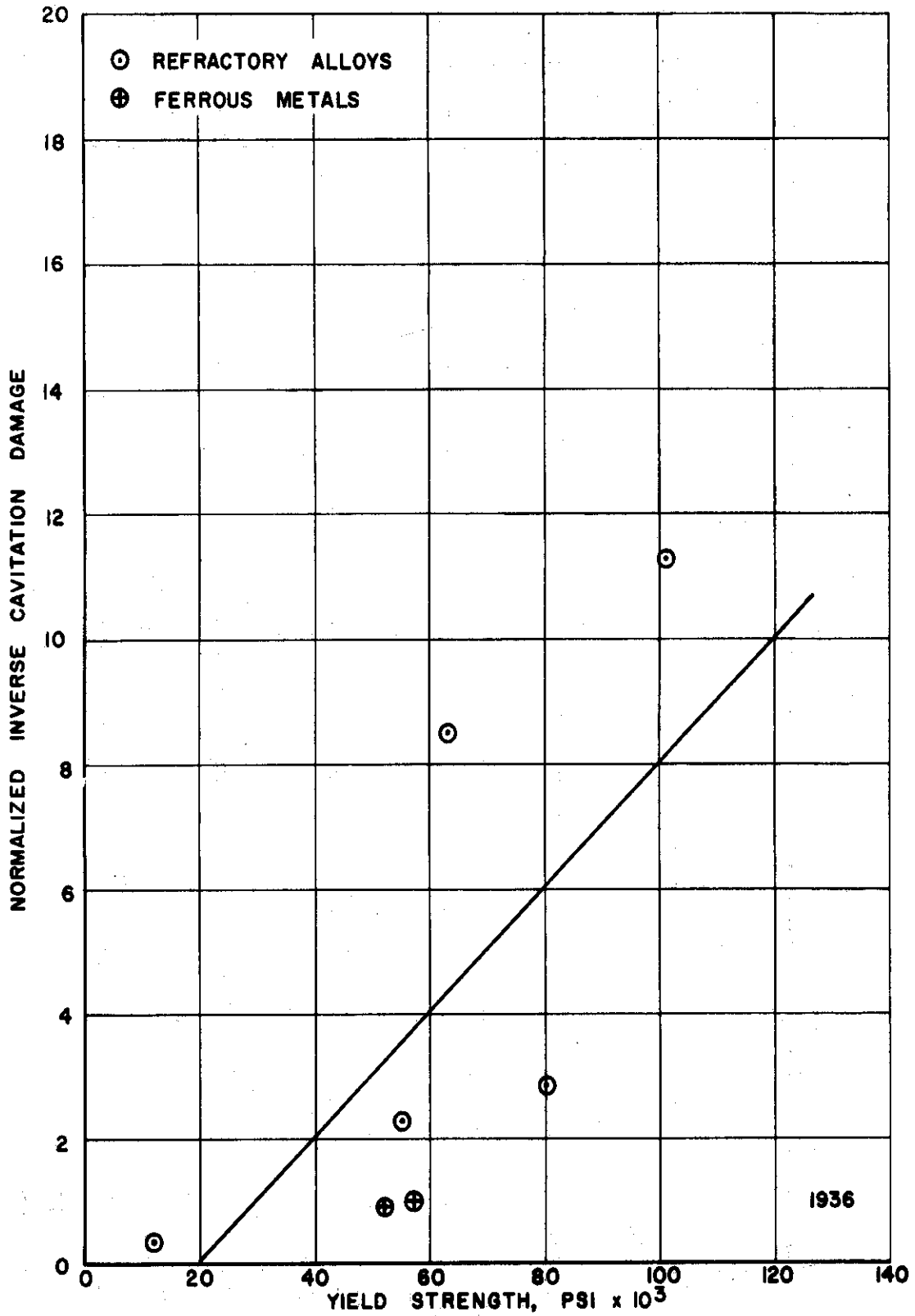
Fig. 113.--Normalized inverse cavitation damage versus yield strength - lithium at 1500°F.
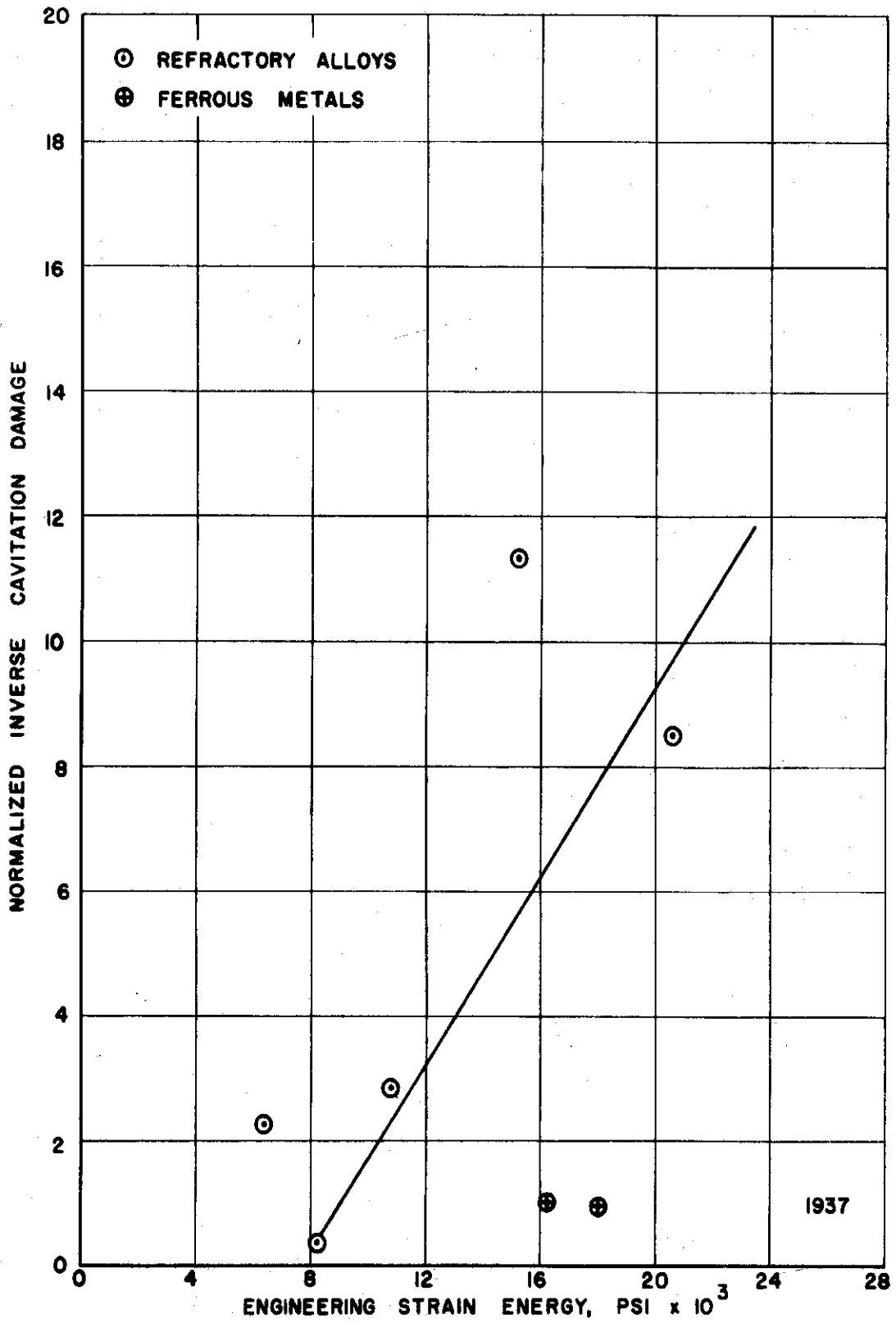
Fig. 114.--Normalized inverse cavitation damage versus engineer-
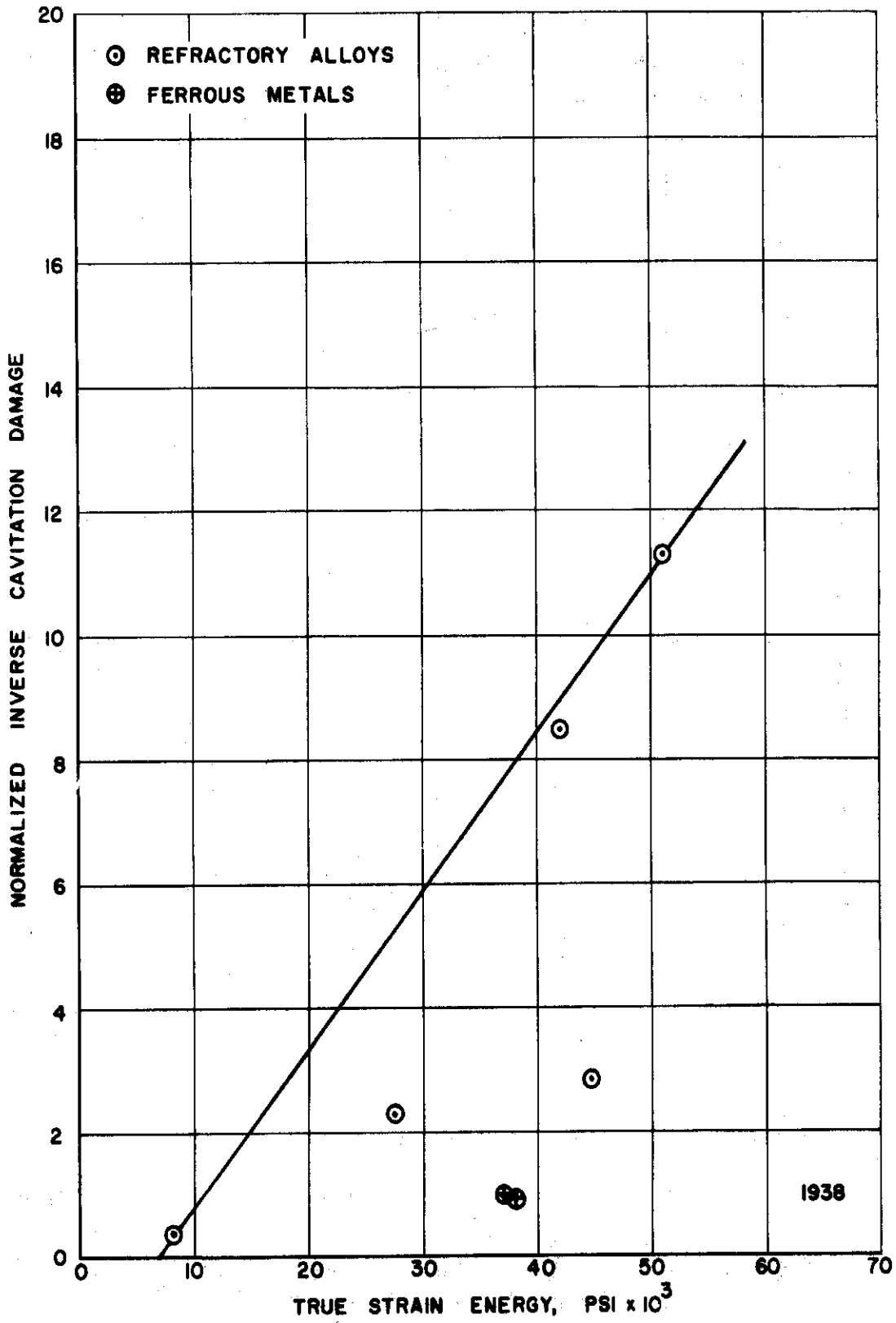ing strain energy - lithium at 1500°F.

Fig. 115.--Normalized inverse cavitation damage versus true
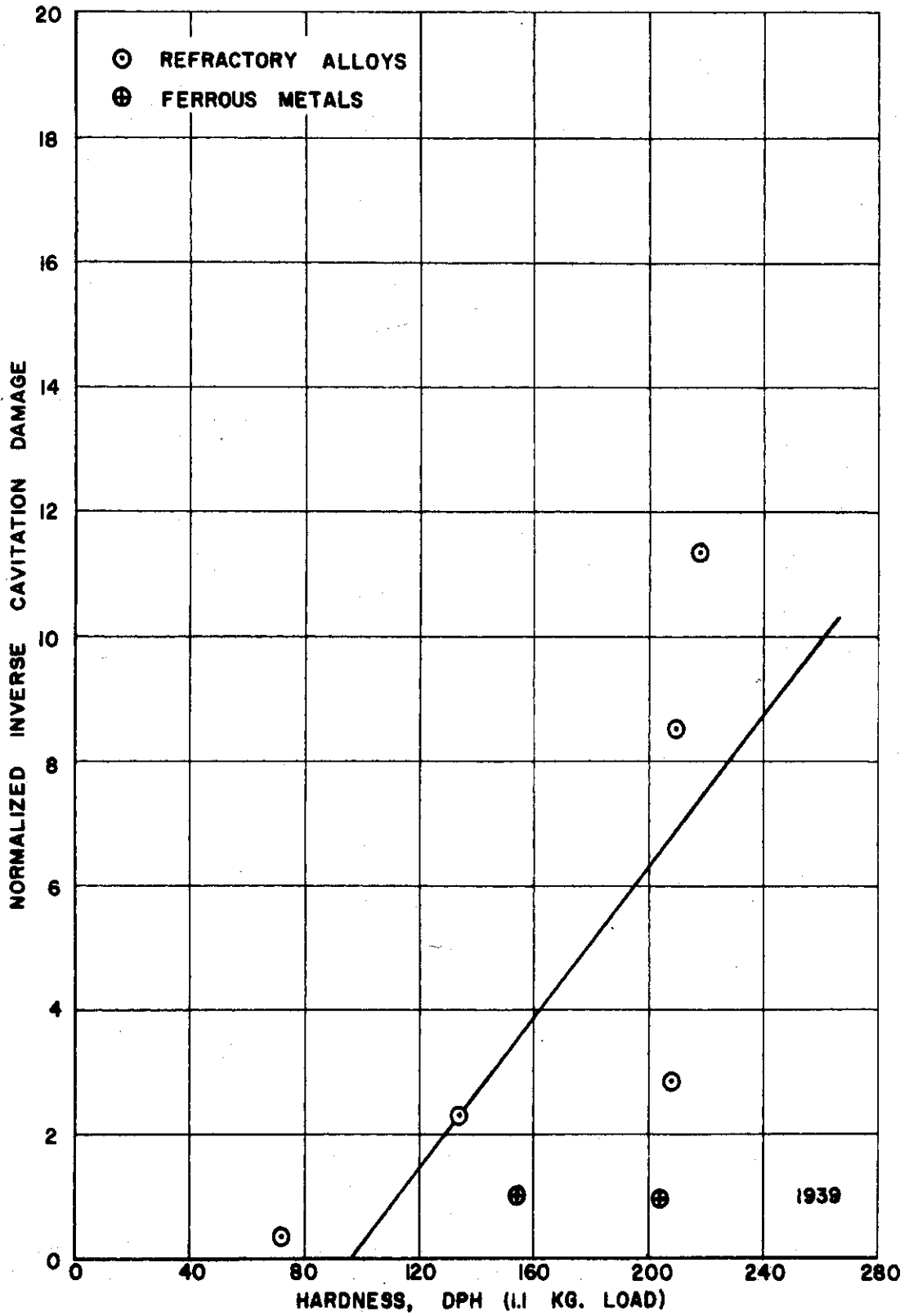strain energy - lithium at 1500°F.

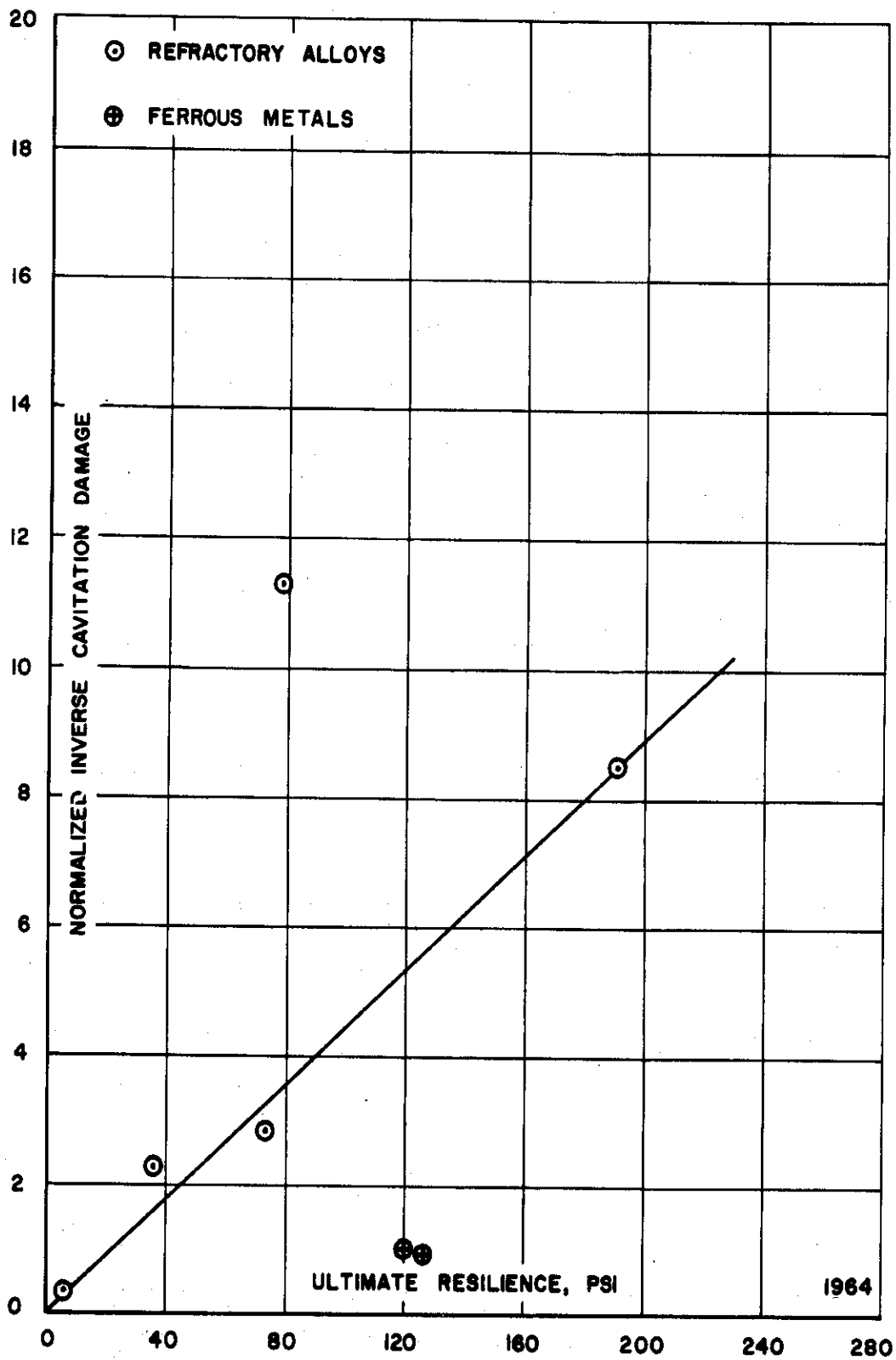Fig. 116.--Normalized inverse cavitation damage versus hardness - lithium at 1500°F.

Fig. 117.--Normalized inverse cavitation damage versus ultimate resilience - lithium at 1500°F.
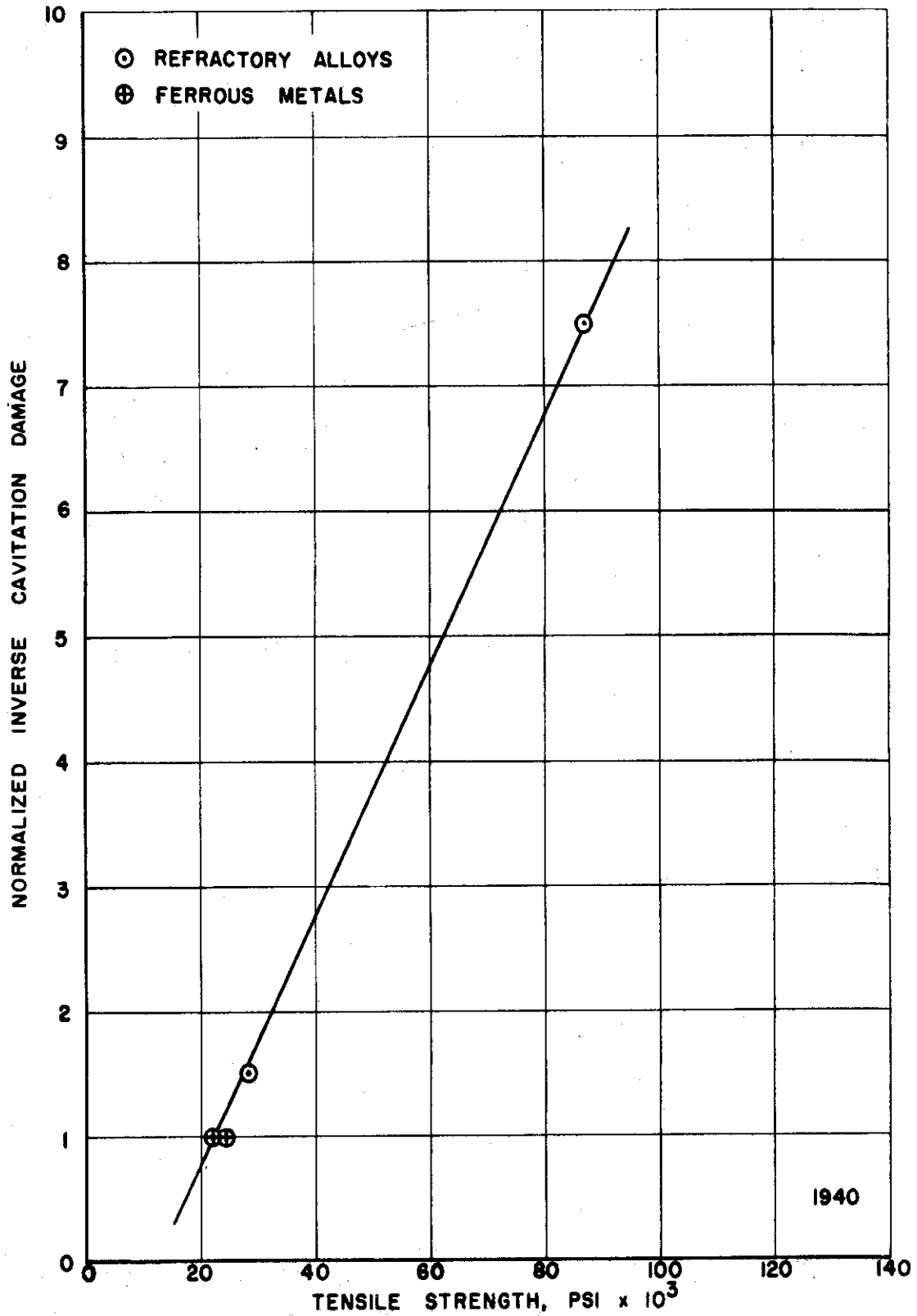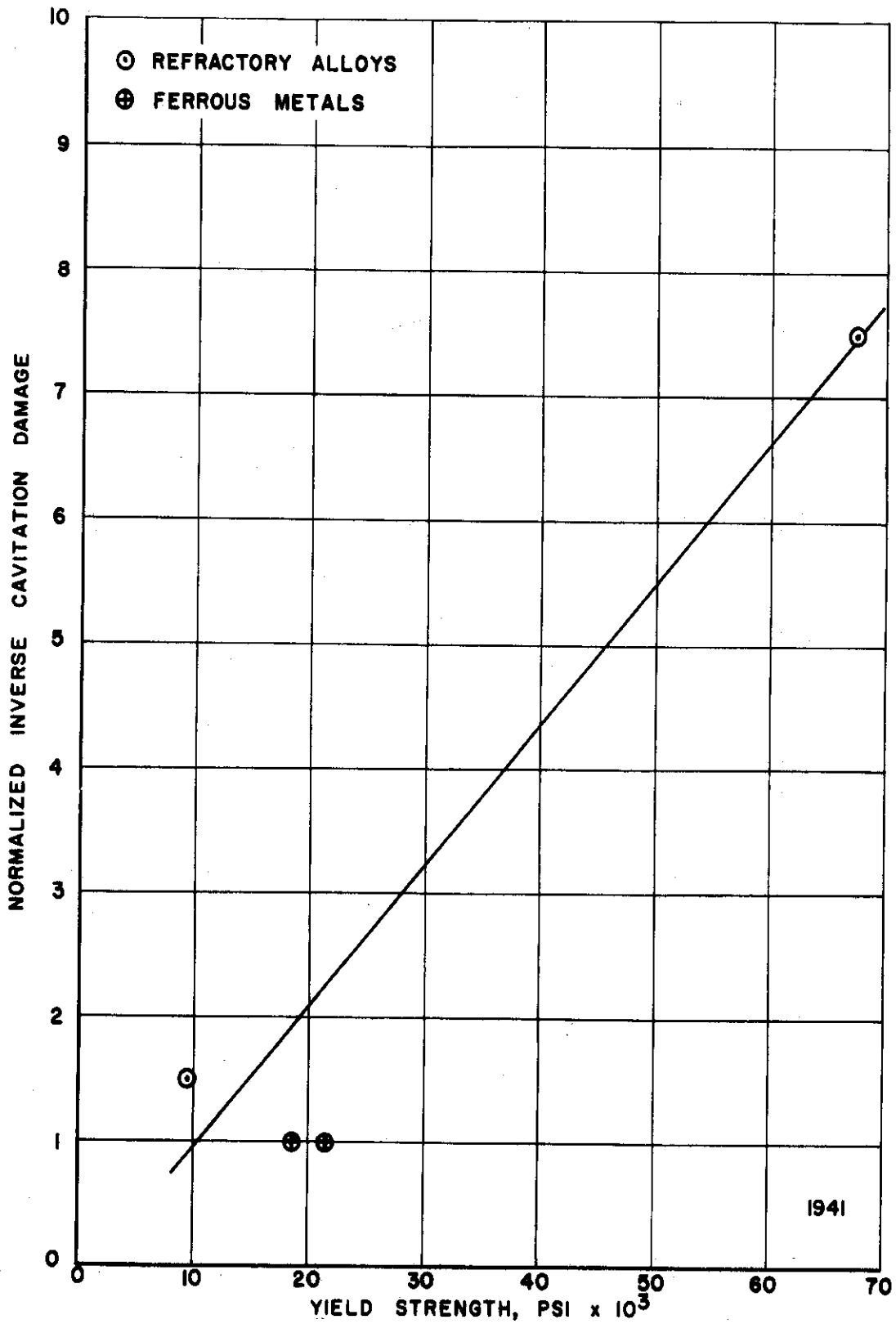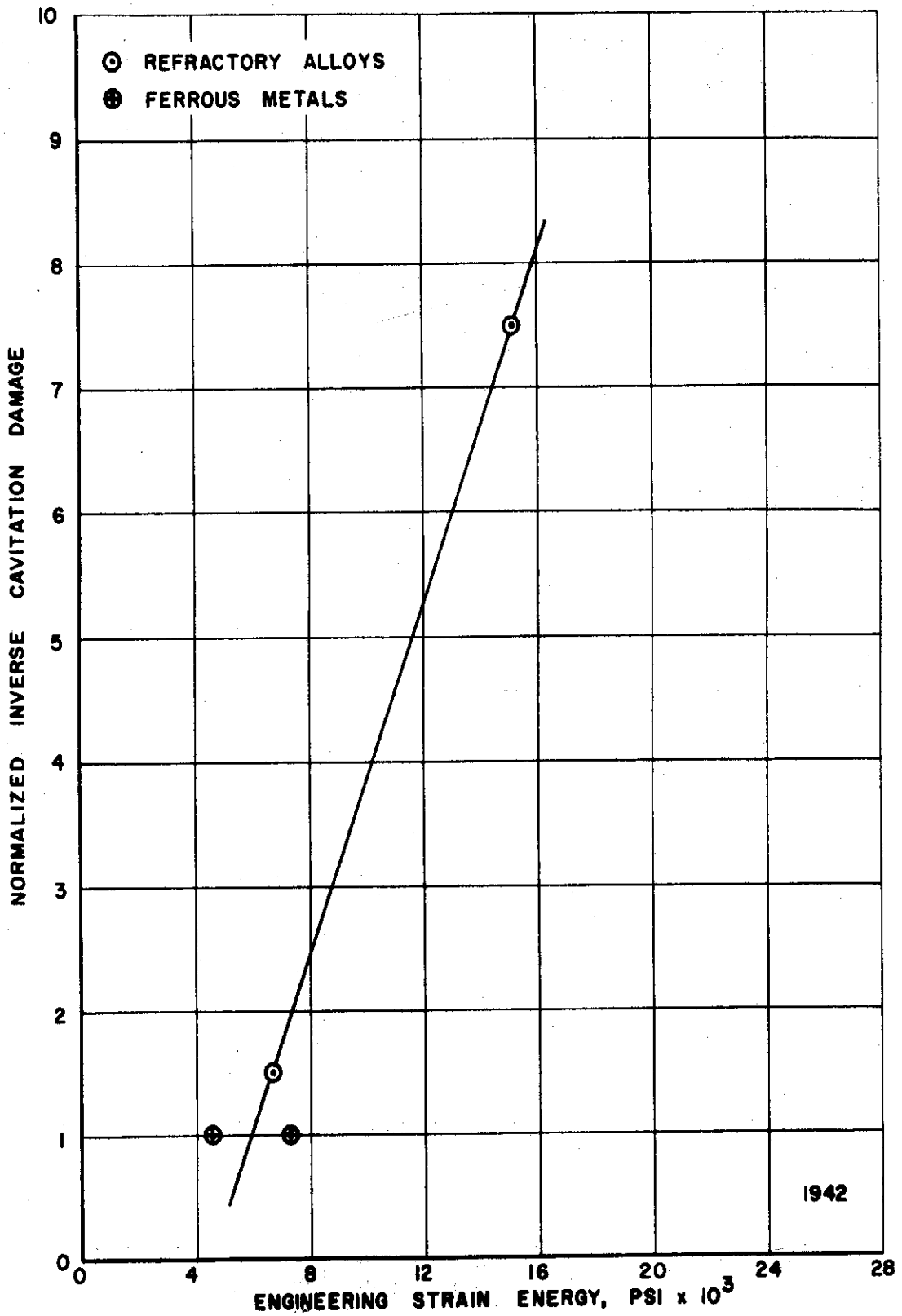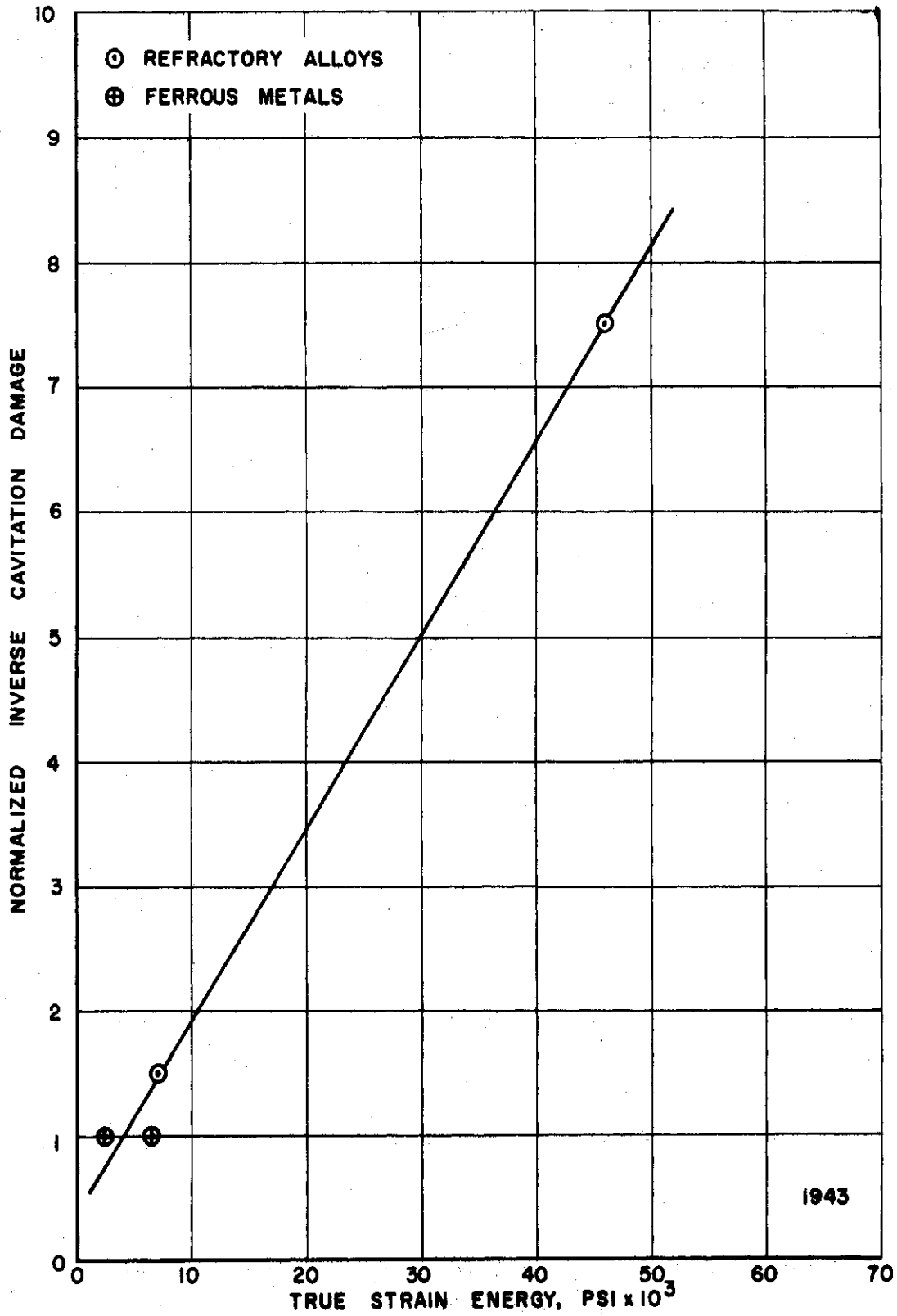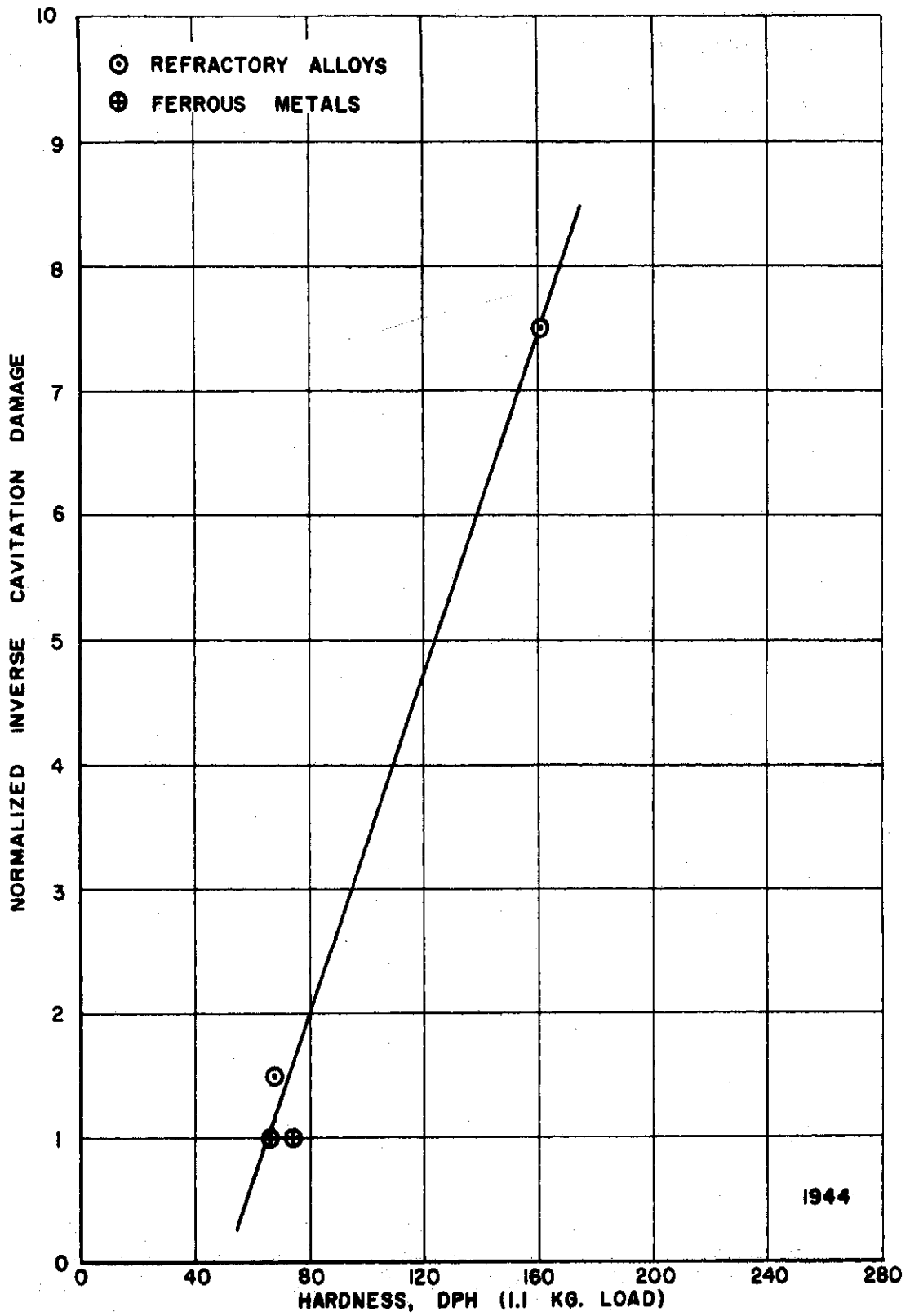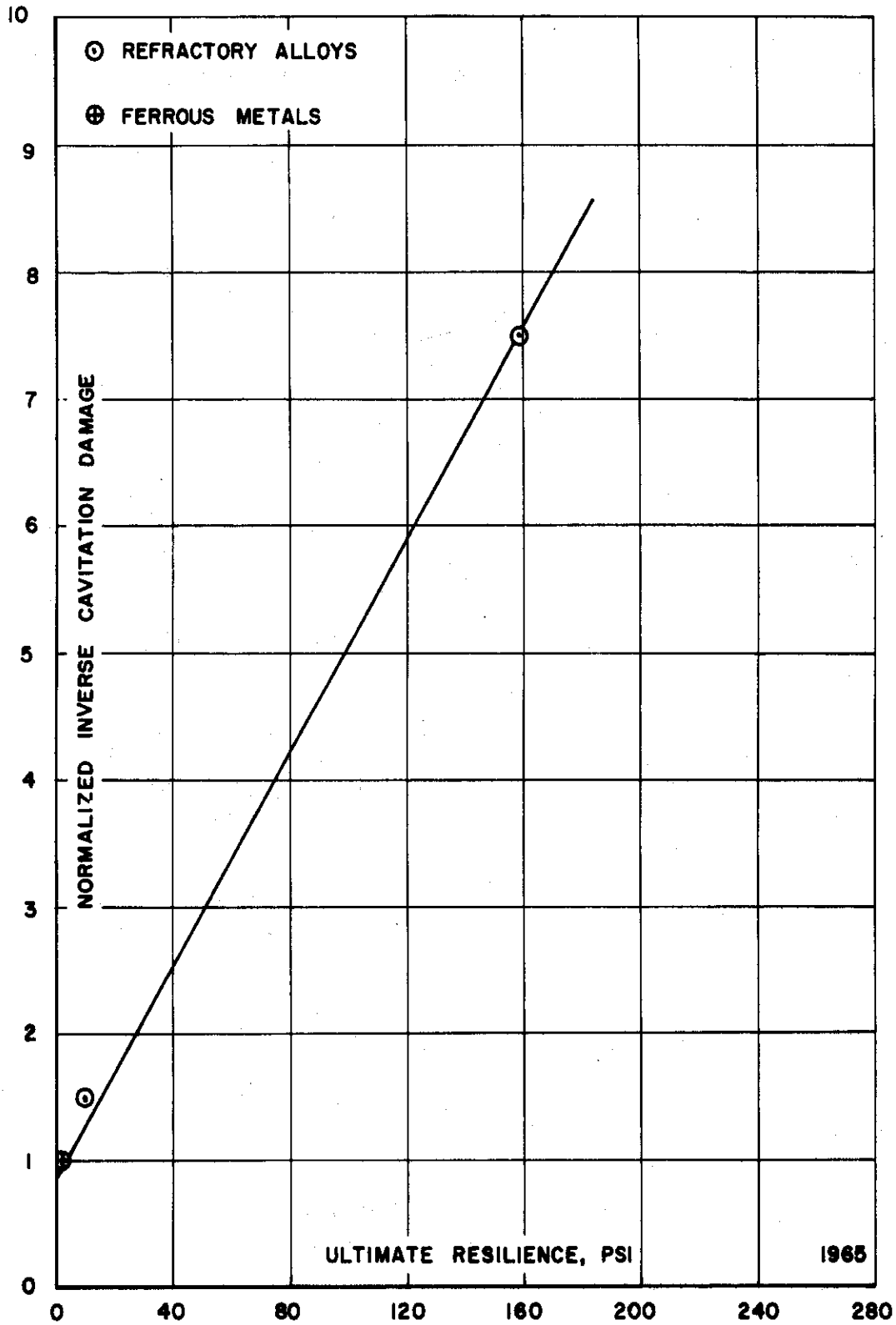
REFERENCES

1. _Royal Society Discussion on Deformation of Solids Due to Liquid Impact_, May 27, 1965; London, England.

2. Decker, O., "Cavitation Erosion Experience in Liquid Mercury Lubricated Journal Bearings," _First Annual Mercury Symposium_, November, 1965, Atomics International, Canoga Park, California, p. 14.

3. Shoudy, A. A. and Allis, R. J., "Materials Selection for Fast Reactor Applications," _Proc. of Michigan ANS Fast Reactor Topical Meeting_, April, 1965, Detroit, Michigan.

4. Wood, G. M., Kulp, R. S. and Altieri, J. V., "Cavitation Damage Investigations in Mixed-Flow Liquid Metal Pumps," _Cavitation in Fluid Machinery_, ASME, November, 1965, pp. 196-214.

5. Smith, P. G., DeVan, J. H. and Grindell, A. G., "Cavitation Damage to Centrifugal Pump Impellers During Operation with Liquid Metals and Molten Salt at 1050-1400°F," _Journal of Basic Engineering_, _Trans. ASME_, September, 1963, pp. 329-337.

6. Hunt, J. B., "Cavitation in Thin Films of Lubricant," _The Engineer_, January 29, 1965, pp. 22-23.

7. Euler, Leonhard, "Theorie plus complete des machines qui sont mises mouvement par la reaction de l'eau" (More Complete Theory of Machines Driven by Hydraulic Reaction), _Historie de l'Academie Royale des Sciences et Belles Lettres, Classe de Philosophie Experimentale_, Germany, 1754.

8. Reynolds, O., "Experiments Showing the Boiling of Water in an Open Tube at Ordinary Temperatures," British Assoc. Adv. Sci. Report, 1894.

9. Besant, W., _A Treatise on Hydrodynamics_, Cambridge University Press, Cambridge, England, 1859.

10. Rayleigh, Lord, "On the Pressure Developed in a Liquid During the Collapse of a Spherical Cavity," _Phil. Mag._, Vol. 34, 1917, pp. 94-98.

11. Thornycroft, J., and Barnaby, S. W., "Torpedo Boat Destroyers," _Proc. Inst. Civil Engineers_, Vol. 122, 1895, p. 51.

12. Barnaby, S. W., "On the Formation of Cavities in Water by Screw Propellers at High Speeds," Trans. Inst. Nav. Arch., Vol. 39, 1898, pp. 139-144.

13. Parsons, C. A. and Cook, S. S., "Investigations into the Causes of Corrosion or Erosion of Propellers," Engineering, Vol. 107, 1919, pp. 515-519.

14. Parsons, Sir Charles, "The Application of the Compound Steam Turbine to the Purpose of Marine Propulsion," Trans. Inst. Nav. Arch., Vol. 38, 1897, pp. 232-242.

15. Wagenbach, W., "Beitrage zur Berechnung und Konstrucktion der Wasserturbinen" (Contribution to the Calculation and Construction of Hydraulic Turbines), Zeitschrift fur das Gesamte Turbinenwesen, Vol. 4, 1907, pp. 273-277.

16. Fottinger, H., "Studies of Cavitation and Erosion in Turbines, Turbopumps, and Propellers" (in German), Hydraulische Probleme, 1926, pp. 107-110.

17. Schroter, Hellmut, "Korrosion durch Kavitation in einen Diffusor" (Erosion by Cavitation in a Diffusor), Zeitschrift Verein Deutscher Ingenieure, Vol. 76, 1932, pp. 511-512.

18. Mousson, J. M., "Pitting Resistance of Metals Under Cavitation Conditions," Trans. ASME, Vol. 59, 1937, pp. 399-408.

19. Lichtman, J. Z., Kallas, D. H., Chatten, C. K. and Cochran, E. P., Jr., "Study of Corrosion and Cavitation-Erosion Damage," Trans. ASME, Vol. 80, No. 6, August, 1958, pp. 1325-1339.

20. Hammitt, F. G., "Observations on Cavitation Damage in a Flowing System," Journal of Basic Engineering, Trans. ASME, Series D, Vol. 85, 1963, pp. 347-359.

21. Hammitt, F. G., Barinka, L. L., Robinson, M. J., Pehlke, R. D. and Siebert, C. A., "Initial Phases of Damage to Test Specimens in a Cavitating Venturi as Affected by Fluid and Material Properties and Degree of Cavitation," Journal of Basic Engineering, Trans. ASME, June, 1965, pp. 453-464.

22. Robinson, M. John, "On the Detailed Flow Structure and the Corresponding Damage to Test Specimens in a Cavitating Venturi," Ph.D. Thesis and ORA Technical Report No. 03424-16-T, Department of Nuclear Engineering, The University of Michigan, August, 1965.

23. Robertson, J. M., "Water Tunnels for Hydraulic Investigations," Trans. ASME, Vol. 78, No. 1, January, 1956, pp. 95-104.

24. Wright, E. A., "Some International Aspects of Ship Model Research," David Taylor Model Basin Report 1220, April, 1958.

25. Knapp, R. T., "Recent Investigations of the Mechanics of Cavitation and Cavitation Damage," Trans. ASME, Vol. 77, No. 7, October, 1955, pp. 1045-1054.

26. Rasmussen, R. E. H., "Some Experiments on Cavitation Erosion in Water Mixed with Air," Cavitation in Hydrodynamics, Proc. National Phys. Lab. Symposium, Paper No. 20, H. M. Stationery Office, London, England, 1956.

27. Wood, G. M., Knudsen, L. K. and Hammitt, F. G., "Cavitation Damage Studies with Rotating Disk in Water," ASME Paper No. 66-FE-11, April, 1966.

28. Kelly, R. W., Wood, G. M., Marman, H. V. and Milich, J. J., "Rotating Disk Approach for Cavitation Damage Studies in High Temperature Liquid Metal," ASME Paper No. 63-AHGT-26, March, 1963.

29. Gaines, N., "A Magnetostriction Oscillator Producing Intense Audible Sound and Some Effects Obtained," Physics, Vol. 3, No. 5, 1932, pp. 209-229.

30. Kerr, S. Logan, "Determination of the Relative Resistance to Cavitation Erosion by the Vibratory Method," Trans. ASME, Vol. 59, July, 1937, pp. 373-397.

31. Schumb, W. C., Peters, H. and Milligan, L. H., "New Method for Studying Cavitation Erosion of Metals," Metals and Alloys, Vol. 8, May, 1937, pp. 126-132.

32. Nowotny, H., "Destruction of Materials by Cavitation," VDI-Verlag, Berlin, Germany, 1942. Reprinted by Edwards Brothers, Inc., Ann Arbor, Michigan, 1946. English Translation available as ORA Internal Report No. 03424-15-I, Department of Nuclear Engineering, The University of Michigan, 1962.

33. Leith, W. C. and Thompson, A. Lloyd, "Some Corrosion Effects in Accelerated Cavitation Damage," ASME Paper No. 59-A-52, November, 1959.

34. Rheingans, W. J., "Accelerated Cavitation Research," Trans. ASME, Vol. 72, No. 5, July, 1950, pp. 705-719.

35. Plesset, M. S., "On Cathodic Protection in Cavitation Damage," Journal of Basic Engineering, Trans. ASME, Series D, Vol. 82, No. 4, 1960, pp. 808-820.

36. Thiruvengadam, A. and Preiser, H. S., "On Testing Materials for Cavitation Damage Resistance," Hydronautics, Inc., Technical Report No. 233-3, December, 1963.

37. Thiruvengadam, A., Preiser, H. S. and Rudy, S. L., "Cavitation Damage in Liquid Metals," Technical Progress Report 467-2 (NASA CR-54391) For the Period January 1, 1965, to March 31, 1965, Hydronautics, Inc., April 28, 1965.

38. Thiruvengadam, A., Preiser, H. S. and Rudy, S. L., "Cavitation Damage in Liquid Metals," Technical Progress Report 467-3 (NASA CR-54459) For the Period April 1, 1965, to May 31, 1965, Hydronautics, Inc., June 30, 1965.

39. Young, S. G. and Johnston, J. R., "Accelerated Cavitation Damage of Steels and Super-Alloys in Sodium and Mercury," presented at ASTM Annual Meeting, Symposium on Erosion by Cavitation or Impingement, Atlantic City, New Jersey, June, 1966; to be published by ASTM.

40. Garcia, R. and Hammitt, F. G., "Ultrasonic-Induced Cavitation in Liquid Metals at 1500°F," Internal Report No. 05031-1-I, Department of Nuclear Engineering, The University of Michigan, February, 1965; also Transactions of the American Nuclear Society, Vol. 8, No. 1, June, 1965, pp. 18-19.

41. Garcia, R. and Hammitt, F. G., "Ultrasonic-Induced Cavitation Studies in Lead-Bismuth Alloy, 500-1500°F," Corrosion, Vol. 22, No. 6, June, 1966, pp. 157-167.

42. Garcia, R., Nystrom, R. E. and Hammitt, F. G., "Ultrasonic-Induced Cavitation Studies in Mercury and Water," ORA Technical Report No. 05031-3-T, Department of Nuclear Engineering, The University of Michigan, December, 1965. See also "Comprehensive Cavitation Damage Data for Water, Mercury and Lead-Bismuth Alloy Including Correlations with Material and Fluid Properties," presented at ASTM Annual Meeting, Symposium on Erosion by Cavitation or Impingement, Atlantic City, New Jersey, June, 1966; to be published by ASTM.

43. Garcia, R. and Hammitt, F. G., "Ultrasonic-Induced Cavitation Studies in Lithium at Elevated Temperatures," ORA Technical Report No. 05031-5-T, Department of Nuclear Engineering, The University of Michigan, May, 1966.

44. Ellis, A. T., "Production of Accelerated Cavitation Damage by an Acoustic Field in a Cylindrical Cavity," Journal of the Acoustical Society of America, Vol. 27, No. 5, September, 1955, pp. 913-921.

45. de Haller, P., "Untersuchungen uber die durch Kavitation Hervorgerufenen Korrosionen," Schweiz. Bauztg., Vol. 101, 1933, pp. 243-246, 260-264.

46. Hobbs, J. M., "Problems of Predicting Cavitation Erosion from Accelerated Tests," ASME Paper No. 61-HYD-19, 1961.

47. Petracchi, G., "Investigations of Cavitation Corrosion," La Metallurgia Italiana, Vol. 41, No. 1, 1949, pp. 1-6. See also Engineering Digest, Vol. 10, No. 9, September, 1949, p. 314.

48. Plesset, M. S., "The Pulsation Method for Generating Cavitation Damage," Journal of Basic Engineering, Trans. ASME, Vol. 85, Series D, No. 3, 1963, pp. 360-364. See also "Pulsing Technique for Studying Cavitation Erosion of Metals," Corrosion, Vol. 18, No. 5, May, 1962, pp. 181-188.

49. Wheeler, W. H., "Indentation of Metals by Cavitation," Journal of Basic Engineering, Trans. ASME, March, 1960, pp. 184-194.

50. Hammitt, F. G., "Cavitation Damage and Performance Research Facilities," Symposium on Cavitation Research Facilities and Techniques, pp. 175-184, ASME Fluids Engineering Division, May, 1964. See also ORA Technical Report No. 03424-12-T, Department of Nuclear Engineering, The University of Michigan, November, 1963.

51. Garcia, R. and Hammitt, F. G., "Ultrasonic-Induced Cavitation Studies," ORA Technical Report No. 05031-1-T, Department of Nuclear Engineering, The University of Michigan, October, 1964.

52. Blitz, J., Fundamentals of Ultrasonics, Butterworth & Co., Ltd., London, England, 1963.

53. Frederick, J. R., Ultrasonic Engineering, John Wiley & Sons, Inc., New York, 1965.

54. Mason, W. P., "Internal Friction and Fatigue in Metals at Large Strain Amplitudes," Journal of the Acoustical Society of America, Vol. 28, No. 6, November, 1956, pp. 1207-1218.

55. Aydinmakine, F. A., "High-Temperature Vibratory Cavitation Damage Research Facility of the University of Michigan," Term Paper Submitted for the Course Mechanical Engineering 600, May 15, 1964, University of Michigan, Ann Arbor, Michigan.

56. Kerr, S. Logan and Leith, W. C., "A Review of Cavitation Damage by the Vibratory Method at the Dominion Engineering Works, Limited," Dominion Engineering Works, Limited, Technical Report, 1955.

57. Garcia, R. and Hammitt, F. G., "Amplitude Determination of an Ultrasonic Transducer by Means of an Accelerometer Assembly," Internal Report No. 05031-7-I, Department of Nuclear Engineering, The University of Michigan, December, 1965.

58. Hammitt, F. G., "Damage to Solids Caused by Cavitation," to be published Proc. Royal Society; presented at Royal Society Discussion on Deformation of Solids Due to Liquid Impact, May 27, 1965, London, England.

59. Plesset, M. S. and Devine, R. E., "Effect of Exposure Time on Cavitation Damage," ASME Paper No. 65-WA/FE-23; to be published Journal of Basic Engineering, Trans. ASME.

60. Olson, H. G., "High Speed Photographic Studies of Ultrasonically-Induced Cavitation and Detailed Examination of Damage to Selected Materials," Ph.D. Thesis and ORA Technical Report No. 07738-2-T, Department of Nuclear Engineering, The University of Michigan, August, 1966.

61. Jackson, F. J. and Nyborg, W. L., "Sonically-Induced Microstreaming Near a Plane Boundary. I. The Sonic Generator and Associated Acoustic Field," The Journal of the Acoustical Society of America, Vol. 32, No. 10, October, 1960, pp. 1243-1250.

62. Jackson, F. J., "Sonically-Induced Microstreaming Near a Plane Boundary. II. Acoustic Streaming Field," The Journal of the Acoustical Society of America, Vol. 32, No. 11, November, 1960, pp. 1387-1395.

63. Crofford, W. N., Kovacina, T. A. and Miller, R. R., "Isothermal Study of Concentration and Transport of Radioactive Stainless Steel Components in Liquid Lithium," NRL Report 5572, U.S. Dept. of Commerce, Dec. 29, 1960.

64. Garcia, R. and Hammitt, F. G., "Ultrasonic-Induced Cavitation Studies in Lead-Bismuth Alloy at Elevated Temperatures," ORA Technical Report No. 05031-2-T, Department of Nuclear Engineering, The University of Michigan, June, 1965. See also "Ultrasonic-Induced Cavitation Studies in Lead-Bismuth Alloy at Elevated Temperatures," Internal Report No. 05031-4-I, Department of Nuclear Engineering, The University of Michigan, September, 1965.

65. Leith, W. C., "Prediction of Cavitation Damage in the Alkali Liquid Metals," to be published in ASTM Proceedings, 1965.

66. Devine, R. E. and Plesset, M. S., "Temperature Effects in Cavitation Damage," Report No. 85-27, Division of Engineering and Applied Science, California Institute of Technology, Pasadena, California, April, 1964.

67. Hobbs, J. M., "Experience with a 20-Kc. Cavitation Erosion Test," Paper #120 presented at 1966 Annual ASTM Meeting, Symposium on Erosion by Cavitation or Impingement, Atlantic City, New Jersey, June, 1966.

68. Kemppainen, D. J. and Hammitt, F. G., "Effect of Temperature on Cavitation Damage," ORA Internal Report No. 05031-10-I, Department of Nuclear Engineering, The University of Michigan, July, 1966.

69. Stahl, H. A. and Stepanoff, A. J., "Thermodynamic Aspects of Cavitation in Centrifugal Pumps," Trans. ASME, Vol. 78, 1956, pp. 1691-1693.

70. Plesset, M. S. and Ellis, A. T., "On the Mechanism of Cavitation Damage," Trans. ASME, Vol. 77, No. 7, October, 1955, pp. 1055-1064.

71. Harrison, Curtis A., Robinson, M. John, Siebert, Clarence A., Hammitt, Frederick G. and Lawrence, Joe, "Complete Mechanical Properties Specifications for Materials as Used in Venturi Cavitation Damage Tests," Internal Report No. 03424-29-I, Department of Nuclear Engineering, The University of Michigan, August, 1965.

72. Shalnev, K. K., "The Energetics Parameter and Scale Effect in Cavitation Erosion," Akademiya nauk SSSR, Izvestiya Otdeleniye tekhnicheskikh nauk. Mekhanika i mashinomostroyeniye, No. 5, 1961, pp. 3-10.

73. Thiruvengadam, A., "A Unified Theory of Cavitation Damage," Journal of Basic Engineering, Trans. ASME, Vol. 85, Series D, No. 3, September, 1963, pp. 365-376.

74. Thiruvengadam, A., "Prediction of Cavitation Damage," Ph.D. Thesis, Dept. of Hydraulic Eng., Indian Institute of Science, Bangalore, India, 1961.

75. Personal Communication from Henry P. Leeper, Project Metallurgist, Pratt & Whitney Aircraft (CANEL), to F. G. Hammitt; February 26, 1965, and May 13, 1965.

76. Plesset, M. S., "Bubble Dynamics," Report No. 85-23, Division of Engineering and Applied Science, California Institute of Technology, February, 1963.

77. Hammitt, F. G. and Smith, W., "Bubble Dynamics," Department of Nuclear Engineering, The University of Michigan, October, 1962, to be published.

78. Hammitt, F. G., "Liquid-Metal Cavitation--Problems and Desired Research," ASME Paper No. 60-HYD-13, March, 1960.

79. Florschuetz, L. W. and Chao, B. T., "On the Mechanics of Vapor Bubble Collapse--A Theoretical and Experimental Investigation," Report ME-TN-1069-2, Department of Mechanical and Industrial Engineering, The University of Illinois, Urbana, Illinois, October, 1963.

80. Hoff, G., Langbein, G. and Rieger, H., "Investigations of Material-Destruction Due to Liquid Impact," Dornier-System Technical Report, translated from the German.

81. Wilson, R. W. and Graham, R., "Cavitation of Metal Surfaces in Contact with Lubricants," Conference on Lubrication and Wear, The Institution of Mechanical Engineers, London, England, October, 1957.

82. Ivany, R. D., "Collapse of a Cavitation Bubble in Viscous, Compressible Liquid--Numerical and Experimental Analyses," Ph.D. Thesis, Department of Nuclear Engineering, The University of Michigan, April, 1965; Also available as ORA Technical Report No. 03424-15-T, The University of Michigan.

83. Ivany, R. D. and Hammitt, F. G., "Cavitation Bubble Collapse in Viscous Compressible Liquids--Numerical Analyses," ASME Paper No. 65-FE-16; to be published Journal of Basic Engineering, Trans. ASME.

84. Hickling, Robert and Plesset, Milton S., "Collapse and Rebound of a Spherical Bubble in Water," The Physics of Fluids, Vol. 7, No. 1, January, 1964, pp. 7-14.

85. Liquid Metals Handbook, Richard N. Lyon, Editor-in-Chief, Second Edition, June, 1952.

86. International Critical Tables, Compiled by Clarence J. West and Callie Hull, McGraw-Hill Book Company, New York, 1933.

87. Westervelt, Franklin H., "Automatic System Simulation Programming," Ph.D. Thesis, College of Engineering, The University of Michigan, November, 1960.

88. Crandall, Richard L., "The Mathematical and Logical Procedures of the Stepwise Regression Program with Learning," University of Michigan Computing Center Internal Report, 1965.

89. Rohsenow, W. M., Editor, Developments in Heat Transfer, The MIT Press, Cambridge, Massachusetts, 1964.

90. Proceedings of the Conference on Selected Technology for the Petroleum Industry, NASA Lewis Research Center, Cleveland, Ohio, December 8-9, 1965.

91. Collier, J. G., "The Boiling of Sodium and its Significance to the Safety of Fast Reactors," Internal Document, Chemical Engineering Division, A.E.R.E. Harwell, January, 1966.

92. Simpson, H. C. and Silver, R. S., "Theory of One-Dimensional, Two-Phase Homogeneous Non-Equilibrium Flow," _Symposium on Two-Phase Fluid Flow_, Institution of Mechanical Engineers, London, February 7, 1962.

93. Plesset, M. S. and Zwick, S. A., "The Growth of Vapor Bubbles in Superheated Liquids," _Journal of Applied Physics_, Vol. 25, No. 4, April, 1954, pp. 493-500.

94. Plesset, M. S., "The Dynamics of Cavitation Bubbles," _Journal of Applied Mechanics_, September, 1949, pp. 277-282.

95. Private Communication from Robert S. Ruggeri, NASA Lewis Research Center, Cleveland, Ohio, May 10, 1966, File No. 2751.

96. Hollander, A., "Thermodynamic Aspects of Cavitation in Centrifugal Pumps," _American Rocket Society Journal_, October, 1962, pp. 1594-1595.

97. Sears, Francis W., _Mechanics, Wave Motion, and Heat_, Addison-Wesley Publishing Co., Inc., Reading, Massachusetts, 1958, pp. 602-604.

98. Van Wylen, Gordon J. and Sonntag, Richard E., _Fundamentals of Classical Thermodynamics_, John Wiley & Sons, Inc., New York, 1965, pp. 331-332.

99. Hammitt, F. G., Robinson, M. John, Siebert, C. A. and Aydinmakine, F. A., "Cavitation Damage Correlations for Various Fluid-Material Combinations," ORA Technical Report No. 03424-14-T, Department of Nuclear Engineering, The University of Michigan, October, 1964.

100. Heymann, F. J., "On the Time Dependence of the Erosion Rate Due to Impingement or Cavitation," Paper #136 presented at 1966 Annual ASTM Meeting, Symposium on Erosion by Cavitation or Impingement, Atlantic City, New Jersey, June, 1966.

101. Hammitt, F. G., Discussion of Paper #136, ASTM Symposium on Erosion by Cavitation or Impingement, June, 1966, entitled "On the Time Dependence of the Erosion Rate Due to Impingement or Cavitation," by F. J. Heymann.

SELECTED BIBLIOGRAPHY
(RELATED BACKGROUND MATERIAL)

1. Albers, Vernon M., _Underwater Acoustics Handbook--Volume II,_ Pennsylvania State University Press, 1965.

2. Blitz, J., _Fundamentals of Ultrasonics_, Butterworth & Co., Ltd., London, England, 1963.

3. Blitz, J., _Elements of Acoustics_, Butterworth & Co., Ltd., London, England, 1964.

4. Cady, Walter G., _Piezoelectricity, Volumes One and Two_, Dover Publications, Inc., New York, 1964.

5. Coleman, B. D., Gurtin, M. E., Herrera, I., Truesdell, R. and Truesdell, C., _Wave Propagation in Dissipative Materials_, Springer-Verlag, Inc., New York, 1965.

6. Crandall, I. B., _Theory of Vibrating Systems and Sound_, D. Van Nostrand Co., New York, 1926.

7. El'piner, Isaak E., _Ultrasound: Physical, Chemical, and Biological Effects_, Translated from the Russian by K. L. Sinclair, Consultants Bureau, New York, 1964.

8. Frederick, Julian R., _Ultrasonic Engineering_, John Wiley & Sons, Inc., New York, 1965.

9. Hueter, T. F. and Bolt, R. H., _Sonics_, John Wiley & Sons, Inc., New York, 1955.

10. Kinsler, L. E. and Frey, A. R., _Fundamentals of Acoustics_, John Wiley & Sons, Inc., New York, 1950.

11. Krasil'nikov, V. A., _Sound and Ultrasound Waves in Air, Water, and Solid Bodies_, Jerusalem, Israel Program for Scientific Translations, Available from Office of Technical Services, U.S. Dept. of Commerce, 1963.

12. Mason, W. P., _Physical Acoustics, Principles and Methods, Volume I, Part B,_ Academic Press, New York, 1964.

13. Mason, W. P., _Piezoelectric Crystals and Their Applications to Ultrasonics_, D. Van Nostrand Co., New York, 1950.

14. Sharman, R. V., _Vibrations and Waves_, Butterworth & Co., Ltd., London, England, 1963.